

For Reference

NOT TO BE TAKEN FROM THIS ROOM

Ex LIBRIS
UNIVERSITATIS
ALBERTAEENSIS





Digitized by the Internet Archive
in 2019 with funding from
University of Alberta Libraries

<https://archive.org/details/Corbett1984>

THE UNIVERSITY OF ALBERTA

RELEASE FORM

NAME OF AUTHOR Ivan Corbett
TITLE OF THESIS LOAD AND DISPLACEMENT VARIATIONS ALONG A
 SOFT GROUND TUNNEL
DEGREE FOR WHICH THESIS WAS PRESENTED MASTER OF SCIENCE
YEAR THIS DEGREE GRANTED FALL 1984

Permission is hereby granted to THE UNIVERSITY OF ALBERTA LIBRARY to reproduce single copies of this thesis and to lend or sell such copies for private, scholarly or scientific research purposes only.

The author reserves other publication rights, and neither the thesis nor extensive extracts from it may be printed or otherwise reproduced without the author's written permission.

THE UNIVERSITY OF ALBERTA

LOAD AND DISPLACEMENT VARIATIONS ALONG A SOFT GROUND TUNNEL

by



Ivan Corbett

A THESIS

SUBMITTED TO THE FACULTY OF GRADUATE STUDIES AND RESEARCH
IN PARTIAL FULFILMENT OF THE REQUIREMENTS FOR THE DEGREE
OF MASTER OF SCIENCE

Department of Civil Engineering

EDMONTON, ALBERTA

FALL 1984

THE UNIVERSITY OF ALBERTA
FACULTY OF GRADUATE STUDIES AND RESEARCH

The undersigned certify that they have read, and recommend to the Faculty of Graduate Studies and Research, for acceptance, a thesis entitled LOAD AND DISPLACEMENT VARIATIONS ALONG A SOFT GROUND TUNNEL submitted by Ivan Corbett in partial fulfilment of the requirements for the degree of Master of Science.

Abstract

Contained within are field measurements and subsequent analysis associated with the investigation of loads and displacements along a 500m length of tunnel. The tunnel, 3.2m in diameter with an approximate depth of burial of 12.2m above crown, was excavated using a Tunnel Boring Machine with a steel set and wood lagging primary liner. Data presented covers a wide spectrum of tunnelling conditions, a result of variable ground conditions encountered along the tunnel.

Displacements, investigated using 26 surface settlement points, 5 multipoint extensometers and 2 slope indicators showed increases in movement which could be closely correlated with changing geologic conditions. It was also found, in an area where all indicators suggested non-yielding ground, that small equal vertical displacements existed above the tunnel crown. These movements were considered analogous to the deflections at the centre of a deep elastic beam as opposed to an indication of block like failure into the tunnel.

Load measurement along the tunnel necessitated the development of an inexpensive but accurate system. It was thus decided that deflections occurring at the centre of regular construction laggings could be utilised to back calculate pressure magnitudes if certain assumptions were made. Development of a system to detect such deflections resulted in the first "University of Alberta Deflectometer".

Measurement of steel set loads was achieved using 16 load cells.

Local tunnel behaviour, together with accuracy determination of wood lagging pressures, was investigated using four formal test sections. These sections indicated pressure distributions typical of a flexible lining system. Ratios of steel set load to lining load were found to vary between 1.2 and 3.8 with the lower values being observed under the poorest ground conditions.

The accuracy of a single pressure prediction by a wood lagging was found to be influenced by several factors. Further investigation of the method, however, especially in Test Section 3, indicated that "average" pressure values could be obtained if more measurements than is usually considered economical were made.

Finally, a new measurement technique based on information gained from Test Sections 1 to 4, was applied at 16 sections along the tunnel. This resulted in crown pressure magnitudes which varied from 4.8% to 49.3% full overburden. All sections, located directly underneath a surface settlement point, allowed investigation of the interrelationship between loads and displacements. This gave a trend of increasing load with increasing displacements although no direct numerical relationship was evident.

Conventional methods of lining load prediction, with the exception of Terzaghi, proved to be overconservative and insensitive to changing ground conditions. To investigate

the full spectrum of encountered ground conditions a method referred to as the Convergence Confinement Method (CCM) was used. In this method changing ground conditions were modeled by imposing decreased strength parameters to material within an expanding circular yield zone. These strength parameters, defined as the "apparent shear strength parameters ϕ^* and c^* ", were chosen to model temporary effects such as excess pore pressures and loosening, present around the tunnel face. While more investigation is required into ϕ^* and c^* values, results indicate that trends of pressure dependence and magnitude could quite accurately be predicted given correct apparent shear strength parameters.

Acknowledgements

I would like to extend a very special thanks to my supervisor Dr. P.K. Kaiser for his guidance, enthusiasm and encouragement throughout this thesis and in other research areas. This thanks is also extended to Dr. Z. Eisenstein who took over my supervisory duties on Peter's absence.

I am gratefully indebted to the Department of Civil Engineering, University of Alberta and the National Science and Engineering Research Council for personal funding, thereby making it possible to study in Canada. Special thanks is extended to the City of Edmonton, Department of Water and Sanitation and the Central Research Fund, University of Alberta for sponsoring the fieldwork presented in this thesis.

To members of the technical support staff within the Department of Civil Engineering, University of Alberta I offer my appreciation for the many hours spent preparing instruments. I especially thank Mr. G. Cyre for his help and guidance during instrument preparation and installation and Christine Hurley for the many hours spent in the field taking measurements.

I thank my fellow graduate students for their companionship during my studies and also for their unselfish help given to me when I needed someone to help with field measurements. Special thanks is given to Dave Korpach for his help, freely given on many occasions, and for many happy hours spent discussing this thesis and other related topics,

playing sports or enjoying a cool beer.

For the fruitful discussions held with many of my peers, I thank them. Special mention is given to Paulo Branco who gladly gave up his time to proof read large portions of this thesis. His input and constructive criticisms had a very positive effect on the quality of the work presented within. I would like to give special mention to Messrs H. Heinz, A. Negro and P. Collins.

To Mr. Ian Humphries I extend my gratitude for editing extensive portions of this thesis.

I thank also Marty and Sandy Lanigan for the friendship and hospitality shown to me during my stay in Edmonton. To members of the Nor'westers Rugby Club, through whom I have made so many good friends, I extend my appreciation and thanks.

Lastly, but certainly not least, I offer a very heartfelt thanks to my parents, James and Edith, for their continual encouragement and support throughout all my academic endeavours.

Table of Contents

Chapter	Page
1. INTRODUCTION	1
1.1 Objectives of this Thesis	1
1.2 Scope of this Thesis	2
2. PROJECT DETAILS AND GEOLOGY	4
2.1 Project Details	4
2.1.1 Location	4
2.1.2 Tunnel Details	4
2.1.3 Tunnel Boring Machine (TBM)	7
2.1.4 Construction Procedure and Excavation Rates	7
2.2 Geological Details	11
2.2.1 General Edmonton Geology	11
2.2.2 Geological Details of the Project Area	13
2.2.3 Geotechnical Properties of the Edmonton Surficial Deposits	17
3. INSTRUMENTATION AND EQUIPMENT	19
3.1 Ground Displacement Measurement	19
3.1.1 Principles of Ground Displacement Measurement	19
3.1.2 Vertical Displacements	20
3.1.2.1 Surface Settlement Points	20
3.1.2.2 Multipoint Extensometers	21
3.1.2.3 Benchmark Installation	26
3.1.2.4 Surveying Details	28
3.1.3 Horizontal Displacement Measurements	28
3.1.3.1 Inclinometers	29
3.2 Tunnel Support Loads	33

3.2.1	Lagging Load Measurement	33
3.2.1.1	University of Alberta Deflectometer	34
3.2.1.2	Simulated Steel Laggings	38
3.2.1.3	Calibrated Wood Laggings	40
3.2.1.4	Calibration of Laggings	40
3.2.1.5	Uncalibrated Laggings	48
3.2.2	Steel Set Load Measurement	50
3.2.2.1	Load Cells	51
4.	GROUND DISPLACEMENTS	56
4.1	Vertical Displacements	57
4.1.1	Surface Displacements	57
4.1.2	Vertical Displacements with Depth	65
4.1.3	Surface Settlement Predictions	79
4.2	Horizontal Displacements	84
5.	TUNNEL SUPPORT PRESSURE MEASUREMENTS	92
5.1	Instrumented Test Sections	92
5.1.1	Test Section 1	92
5.1.2	Test Section 2	100
5.1.3	Test Section 4	109
5.2	Discussion of Tunnel Support Pressure Measurements	119
5.2.1	Performance of Wood Laggings	119
5.2.2	Discussion of Lagging Pressures	125
5.2.3	Discussion of Load Cell Results	132
5.2.4	Interrelation of Lagging Pressures and Steel Set Loads	134
5.2.5	Conclusions	139

5.3 Prediction of Lining Loads	139
5.3.1 Convergence Confinement Method	142
5.3.1.1 Theoretical Prediction of the Ground Convergence Curve	147
5.3.2 Discussion of Predicted Pressures Compared with Field Measurements	159
5.4 Load Variation Along Tunnel	164
5.4.1 Test Section 3	164
5.4.1.1 Section Details and Purpose	164
5.4.1.2 Lagging Pressure Details	166
5.4.1.3 Load Cell Results	170
5.4.2 Measurement of Lining Pressure Along the Tunnel	172
5.4.3 Discussion on Load Variation along the Tunnel	173
6. SUMMARY AND CONCLUSIONS	195
REFERENCES	203
APPENDIX A	212
APPENDIX B	217
APPENDIX C	221
APPENDIX D	226
APPENDIX E	241

List of Tables

Table	Page
3.1	Details of the Inclinator System.....31
3.2	Axial Load Predictions from Load Cell Calibration Tests.....52
5.1	Comparison Values Between Steel and Wood Lagging Pressures.....120
5.2	Average Lagging Pressures for Test Section 1, 2 and 4.....126
5.3	Steel Set to Lagging Load Calculation Values.....136
5.4	Uncalibrated Section Pressures.....185

List of Figures

Figure	Page
2.1	Location of Project Area in Edmonton.....5
2.2	Detailed Map of Project Area.....6
2.3	Three Dimensional Presentation of the Top Surface of a Water Bearing Sand Layer present in Project Area.....15
2.4	Defined Geologic Areas along the Tunnel.....16
3.1	Location of Ground Displacement Instruments.....22
3.2	Details of Multipoint Extensometer Probe.....24
3.3	Installed Multipoint Extensometer Details.....25
3.4	University of Alberta Deflectometer.....36
3.5	Simulated Steel Lagging.....39
3.6	Wood Lagging Details.....41
3.7	Laboratory Arrangement for Calibrated Laggings.....42
3.8	Typical Load-Deflection Record for a Wood Lagging...42
3.9	Distribution of Wood Lagging Flexural Rigidities....45
3.10	Distribution of Steel Lagging Flexural Rigidities...47
3.11	Distribution of Measured Zero Deflections.....47
3.12	Load Cell Cross Section Details.....53
4.1	Compilation plot of all Settlement Point Displacements varying with Tunnel Face Position.....58
4.2	Qualitative Distribution of Total Expected Surface Settlement with Tunnel Face Advance.....61
4.3	Normalized plot of seven Settlement Points with Different Total Settlements.....62
4.4	Observed Settlements in the Defined Geologic Regions.....63
4.5	Vertical Displacements with Depth as Measured by the Multipoint Extensometers.....66

Figure	Page
4.6 Qualitative Development of Plasticity around a Tunnel.....	69
4.7 Block Failure Mechanism for the Kennedale Tunnel - Undrained Analysis.....	73
4.8 Block Failure Mechanism for the Kennedale Tunnel - Effective Stress Analysis.....	74
4.9 Vertical Displacements with Depth in Yielding Ground(after El-Nahhas, 1980: modified)....	76
4.10 Progressive Failure Mechanism for Block Failure.....	78
4.11 Gaussian Probability Curve (after Peck, 1969: modified).....	81
4.12 Probability Curve Parameter "i" varying with Z/D ratio (after Peck et al., 1969: modified)..	81
4.13 Volume Loss of Material with Increasing Overload Factor (after Peck et al., 1969: modified).	83
4.14 Horizontal Displacements recorded in the Longitudinal Plane containing the Tunnel axis by Slope Indicator 1.....	85
4.15 Horizontal Displacements Transverse to the Tunnel axis as recorded by Slope Indicator 1.....	86
4.16 Horizontal Displacements recorded in the Longitudinal Plane containing the Tunnel axis by Slope Indicator 2.....	87
4.17 Horizontal Displacements Transverse to the Tunnel axis as recorded by Slope Indicator 2.....	88
5.1 Location of Test Sections along Tunnel.....	93
5.2 Configuration of Test Section 1.....	95
5.3 Test Section 1 : Rib 1 Lagging Pressures.....	96
5.4 Test Section 1 : Rib 2 Lagging Pressures.....	97
5.5 Test Section 1 : Rib 3 Lagging Pressures.....	98
5.6 Test Section 1 : Load Cell Axial Loads.....	99

Figure	Page
5.7	Configuration of Test Section 2.....101
5.8	Test Section 2 : Rib1 Tunnel Springline Pressures..102
5.9	Test Section 2 : Rib1 Tunnel Crown Pressures.....103
5.10	Test Section 2 : Rib2 Tunnel Springline Pressures..104
5.11	Test Section 2 : Rib2 Tunnel Crown Pressures.....105
5.12	Test Section 2 : Rib3 Tunnel Springline Pressures..106
5.13	Test Section 2 : Rib3 Tunnel Crown Pressures.....107
5.14	Test Section 2 : Load Cell Axial Loads.....108
5.15	Configuration of Test Section 4.....110
5.16	Overburden Details at Test Section 4.....111
5.17	Test Section 4 : Rib1 Tunnel Springline Pressures..112
5.18	Test Section 4 : Rib1 Tunnel Crown Pressures.....113
5.19	Test Section 4 : Rib2 Tunnel Springline Pressures..114
5.20	Test Section 4 : Rib2 Tunnel Crown Pressures.....115
5.21	Test Section 4 : Rib3 Tunnel Springline Pressures..116
5.22	Test Section 4 : Rib3 Tunnel Crown Pressures.....117
5.23	Test Section 4 : Load Cell Axial Loads.....118
5.24	Mechanisms for TBM Induced Lagging Moments.....122
5.25	Average Pressures for Test Section 1.....127
5.26	Average Pressures for Test Section 2.....128
5.27	Average Pressures for Test Section 4.....129
5.28	Facets of the Convergence Confinement Method.....143
5.29	Typical Shapes of Ground Convergence Curves.....146
5.30	Boundary Conditions for Analysis of Daemen(1975)149

Figure	Page
5.31 Ground Convergence Curves Generated under the assumption of $\phi=35^\circ$; $\phi^*=35^\circ$; $c = 10\text{kPa}$; $c^* = 10\text{kPa}$	155
5.32 Ground Convergence Curves Generated under the assumption of $\phi=35^\circ$; $\phi^*=19.5^\circ$; $c = 10\text{kPa}$; $c^* = 0\text{kPa}$	156
5.33 Ground Convergence Curves Generated under the assumption of $\phi=35^\circ$; $\phi^*=0^\circ$; $c = 10\text{kPa}$; $c^* = 0\text{kPa}$	157
5.34 Crown Convergence Curves for the three Strength Cases Considered.....	158
5.35 Configuration of Test Section 3.....	165
5.36 Crown Pressure Measurements of Test Section 3.....	167
5.37 Pressure Comparison Obtained between "Correct Pressures" and those Obtained Under the Assumption of Zero Initial Deflection....	169
5.38 Load Cell Axial Loads for Test Section 3.....	171
5.39 Crown Pressure Distributions for Uncalibrated Sections UC a and UC b.....	174
5.40 Crown Pressure Distributions for Uncalibrated Sections UC c and UC d.....	175
5.41 Crown Pressure Distributions for Uncalibrated Sections UC e and UC f.....	176
5.42 Crown Pressure Distributions for Uncalibrated Sections UC g and UC h.....	177
5.43 Crown Pressure Distributions for Uncalibrated Sections UC i and UC j.....	178
5.44 Crown Pressure Distributions for Uncalibrated Sections UC k and UC l.....	179
5.45 Crown Pressure Distributions for Uncalibrated Sections UC m and UC n.....	180
5.46 Crown Pressure Distributions for Uncalibrated Sections UC o and UC p.....	181

Figure	Page
5.47 Uncalibrated Section Crown Pressures versus Surface Settlement.....	186
5.48 Uncalibrated Section Pressures in terms of Percentage Overburden versus Surface Settlement.	190

List of Plates

Plate	Page
3.1 University of Alberta Deflectometer.....	37
3.2 Calibrated Wood Lagging.....	43
3.3 Installed Load Cell.....	55

1. INTRODUCTION

Edmonton, located in central Alberta, has had an active tunnelling history over the last forty years with an approximate total of 90 kilometers being constructed in the past ten years alone. The vast majority of these tunnels have been constructed for storm and sanitary purposes, e.g., 80km of these tunnels in the past 10 years have been for this purpose. In recent years tunnelling activities associated with the extension of the Light Rail Transit System within Edmonton have been major undertakings although in total distance it has only accounted for approximately 1.6 km.

In an effort to understand the complex problems of tunnelling in relation to the development of lining loads and soil displacements, several studies, sponsored by the City of Edmonton, have been undertaken by the Department of Civil Engineering, University of Alberta, Edmonton, (El-Nahhas, 1977; El-Nahhas, 1980; Branco, 1981). This present study is a continuation of these efforts to obtain a better understanding of the interdependency of construction procedure and ground conditions upon measured loads and displacements.

1.1 Objectives of this Thesis

Unlike the previous studies already cited which investigated the performance of short, heavily instrumented sections, this project wished to examine the variability of

loads and displacements along a larger portion of tunnel. While surface displacements can be measured relatively cheaply the measurement of lining loads generally requires more sophisticated and hence more expensive methods. Although, economics did dictate development of an inexpensive measuring technique to enable measurement of load along the tunnel, it was also an initial objective of this project to develop and investigate the accuracy of such a system. In this respect the first "University of Alberta Deflectometer" was designed and constructed for use in this study. This instrument, which measures lagging deflections, satisfied a request of the City of Edmonton, Department of Water and Sanitation (co-sponsors of the project) to have a simple but still accurate inexpensive monitoring system developed for use in future similar works.

1.2 Scope of this Thesis

In the following Chapters the techniques and approaches taken in pursuit of the aforementioned objectives are presented.

Project details and geology are contained in Chapter 2 while Chapter 3 introduces the instrumentation chosen, why it was selected, how it was calibrated and finally how it was installed.

Chapter's 4 and 5 present the data obtained from all installed instruments. Chapter 4 contains ground displacement measurements while Chapter 5, the backbone of

this thesis, presents information on load measurements along the tunnel. It also contains details of the measuring technique used to obtain the load measurements. After developing theoretical relationships between assumed ground strength parameters and expected tunnel lining loads, the interrelationship between measured loads, displacements and theoretical predictions are investigated.

Chapter 6 summarizes the conclusions of this project.

2. PROJECT DETAILS AND GEOLOGY

2.1 Project Details

2.1.1 Location

Edmonton, a city of approximately 500,000 inhabitants, is located in central Alberta on the banks of the North Saskatchewan River. Figure 2.1 shows the general location of the project area within Edmonton. A more detailed map of the site area together with the location of the tunnel centre line is given in Figure 2.2. The tunnel, constructed in glacial deposits, is intended to convey storm water to the North Saskatchewan River. At present the site area is largely undeveloped.

2.1.2 Tunnel Details

The tunnel, 3.2m (126inches) in diameter had a total plan length of 1670m. Construction followed usual City of Edmonton procedures utilising a Tunnel Boring Machine (TBM or Mole) together with a steel set and wood lagging primary liner. Generally, steel set spacing was 1.22m (4feet) although this was reduced to 0.91m (3feet) if ground conditions deteriorated. The decision to reduce the rib spacing was taken if rib expansion resulted in consistent wood lagging breakages. Lagging was 80mm (3inches) thick and 130mm (5inches) wide in the crown area while below the springline 50mm (2inches) thick and 250mm (10inches) wide

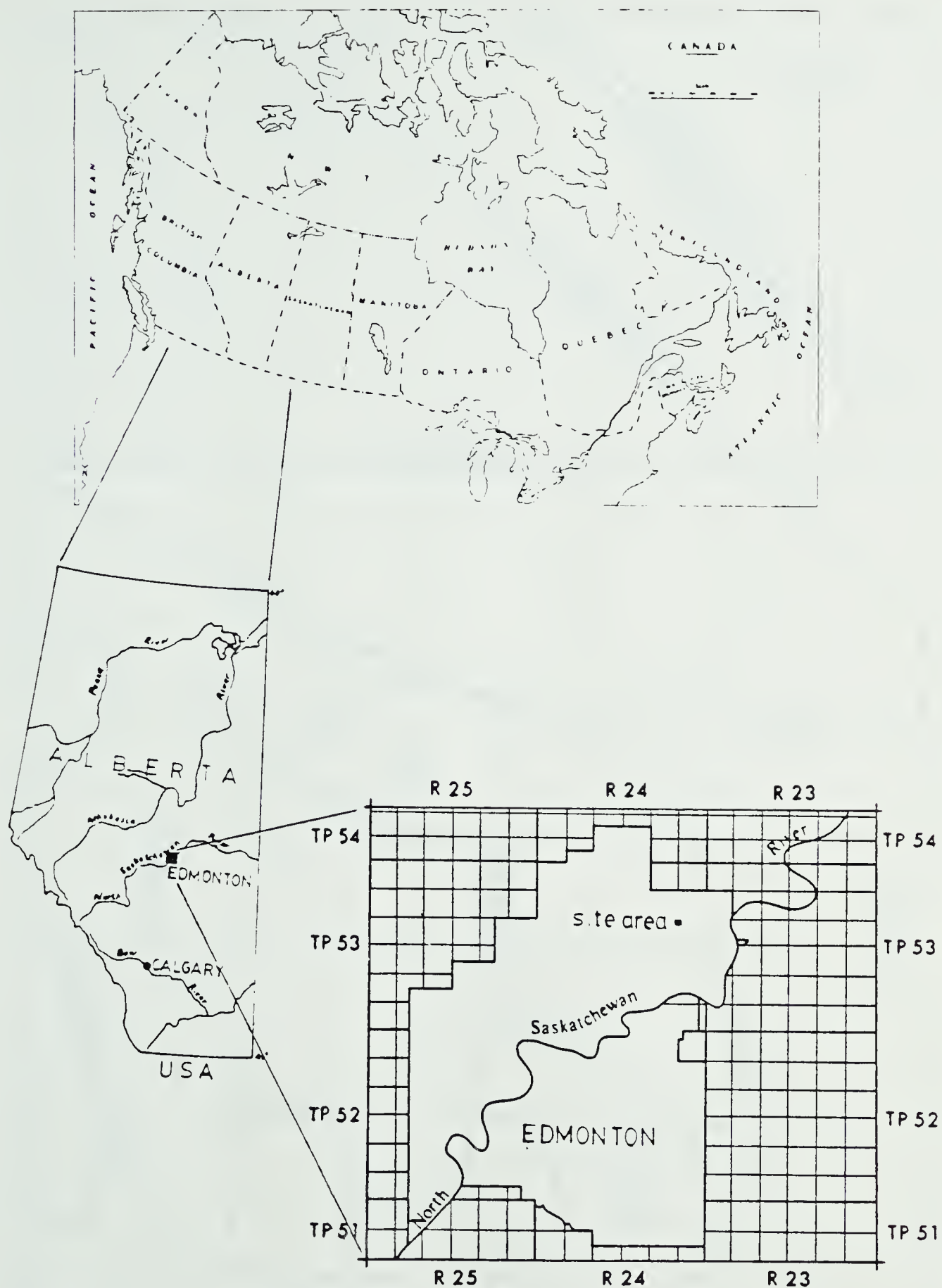


Figure 2.1 Location of Project Area in Edmonton

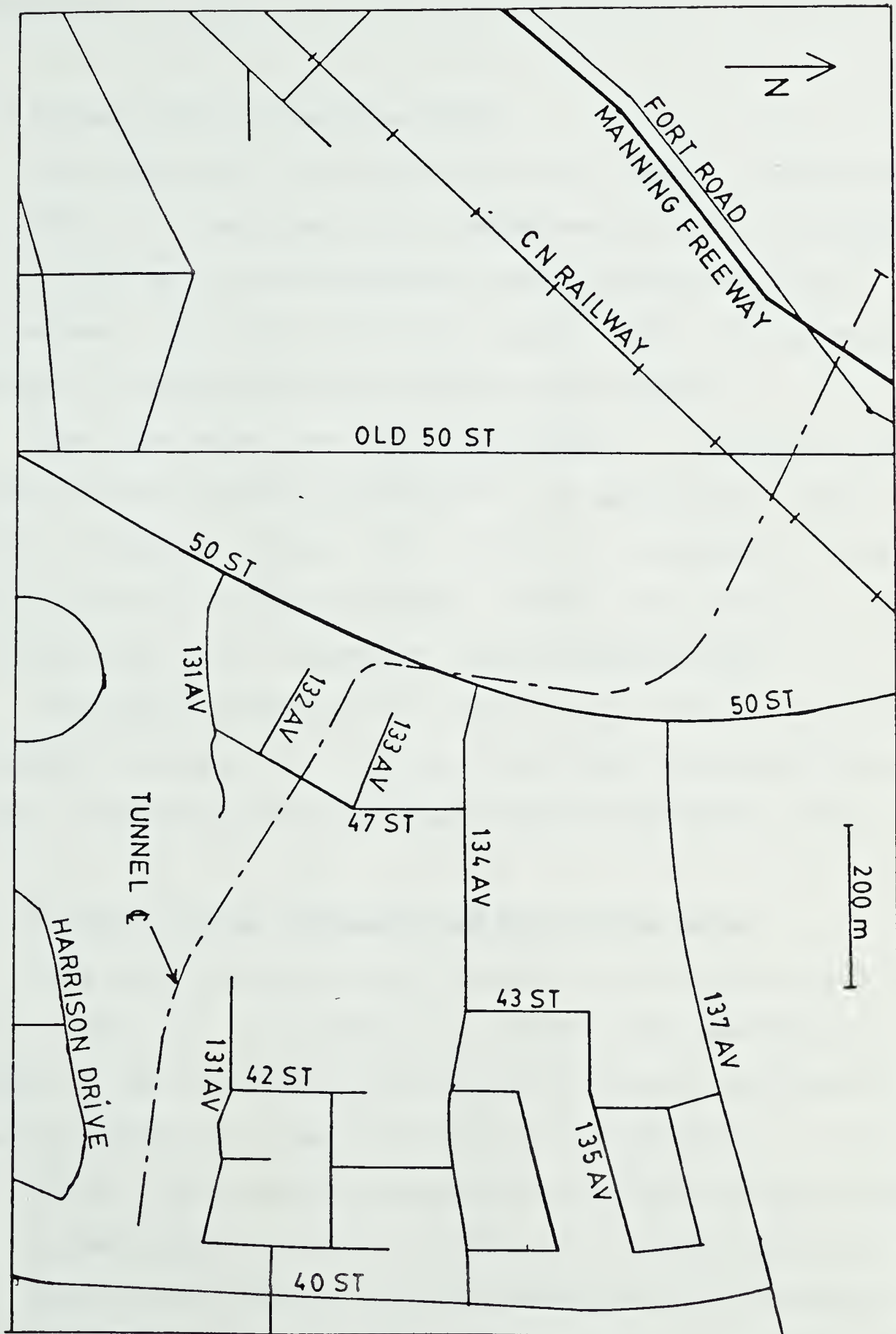


Figure 2.2 Detailed Map of Project Area

boards were used.

2.1.3 Tunnel Boring Machine (TBM)

The TBM used in this project was a Lovatt M126-series No 4800 with a maximum of 485 horsepower. Power was supplied to the TBM by two 200 horsepower electric motors and a 75 horsepower auxiliary electric motor. The 10 horsepower deficit is obtained using a charge pump system.

The TBM which was 3.2m (126 inches) in diameter pushed itself forward using a maximum of 10 propulsion jacks. A total maximum thrust of 5.3MN is available although typically only 1.5MN was used. Using the jacks a total maximum advance of 1.68m (66 inches) was possible.

The total length of the TBM was 6.1m (20feet) although a feeder conveyor belt, designed to remove material from the face, extended approximately another 9m (30 feet) rearward.

2.1.4 Construction Procedure and Excavation Rates

The construction of the tunnel involved excavation of the tunnel in increments of length, one increment being equal to the rib spacing. The excavation and installation of each increment utilised the following procedure:

1. Using the installed lining as a reaction force, the TBM pushed itself forward into the soil. During pushing, the head of the TBM was rotated thereby excavating material and advancing the face. The excavated material was removed from the cutting head via a feeder conveyor

belt. The feeder conveyor deposited the spoil onto a second longer belt. The second belt was supported well above the tunnel invert on a hollow steel frame structure. The frame allowed passage of the electrically powered muck train underneath the belt to the tail area of the TBM. Material from the second conveyor was discharged into the waiting empty muck cars. The cars were filled consecutively as the muck train reversed from the frame.

After the TBM had advanced far enough for a rib to be erected within the tailpiece, it halted, at which time the muck train departed to be unloaded. Train unloading was achieved by side dumping capabilities of the muck cars into a hoist skip. Material was lifted to the surface by the hoist and subsequently trucked away.

During excavation wood lagging required for the next rib was stacked on the floor of the tunnel in a convenient manner to aid erection time.

2. The three steel segments required to make the complete circle were erected within the shield such that one rib joint was located at the tunnel invert. To enhance the erection time of a rib the two side steel sets, required for the rib, had been fabricated at the conclusion of the previous rib. For storage, during excavation of the present rib, the fabricated twin steel sets were attached to the top pushing frame of the TBM. The upper steel set, stored up the side of the mole, was manually

lifted over the feeder conveyor belt and the steel set ring completed.

After establishing the correct rib distance by inserting a lagging board at invert and pushing gently on the newly formed steel set ring the lagging boards were placed in position, starting at the invert and working up around both sides.

3. Expansion of the steel sets using radially positioned rams was next performed. Due to the shield tail being behind the now penultimate ring, only the trailing steel set of that ring could be expanded at this time. Expansion was achieved using two similar stages, each one resulting in a 100mm (4inches) expansion of the two upper steel set joints. The expansion spaces were maintained by inserting 100mm long "I" section steel spacers.
4. After the ram was retracted, chains to hold the last three ribs together were placed on both sides of the tunnel. The purpose of the chains was to prevent loosening of the end rib when the TBM push stopped after excavation of the next ring. This was important under high load conditions as movement of the steel set ring would have led to lagging, followed by material, entering the tunnel. The newly formed rib was now used as an extension to the reaction force and the procedure described in 1 to 4 repeated.

The advance rate using the aforementioned procedure varied depending on the ground conditions. In good ground, i.e., ground where the face was self-supporting, that is, excavation could be performed with the shield face doors fully open and where no ground water was present, excavation advances of 12.2m (40 feet; 10 ribs) were not uncommon in an eight hour shift. Occasionally advances in excess of 15m (12-13 ribs) was achieved. In poorer ground conditions where water ingress created major problems, advance rates decreased to approximately 6m (20 feet; 5 ribs) per eight hour shift with advances as low as one rib being recorded under the very worst conditions.

Water ingress through the cohesionless material found at the tunnel level, resulted in the following difficulties, which were manifested in decreased advance rates:

1. Slower excavation due to the inability to fully open the shield doors.
2. Large ground losses due to material being washed into the tunnel by water; and
3. Increased difficulties keeping the TBM on line.

Point 2 had the largest impact as constant mucking out of material during excavation and prior to lagging installation was required. In the areas where large amounts of fine silty material were being washed into the tunnel, the construction technique was modified slightly to incorporate location of a geotextile behind the lagging in an effort to stop the material. While this was effective

away from the tail area it did nothing to improve conditions at the tail and did in fact slow down the installation time of a rib.

Periodic tunnel delays occurred due to TBM maintenance work, e.g., replacing excavating teeth and shut down whilst surveying crews set out the line. Random delays occurred from equipment breakdowns or instances where boulders were located in front of the TBM. Depending on their size some of these boulders required breaking up with a jack hammer before removal. One unique delay involved the hitting of a steel pile belonging to a recently constructed bridge pier.

2.2 Geological Details

2.2.1 General Edmonton Geology

The dominating factor of Edmonton surficial deposits was the occurrence of glaciation by the Wisconsin ice sheet which left the area approximately 10,000 years ago. Westgate (1969) postulated advance and readvance of this ice sheet which deposited two individual till sheets. Kathol and Macpherson (1975), however, question the existence of two separate sheets explaining colour differences of the two layers as a product of oxidation. Recent personal communication (S. Thomson, Department of Civil Engineering, University of Alberta) indicates also that the till in the Edmonton area is from one depositional episode. Tiedemann (1984) presents evidence in support of a single till sheet

comprised of three different till types.

The underlying bedrock which controls to a large extent the surface topography is known as the Edmonton formation (Kathol and Macpherson, 1975) although Irish (1970) refers to it as the Horseshoe Canyon formation. The formation consists primarily of fine grained bentonitic sandstones and siltstones interbedded with bentonitic silty claystones (Kathol and Macpherson, 1975). Coal seams, a product of a shallow inland sea which used to cover much of North America and bentonite beds of variable thickness are common. The bentonite beds are attributed to volcanic ash.

The topography of the bedrock was established prior to glaciation by a well defined dendritic drainage system flowing eastwards from the Rocky Mountains. The thalwegs of these preglacial valleys have been mapped in the Edmonton area by Carlson (1967).

The preglacial channels have an important bearing on tunnel construction in the Edmonton area as they are generally floored with water bearing sands and gravels known as Saskatchewan Sands and Gravels. The valleys were infilled as the Wisconsin ice sheet advanced up the regional slope of the land. The advancing ice sheet caused damming of the rivers resulting in a velocity decrease and deposition of some bedload and hence aggrading of the valleys. These sediments, due to velocity changes as the ice sheet approached, generally show a gradation of finer to coarse material with depth. After advance of the ice sheet these

the following are the main results of the study.

- (1) The first result is that the model is able to explain the observed pattern of results. The model predicts that the effect of the treatment will be significant for the first two groups, but not for the third group. This is exactly what was found in the data.
- (2) The second result is that the model is able to explain the observed pattern of results. The model predicts that the effect of the treatment will be significant for the first two groups, but not for the third group. This is exactly what was found in the data.
- (3) The third result is that the model is able to explain the observed pattern of results. The model predicts that the effect of the treatment will be significant for the first two groups, but not for the third group. This is exactly what was found in the data.
- (4) The fourth result is that the model is able to explain the observed pattern of results. The model predicts that the effect of the treatment will be significant for the first two groups, but not for the third group. This is exactly what was found in the data.
- (5) The fifth result is that the model is able to explain the observed pattern of results. The model predicts that the effect of the treatment will be significant for the first two groups, but not for the third group. This is exactly what was found in the data.
- (6) The sixth result is that the model is able to explain the observed pattern of results. The model predicts that the effect of the treatment will be significant for the first two groups, but not for the third group. This is exactly what was found in the data.
- (7) The seventh result is that the model is able to explain the observed pattern of results. The model predicts that the effect of the treatment will be significant for the first two groups, but not for the third group. This is exactly what was found in the data.
- (8) The eighth result is that the model is able to explain the observed pattern of results. The model predicts that the effect of the treatment will be significant for the first two groups, but not for the third group. This is exactly what was found in the data.
- (9) The ninth result is that the model is able to explain the observed pattern of results. The model predicts that the effect of the treatment will be significant for the first two groups, but not for the third group. This is exactly what was found in the data.
- (10) The tenth result is that the model is able to explain the observed pattern of results. The model predicts that the effect of the treatment will be significant for the first two groups, but not for the third group. This is exactly what was found in the data.

valleys and their sediments were filled with till. The final cap in the Edmonton surficial lithology is the Lake Edmonton Clay which is a sediment from glacial Lake Edmonton which formed during ice retreat.

Present drainage of the area is achieved by the North Saskatchewan River (and tributaries) which since deglaciation has down cut through the glacial sediments to bedrock. The North Saskatchewan generally follows the old preglacial valleys and only in some regions has it eroded a new channel.

2.2.2 Geological Details of the Project Area

Surficial deposits in the project area are in excess of 30m (100 feet) due to the presence of an infilled preglacial valley. A report by Kathol and Macpherson (1975) suggested the lithology in the area consisted of 3-5m (10-15 feet) of glacio lacustrine (Lake Edmonton Clay) material, 16-22m (50-75 feet) of glacial till overlying 6-8m (20-25 feet) of Saskatchewan Sands and Gravels.

Site investigations at the project area confirm that these numbers are correct. The presence however of a 3-5m (10-15 feet) thick layer of fine silty, water-bearing cohesionless material was not expected. This layer, which was located beneath the tunnel invert for the first 650m from the east portal, appeared at or above crown level for the remainder of the project and resulted in severe tunnelling difficulties. Using information obtained from the

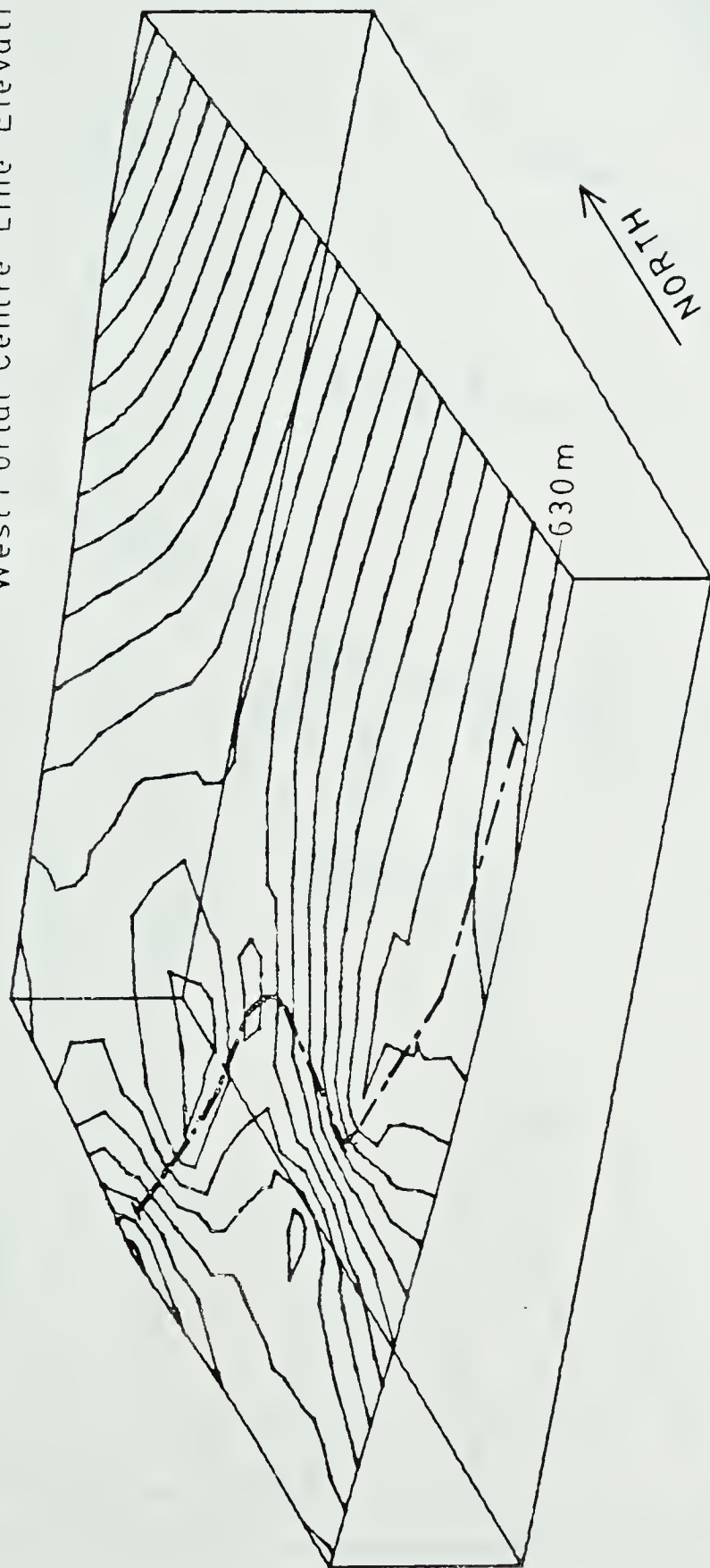
site investigation for this project plus other borehole logs from the area, kindly supplied by Edmonton Geotechnical Consulting firms, a three dimensional plot of the top surface of this sand layer(Figure 2.3) was prepared for the project area. The approximate position of the tunnel centre line is also given in Figure 2.3.

Figure 2.3 shows this layer to have a shape closely approximated by a quarter basin with its low point located in the south east corner of the area. Geologically this may be explained by deposition close to the ice front in an ice marginal lake. This is postulated since the present site area was a large distance from the western lake margin which resulted in all the coarse material contained in the current flowing along the edge of the ice being deposited prior to reaching the site location. The stagnant ice front known to exist in the area (St Onge, 1972) had a sudden change in shape, i.e., a change from running approximately east-west to running north-south. The sudden change in flow direction of the current along the ice edge undoubtedly resulted in a velocity decrease and subsequent deposition of the silts while smaller sized fines were carried on. The occurrence of till on top of this layer is believed to be a product of either a flow till or an ablation till.

With reference to Figure 2.3 and personal knowledge of geological conditions along the tunnel the four geological regions as presented in Figure 2.4 were delimited. A brief description of these regions follows.

East Portal Centre Line Elevation 636.00m

West Portal Centre Line Elevation 640.25m



Contour Interval 1m

----- Tunnel Centre Line

Figure 2.3 Three Dimensional Presentation of the Top Surface of a Water Bearing Sand Layer present in Project Area



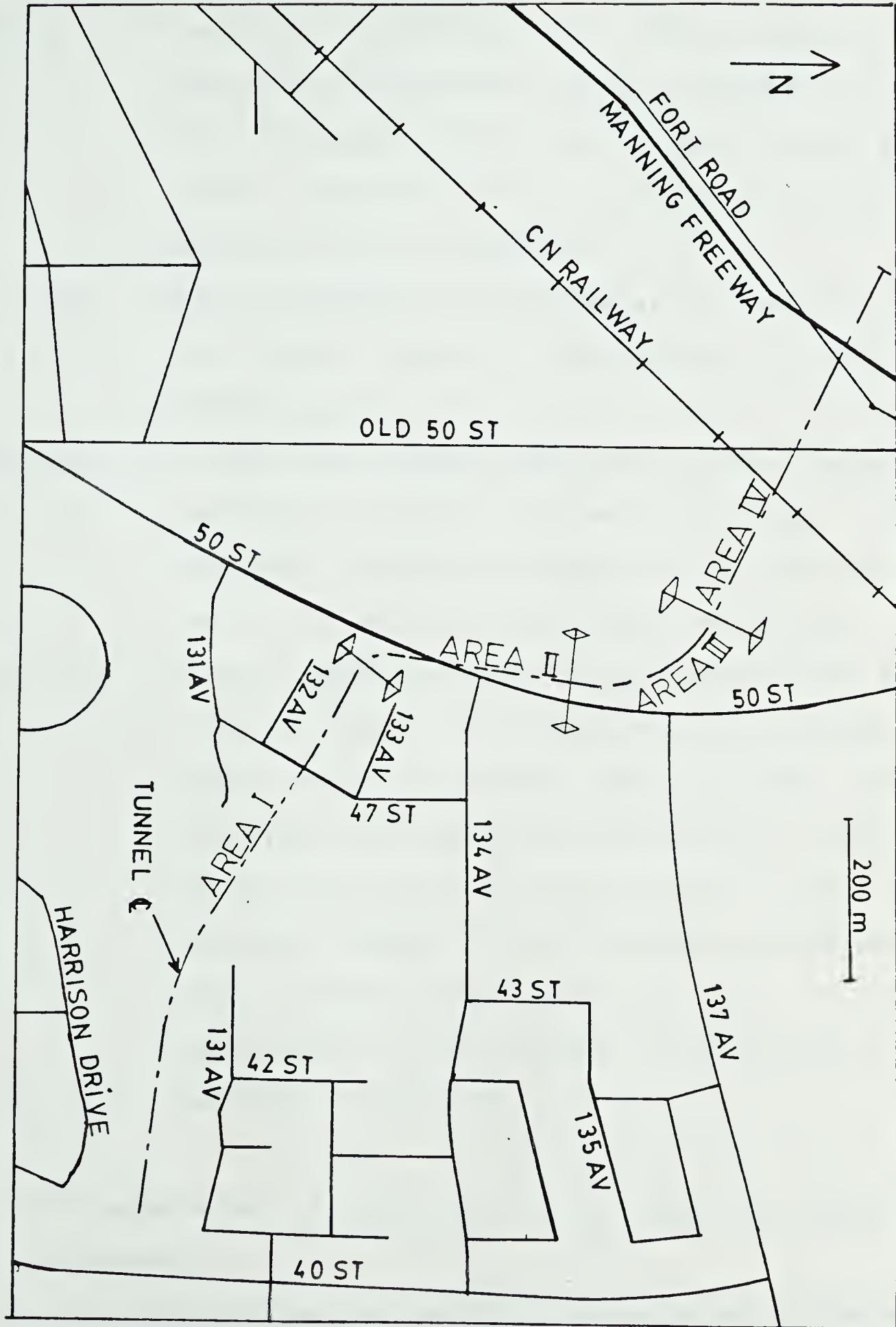


Figure 2.4 Defined Geologic Areas along the Tunnel

- Area I Tunneling conditions in this region were excellent with material being a competent till. Minor problems arose when discontinuous sand lenses, typical of the glacial deposits in Edmonton, were encountered.
- Area II Major problems concerning water ingress from the sand layer delayed construction activities considerably.
- Area III In this area slightly more clay binder increased the cohesive forces in the sand layer. This decreased the permeability and thus reduced the severity of the water problems encountered.
- Area IV In this region the material was similar to Area II but increased water problems, due to apparent higher water pressures, created the worst conditions for tunnelling in the entire project. The increased water pressure may be a result of increased height of the top sand surface above crown. Excess water pressures were further complicated by the recent construction of an embankment on surface.

2.2.3 Geotechnical Properties of the Edmonton Surficial Deposits

Published information regarding geotechnical parameters of the Edmonton till have been largely associated with results obtained from the till in the downtown Edmonton

area. Edmonton till in the downtown sector is known to be very dense with typical blow counts in the order of 35-60 (DeJong and Morgenstern, 1973) although values in excess of 100 are not uncommon. In regions away from the downtown sector the blow counts are generally less.

The unconfined compressive strength of intact samples have been reported by May and Thomson (1978) as varying between 140-245kPa at a depth of 15m with stronger strengths being obtained with depth. Information contained in the unpublished borehole logs used in the generation of Figure 2.3 suggest a value of 300kPa for the till in the project area.

Deformation modulus values as determined from pressuremeter studies conducted in the Edmonton downtown (Eisenstein and Morrison, 1972) indicate a value of 160MPa at a depth equal to that of the tunnel axis in this project. Considering the downtown till is known to be extremely dense a value of 60MPa was arbitrarily chosen as representative for the till in the project area.

Few friction angle values have been reported in the literature, however assumptions of 30-35 degrees is usual for sound tills. This range is validated by quoted values of 27° by Thomson and Yacyshyn (1977) and 34° by Wittebole (1983).

A summary of quoted material properties for the Edmonton till considering unit weights, gradation curves and strengths can be found in Thomson and El-Nahhas (1980).

3. INSTRUMENTATION AND EQUIPMENT

3.1 Ground Displacement Measurement

3.1.1 Principles of Ground Displacement Measurement

The ultimate aim of any ground displacement instrumentation program is to obtain a complete and accurate record of displacements that occur with time. Time dependent displacements, reflecting time dependent soil responses may be long term (months or years), whereas movements associated with construction activities are of shorter duration (days or weeks). The relative contributions of these two displacement components may affect selection of instrument type. While sensitivity is of paramount importance for long term movements continuous reliability and robustness are also important considerations.

In many instances, as in the project presented here, the two types of displacement occur simultaneously, necessitating that one instrument type provides both short and long term records. Economy generally dictates the need for dual purpose instruments. A criterion of sensitivity and robustness which also satisfied the desire for economy was applied in this study such that short and long term records of displacements could be obtained.

Details concerning instrument type, location and installation are presented in the following sections. It should be noted that these instruments were chosen largely

because of experience within the Department of Civil Engineering, University of Alberta (EL-Nahhas, 1980; Savigny, 1980; Branco, 1981).

3.1.2 Vertical Displacements

3.1.2.1 Surface Settlement Points

Various types of surface settlement points are available and described in the literature (Dunnicliff, 1971; Hanna, 1973). All are designed to fulfill the same basic requirement, i.e., that they be firmly anchored in the ground so that the detected movements are only associated with the particular activity in question and not with external factors such as frost action or seasonal moisture changes. Hence, it is important that the anchors be placed below the level of seasonal movements and that the settlement gauges be protected from damage caused by construction activities or vandalism.

In this project the settlement point used consisted of a 19mm steel reinforcing bar with a 100mm disc welded approximately 100mm from the lower end. The upper end of the bar was marked either by machining a spherical seat or by indenting using a centering punch. This facilitated a consistent repeatable surveying mark. The whole assembly was approximately 2 m in length allowing it to reach below the level of expected frost penetration. Installation followed procedures described

by Branco (1981) which ensured that the settlement point was solidly anchored and isolated from downdrag forces. The point was protected by keeping the top point just below ground level. Each point took approximately twenty minutes to install with all points being installed at least 100m ahead of the tunnel face. The settlement points were located at approximately 15 m intervals along the tunnel centre line (previously set out by a City of Edmonton survey crew).

The instrumented section, which was 500 m in total length, consisted of two separate lengths with a 170 m stretch of road between them. A total of 26 surface settlement points were installed with 10 being installed in the first 157m section. The positions of these settlement points with assigned identification numbers are shown in the location plan ('sp' in Figure 3.1). Measurements were taken using standard leveling techniques as described in section 3.1.2.4.

3.1.2.2 Multipoint Extensometers

Measurement of vertical displacement distribution with depth involves the locating of reference points within the soil mass and measuring their varying position with time. Various systems exist for this purpose as reported by Cording et al.(1975). Because of a long term experience in the Department of Civil Engineering, University of Alberta, a system modified from the magnetic extensometers developed by Burland et

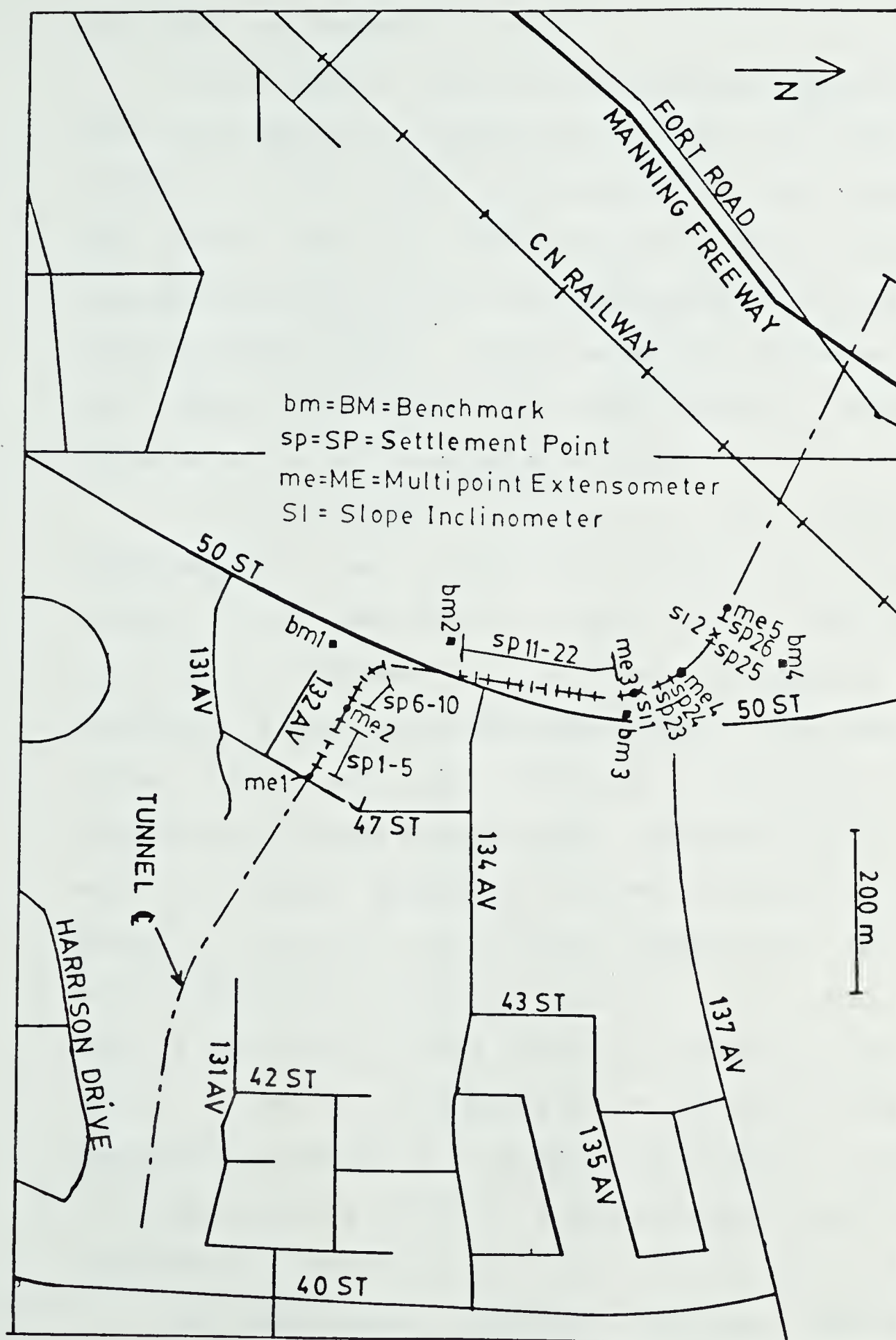


Figure 3.1 Location of Ground Displacement Instruments

al.(1972) was chosen.

In this system a set of ring magnets, combining to form three magnetic fields (Figure 3.2a), are positioned outside a P.V.C. access tube located in the borehole. The probe containing the magnets is held in place by springs which make a positive attachment to the borehole walls (Figure 3.2b) and hence move in unison with the soil. Space limitations would allow placing of measuring units at a minimum separation of 0.5m.

In this project a total of five multipoint extensometers were installed following a procedure similar to that described by Branco (1981) and located as shown in Figure 3.1 as 'me'. In general, it was attempted to have the lowest probe about 1.5m above the tunnel crown with the remaining probes being placed equidistant between bottom probe and ground surface. It was not always possible, however, to have the bottom probe at 1.5m above tunnel crown, because, at the time of installation, the exact distance to the tunnel crown was not known and in some boreholes, notably those for ME 3, 4 and 5, sloughing at the bottom of the holes prevented placement of a probe at full depth. A summary of probe numbers and their distances above tunnel crown is given in Figure 3.3 .

The measurement procedure involved locating the magnetic fields of each gauge by lowering a device containing a reed switch down the access tube. As the

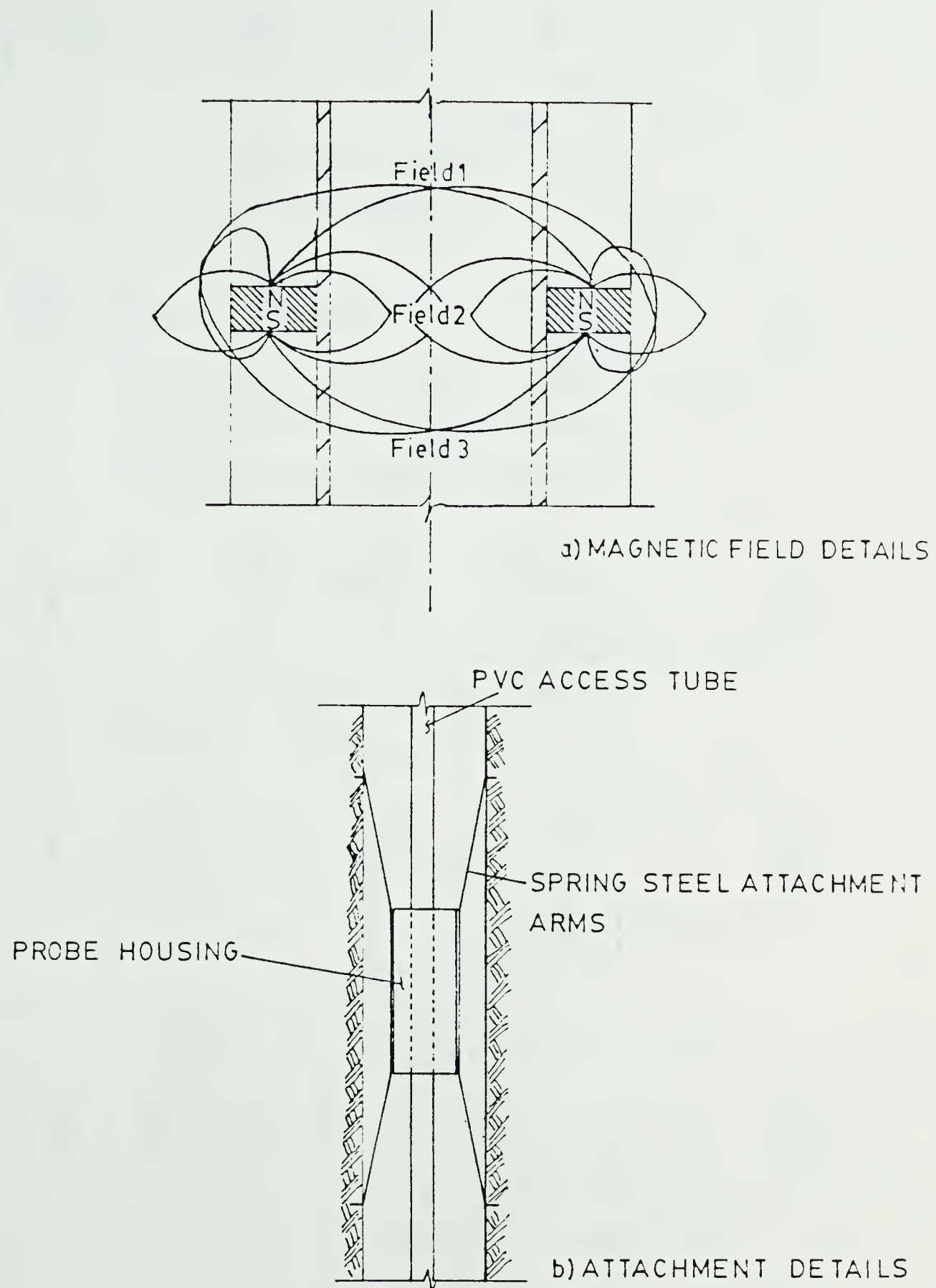


Figure 3.2 Details of Multipoint Extensometer Probe

2.0m VERT SCALE
DIMENSIONS IN METRES

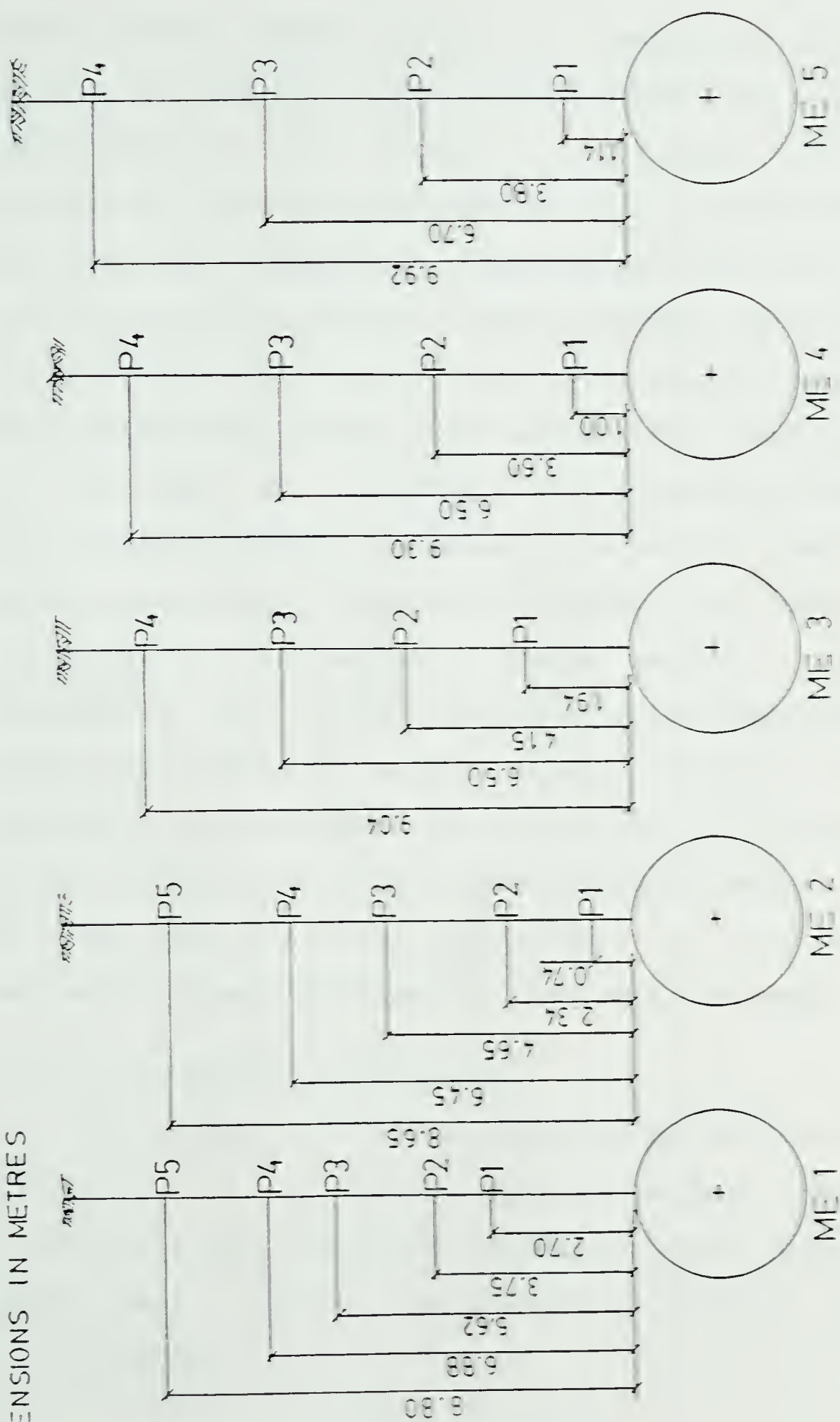


Figure 3.3 Details of Installed Multipoint Interferometer

reed switch passed through the magnetic field, it closed, activating a buzzer at the surface. For optimum repeatability the middle , stronger field, was monitored. Distances from the top of the access tube to the magnets, measured by lowering the measuring device with a tape, were recorded. After optical surveying of the top of the access tube the total movements were calculated from the relative displacements measured.

As well as surveying errors described in section 3.1.2.4 associated with leveling the top of the access tube, errors arose from variability with the reed switch in locating the magnetic fields between readings. Cording et al. (1975) quoted an error magnitude of $\pm 0.1\text{mm}$ for this. A larger error resulted from the variability associated with the use of the measuring tape. Burland et al.(1972) reported additional errors of $\pm 1\text{-}2\text{mm}$ due to this variability. In this project estimated repeatabilities of $\pm 1\text{mm}$ were achieved.

3.1.2.3 Benchmark Installation

The highest levelling accuracies can be achieved by selection of a short circuit between benchmark, instruments and benchmark. Expected error magnitudes have been related to surveying distance by the relationship

$$\text{Error} = \pm 0.0003 N^{1/2} \text{ m} \quad (\text{Mendes et al., 1970})$$

where N is the number of instrument set ups.

It is therefore of paramount importance that the benchmarks are located as close as possible to the test area but also far enough away such that they are unaffected by construction activities

To comply with these requirements four benchmarks('bm') as shown in Figure 3.1, were installed. These benchmarks consisted of a continuous length of 50mm steel pipe, fitted with a surveying point. Installation involved firmly anchoring the assembly at the bottom of a borehole and isolating it from soil downdrag forces by means of a 75mm P.V.C. pipe. Benchmarks Nos. 1, 3 and 4 were anchored at approximately 12.5m below surface while No. 2 was positioned at a depth of 6.5m due to its increased distance from the tunnel axis and the presence of low strength underlying material. Prior to installation of benchmarks 2 and 4 Standard Penetration Tests were performed yielding values of 13 and 22 respectively. The benchmarks were protected from vandalism by special preformed covers.

While field measurements continued, settlement of the benchmarks was monitored. All settlements occurring were within the accuracy limits of the surveying and therefore imperceptible.

3.1.2.4 Surveying Details

All instruments installed to detect vertical soil displacements were surveyed regularly to obtain a continuous record for each point. Readings were taken a minimum of once a day and occasionally twice, although due to inclement weather conditions at the time of surveying some readings had to be discarded.

Good levelling techniques, as outlined by Hanna(1973), which include limiting of sight lengths, balancing of back and foresights, plumbing the staff, clear staff markings and the use of stable turning points were observed. Cording et al. (1975) quoted errors of $\pm 1.5\text{mm}$ on any measured point, obtained using the above precautions.

During excavation of the first test section, between January and March 1983, a slightly sub-standard instrument was used which together with a lengthy survey circuit resulted in errors in excess of $\pm 1.5\text{mm}$. For the second section, however, an instrument with better adjustment was used which coupled with shorter surveying routes reduced the errors to below $\pm 1\text{mm}$. This emphasizes the importance of using good quality surveying equipment in field projects.

3.1.3 Horizontal Displacement Measurements

3.1.3.1 Inclinometers

Inclinometers are the most commonly used instrument for the detection of horizontal movements with depth. They have been employed successfully in monitoring slope instabilities (Wilson, 1967), movements around deep excavations (Burland and Moore, 1974), as well as in detection of horizontal movements around tunnels (Branco, 1981; Palmer and Belshaw, 1979). Hanna (1973) presents a brief overview of available inclinometer types and their working principles. A more detailed description of inclinometer types and a thorough investigation of instrument errors was given by Savigny (1980).

In this project two inclinometers were installed on the assumed tunnel centre line (shown in Figure 3.1 as 'SI'), and anchored at approximately 22m below surface. This depth was chosen with consideration of information contained in Cording et al. (1975) where it is recommended that inclinometers be anchored at least 5m below the expected zone of movement. For this project the expected zone of movement coincided with the tunnel invert, 15m below ground surface. Standard installation procedures were adhered to with both inclinometers being grouted with a 4:1 mix by volume of bentonite and cement. During installation of Inclinometer 2 a stronger more viscous grout was arbitrarily used in a successful attempt to stop excessive losses incurred when the

original mix was placed in the borehole. This necessary addition resulted in an excessively strong grout which subsequently affected the performance of the inclinometer. Inclinometer casings were manufactured by Sinco Inc., Seattle, Washington.

A Sinco Digitilt Inclinometer model 50306, was used as the sensing element. It consists of two servo accelerometer sensing elements mounted at 90 degrees to each other and housed in a 927mm long probe. The torpedo like sensor has an upper and lower wheel assembly each consisting of one fixed and one spring loaded wheel. The gauge length or wheel spacing is 610mm. This unit is connected to the readout device by a 9.5mm neoprene coated six strand cable. The depth is measured by coloured neoprene markers vulcanized to the cable at 305mm(one foot) intervals. The readout device is a digital voltmeter that indicates voltage on a four digit display. Complete specifications of the inclinometer system (Savigny, 1980) are given in Table 3.1 . The accuracy of the complete system allowing for cumulative errors in the sensor, digital readout and casing, provided care is taken to ensure readings are taken at the same depth every time, should not exceed $\pm 5\text{mm}$ at the top of a 30.5m casing(Digitilt Instruction Manual). In this project, using standard inclinometer data recording techniques, as outlined in the Digitilt Instruction Manual, error magnitudes were estimated for the level of

Table 3.1 Details of the Inclinator System

SENSOR: Slope Indicator Company Model 50320

Sensitivity:	± 0.0015 m per 30 m casing
Total System Accuracy:	± 0.0076 m per 30 m casing
Wheel Base:	61 cm
Overall Length:	93 cm
Outside Diameter (not including wheels):	4.3 cm
Sensors:	Two 0.5 g closed loop force-balanced servo accelerometers
Operating Range:	0° to 30° (from vertical)

CABLE: Slope Indicator Company 1.07 cm O.D., six conductor with 0.16 cm stranded-steel core; waterproof neoprene cover with external marks at 0.31 m intervals.

INDICATOR: Slope Indicator Company Model 50306

Dimensions:	14.3 x 6.0 x 22.9 cm
Weight:	2.27 kg
Internal Power:	6V, 6 Ah
Charger:	External; 6 VDC
Operating Time on Batteries:	8 hours
Digital Display:	4 digits
Recording:	Manual

CASING: Slope Indicator Company ABS Plastic Casing & Couplings

Casing Length:	3.05 m
O.D.:	7.0 cm
I.D.:	5.9 cm
Coupling Length:	0.15 m
O.D.:	7.0 cm
I.D.:	6.5 cm

the tunnel axis to be $\pm 1\text{mm}$ for inclinometer's 1 and 2. Errors of $\pm 2\text{mm}$ were estimated for the ground surface.

The frequency of readings taken prior to excavation of the slope indicators were subject to tunnel advance rates. Also a time delay existed between taking a set of readings, entering the tunnel to record face position and returning to the surface to take another set of readings. The object was to obtain a good record of face position and inclinometer movement. As is shown in Chapter 4 a better record was obtained for Inclinometer 2 because poorer ground conditions at this location resulted in slower advance of the tunnel face. It should be noted that although it was attempted to have the Inclinometers on the tunnel centre line, location difficulties on the surface together with alignment deviancies of the mole, resulted in Inclinometer 1 being located close to the edge of the tunnel while Inclinometer 2 remained very close to the final centre line.

Data from the inclinometers was reduced using standard inclinometer equations as set out in the Digitilt Instruction Manual. The related computer program incorporating these equations, formulated by Savigny (1980), was used to reduce the data.

3.2 Tunnel Support Loads

3.2.1 Lagging Load Measurement

To obtain lagging loads the magnitude and distribution of the pressure acting on the lagging must be obtained. Integration of this pressure distribution can be used to give the total load. Alternatively, by application of the integrated measuring technique (Kovari et al., 1977) it is theoretically possible to determine the lagging pressure and load from lagging deflection measurements. However, to obtain pressure and pressure distribution, a large number of measurements per lagging would be required and this is not practically feasible. It was thus decided, to apply this concept but in a simpler form by measuring only one deflection point and assuming a uniform, 'equivalent' pressure distribution. Under these assumptions it is possible to relate distributed load directly to the lagging deflections using simple statics principles as presented in Appendix A 1. This alternative requires knowledge of the stiffness properties of the lagging in terms of its magnitude and variability with time.

Pressure distribution could be obtained using pressure cells inserted between lagging and soil but this is an expensive solution which only yields point measurements. For measuring lagging deflections a variety of systems, of varying sophistication, embracing either strain measurement (Branco, 1981) or deflection measurement (Kovari et al., 1977)

are available.

Both of the above techniques are expensive and only economically feasible for monitoring a few cross sections and then, only if point records are adequate. To obtain inexpensive results along large portions of the tunnel it was necessary to develop a reusable instrument. In addition, it was one of the aims of the project, to develop and calibrate a system for ongoing safety monitoring of future tunnels constructed using the same support techniques.

With all the aforementioned constraints it was decided that single point deflection measurements on lagging boards could be measured relatively cheaply. This could result in a simple, practical monitoring system for the City of Edmonton, allowing it to evaluate the degree of risk (Factor of Safety) and to optimise tunnel construction by comparison of allowable with actual deflection measurements.

For this objective a methodology was developed to measure deflections with sufficient accuracy, and this resulted in the design and construction of the first "University of Alberta Deflectometer".

3.2.1.1 University of Alberta Deflectometer

The deflectometer was designed such that deflections between two measuring points placed near the ends of the lagging boards and a central reference point could be measured. The instrument was designed to incorporate a degree of robustness plus adequate stiffness to ensure that measurement would not be

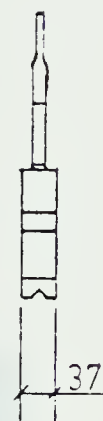
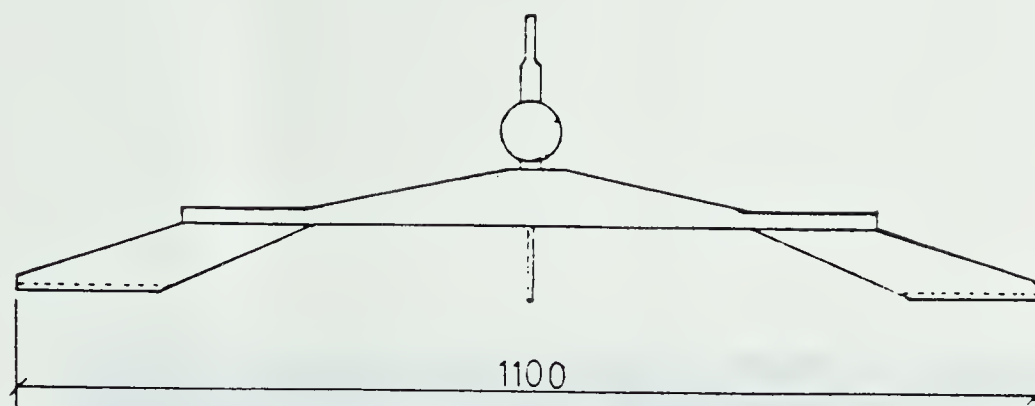
affected by self weight or operator induced forces. With reference to a system used by Kovari et al. (1977) the instrument shown in Figure 3.4 and Plate 3.1 was conceived and built by the Civil Engineering Workshop at the University of Alberta. As the project continued minor modifications were made to the instrument mainly concerning protection of the dial gauge.

The measurement technique involved holding the deflectometer at its extremities to prevent operator bending. This is shown diagrammatically in Figure 3.4. Using this technique one reading took only seconds to perform. However, the instrument proved to be too heavy for continual field use as after a few readings arm fatigue set in. A better design would have included a lighter, but stiffer framework system which would have resulted in less discomfort for the operator. Also, the dial gauge could have been better protected by enclosing it within the frame.

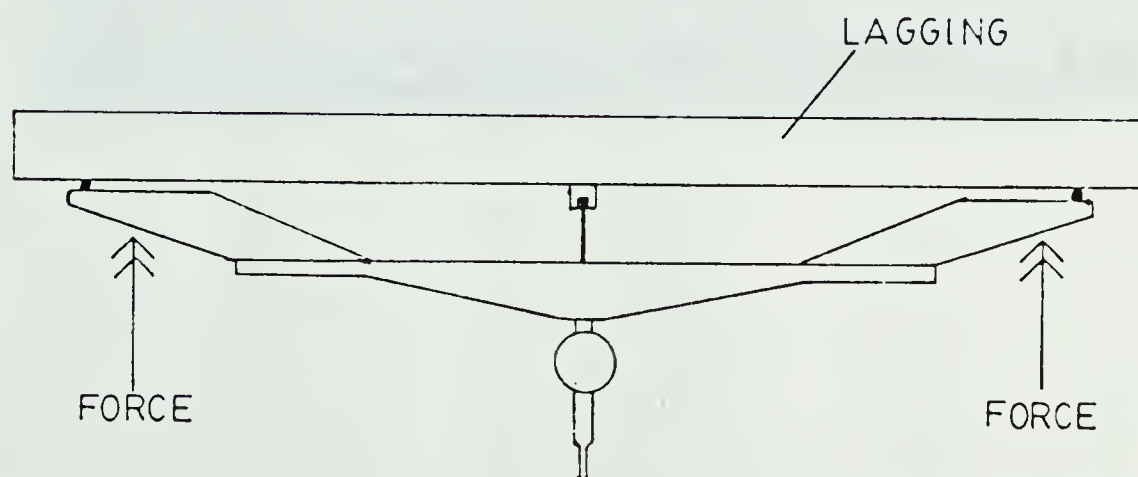
The accuracy of the instrument was user dependent and not close to the sensitivity of the dial gauge (0.1mm graduated, 0.01mm by interpolation). With experience it was possible to reduce the effect of operator influence resulting in repeatable readings with errors close to $\pm 0.2\text{mm}$. Random larger errors did however occur.

Data collection was continuous, resulting in good records of load development with face position and time being obtained in the formal Test Sections. Recorded

200mm



a) SECTION



b) MEASUREMENT

Figure 3.4 University of Alberta Deflectometer



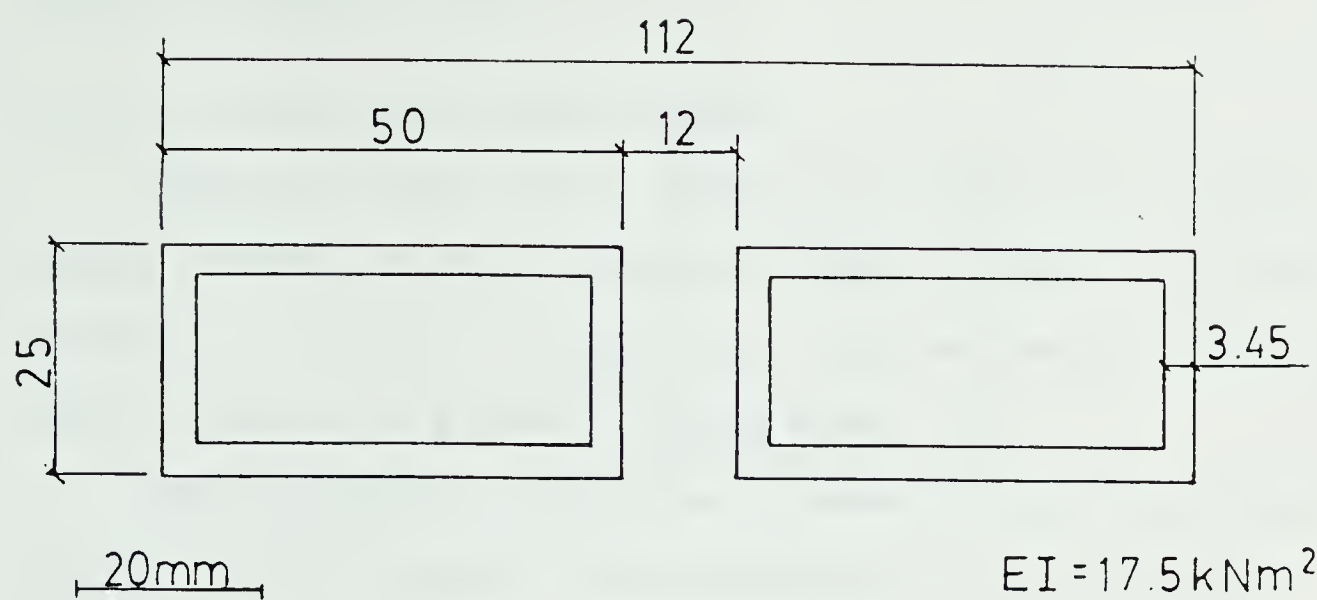
Plate 3.1 University of Alberta Deflectometer

measurements were reduced into equivalent pressures using the computer formulation of equations presented in Appendix A. During installation of instrumented laggings, spacers were placed between boards to prevent development of complicating hoop stresses. At the location of Test Sections 3 and 4, however, this was not possible as it would have led to large losses of ground through the spaces.

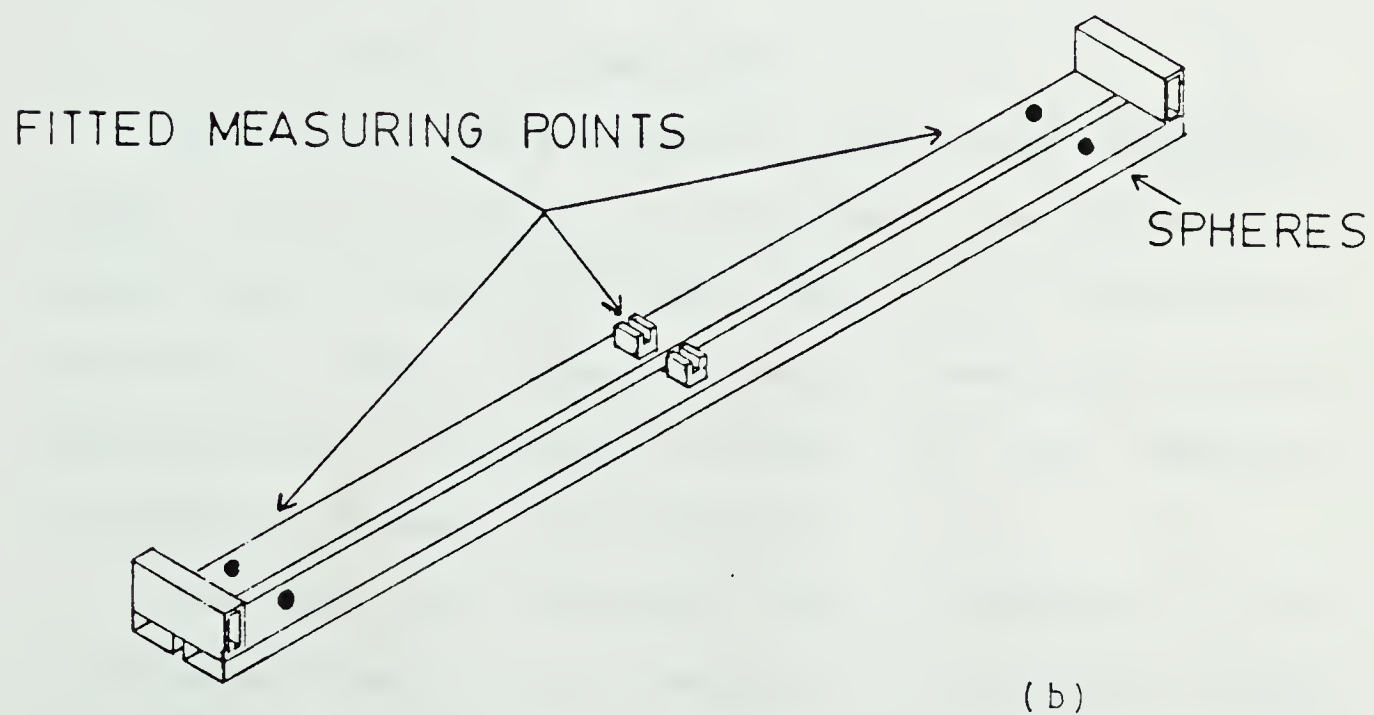
3.2.1.2 Simulated Steel Laggings

Because steel is a much more predictable and consistent material than wood it was decided to produce simulated steel laggings which could be used to validate loads obtained from the wood laggings. To avoid complications involving stiffness variations it was necessary to design a steel cross-section with a similar flexural rigidity (EI) to that of the wood laggings. Designing for a wood lagging 50mm thick and 100mm wide we obtained a rigidity of 10.42kNm^2 by assuming a Young's Modulus (E) for wood of 8GPa (Branco, 1981). Using this information the steel cross-section shown in Figure 3.5a having a slightly higher EI value of 17.5kNm^2 was chosen. Laboratory calibration tests later showed average values of 16.74kNm^2 for the steel laggings and 14.0kNm^2 for the wood laggings.

Before calibration and installation of the steel laggings central reference points and steel balls were fitted to accommodate deflectometer measurements as



(a)



(b)

Figure 3.5 Simulated Steel Lagging

shown in Figure 3.5b.

3.2.1.3 Calibrated Wood Laggings

Typical construction laggings as used on a regular basis during tunnel advance were fitted with three deflection points to comply with deflectometer design. This is shown in Figure 3.6 and Plate 3.2.

The deflection points were screwed into the timbers prior to calibration. Two separate lots of timbers, one being on average 50mm thick and the other being 80mm were calibrated. An increase in lagging thickness proved necessary as a result of the larger loads experienced at the location of the second two test sections (Test Sections 3 and 4).

3.2.1.4 Calibration of Laggings

Calibration was achieved by placing two equal point loads on the lagging at 152.5mm on each side of the centre while simulating simple supports at the ends. The deflection under increasing load was measured using the deflectometer. A diagrammatic sketch of the laboratory arrangement is shown in Figure 3.7.

Initially the laggings were calibrated using incremental loads up to a maximum total value of 2.532kN for P (Figure 3.7). These incremental loads resulted in linearity of deflections as shown in Figure 3.8 and hence, for reasons of time economy the loads were later applied in one increment.

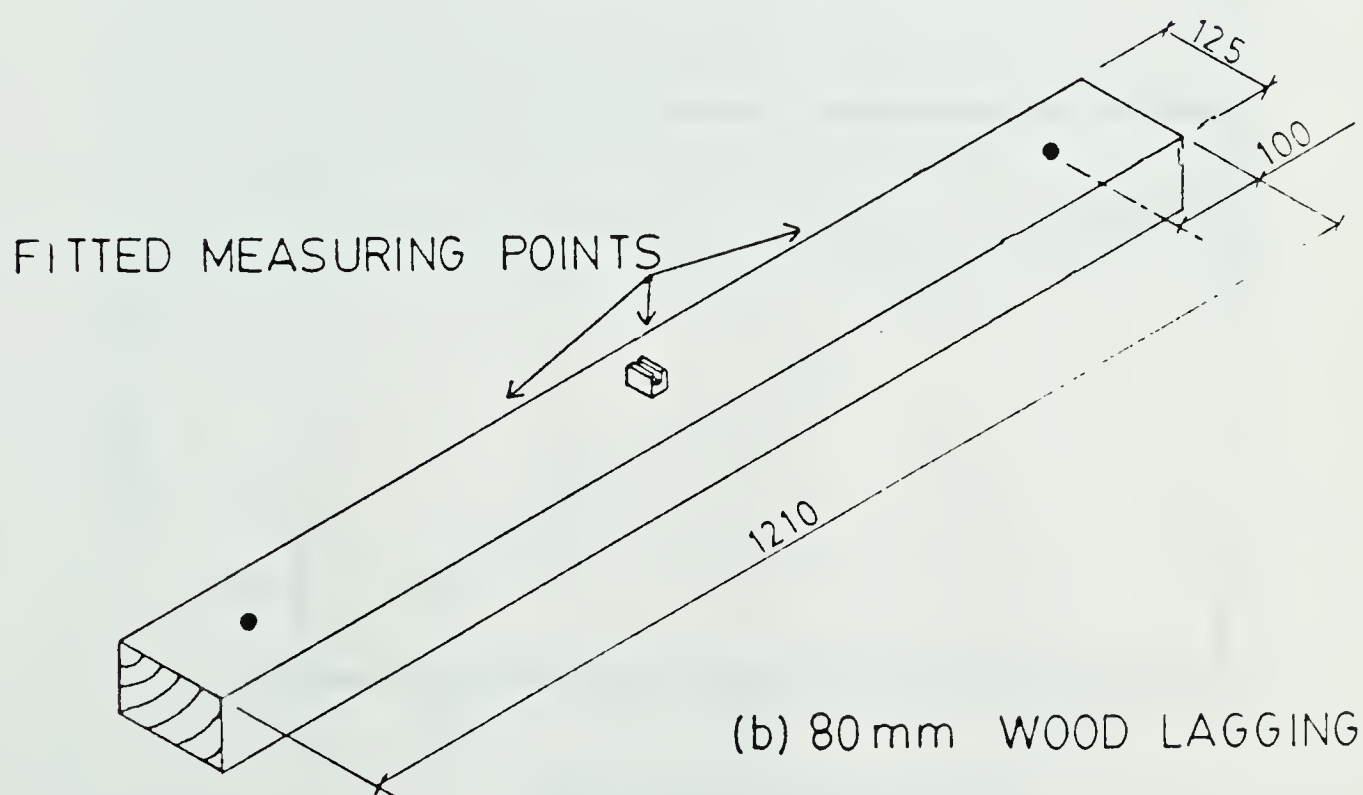
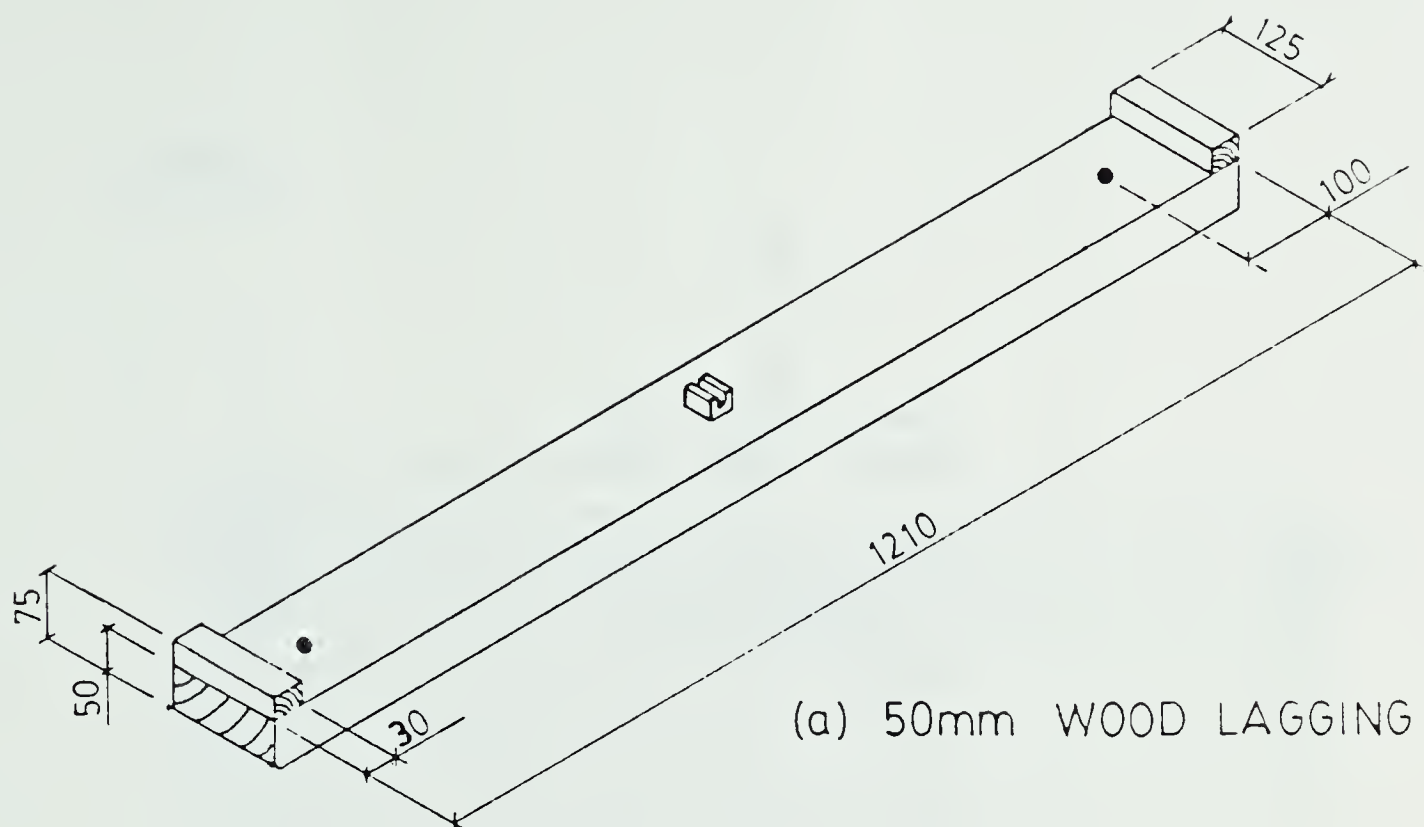


Figure 3.6 Wood Lagging Details

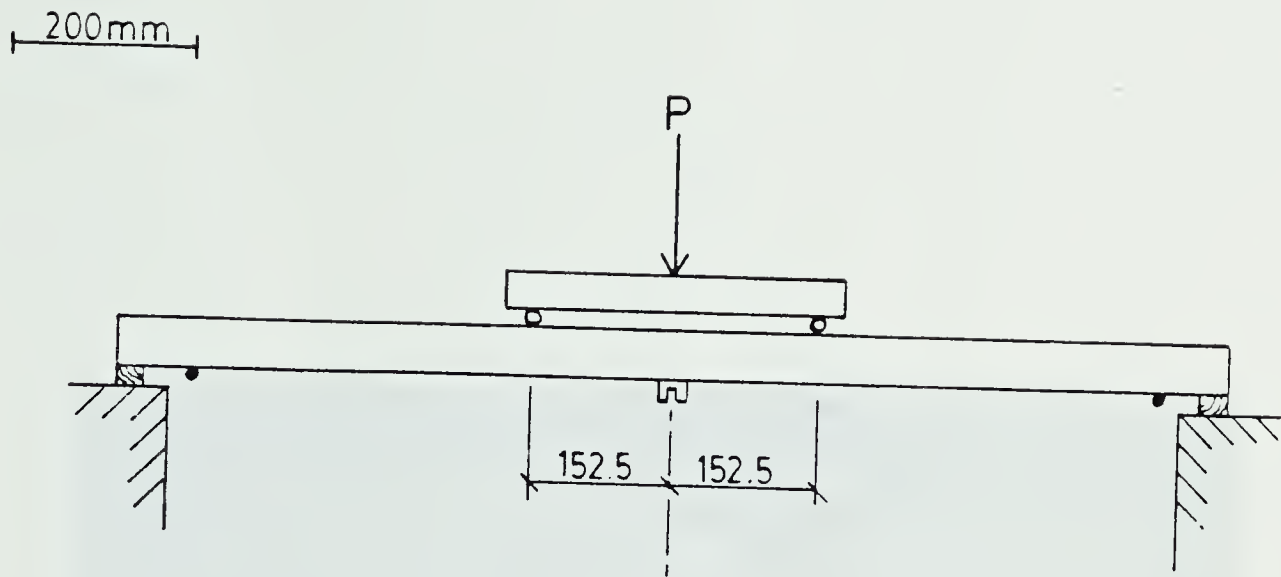


Figure 3.7 Laboratory Arrangement for Calibrated Laggings

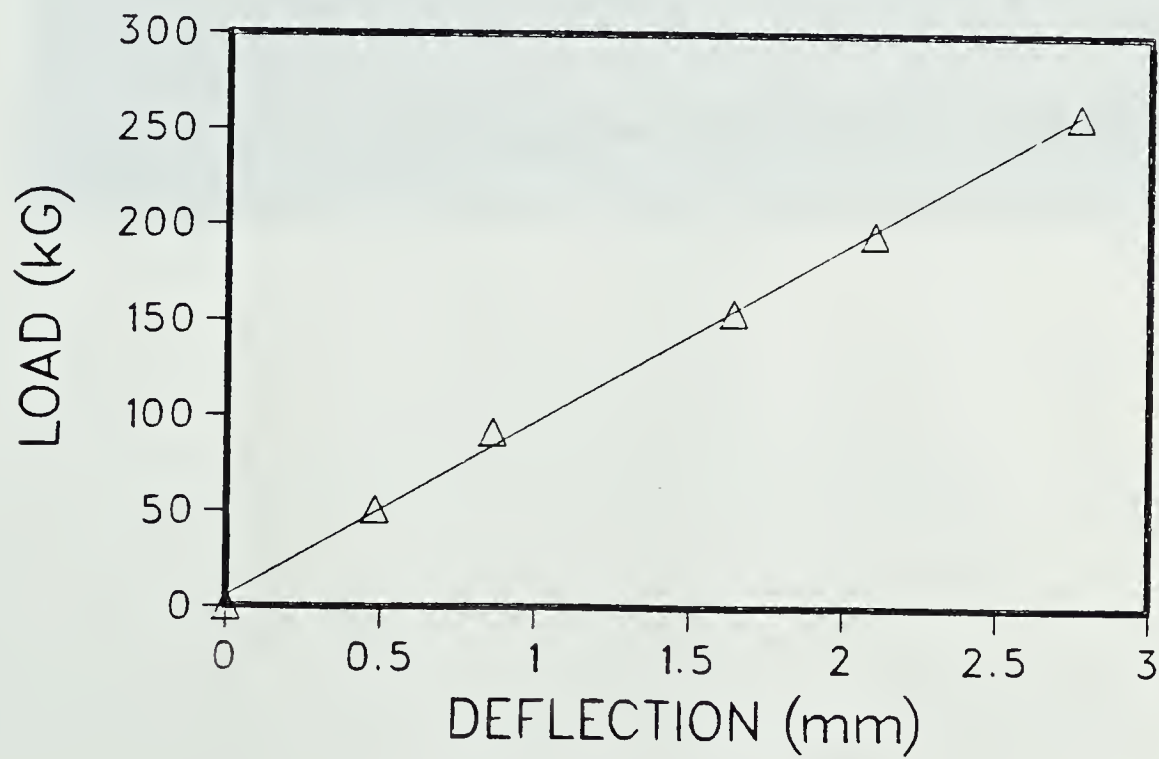


Figure 3.8 Typical Load-Deflection Record for a Wood Lagging

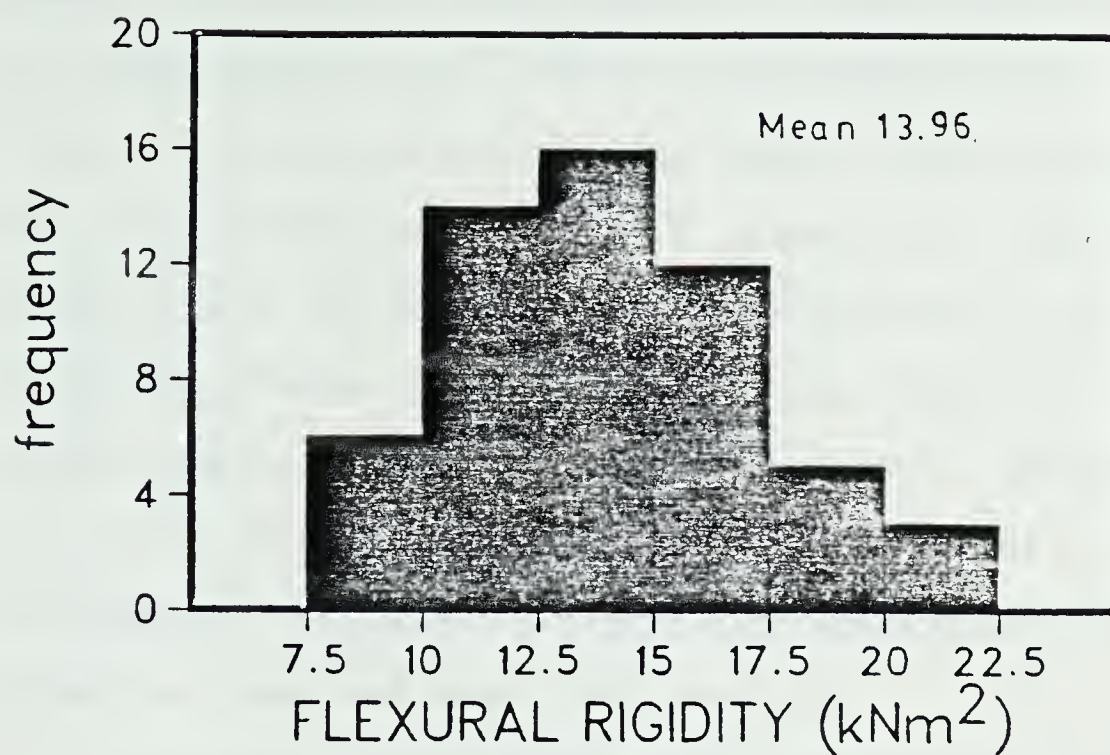


Plate 3.2 Calibrated Wood Lagging

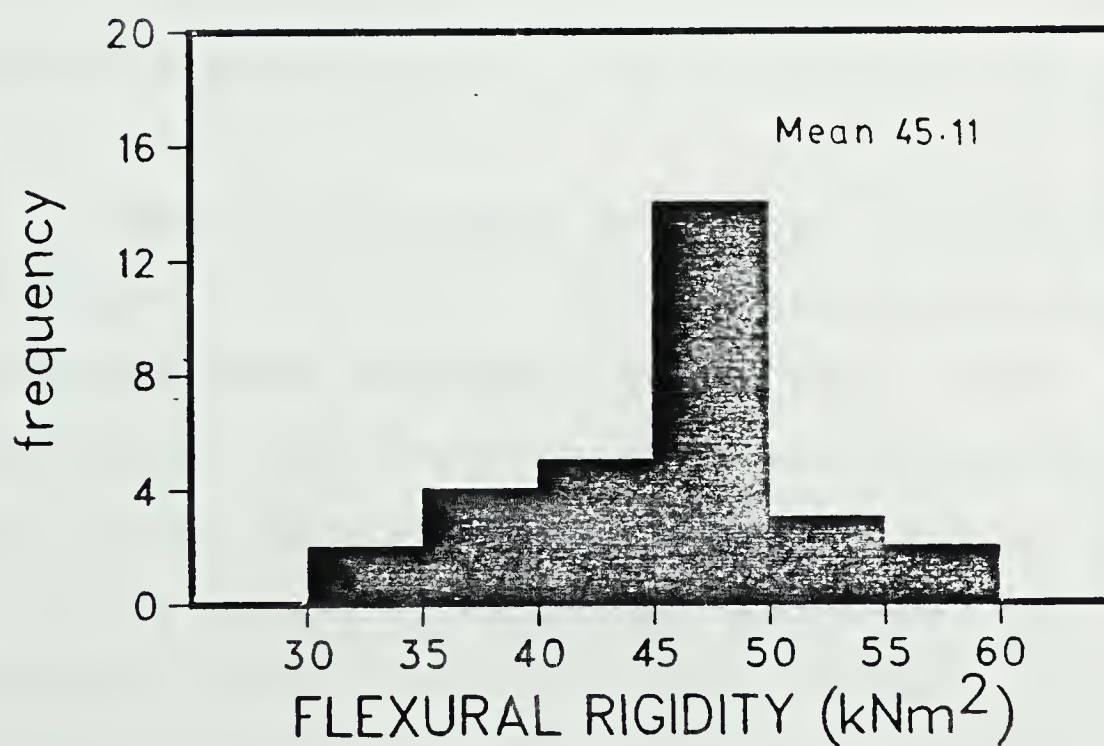
Before a flexural rigidity for a given lagging can be calculated from the measured deflection it is necessary to predict the deflected shape of the board for the given load configuration'. The methodology for this is set out in Benham (1965) or any other elementary mechanics of solids book. Full details of the calculations are contained in Appendix B where final equations can also be found. Once the deflected shape has been calculated, rigidity values can be directly related to the measured deflection. However, due to the fact that the measuring end points were not placed exactly at the end of the beam a correction factor must be applied to the measured deflection. This correction factor is necessary because only the relative deflection between end points and centre point was measured. Analysis without this factor would result in overestimation on the flexural rigidity. Full details on calculation of this factor are given in Appendix B.

It was thus found, after correction, that the average flexural rigidity of the 50mm thick boards was 13.96kNm² with a standard deviation of 3.35 kNm² determined from 56 measurements. Using thirty 80mm thick boards an average value of 45.11kNm² with standard deviation of 6.45kNm² was found. Full distributions of both sets are given in Figure 3.9. These rigidities are

 'The deflection measured is a relative deflection between the two end measuring points and the central reference point.



a) 50mm LAGGING



b) 80mm LAGGING

Figure 3.9 Distribution of Wood Laggings Flexural Rigidities

based on typical displacements of approximately 3mm for the 50mm boards and 1.3mm for the 80mm boards. Although these are quite small deflections a report prepared for the City of Edmonton (City of Edmonton, 1983b) showed linearity of deflection load measurements up to 15mm for the 80mm boards. This is also thought applicable for the 50mm boards. Observed linearity over this range, of which our deflection measurements form a part, increases confidence in the accuracy of calculated rigidities based on measured small deflections.

Eighteen simulated steel laggings yielding an average value of 16.74 kNm^2 with a standard deviation of 0.25 kNm^2 are shown in Figure 3.10.

Moisture Effects

Timber stiffnesses are known to be dependent on moisture content, i.e., with increasing moisture content the stiffness decreases to a lower limit at total saturation, referred to as the "fibre saturation point". The fibre saturation point of most woods is around 30% moisture content by weight. A report by the City of Edmonton(1983a) showed that timber stockpiles on surface prior to being installed had average moisture contents of 24% (80mm boards). Information from the same report showed tunnel average moisture contents of 27.1% in known "dry" conditions and 31.2% in known "wet"

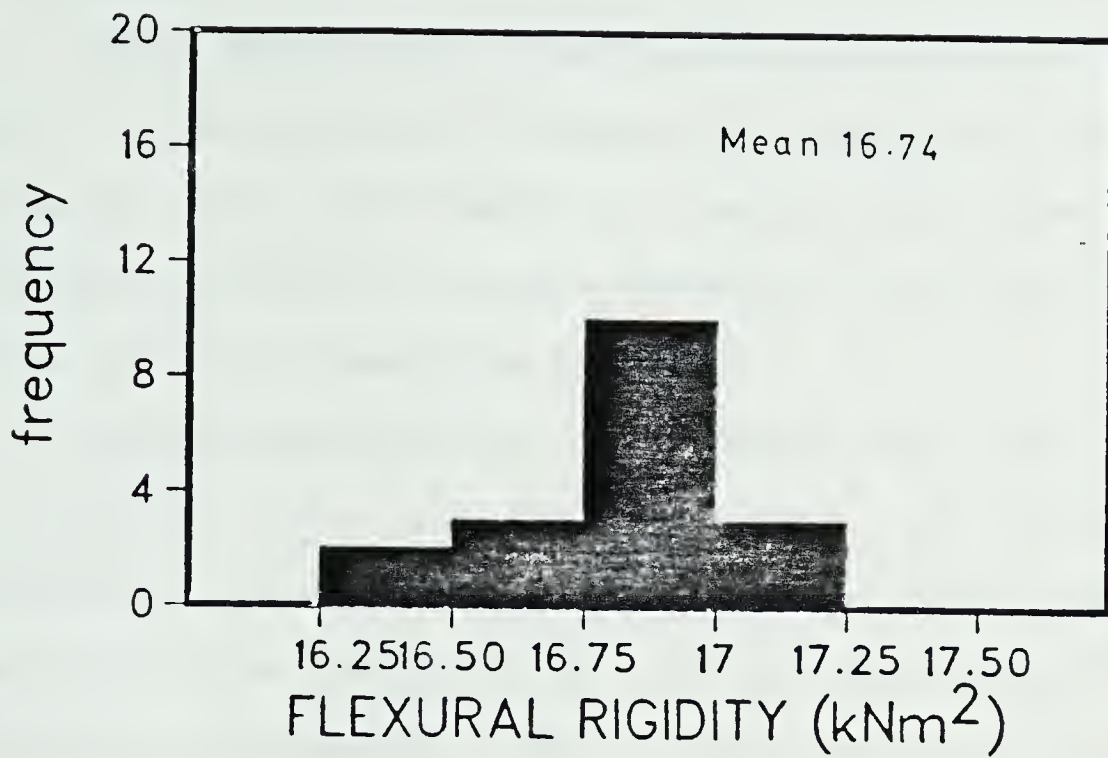


Figure 3.10 Distribution of Steel Lagging Flexural Rigidities

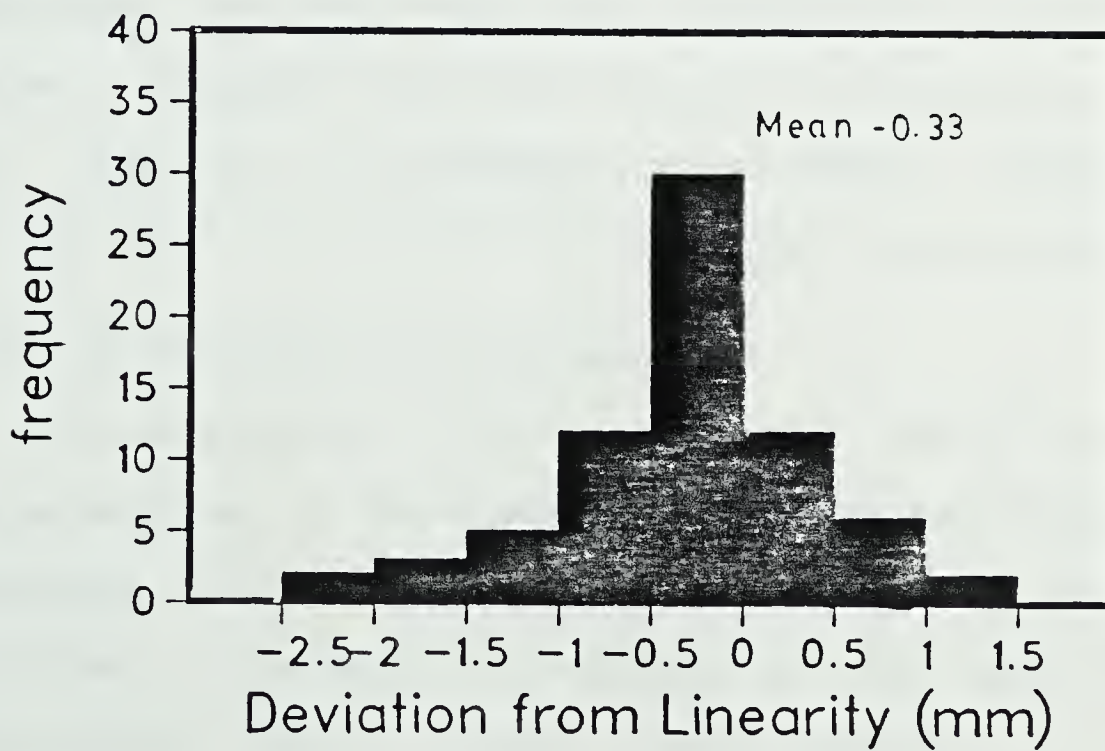


Figure 3.11 Measured Distribution of Zero Deflection

conditions .

Tests performed on boards during calibration showed very little stiffness change after spending 4 days in a moisture room (100% humidity). Tests on the same boards however showed an average decrease in stiffness of 7.7% after 72 hours immersion in water.

No moisture content measurements were performed on the boards prior to field use but the field data indicates boards to be close to the fibre saturation point prior to installation, intimating little stiffness variation thereafter. The 7.7% reduction of stiffness found in the laboratory upon saturation, if representative of all calibrated boards, is thought to be partially self-compensated by an increase in stiffness brought about by unmeasured hoop stresses between laggings. For these reasons and because of lack of time to investigate this aspect properly no corrections for stiffness losses have been included.

3.2.1.5 Uncalibrated Laggings

In an attempt to monitor the load variation along large sections of the tunnel, deflection measurements on laggings installed without any additives, hereafter referred to as uncalibrated laggings, were measured. To facilitate this, slight modifications to the deflectometer proved necessary, such that the measuring points were fitted to the instrument rather than to the laggings. These modifications took the form of two

removable semi-hemispheres fitted equidistant from the dial gauge and a flat disc shaped tip for the dial gauge point. The increased areas of all measuring points was intended to mask the effects of local timber roughnesses. A flat headed nail was also fitted to the midpoint of the board to give a more repeatable central measuring point. Centre nails were used for boards contained in the first two ribs of Test Section 3. During nail installation, zero deflection readings were taken on the boards such that deflections directly attributable to load could be ascertained.

Deflection similarity measurements, between the modified deflectometer and those taken with the standard technique were performed yielding the results shown below.

Board #	Deflectometer Readings (mm)		
	Unaltered	Modified	Difference
1	2.91	3.16	0.25
2	3.52	3.71	0.19
3	3.40	3.58	0.18
4	5.19	5.18	-0.01

These results show that similar deflection measurements are obtained by both methods (less than ± 0.15 mm expected error).

For boards installed without any pretreatment, it was necessary to know the magnitude of zero deflections. For this purpose readings were taken on 72 unloaded laggings. This yielded a mean deviation from linearity of -0.33mm with a standard deviation of 0.7mm and a distribution as shown in Figure 3.11. From these results an average deviation from linearity of zero was assumed for all uncalibrated untreated laggings.

3.2.2 Steel Set Load Measurement

In a Steel and Wood lagging lining system it is important to know what percentage of loads in the steel sets are directly attributable to lagging pressures. In the preceding sections the various techniques used in this project for determination of lagging pressures have been expanded. However, to obtain the aforementioned relationship between lagging and steel set loads we must now determine active loads in the steel sets for comparison with those measured in the lagging. To obtain full details of steel set load, the magnitude and distribution of bending moment, shear force and axial thrust around the steel set is required. Kovari et al. (1977) proposed a load cell from which all of the above could be ascertained which was thus chosen for use in this project. Due to difficulties arising from the cell being too short (product of steel set ring fabrication) it proved impossible to use the cell to its full potential. It was possible however, to obtain axial

thrust from the load cells which unfortunately results in an increased need for assumptions regarding load distribution around the steel set. Assumptions regarding load distribution will be presented in Chapter 5 .

3.2.2.1 Load Cells

Details concerning the design and calibration of the load cells are given in Appendix C. A total of 16 load cells were manufactured with cross section details as shown in Figure 3.12. The reduction of cross section for Load Cells 9 to 16 proved necessary because load build up calculated from the first 8 load cells, installed in Test Sections 1 and 2 proved to be less than 10% of design load. The original cross section was therefore halved in area to increase the sensitivity of the remaining load cells .

From the cross sections shown in Figure 3.12 it can be seen that each cell consists of an upper small cell and a lower large cell. As a function of the original design criterion, calibration tests with applied inclined loads were performed on five load cells. These inclined load tests were thus used to compare predicted axial loads, from the two portions of each cell, with those actually applied. The results from this are presented in Table 3.2.

For Load Cells 5 through 8 it can be seen that the smaller cell consistently gives predictions closer to the actual value. Based on this information it was

Table 3.2 Axial Load Predictions from Load Cell Calibration Tests

LOAD CELL #	APPLIED LOAD (kN)	LOAD CELL AXIAL LOAD (kN)		
		Smallcell	Largecell	Average
5	0.0	0.0	0.0	0.0
	30.0	27.9	18.7	23.3
	60.0	58.2	41.3	49.7
	90.0	88.2	65.0	76.6
	120.0	118.5	91.5	105.0
	150.0	144.3	120.4	132.3
	180.0	176.1	147.4	161.7
6	0.0	0.0	0.0	0.0
	30.0	27.7	31.3	29.5
	60.0	60.6	55.8	58.2
	90.0	88.4	80.3	84.3
	120.0	117.8	107.6	112.6
	150.0	146.0	134.6	140.2
	180.0	176.2	161.2	168.7
7	0.0	0.0	0.0	0.0
	30.0	28.0	26.7	27.4
	60.0	55.6	54.5	55.1
	90.0	83.3	79.6	81.4
	120.0	110.9	106.5	108.7
	150.0	138.9	132.7	135.8
	180.0	176.6	165.8	171.2
8	0.0	0.0	0.0	0.0
	30.0	30.2	28.0	29.1
	60.0	60.5	52.1	56.3
	90.0	91.3	78.1	84.7
	120.0	120.6	103.8	112.2
	150.0	151.8	130.5	141.1
	180.0	183.7	159.6	171.6
9	0.0	0.0	0.0	0.0
	30.0	28.9	29.5	29.2
	60.0	57.4	57.8	57.6
	90.0	86.2	88.8	87.6
	120.0	117.1	118.9	118.1
	150.0	145.6	149.6	147.6
	200.0	195.7	198.9	197.3

DIMENSIONS IN mm

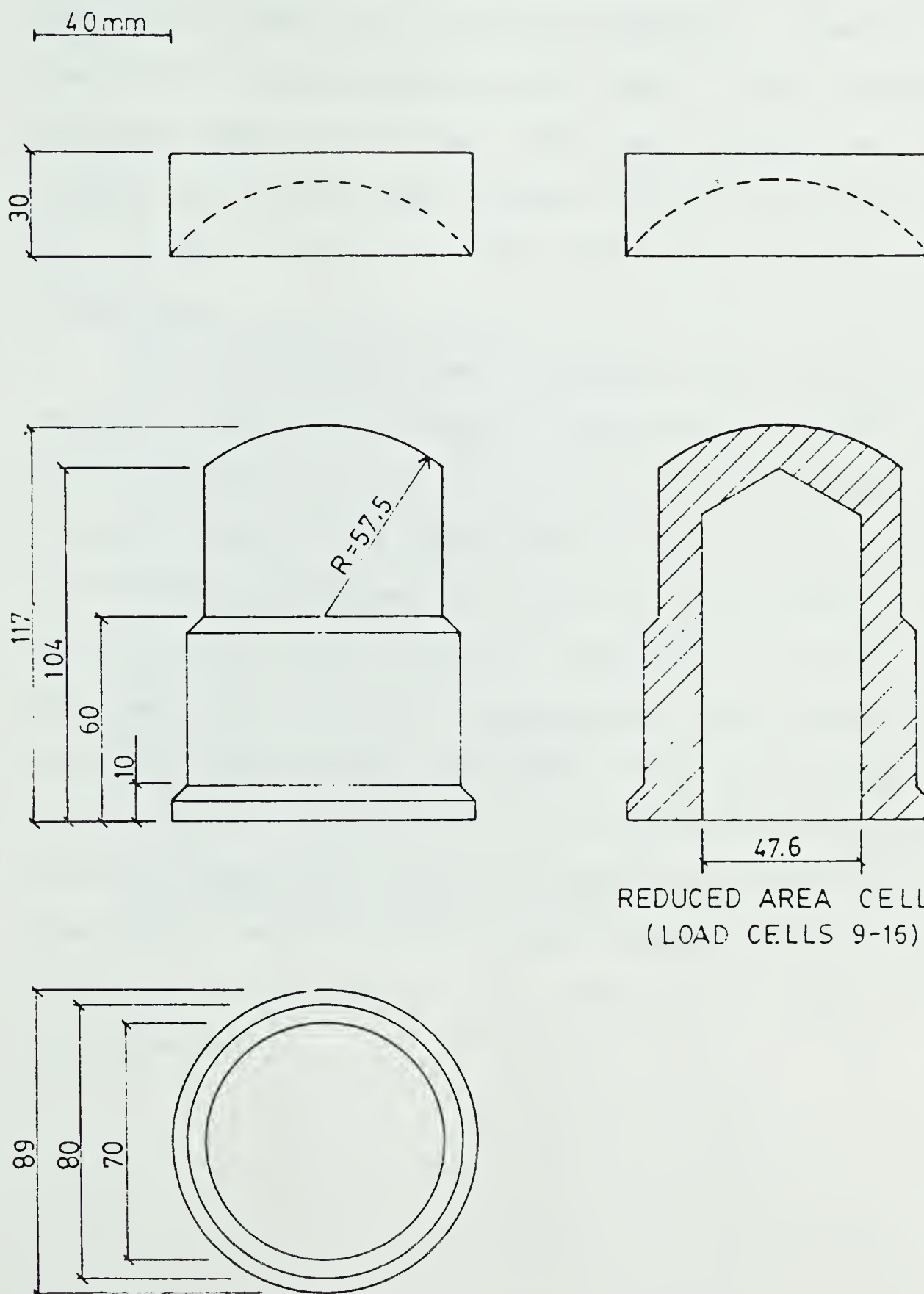


Figure 3.12 Load Cell Cross Section Details

decided to use loads predicted from the small cell portion of Load Cells 1 to 8 in Chapter 5 . Results from Load Cell 9 (reduced area cell) show little variation between upper and lower cell and calculated values compare well with actual values. Hence, for Load Cells 9 to 16 the average of upper and lower portions will be presented.

The load cells were installed when the ribs were expanded as part of the usual tunnelling procedure. They were installed, such that one set of strain gauges faced perpendicular to the tunnel axis. Plate 3.3 shows a load cell immediately after installation. Measurements, using an electronic strain readout, were taken on each gauge of the load cell during measurement. Measurements were taken at varying time intervals such that good load versus face position and time records were obtained. Prior to installation the load cells were given at least one hour to acclimatize to tunnel temperatures with zero readings being taken as close as feasible to installation.



Plate 3.3 Installed Load Cell

4. GROUND DISPLACEMENTS

In the design of a tunnel there are two major concerns:

1. What will be the magnitude and distribution of tunnel induced ground movement?
2. What will be the magnitude and distribution of tunnel lining load ?

The former is the topic of this chapter while the latter will be discussed in detail in Chapter 5.

With ground movements, major concerns involve an estimation of the complete ground displacement field around the tunnel. These estimates include, maximum settlements, maximum distortion gradients and the width of the settlement trough. In rural areas these concerns are only of academic interest but in urban areas, where the vast majority of soft ground tunnels are constructed, accurate knowledge of these variables are essential if dangers to surface buildings are to be fully realized and adequate preventive measures taken.

In conjunction with vertical movements, horizontal movements occur which can also have detrimental effects on surface structures. Measurements of both vertical and horizontal displacements observed during this present project, will be presented in the following sections and their compliance with accepted theories investigated.

4.1 Vertical Displacements

A Total of 26 surface settlement points and 5 multipoint extensometers, installed according to procedures outlined in Chapter 3 and located as shown in Figure 3.1, were used to monitor vertical ground movements over a total plan distance of 500 m.

4.1.1 Surface Displacements

Individual Settlement Point (SP) records for each point are presented in Appendix D while here only trends emerging from the data shall be presented. In this respect, a compilation plot of measured settlement at SP1 to SP24, which shows variations with face position is presented in Figure 4.1. After studying this plot, three regions as indicated on Figure 4.1 emerge:

1. Pre-Construction Region
2. Construction Region (approximately 10 diameters)
3. Post-Construction Region.

Pre-Construction Region

In this region, where movements ahead of the face would occur, it is seen that little movements (+1 to -5mm) have been measured. Downward, and occasionally upward, movements prior to passage of the tunnel face have been quite commonly

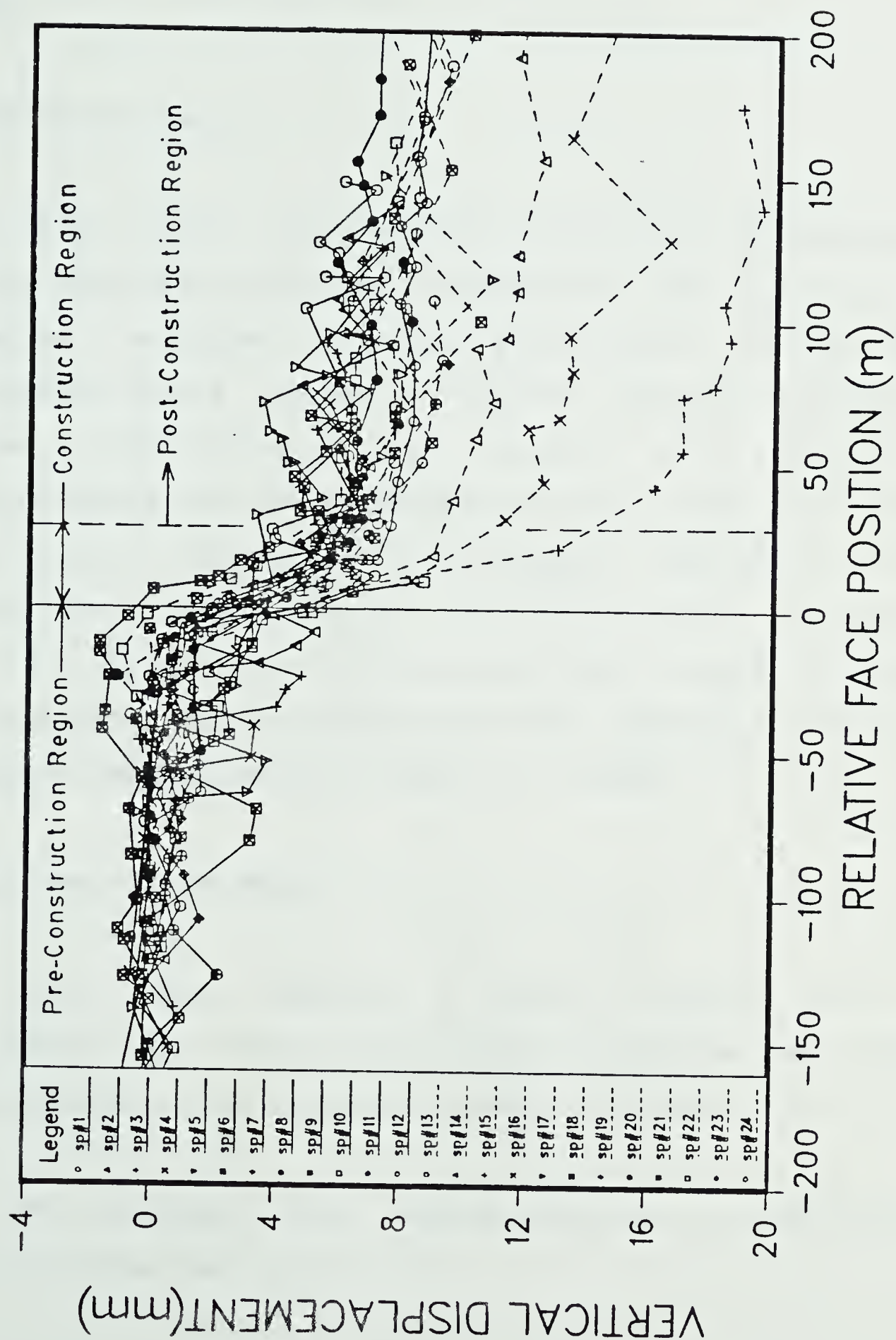


Figure 4.1 Compilation Plot of all Settlement Point Displacements varying with Tunnel Face Position

observed (Branco, 1981; EL-Nahhas, 1980; Palmer and Belshaw, 1980).

Construction Region

This region, which extends approximately 10 diameters (30 m) from the tunnel face, accounts for the majority of observed settlement for any given point. As all the settlement points are at a similar distance above the tunnel, the stress release for each point should be approximately constant which leads to the conclusion that the observed difference in settlement magnitudes are a direct result of construction activities and/or decreasing ground strength and stiffness. From this it may be inferred that observed surface displacements are dependent on more than the commonly used Z/D ratio of a tunnel.

Post-Construction Region

This region exhibits a largely constant rate of settlement which reflects consolidation processes and other time dependent soil responses around the tunnel.

To investigate these regions further, a compilation plot of normalized curves, i.e.,

$$\frac{S_i}{S_{\max}},$$

where S_i = Settlement at a specific data point
 S_{max} = Maximum observed Settlement

was prepared and is presented in Appendix D.

Resulting from these plots, a general trend, as indicated in Figure 4.2, is observed. This figure shows that the same relative displacement occurred in the construction area irrespective of the final displacement value. This point is further emphasized in Figure 4.3 which presents seven normalized curves of settlement points with varying total settlements. This Figure shows approximately 60-70% of all observed settlements in this project occurred within the construction region.

Having discerned that the same relative amount of settlement can be expected in the construction region, it becomes of paramount importance to understand the factors which resulted in the observed settlement differences. Knowledge of these factors and their remedies can then be implemented in future similar works to reduce ground displacements.

In Chapter 2 the length of instrumented section was divided into four areas based on observed geologic and tunnel performance conditions. Figure 4.4, as well as delimiting these areas, has observed average settlements recorded for that area. Using an empirical criterion of increasing severity of tunnelling conditions these four areas (Figure 4.4) would be ranked in the following manner:

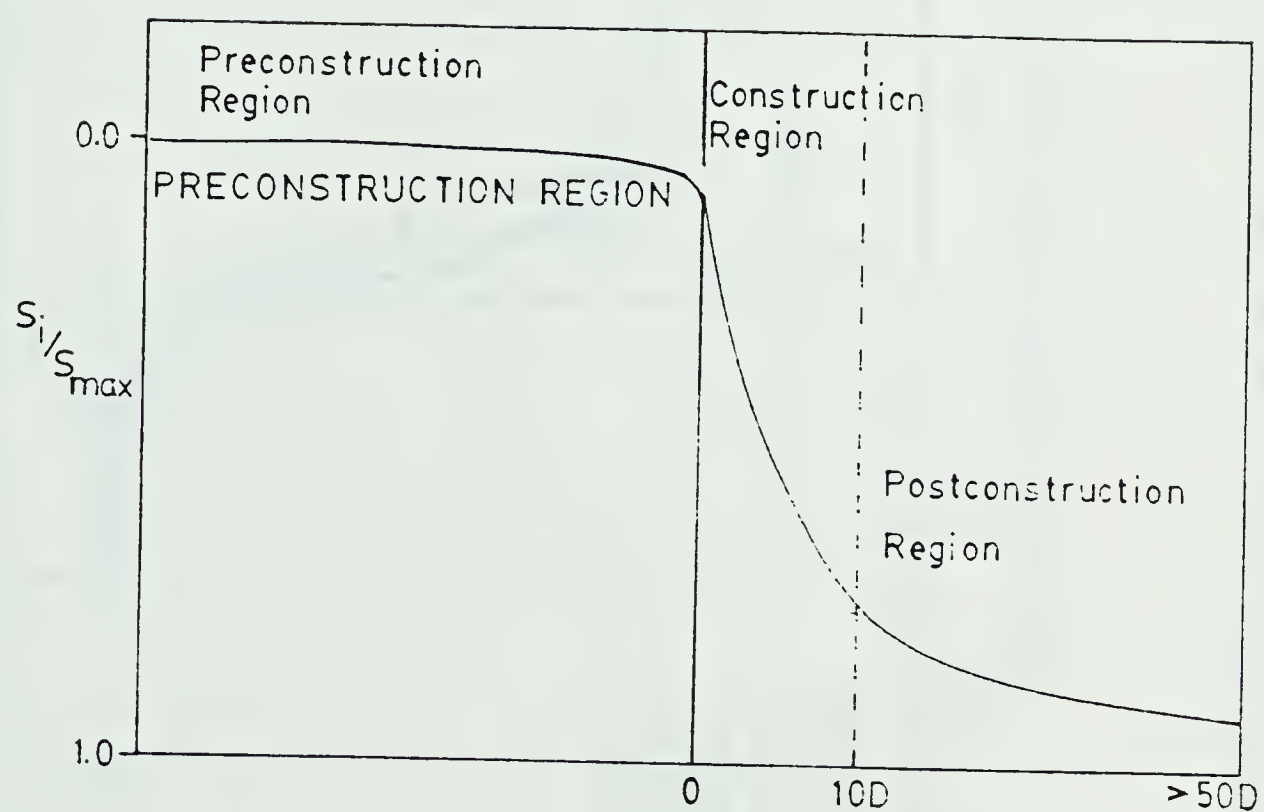


Figure 4.2 Qualitative Distribution of Total Expected Surface Settlement with Tunnel Face Advance

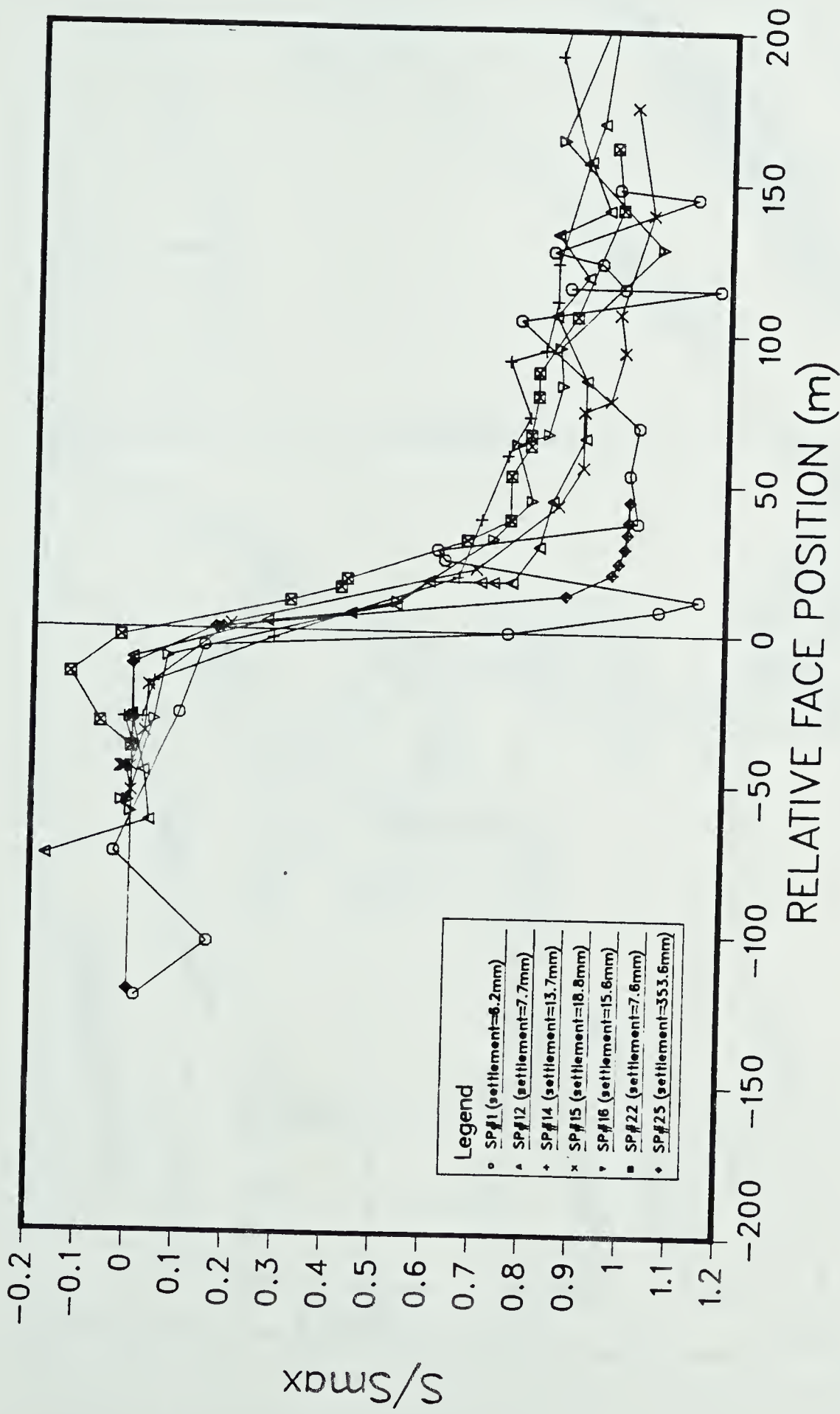


Figure 4.3 Normalized plot of seven Settlement Points with Different Total Settlements

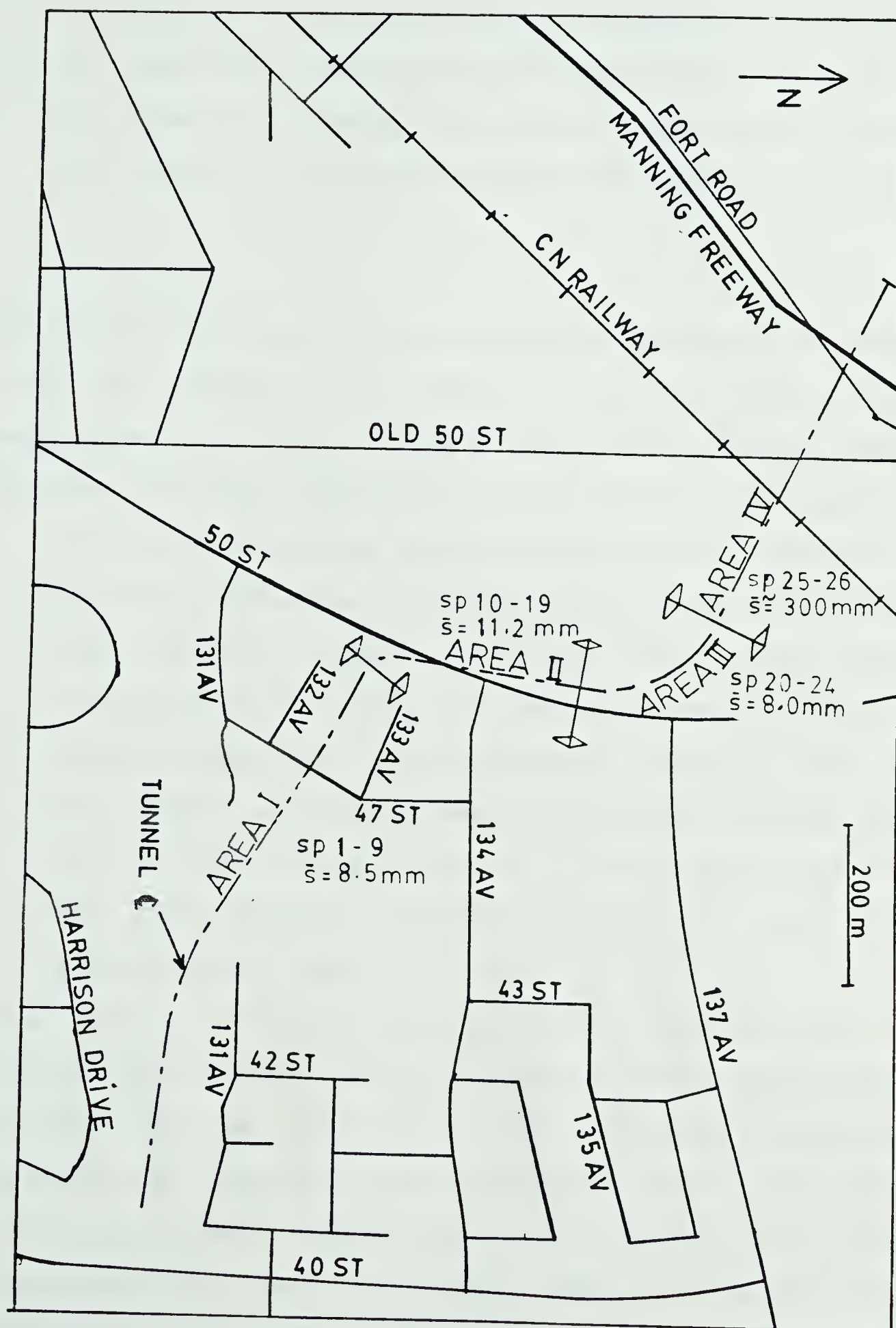


Figure 4.4 Observed Settlements in the Defined Geologic Regions

1. Area I - Average Observed Settlement $s = 8.5\text{mm}$
2. Area III - Average Observed Settlement $s = 8.0\text{mm}$
3. Area II - Average Observed Settlement $s = 11.2\text{mm}$
4. Area IV - Average Observed Settlement $s = 300.0\text{mm}$

These ranks correspond with increasing observed settlements with the exception of area's I and III. This therefore emphasizes that one of the main factors influencing observed surface settlement magnitude, is the ground conditions.

The effects of poor ground conditions are twofold:

1. The ground has less stiffness and strength and therefore less ability to absorb the stress loss brought about by insertion of the stress free boundary (tunnel wall).
2. Ground losses, i.e., the volume of material lost over and above the nominal excavated volume increase due to more difficult ground control. Ground loss at the tunnel has been related to volume of settlement trough at the surface (Peck, 1969).

The former has been investigated in Section 5.3.1 in relation to varying lining pressures with radial inward movement of the soil for differing strength parameters. Briefly, the results show increasing load and slightly increasing crown displacements for deteriorating ground conditions. It can be assumed that increasing crown movements will be manifested in increased surface displacements.

Literature regarding ground losses only reports quantitative values of ground loss for clays (Peck, 1969). Cohesionless ground conditions such as were present in Areas II and IV of this project, together with high water tables are known to lead to large ground losses, often with catastrophic results (Heuer, 1976). The subject of ground losses and expected surface settlements is discussed in Section 4.1.3.

4.1.2 Vertical Displacements with Depth

The vertical displacement profile with depth can be used as an indicator of the extent and magnitude of developed shear strains within the soil mass above the tunnel. In the present project a total of five Multipoint Extensometers (ME's), installed as outlined in Chapter 3 and located as shown in Figure 3.1, were used to detect vertical displacements with depth. Measured displacement records varying with face position and time are given in Appendix E while Figure 4.5 contains the final measured vertical displacement profile for each multipoint extensometer.

The observed records in Appendix E are similar to those of the settlement points in that the majority of the settlement occurred within the construction region. Conclusions cannot be drawn from the movement-time records as they are too short to overcome measurement accuracy. The records of ME 3 and 5 require additional explanation. At ME 3 a construction void approximately 2m in height and equal

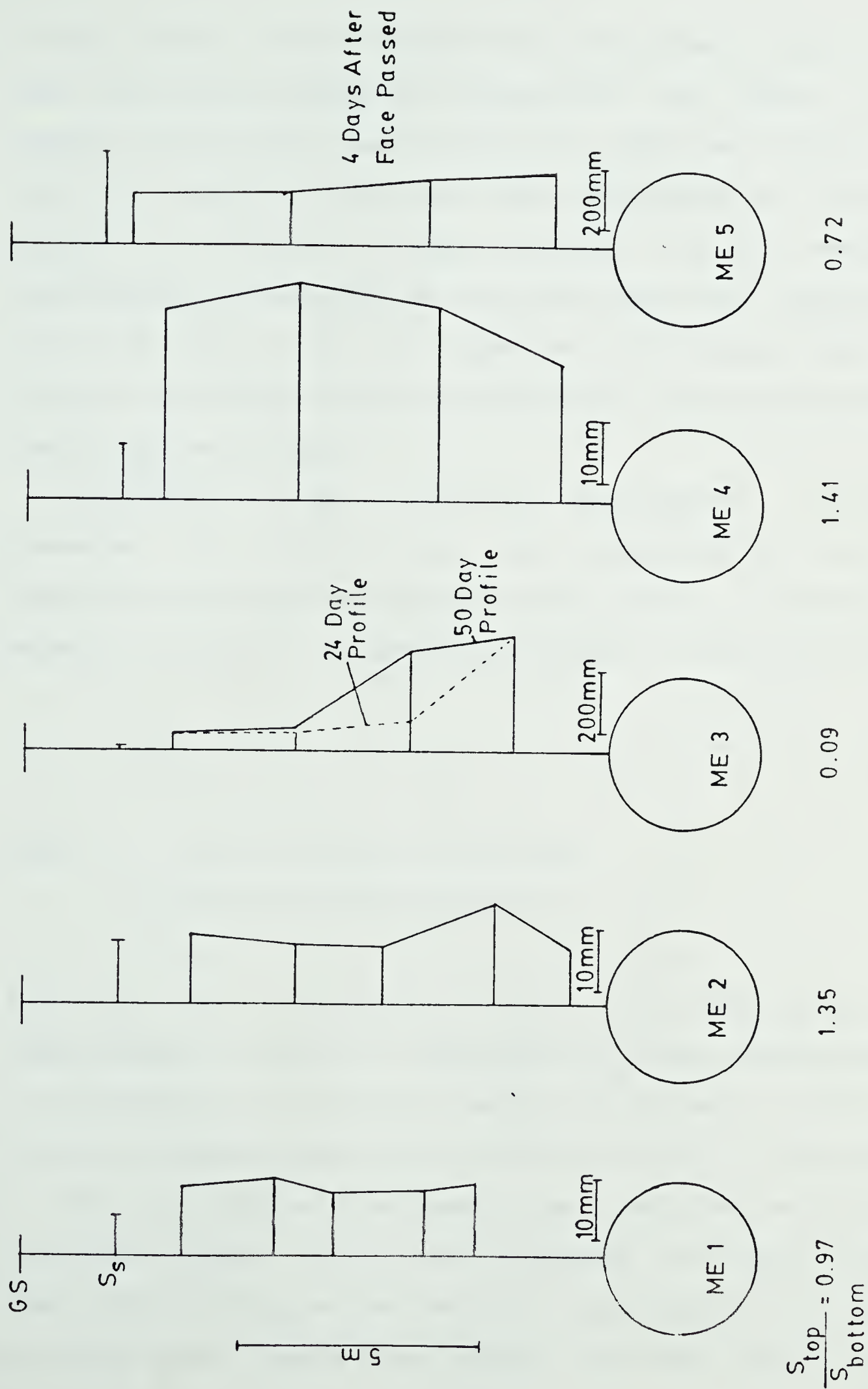


Figure 4.5 Vertical Displacements with Depth as Measured by Multipoint Extensometers

to the tunnel width occurred above the crown. After a few days this void collapsed as evidenced by the sudden large movement of the lower probe (Probe #1). Sometime between the last two readings this void had propagated far enough upwards to induce a large increase in the vertical displacement of Probe #2. ME 5 was destroyed by excavation activities four days after passage of the tunnel face. An attempt was made to find the extensometer sometime later but results proved useless.

Referring to the vertical displacement profiles presented in Figure 4.5, an investigation of the distribution of vertical movements with depth is possible. Relative to this, it is considered prudent to use the ratio:

$$\frac{S_s}{S_c}$$

where S_s = observed surface settlement
 S_c = observed crown settlement.

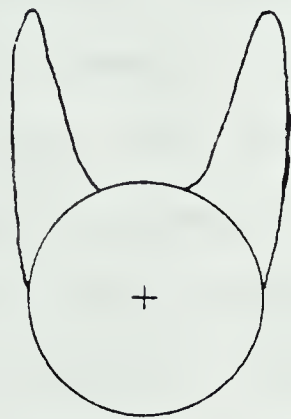
This ratio is a measure of the "degree of uniformity" of displacements. However, measurement of crown displacements is practically very difficult and as can be seen in Figure 3.3 the nearest probe to crown level was still 0.74m above it (ME 4). Surface Settlements as recorded at nearby settlement points have been presented in Figure 4.5 but their applicability to the section in question is in doubt as they were obtained at least 15m away. With these

shortcomings it was decided to calculate S_c/S ratios for each ME based on the ratio of settlement recorded at the upper probe with that of the lowest probe. The results are given in Figure 4.5, and show a range of values of 1.42 (ME 4) to 0.72 (ME 5) if the anomalous value of ME 3 is ignored.

The decreasing vertical movement with depth observed in ME 4 is believed to be a result of placing the probes in a sloughing fine sand. Upon excavation of the tunnel the loose sloughed zone around the original borehole recompressed as a result of downward drainage towards the tunnel.

Attention will now be focussed on observed S_c/S ratios found in this project and their implications on the estimation of shear strains within the soil mass. Work in this area has been aided by the advent of instruments with sufficient accuracy to determine soil movements in three mutually perpendicular directions and the ability of computers to quickly and cheaply convert these measurements into contour plots of displacements from which shear strains can be calculated (El-Nahhas, 1980). Resulting from these advances, El-Nahhas (1980) and others (Atkinson and Potts, 1977; Atkinson et al. 1975; Cording and Hansmire, 1975) have delimited areas of consistently high shear strain as shown qualitatively in Figure 4.6 ,

The reported magnitudes of shear strain in these zones vary but all are larger than that required to reach maximum shear strength of most soils (1-2%). This straining beyond peak creates plastic zones which have been dubbed "plastic



Zones of High Shear Strain
"Plastic Ears"

Figure 4.6 Qualitative Development of Plasticity around a Tunnel

ears". Creation of these plastic zones indicates that the material contained between the ears may bodily move downwards thereby representing a volume loss around the tunnel. With the development of these plastic ears, the propagation of movements through the soil mass becomes more oriented. The result is a narrower settlement trough. Atkinson and Potts (1974) reported narrower, deeper settlement troughs with associated greater distortions when the plastic zones propagated to the surface. They did not however report any intermediate conditions. Accepting that narrower, steeper settlement troughs, potentially more dangerous to buildings, will occur under conditions of plastic ear development around tunnels, predictions are necessary as to where such conditions are likely to prevail and to what extent they occur. Any effects on surface displacements and lining loads would also be of interest.

Broms and Bennermark (1967) introduced the term "Simple Overload Factor" (OFS) in respect to face stability of tunnels, i.e.,

$$\text{Simple Overload Factor} = (p_z - p_i) / c_u$$

where p_z = insitu vertical stress
 p_i = internal pressure (if any)
 c_u = undrained shear strength

This term has been used quite extensively in tunnelling and Peck et al. (1969) have related estimated ground loss to its value. It is generally agreed that for OFS values < 1 movements should be elastic with little additional movement for values < 2.0 . For values such that $2 < \text{OFS} < 4$, settlements on surface become larger and as OFS increases beyond 4 settlements increase and become uncontrollable at values of 5 and 6 (Peck 1969). As a corollary to OFS, Attewell (1977) suggested a "Modified Overload Factor" (OFM) such that

$$\text{OFM} = (\sigma_{\theta \text{ max}} - 2p_i) / q_u$$

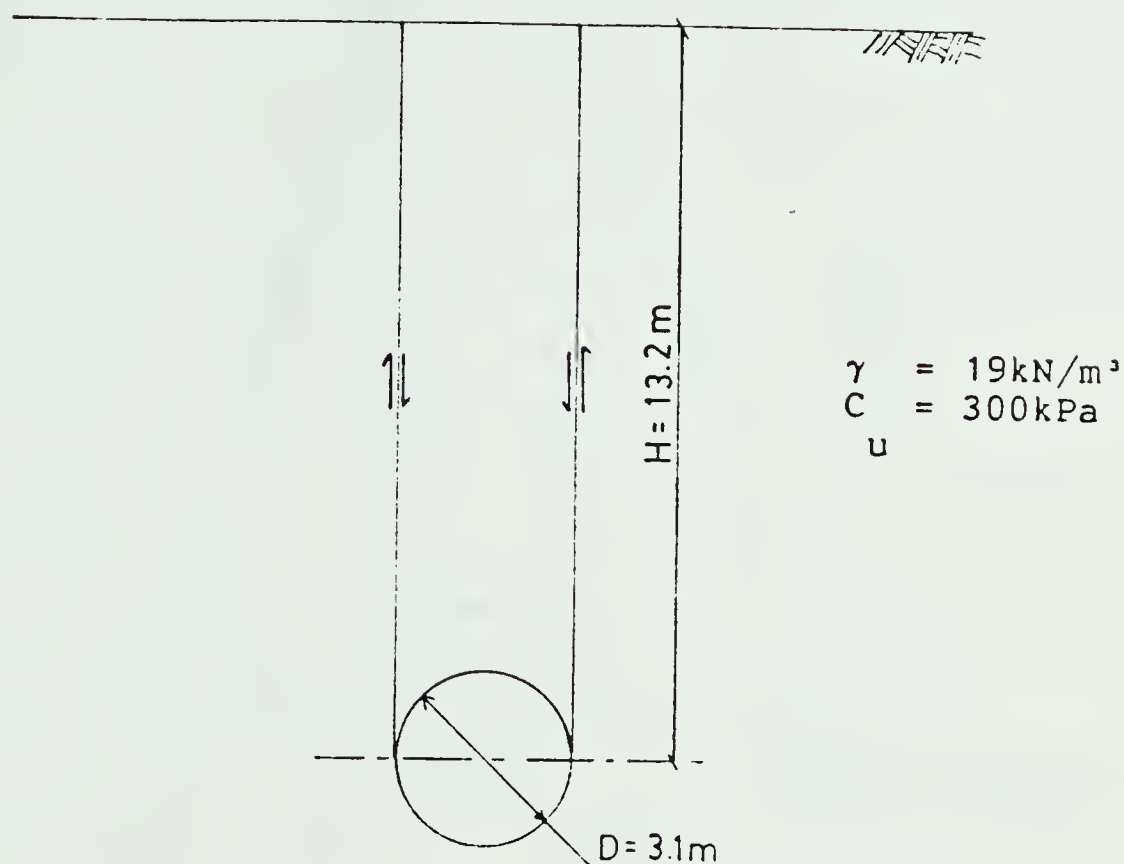
where $\sigma_{\theta \text{ max}}$ = maximum tangential stress
 p_i = internal pressure (if any)
 q_u = unconfined compressive strength of clay.

For conditions of a deep tunnel under $K_0 = 1$, $\text{OFM} = \text{OFS}$, however for shallow tunnels with $K_0 < 1$ the problem of determining $\sigma_{\theta \text{ max}}$ is slightly more complicated. In reality OFM values express the extent to which shearing in the clay can occur (Attewell, 1977). An OFM value of 1.0 implies that material located around the periphery of the tunnel is at the point of yielding ($\sigma_{\theta} = q_u$), and for all values greater than 1.0 yielding will start to propagate from the tunnel wall into the soil mass, i.e., the development of a yield

zone. For deep tunnels and perfect elasto plastic behaviour, this yield zone should be circular but for shallow tunnels the effect of the surface boundary condition causes this yield zone to take an axially asymmetric form leading eventually to development of the plastic ears which propagate towards the surface.

The usefulness of the vertical displacement profile in regard to predicting the extent to which plastic shearing has occurred shall now be examined. What is required to aid this are typical profiles obtained in the no yield, partially yielded and fully yielded conditions. In the following discussion an attempt is made to elucidate these stages more clearly based on empirical measurements in cohesive materials.

In the present project, ME 1 and 2 which show near constant displacement with depth (Figure 4.5), are located in an area where the OFS value is 0.86 from which only minor yielding of the material, if any, would be expected. The profiles however indicate constant but small shearing with depth, i.e. the material above the tunnel behaves in a block like manner but should not be failing. If a factor of safety against the block mechanism of failure as shown in Figure 4.7 is calculated based on a criterion of $\frac{\tau_{\text{available}}}{\tau_{\text{mobilised}}}$ (Negro and Eisenstein, 1981) a value of 10 is found. Using an effective stress analysis as outlined in Figure 4.8 a factor of safety of 3.3 is obtained. Although, the effective stress factor of safety is



$$\tau_{\text{mobilised}} = DH\gamma/2H = D\gamma/2 = 29.5 \text{ kPa}$$

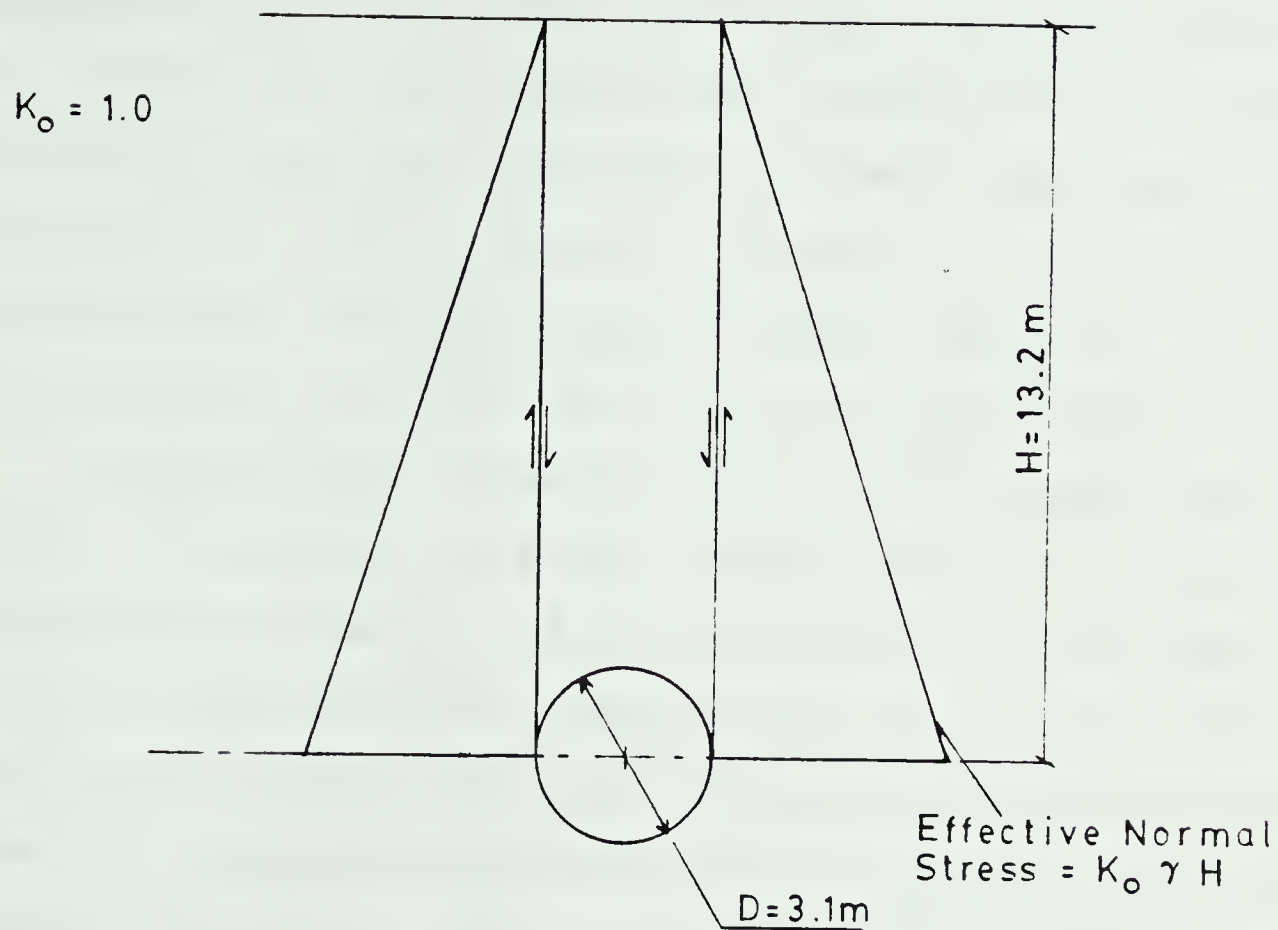
$$\text{Factor of Safety} = \tau_{\text{available}} / \tau_{\text{mobilised}}$$

$$\tau_{\text{mobilised}} = 29.5 \text{ kPa}$$

$$\tau_{\text{available}} = 300 \text{ kPa}$$

$$\text{Factor of Safety} = 10$$

Figure 4.7 Block Failure Mechanism for the Kennedale Tunnel
- Undrained Analysis



Factor of Safety Calculation

Activating Force = $\gamma DH = 778 \text{ kN}$

Effective Resistance Force (F)

$$F = c'H + \sigma_n \tan \phi'$$

$$\sigma_n = \text{integrated normal force} = \gamma H^2 / 2$$

$$\sigma_n = 1655 \text{ kN}$$

$$F = 2[(10 * 13.2) + (1655 * \tan 35^\circ)]$$

$$F = 2582 \text{ kN}$$

Factor of Safety = $2582 / 778$

Factor of Safety = 3.3

Figure 4.8 Block Failure Mechanism for the Kennedale Tunnel
- Effective Stress Analysis

smaller than the undrained value it still indicates conditions to be well away from failure. Further evidence of the ground in the region of ME 1 and 2 being far removed from failure has been obtained by small measured lining pressures at their location (Chapter 5). This shows that equal vertical displacements with depth, similar to block type movement, can also occur in non yielding ground.

Accepting that the block is not failing but behaving nearly elastically, a simple elastic analysis (assuming an infinite continuum) of the problem predicts a settlement at crown of 5.8mm tapering asymptotically to 0.1mm at surface. This is at variance with the constant measured value of $10\text{mm} \pm 2\text{mm}$. The observed equal displacements above the tunnel are, however, similar to those at the centre of a deep elastic deflecting beam. This constant measured displacement could also be a result of decreasing material stiffness towards the surface.

As an example of yielding ground, work done by EL-Nahhas (1980) and reproduced in Figure 4.9 shows the extent of developed yielding which corresponds to the observed non linearity in the vertical displacement profile. In this project the OFS value was 1.86 which indicates some degree of yielding should be expected. Finally with regard to a fully yielded profile, i.e. when the whole block has moved downwards bodily, a large near constant movement with depth would be expected. Such results have been reported by Cording and Hansmire (1975) and Atkinson et al. (1975). In

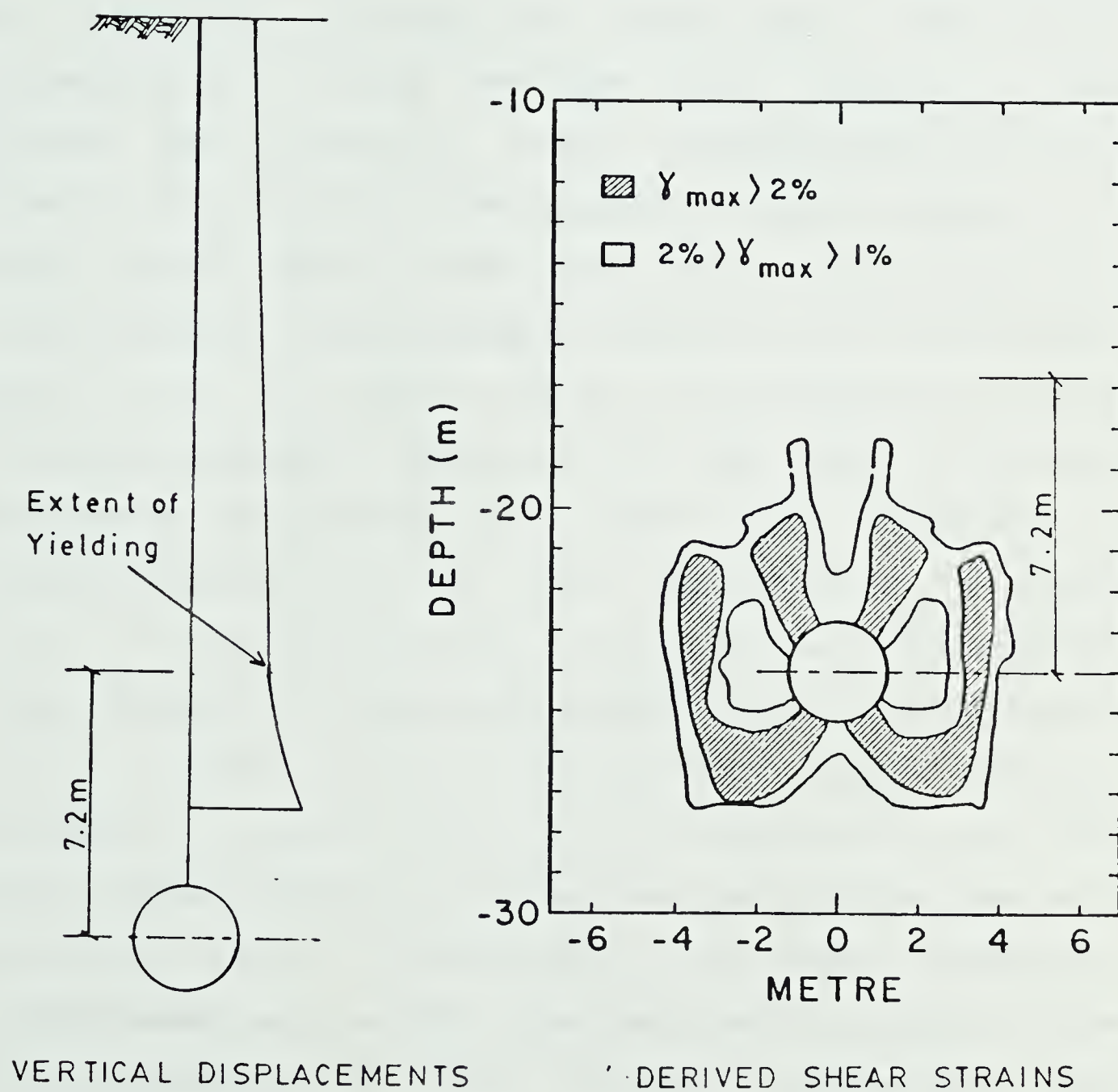


Figure 4.9 Vertical Displacements with Depth in Yielding Ground(after El Nahhas, 1980: modified)

addition those of ME 5 in this project with displacements greater than 300mm are another example.

From these three conditions, the qualitative diagram shown in Figure 4.10 has been compiled. The distributions for unyielded, yielding and yielded cast light on the kinematics of a fully developed block failure. As has already been presented, stress concentrations around the opening will dictate the development of plastic zones, i.e. zones beyond peak strains. These zones originating at the tunnel periphery and propagating upwards towards the surface must do so in a manner similar to the progressive failure mechanism proposed by Bjerrum (1967). The expected vertical settlement distribution with depth under conditions of advancing plastic ears are shown qualitatively in Figure 4.10. If the material has a pronounced post peak strength loss, yielding will propagate further and soil displacements will increase resulting in increased support pressure necessary to achieve stability of the opening. As the yield zone expands towards the surface the non-yielding zone with near equal vertical displacements with depth disappears, leading eventually to full block failure. This aspect of the interrelationship of ground strength, displacements and lining loads has been investigated in detail in Chapter 5. The extent of plastic development was modelled as a circular yield zone of radius R from which estimated support-displacement curves for the crown region were developed. The foregoing presentation shows that in the

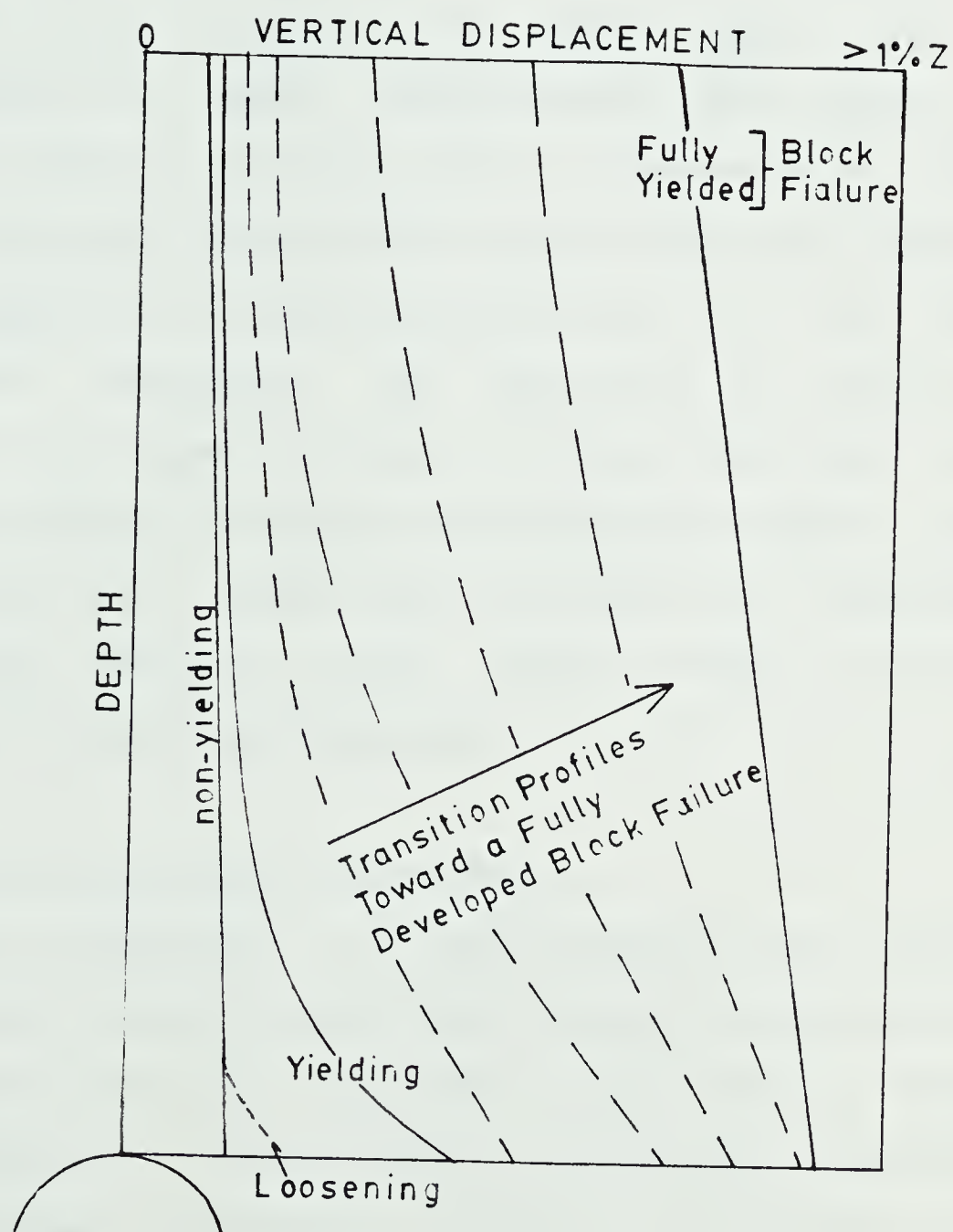


Figure 4.10 Progressive Failure Mechanism for Block Failure

crown region, the area of most interest, the radius R actually represents the extent to which the plastic ears have propagated above the tunnel crown. This is explained in more detail in Chapter 5.

While this section has cast light upon the interrelation of loads, displacements and strains, the extent can only be estimated using a value such as OFS or possibly the more theoretically correct OFM value. These can only be applied to cohesive materials and in this respect more work concerning the mechanisms of plastic ear development and expected widths of shear bands which govern the magnitude of the shear strain magnitude must be carried out. Further work is also required concerning responses of cohesionless materials under varying heads of water and subsequent strength mobilisation.

4.1.3 Surface Settlement Predictions

Loss of ground due to overexcavation and subsequent soil invasion around tunnels has long been recognised as the major cause of surface settlement above shallow tunnels. Quantification of these losses in and around shield driven tunnels has been attempted by Cording and Hansmire (1975) for various overexcavations required as a function of steering the shield. Work in the preceding section indicates that further loss of ground may occur if plastic zones due to overstressing occurs resulting in the bodily downward movement of soil above the tunnel. When an estimated volume

loss is obtained per unit length the problem of surface settlement prediction becomes one of how these volume losses propagate to the surface.

With regard to this propagation, the most common method in use is that proposed by Peck (1969) which is based on a stochastic analysis of how the soil particles will occupy the void caused by the lost ground. This analysis, strongly criticised by De Mello (1981) because of its complete divorce from engineering parameters, results in a predicted surface settlement shape given by a Gaussian probability curve. Details of the curve are given in Figure 4.11 where it is seen that the width of trough is dependent on the value of "i", i.e. width of trough = $6i$. Empirical relationship of "i" with depth of tunnel burial and tunnel diameter for varying ground conditions (Peck, 1969) is shown in Figure 4.12. In the author's opinion too many geological and geotechnical variables such as shear strength, water conditions, stress-strain history, non-homogeneity, etc, are masked in the material boundaries as presented in Figure 4.12. This leads to the false impression that the width of trough and ultimately S_{\max} are most prominently dependent on tunnel depth to crown. This was also an observation of De Mello (1981). Information in the preceding sections showed how settlements can become more oriented if yielding around the tunnel is present, resulting in a narrower settlement trough. This fact has been noticed by Cording and Hansmire (1975) and Attewell (1977) who put a limit of $S_{\max}/z > 0.5\%$

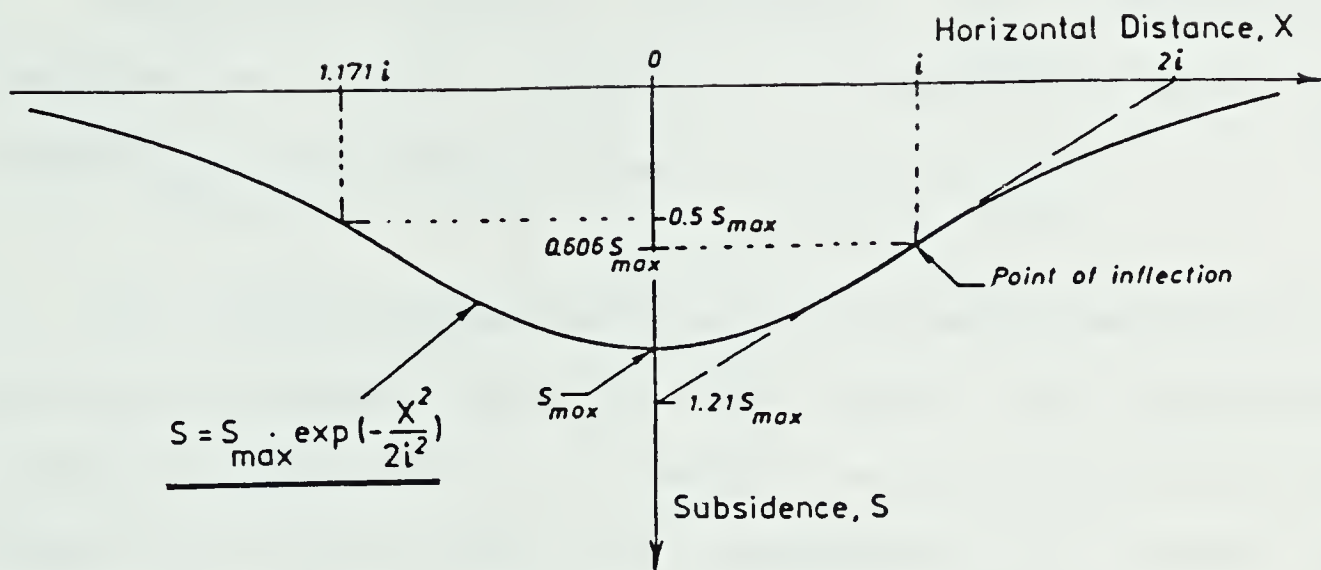


Figure 4.11 Gaussian Probability Curve (after Peck, 1969: modified)

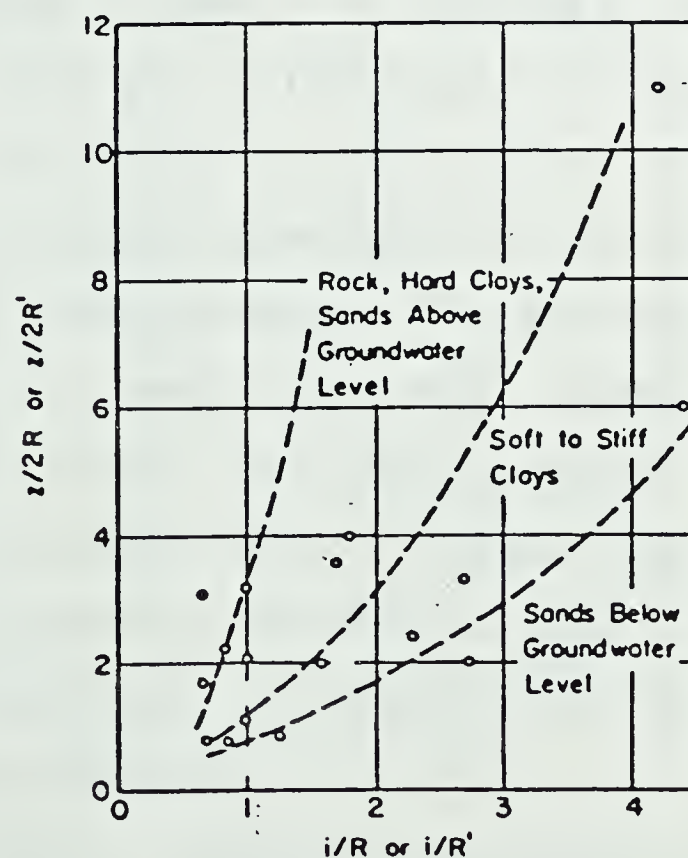


Figure 4.12 Probability Curve Parameter " i " varying with Z/D ratio (after Peck et al., 1969: modified)

above which the normal probability curve fails to match measured profiles by overprediction of width.

Volume of surface settlement (V) obtained by integration of the probability curve yields $V = 2.5 i S_{\max}$ where S_{\max} for a single tunnel = $S_{\text{centre line}}$.

For tunnel design conditions the problem becomes one of estimating volume losses at the tunnel and subsequently equating this value to surface volume after obtaining a value for i from Figure 4.12. Estimations of volume loss varying with OFS values have been presented by Peck et al. (1969) and are reproduced in Figure 4.13. This figure is based on the estimated encroachment volume, relative to the nominal excavated volume, of material into an unlined tunnel. Also plotted in the figure are reported values of ground loss for differing OFS values which show good agreement in the elastic zone ($\text{OFS} < 1$) with decreasingly poor compliance as the OFS increases. The discrepancy at higher OFS values is a result of real tunnels having liners installed which arrest the displacements. In this, the author is in agreement with El-Nahhas (1980) that measured tunnel lining pressures should be used as an internal pressure in obtaining an OFS such that smaller estimated volumes would be obtained.

If the design procedure, as outlined previously, are followed for Area I (Figure 4.4), the only cohesive section, an estimated surface settlement magnitude of 7.8mm at the

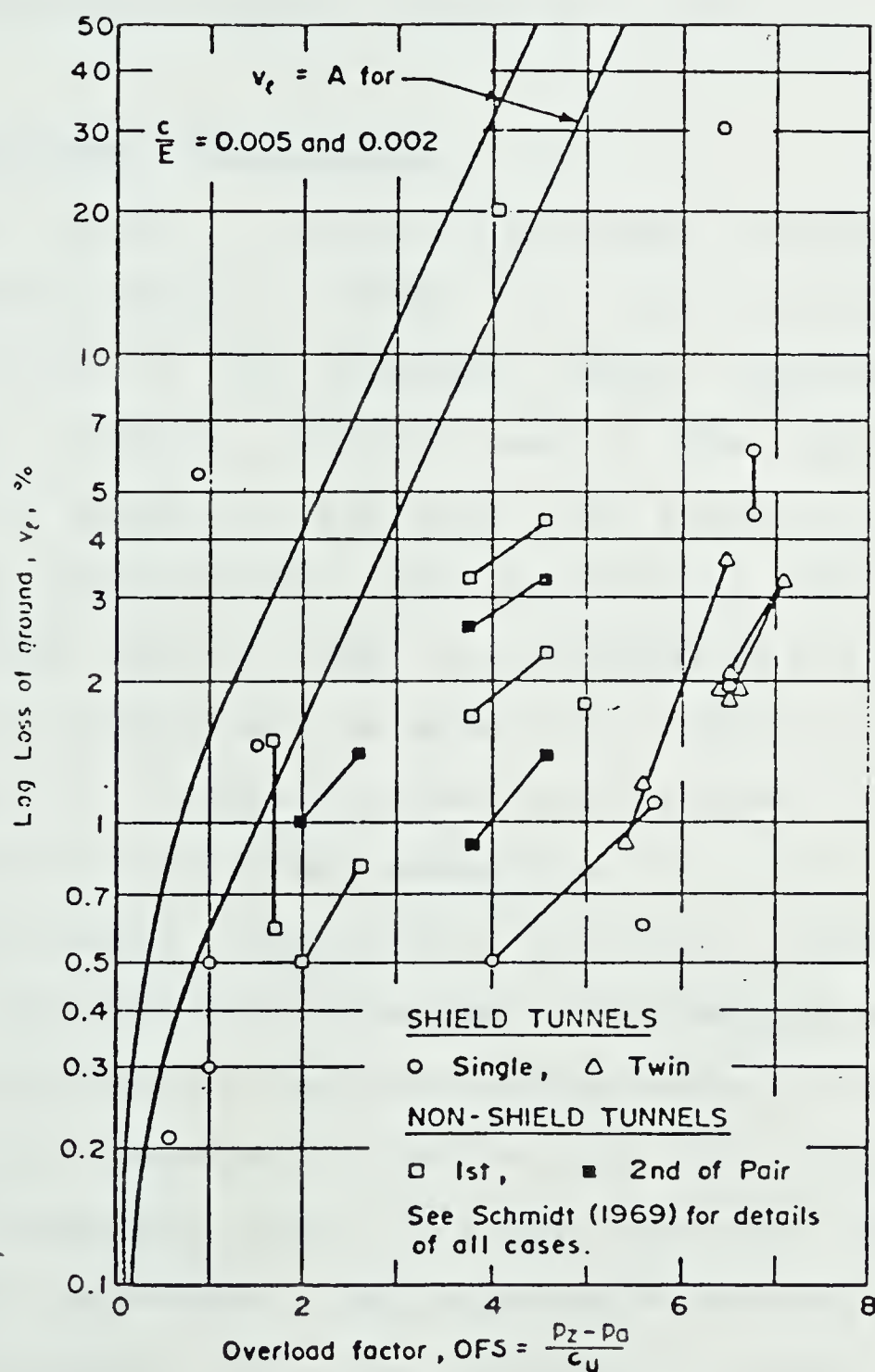


Figure 4.13 Volume Loss of Material with Increasing Overload Factor (after Peck et al., 1969: modified)

centre line is obtained. This is in quite good agreement with the typically measured 8.0mm of this section although there is no data for verification of the i value. The i value was taken at the interface of Rock, Hard Clays, etc and Stiff Clays yielding a value of 3.875m.

4.2 Horizontal Displacements

As stated in Chapter 3 two slope indicators (SI1 and SI2) shown located in Figure 3.1 were installed on the centre line of the proposed tunnel. Because of their location, primary interest was in the development of movements ahead of and into the advancing tunnel face. Obtained displacements in the longitudinal plane containing the tunnel centre line, as recorded by SI1 and SI2, are presented in Figures 4.14 and 4.16 respectively. Figures 4.15 and 4.17 present movements as recorded by SI1 and SI2 transverse to the tunnel centre line.

Considering longitudinal movements (Figures 4.14 and 4.16), large differences between inclinometers was observed, i.e., approximately 4mm maximum displacement into the tunnel face at SI1 compared with 8mm at SI2. The development of ground movements above the tunnel crown was also different for each inclinometer. This observed difference in behaviour was in keeping with the different geologic regions, as defined in Figure 2.4, in which the inclinometers were located, i.e., SI1 was located in Area III while SI2 was in Area IV.

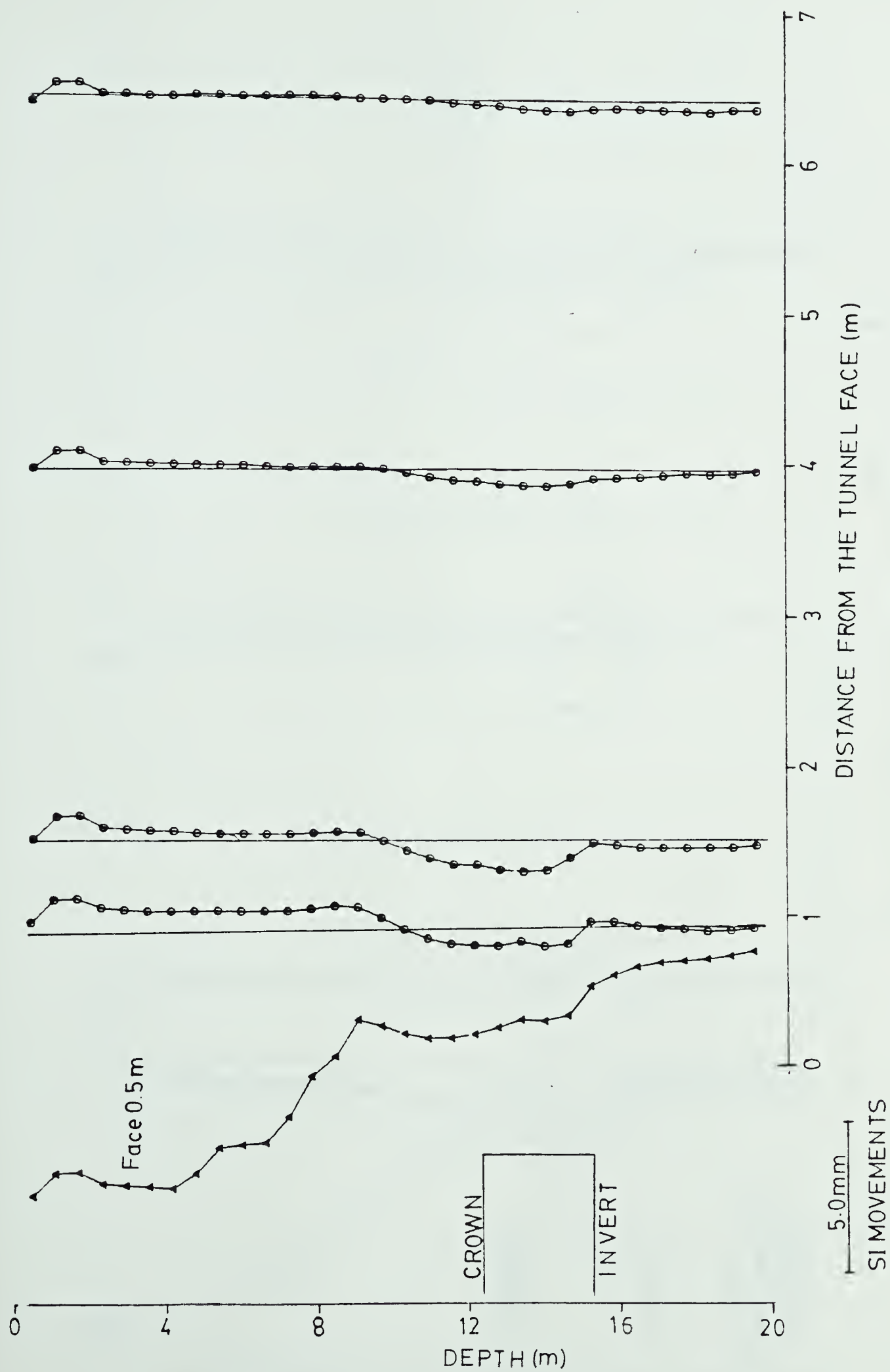


Figure 4.14 Horizontal Displacements recorded in the Longitudinal Plane containing the Tunnel axis by Slope Indicator 1

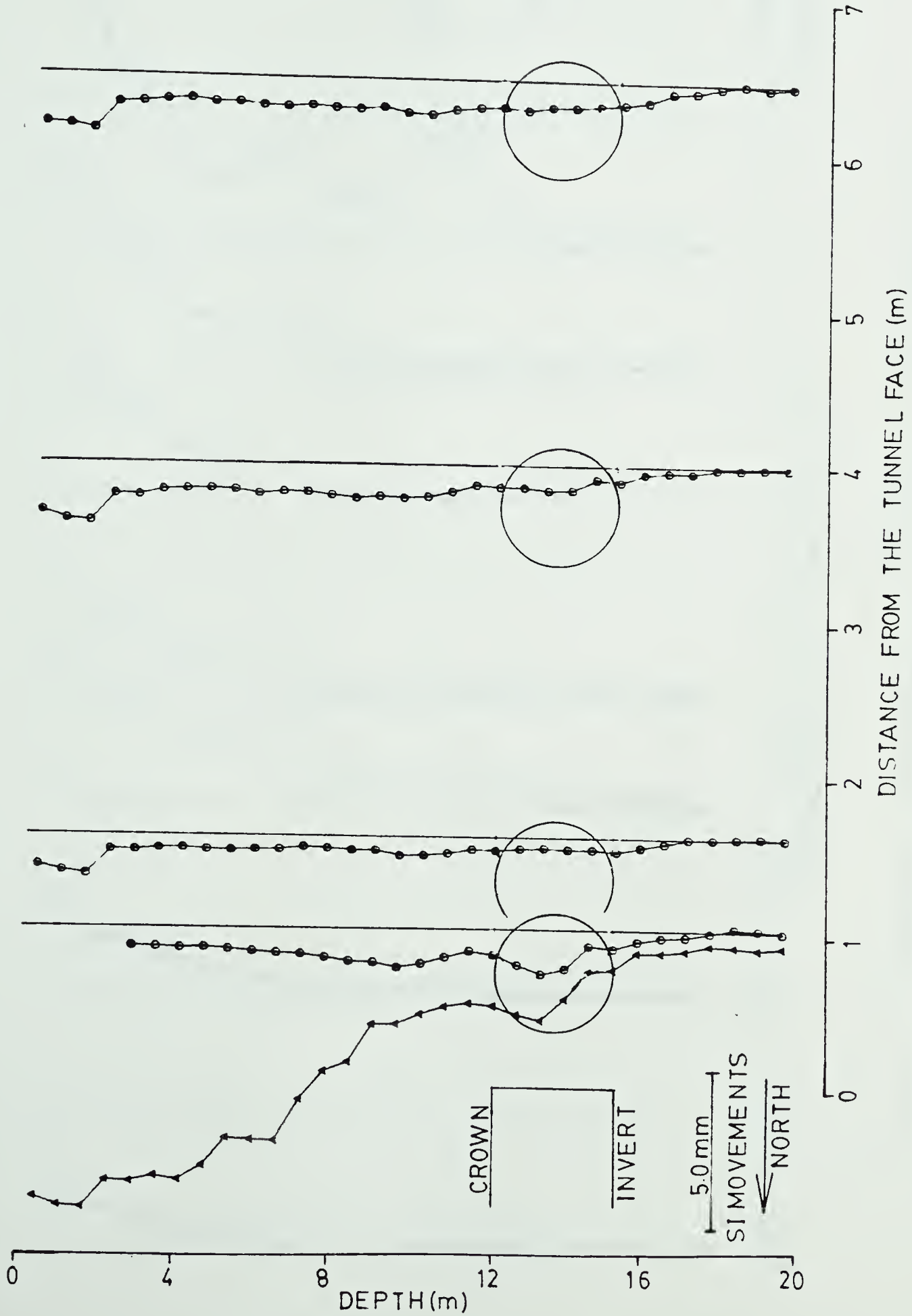


Figure 4.15 Horizontal Displacements Transverse to the Tunnel axis as recorded by Slope Indicator 1

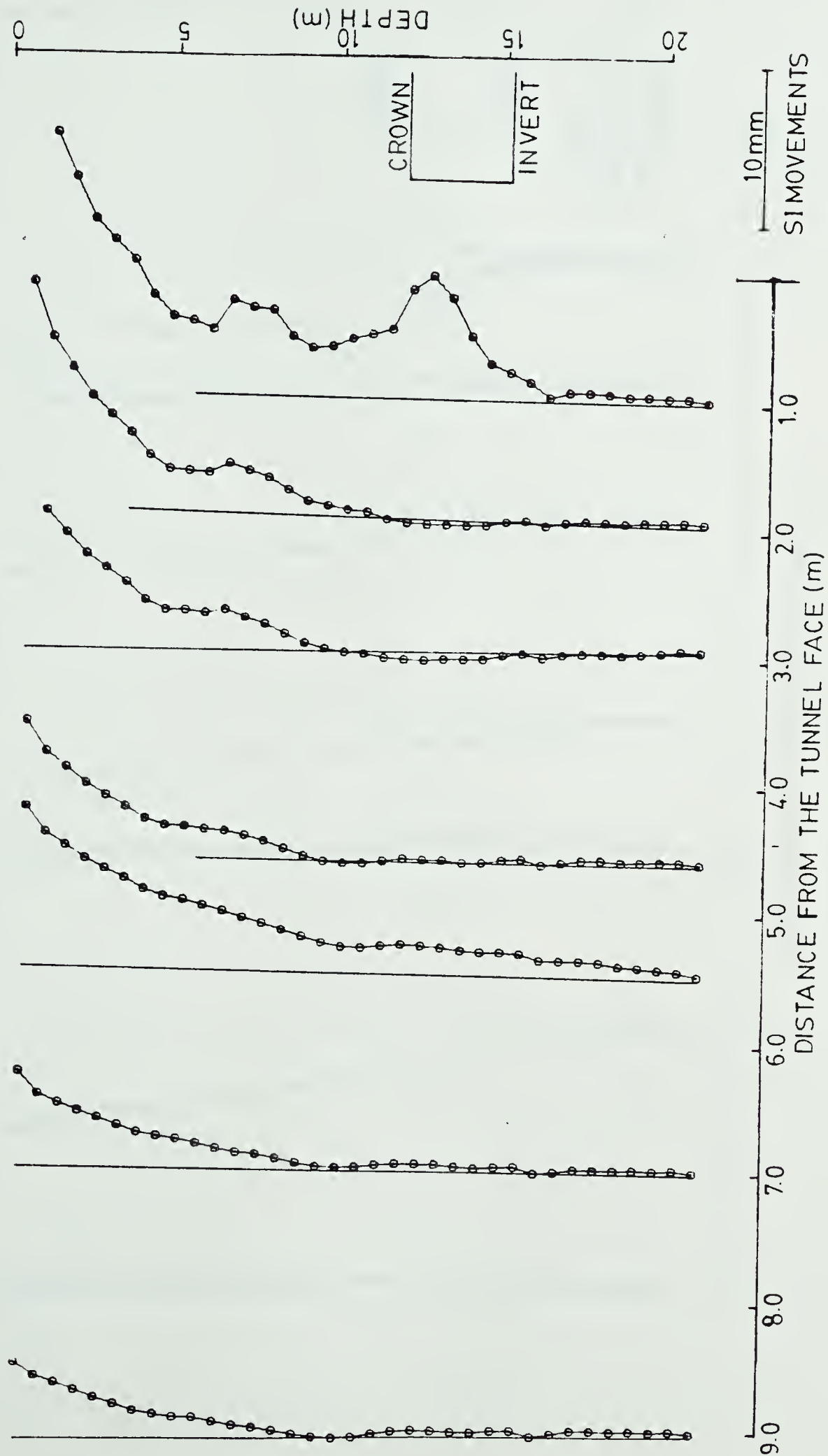


Figure 4.16 Horizontal Displacements recorded in the Longitudinal Plane containing the Tunnel axis by Slope Indicator 2

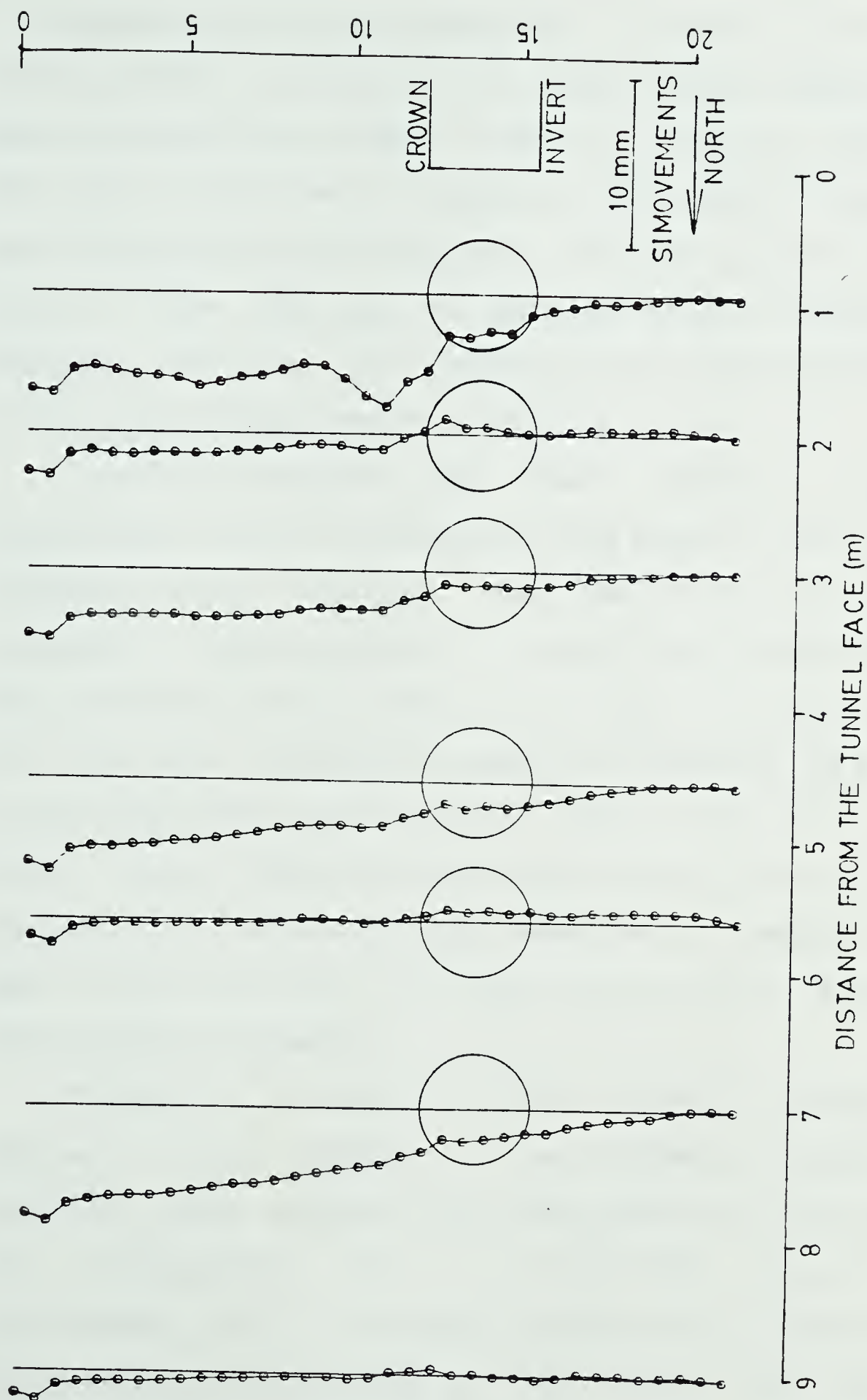


Figure 4.17 Horizontal Displacements Transverse to the Tunnel axis as recorded by Slope Indicator 2

Considering in more detail SI1, located in a region where surface settlement was typically 8mm, displacements show no perceptible movement beyond 4m ahead of the face. The final displacement profile as presented in Figure 4.14 was influenced by the development of quite a large void in front of the TBM and as such can only be considered as anomalous. The same void resulted in the anomalous behaviour of Multipoint Extensometer 3 (Section 4.1.2).

Ignoring therefore the final profile a maximum displacement of 1mm was observed 1.6m ahead of the face. The subsequent set of readings, when the face was 1m away, indicates a displacement of only 0.5mm towards the face. This reduction was believed to be a result of pushing forces from the mole. Evidence of pushing of the soil is also seen by the displaced position of SI1 above the level of the crown. These observed movements, although within the error reported from calibration zero readings in Chapter 3, are seen to be consistent with time and apparently sensitive to minor ground movements.

Transverse movements of SI1 shown in Figure 4.15 indicate little movement or no movement trends. Final measured large movements were believed to be influenced by the construction void as mentioned earlier. This inclinometer due to alignment problems had a final position just inside the springline of the tunnel and while some lateral displacement might be expected at this location, results presented show no perceptible movements until

influenced by the construction void.

Figure 4.16 shows displacements as recorded by SI2. Unlike SI1 no anomalous happenings occurred during excavation and therefore displacements can be assumed as typical of those occurring under ground conditions such as present at SI2. Presented movements at the level of the tunnel axis indicate behaviour similar to that observed by in SI1, i.e., the ground initially moved toward the face up to a distance of 5m away from it and thereafter with the exception of the last recorded reading appears to have been pushed away from the face. The final measurement of approximately 8mm into the face was expected as during excavation material could visibly be seen flowing through the TBM face. It is believed that detected movements may have been larger had an exceptionally strong grout not been used during installation of the slope indicator. The grout, required due to stop excessive grout loss (Chapter 3), resulted in the casing being too rigid allowing ground to flow around it (especially pronounced closer to the face).

Movements above crown level of SI2 was different to that of SI1 in that movements of SI2 show tilting toward the face as early as 9m (3 diameters) ahead of the face. This tilting increased as the tunnel face advanced up to a maximum of 16mm at the surface when the face was 1m away. Recorded vertical displacements in this area showed values in excess of 300mm (SP25 and SP26; Appendix D). This large vertical movement resulted in slumping or doming of the

ground in front of the face as detected by SI2 measurements. Large horizontal displacements ($> 10\text{mm}$) such as were detected here would be very dangerous to surface buildings. The mechanism of doming ahead of the face with associated horizontal movements has been identified by Attewell (1977) as potentially dangerous to surface buildings.

Evidence again of too strong a grout is seen from areas of very sudden profile changes of the inclinometer, eg., the 5m depth level in the last three reported measurements of Figure 4.16. These sudden changes are believed to be a result of cracking of the grout.

Transverse movements as shown in Figure 4.17 indicate no real discernable trend although lateral movement to the north of approximately 1mm occurred at the surface. This value can be compared with approximately 15mm horizontal displacement toward the tunnel face at the same location. The final recorded reading has showed quite large transverse movements (approximately 6mm) although the zone of maximum movement does not start until two metres above crown. This strange location may be related to the strong grout surrounding this inclinometer.

Measurements from both inclinometers show little movement below invert level.

5. TUNNEL SUPPORT PRESSURE MEASUREMENTS

5.1 Instrumented Test Sections

A total of four test sections, located as shown in Figure 5.1 were installed between January 18, 1983 and July 26, 1983. These four sections totaled 16 load cells; 78 calibrated wood laggings and 27 simulated steel laggings. The design and calibration of these instruments has been explained in Chapter 3.

Test Sections 1, 2 and 4 were designed to validate wood lagging pressures with those obtained using the more predictable steel laggings. Test Section 3, described later in Section 5.4, differed significantly both in design and purpose from the other sections. In brief, it was designed to validate measurements taken on dubbed "uncalibrated laggings", also described in Section 5.4.

5.1.1 Test Section 1

Located as shown in Figure 5.1, this section consisted of 4 load cells, 18 wood laggings of nominal thickness (t) 50mm and 9 simulated steel laggings arranged as shown in Figure 5.2. Depth of overburden to the tunnel centre line was approximately 13.7m.

Observed "equivalent" lagging pressures obtained using the method set out in Appendix A, are presented in Figures 5.3, 5.4 and 5.5 for Ribs 1, 2 and 3 respectively. Calculated axial forces as recorded by Load Cells 1 to 4,

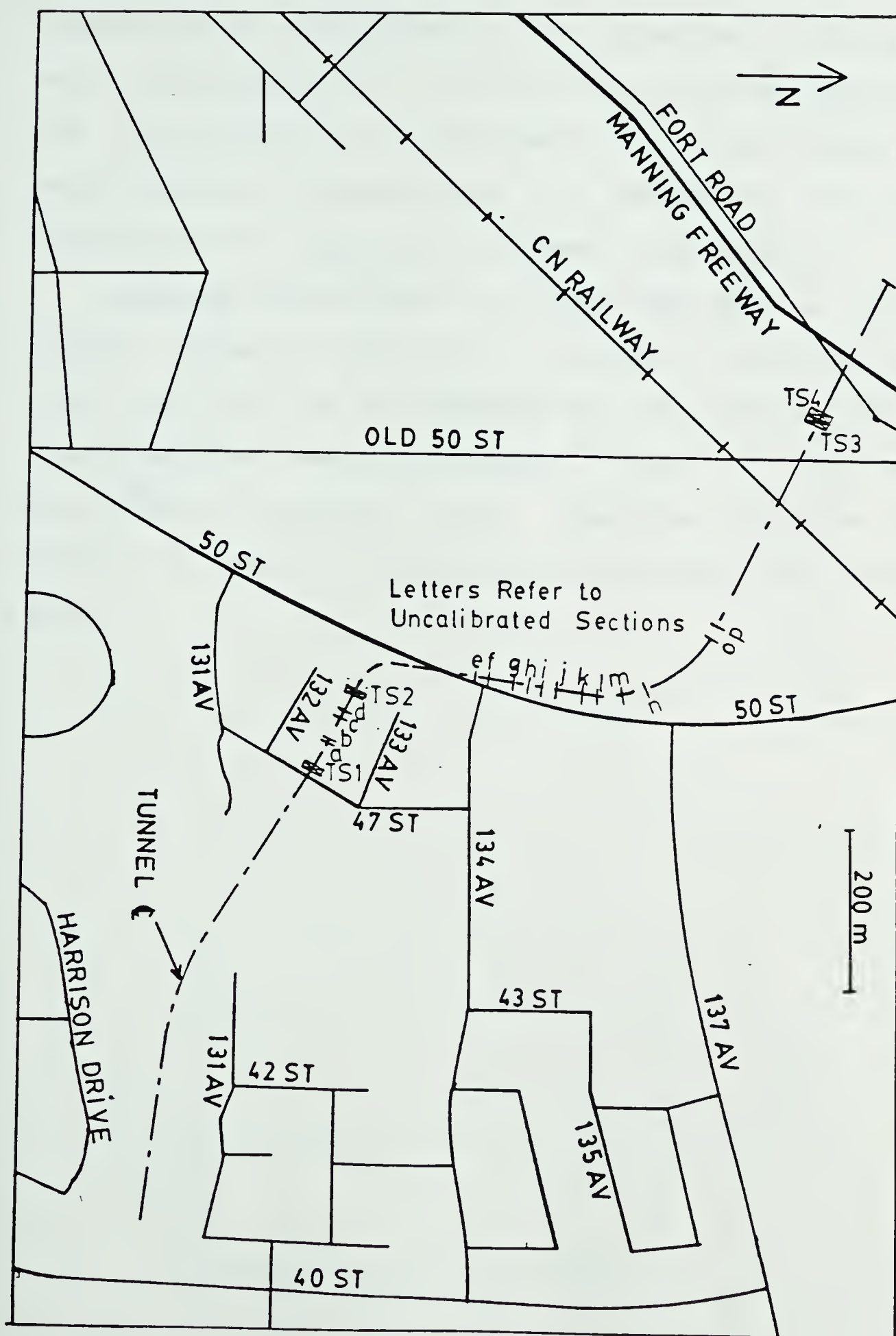


Figure 5.1 Location of Test Sections along Tunnel

located in this Test Section, are presented in Figures 5.6a and b. On Figures 5.3 to 5.6 the face location relative to the test section and normalized to the tunnel diameter, has been presented to demonstrate any dependence of pressure build up on the laggings with tunnel face advance.

Lagging pressures and rib loads both show a generally steady increase which had not tapered off after 50 days by which time the face had advanced well past the section. The irregularities observed between 5 and 10 days can be attributed to operator error. Negative pressures are a result of mole related activities as explained in Section 5.2.1 .

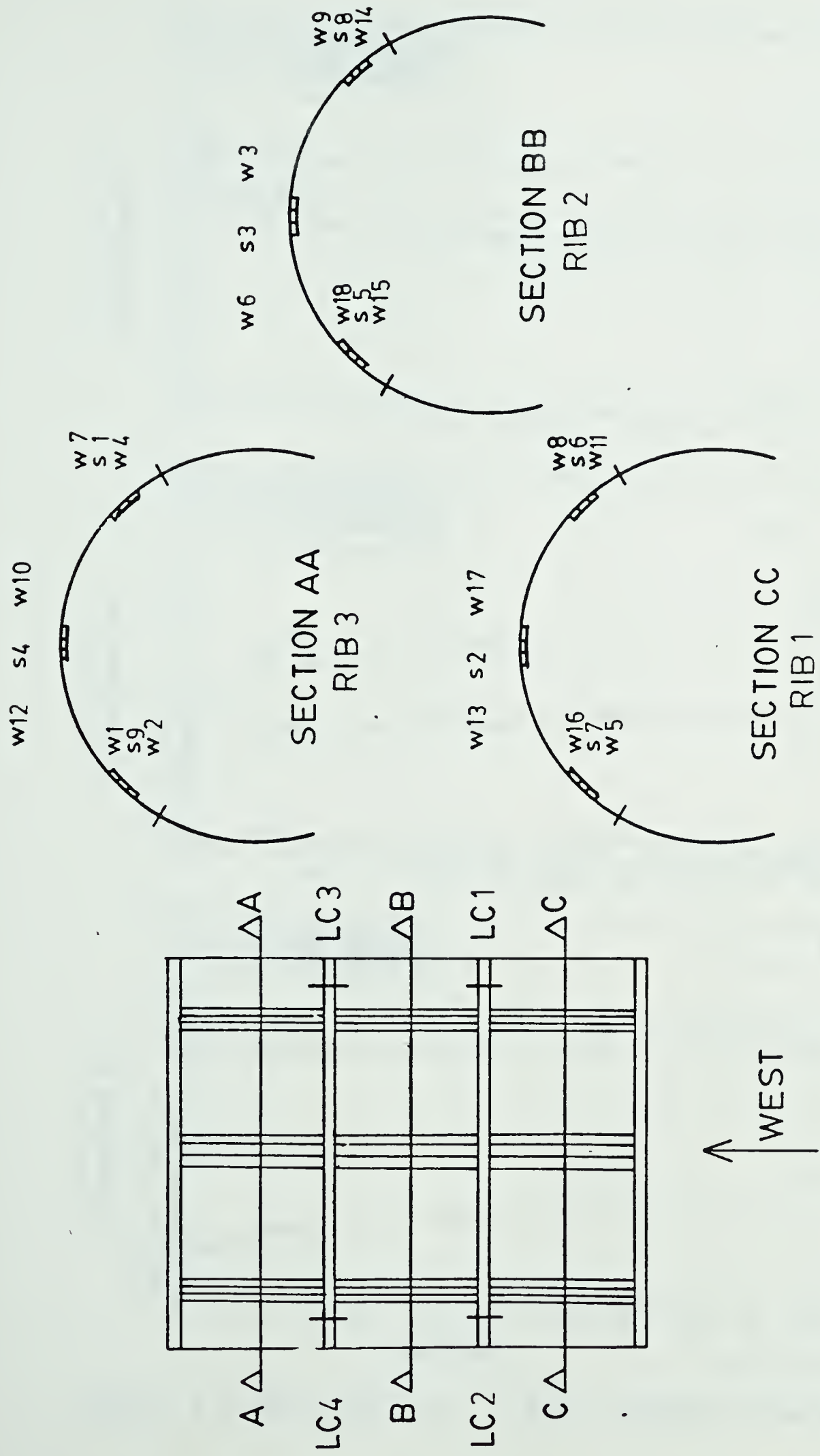


Figure 5.2 Configuration of Test Section 1

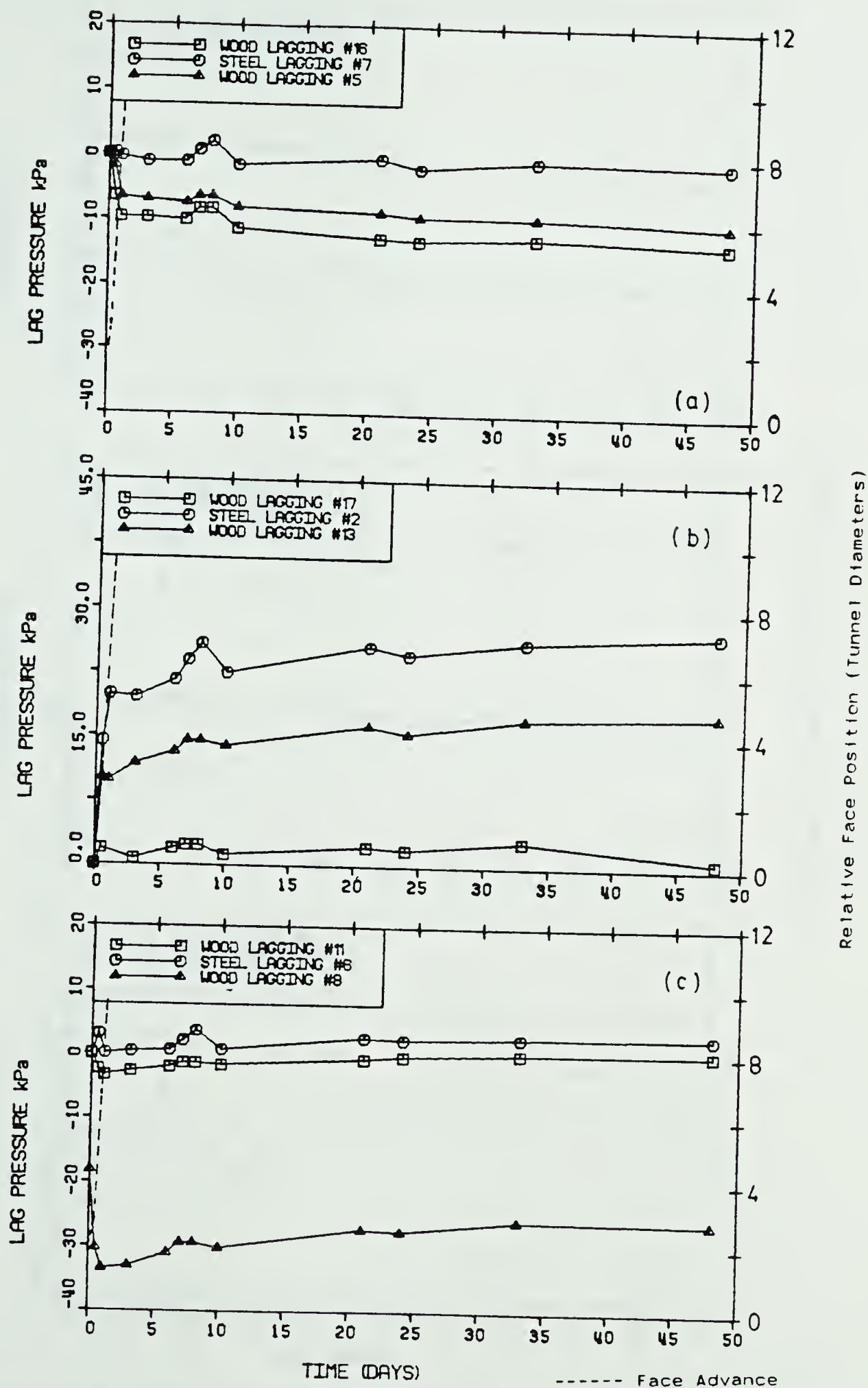


Figure 5.3 Test Section 1 : Rib 1 Lagging Pressures

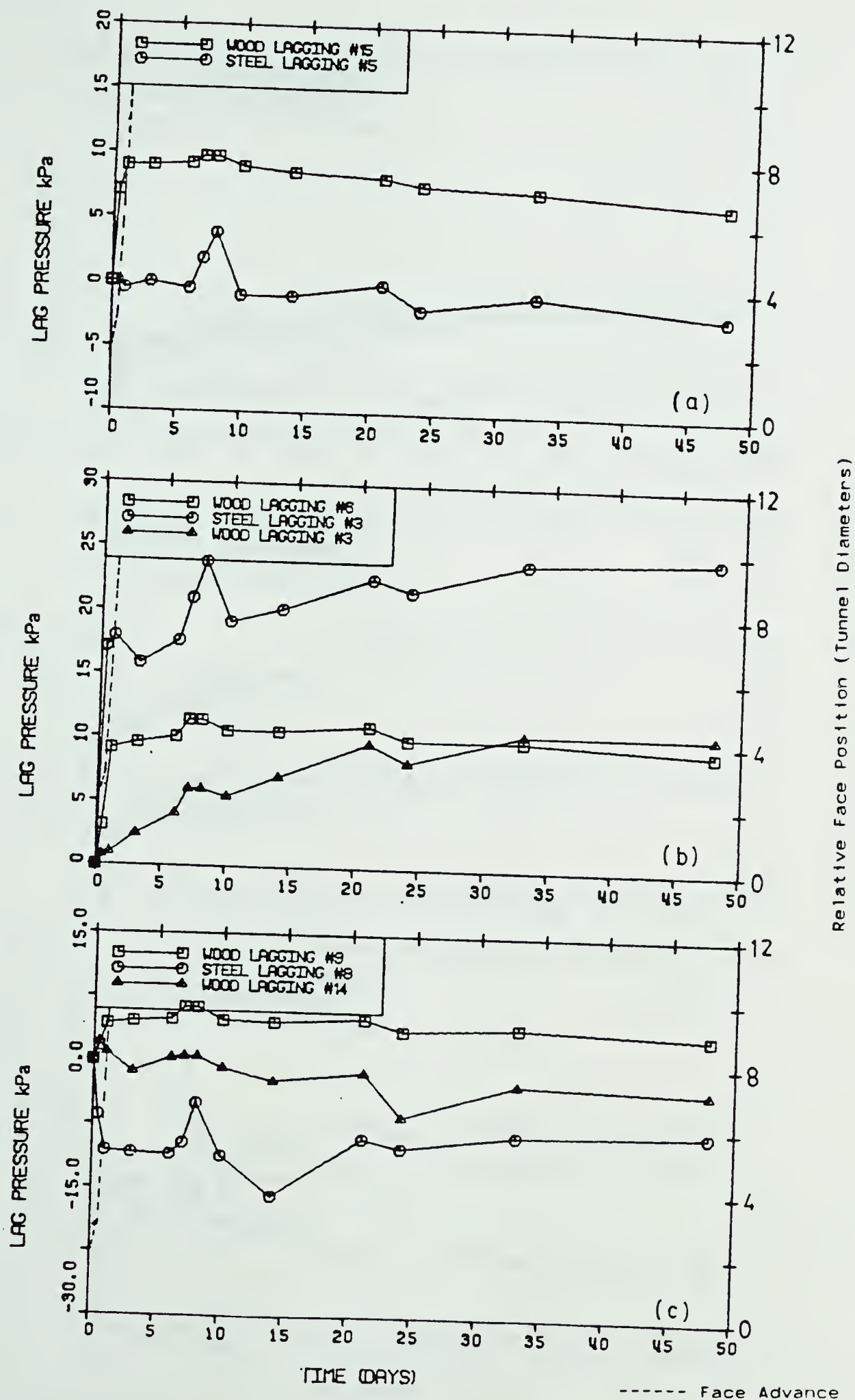


Figure 5.4 Test Section 1 : Rib 2 Lagging Pressures

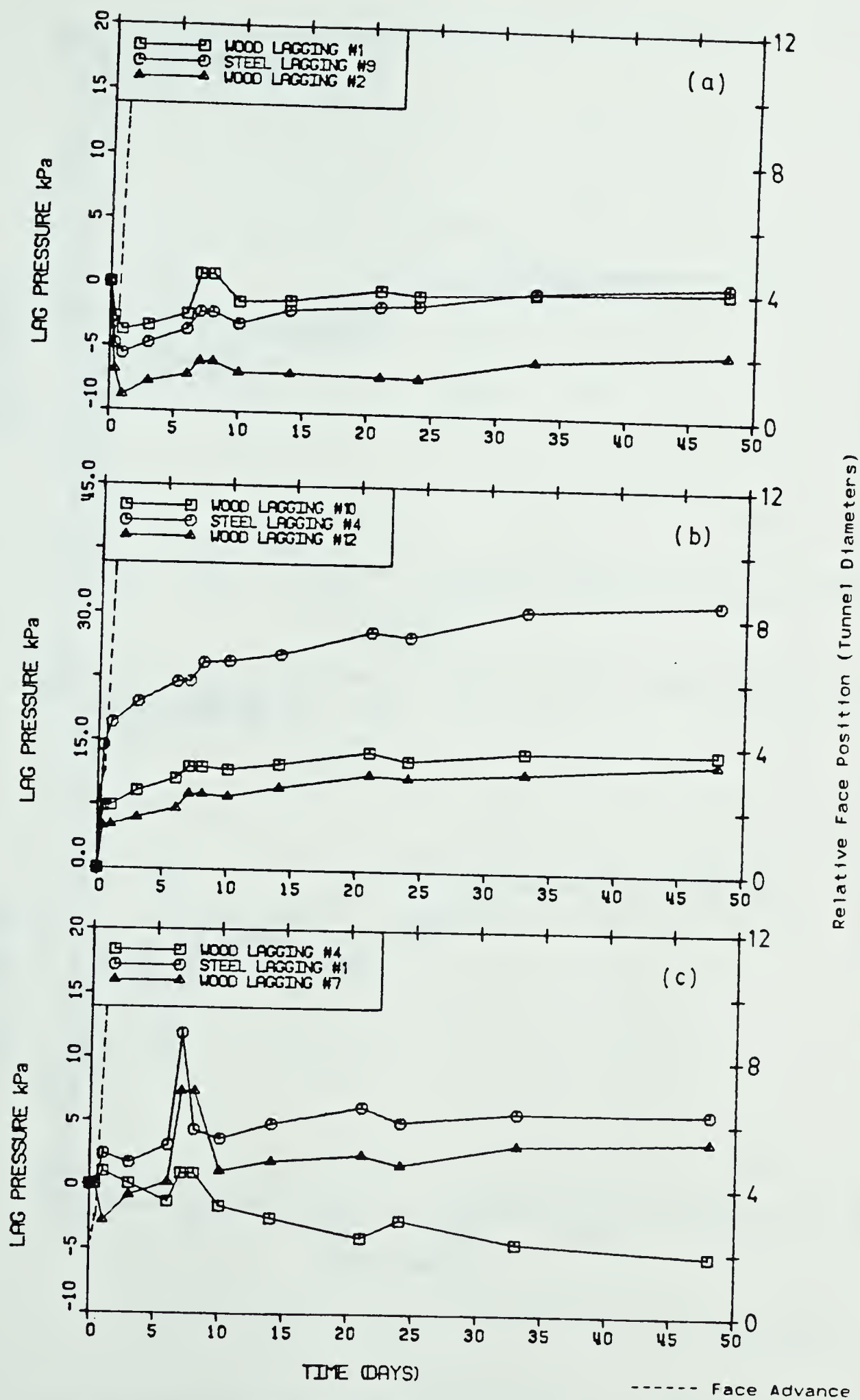


Figure 5.5 Test Section 1 : Rib 3 Lagging Pressures

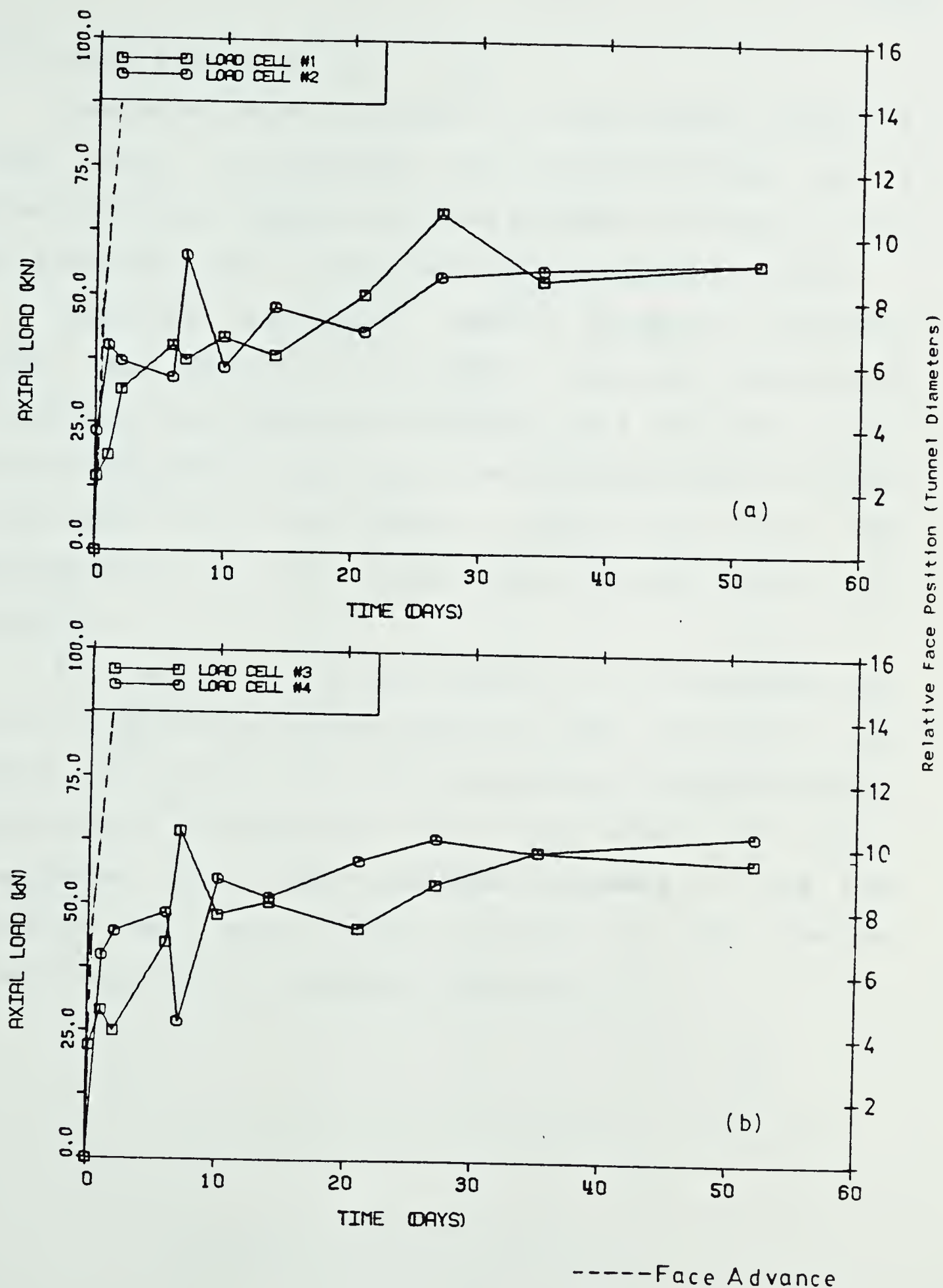


Figure 5.6 Test Section 1 : Load Cell Axial Loads

5.1.2 Test Section 2

Located as shown in Figure 5.1, this section totaled 4 load cells, 30 calibrated wood laggings($t=50\text{mm}$) and 9 simulated steel laggings arranged as shown in Figure 5.7. As with Test Section 1, overburden was approximately 13.7m.

Resulting "equivalent" lagging pressures calculated under the assumption of uniform pressure distribution (Appendix A) are presented in Figures 5.8 to 5.13. Axial forces measured by Load Cells 5 to 8 are presented in Figure 5.14a and b. As in Test Section 1 pressure and axial load developments are shown varying with time and relative face position.

In comparison with Test Section 1, it is observed that a 4 to 5 day delay between expansion and significant load build up exists. This is believed to be attributable to construction shut down for three days which left rib 3 unexpanded until tunnel progress resumed. It is also possible that extra overcut occurred at this section resulting in smaller expansion pressures.

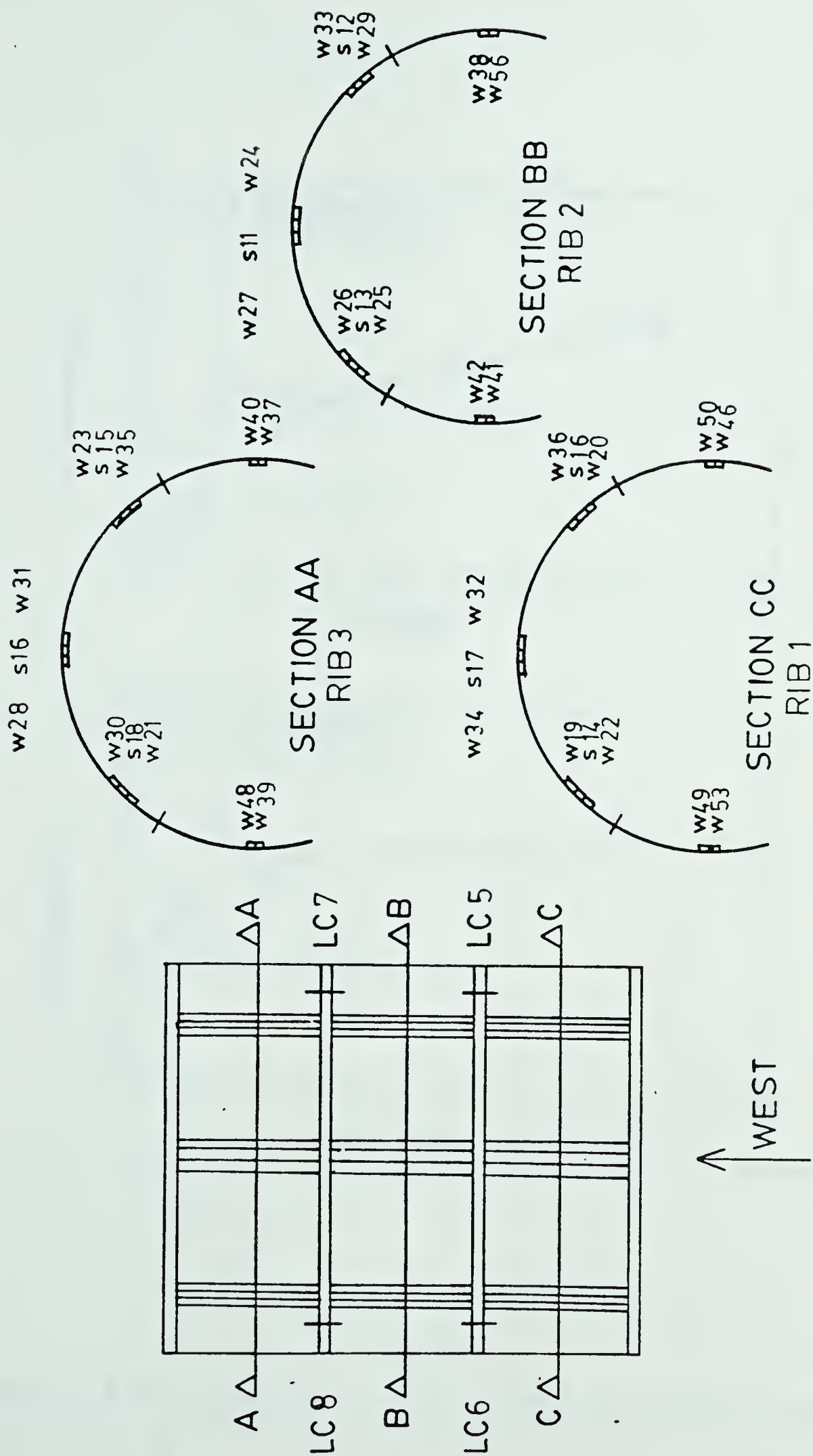


Figure 5.7 Configuration of Test Section 2

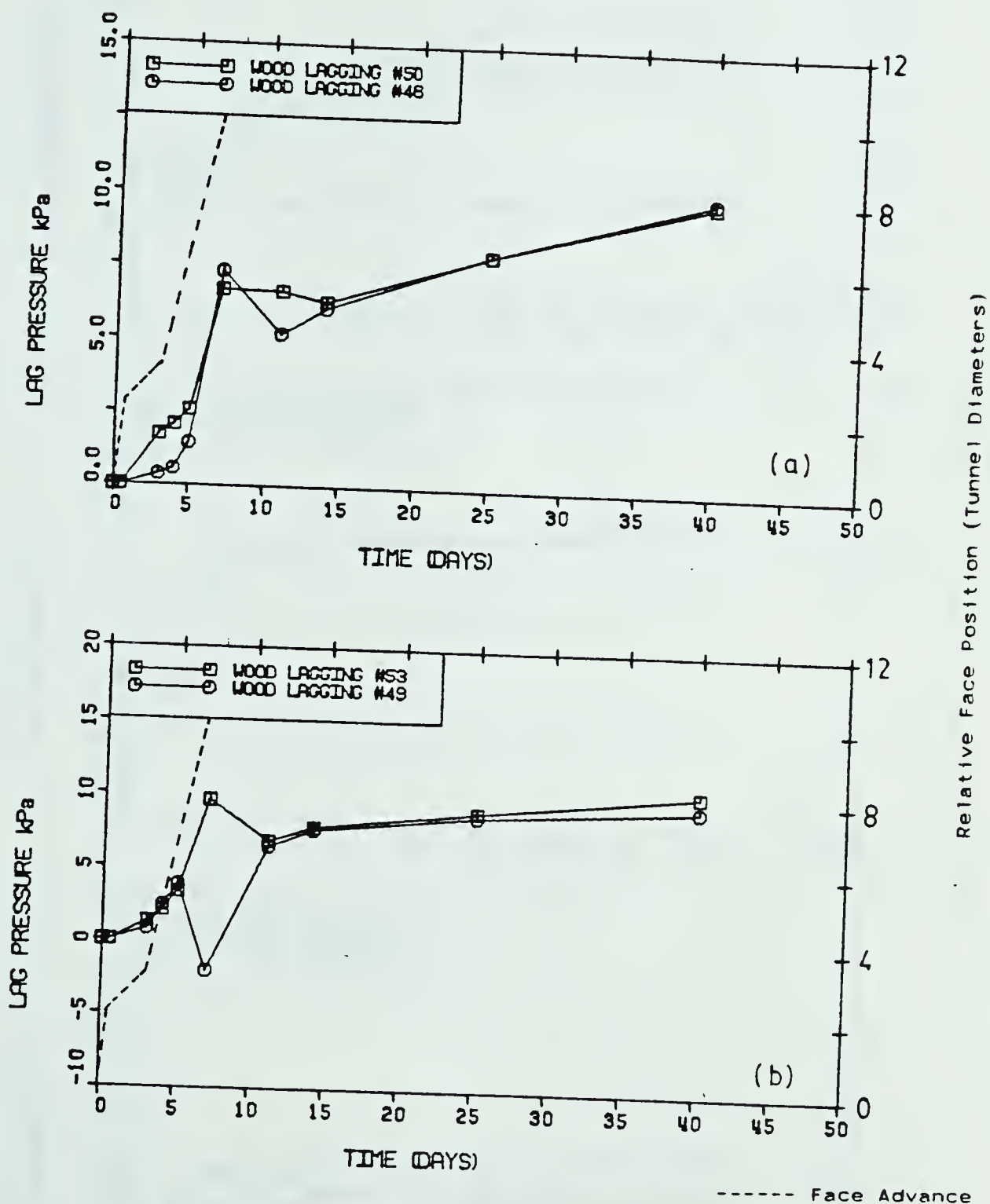


Figure 5.8 Test Section 2 : Rib1 Tunnel Springline Pressures

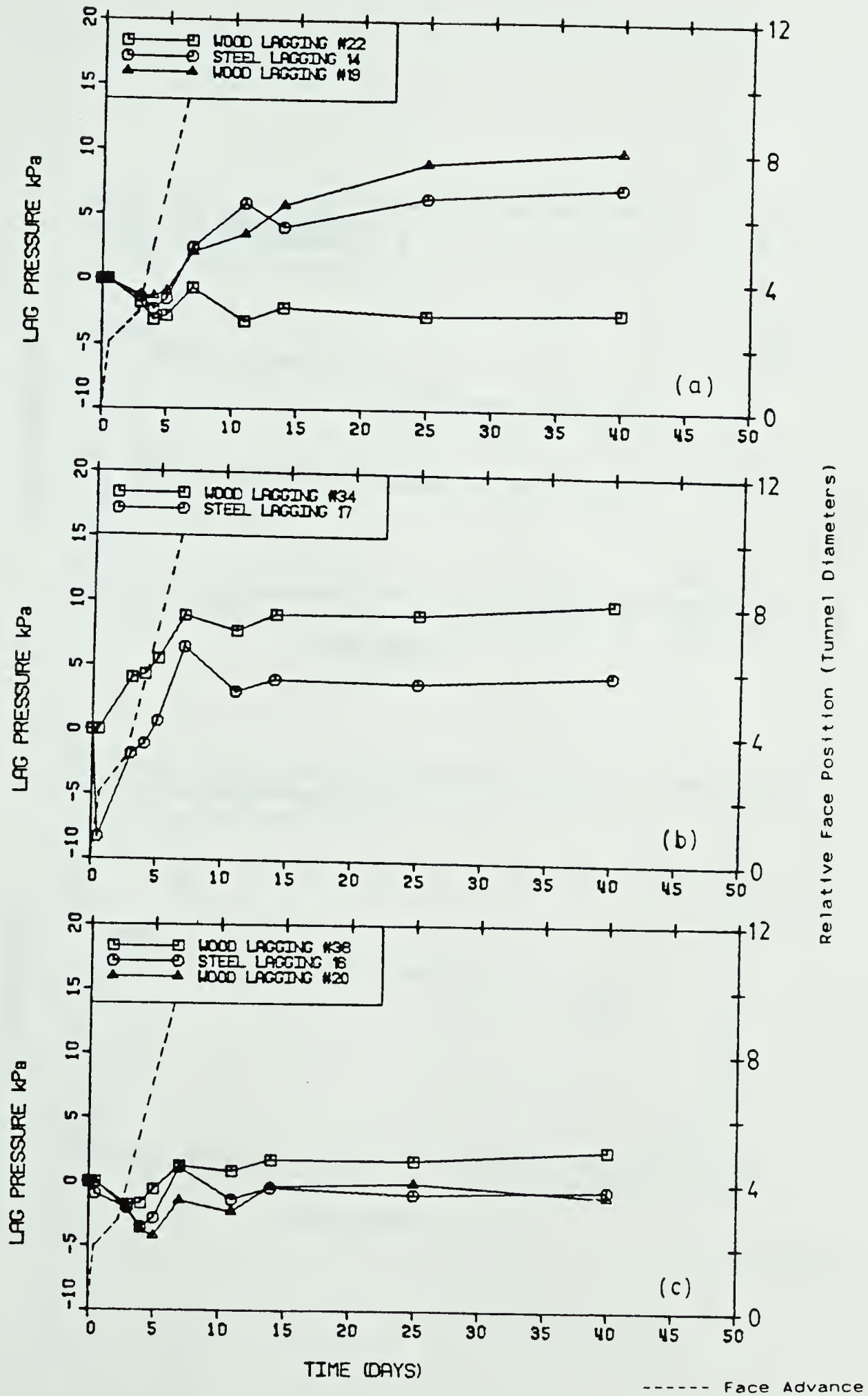


Figure 5.9 Test Section 2 : Rib1 Tunnel Crown Pressures

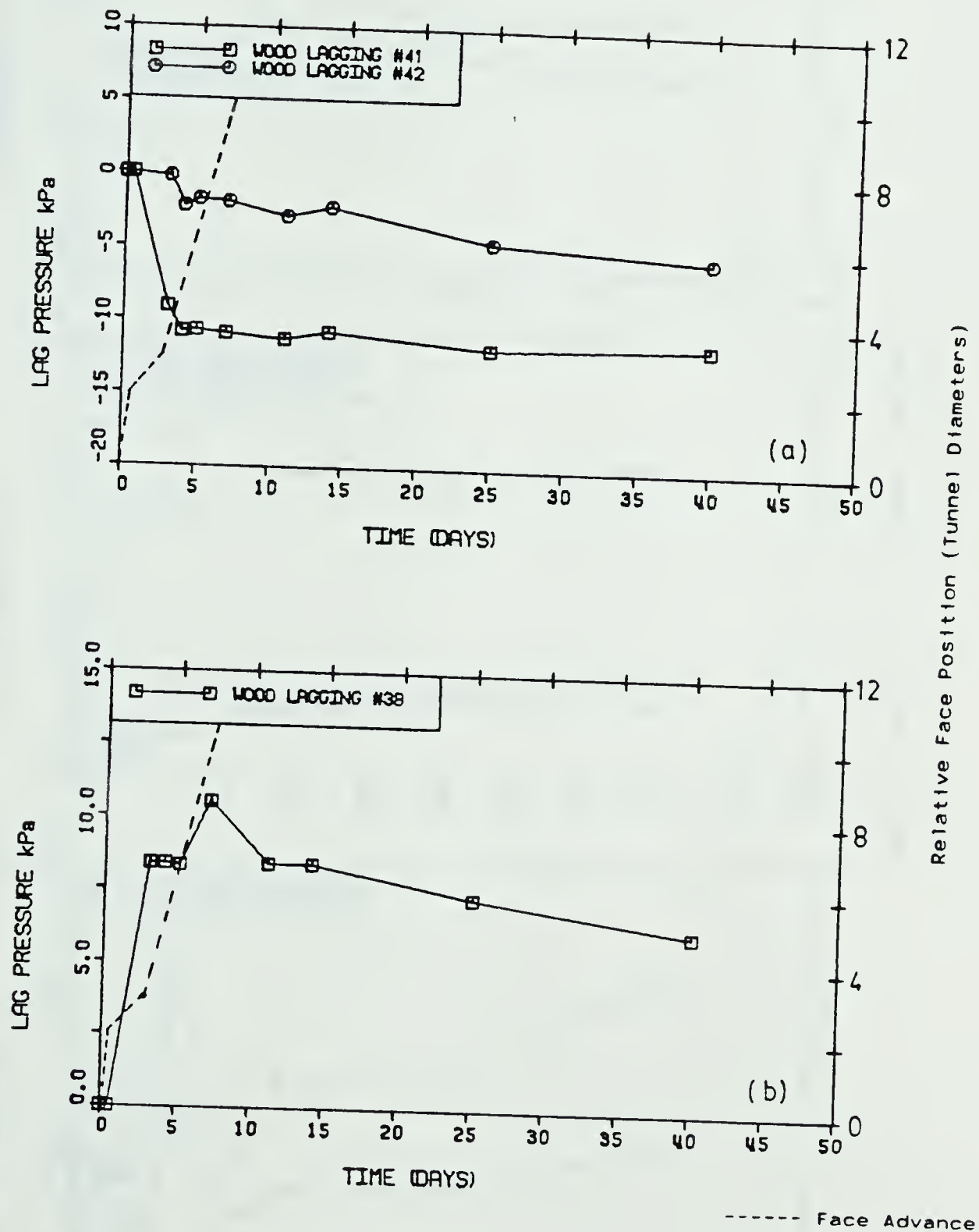


Figure 5.10 Test Section 2 : Rib2 Tunnel Springline Pressures

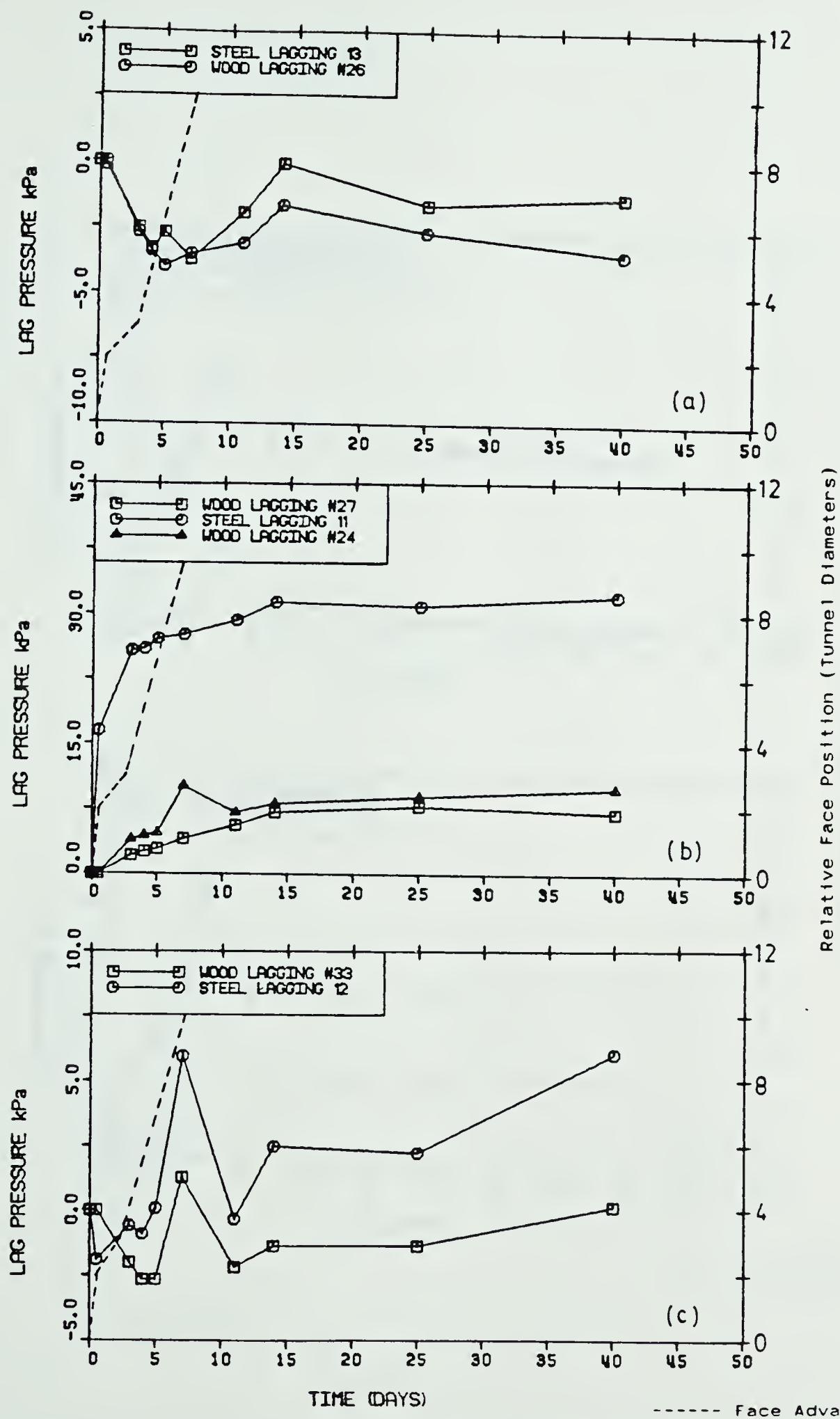


Figure 5.11 Test Section 2 : Rib2 Tunnel Crown Pressures

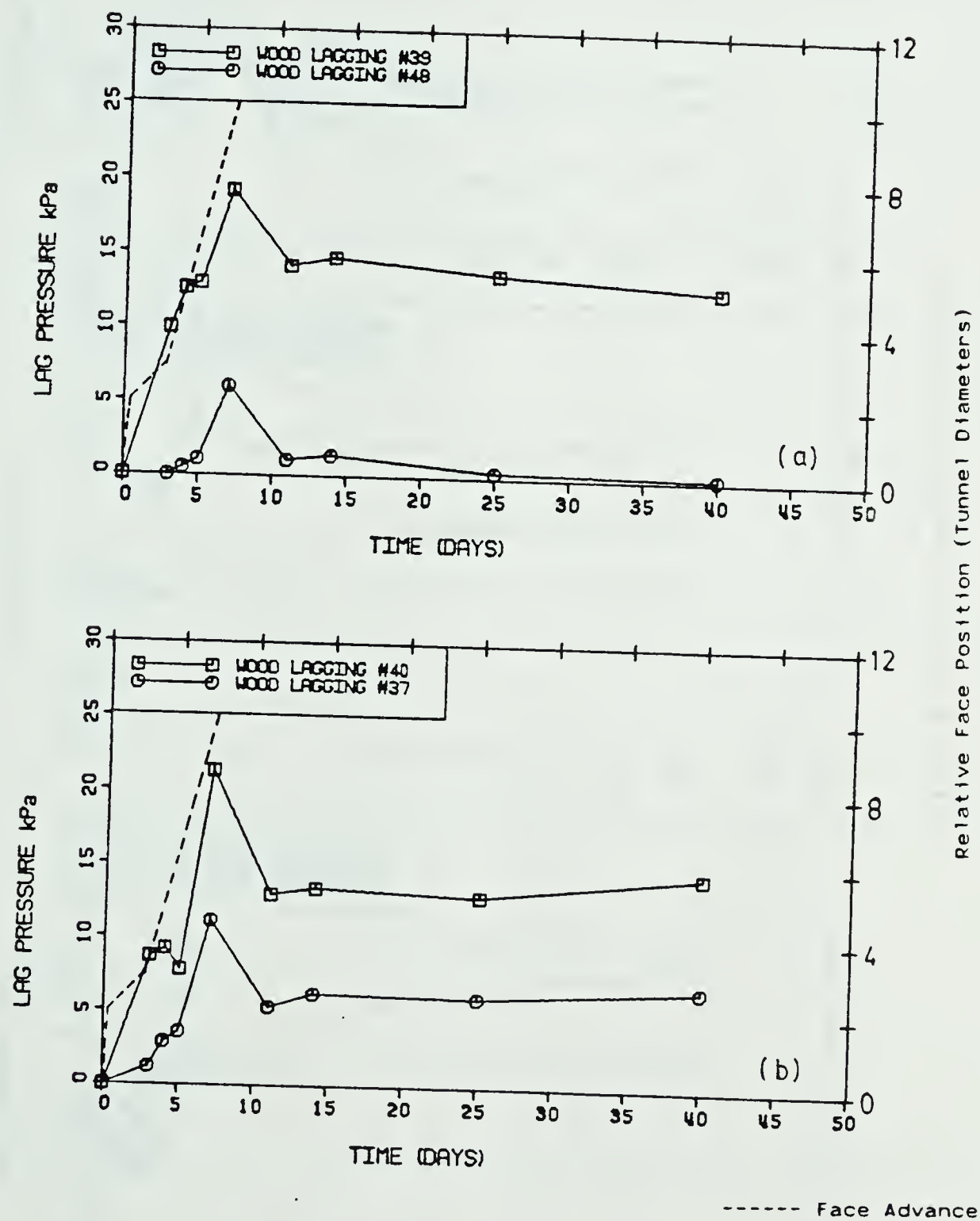


Figure 5.12 Test Section 2 : Rib3 Tunnel Springline Pressures

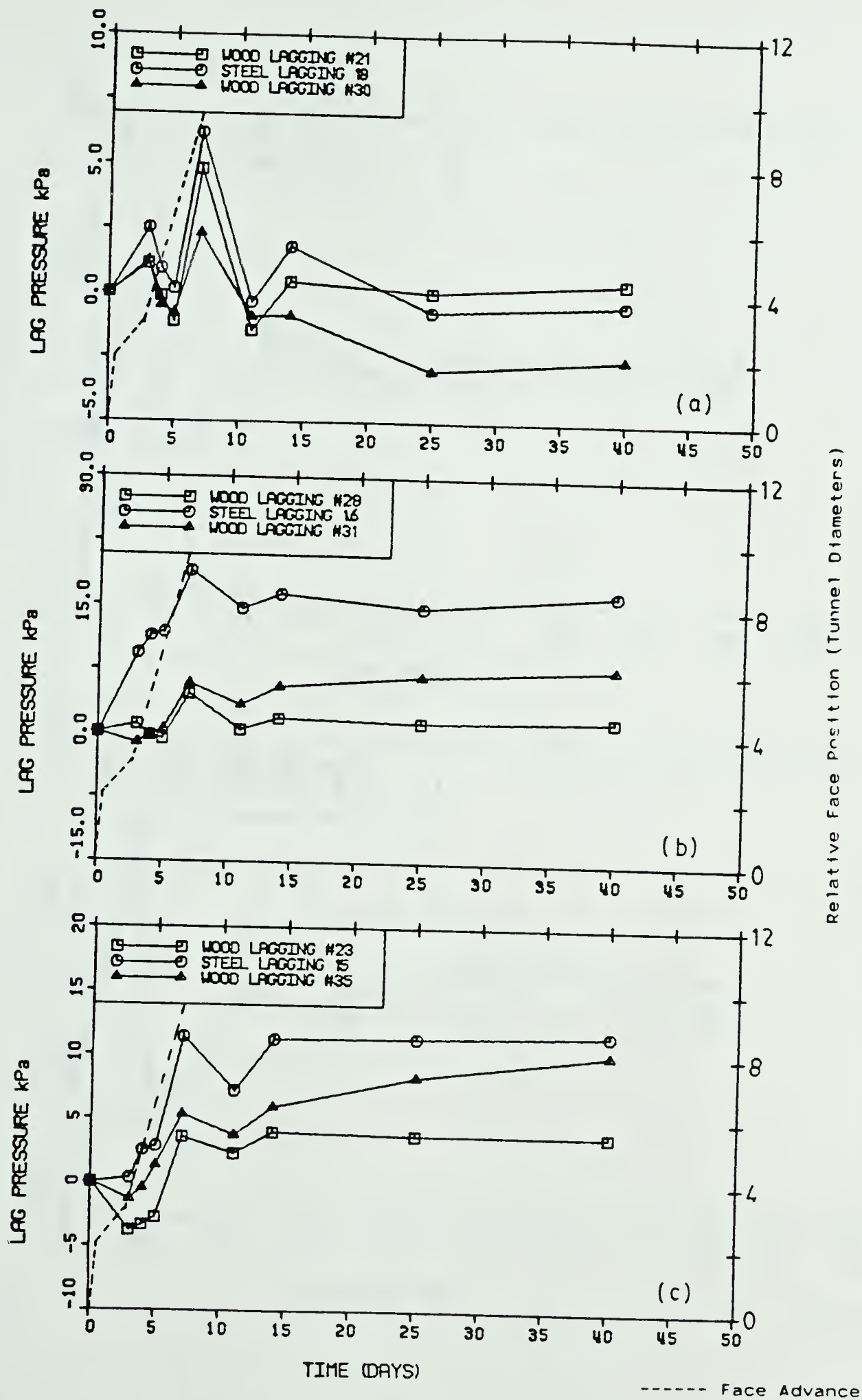


Figure 5.13 Test Section 2 : Rib3 Tunnel Crown Pressures

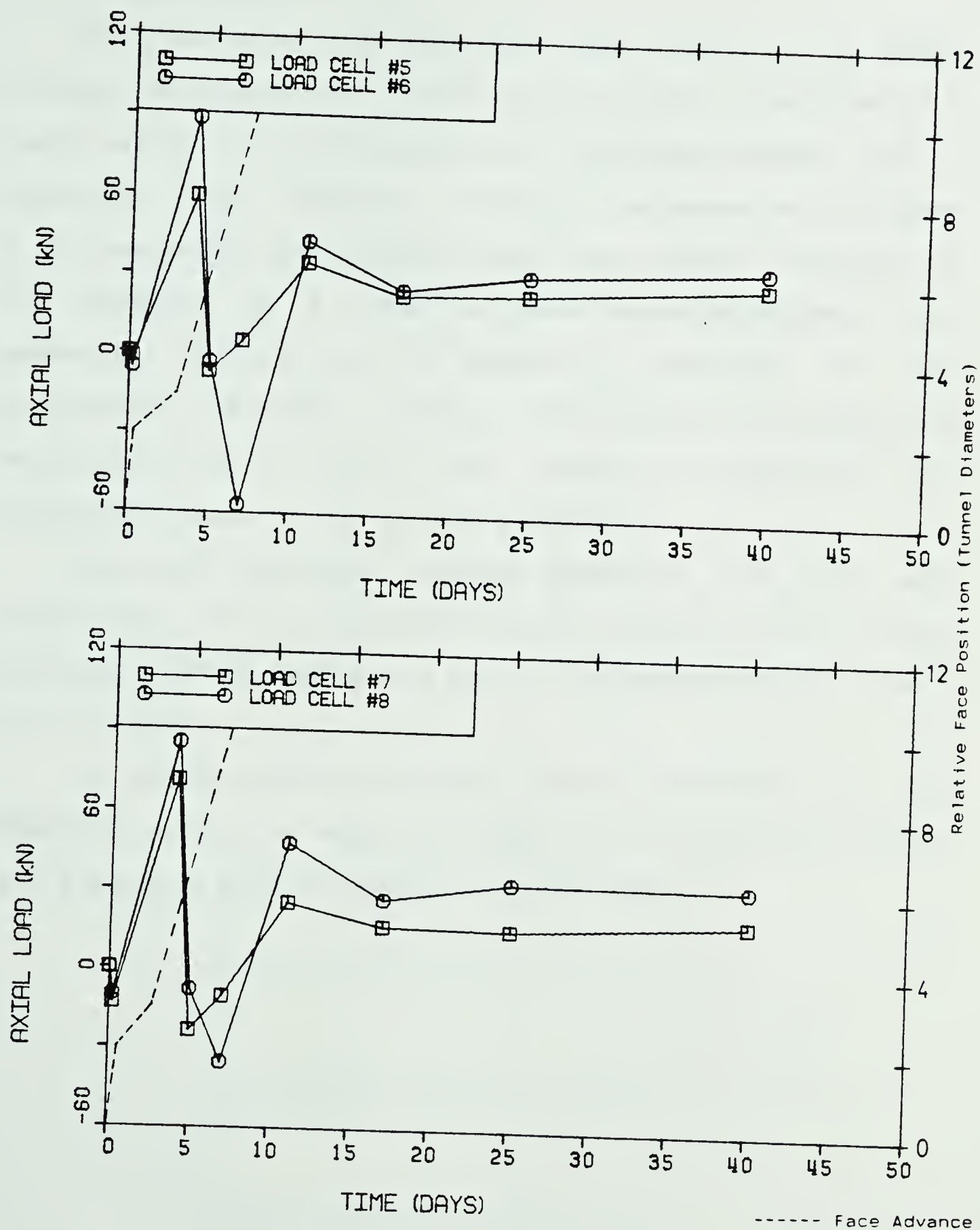


Figure 5.14 Test Section 2 : Load Cell Axial Loads

5.1.3 Test Section 4

Like the other test sections, Test Section 4 is shown located on Figure 5.1 . In total the section consisted of 4 load cells, 30 calibrated wood laggings($t=80\text{mm}$) and 9 simulated steel laggings arranged as presented in Figure 5.15. Overburden depth varied near the section because of the presence of a recently constructed embankment. Full geometric details of the tunnel in relation to the embankment are given in Figure 5.16 . Using a rectangle, of equivalent area to that of the triangular embankment, an overburden depth of 16.7m was calculated.

Derived "equivalent" lagging pressures and load cell axial loads, calculated using similar assumptions and method as those in Test Sections 1 and 2, are presented in Figures 5.17 to 5.23.

It should be noted that all figures presented in this Chapter containing measured lagging and/or load cell values are presented with a viewpoint facing WEST.

AMERICAN MEDICAL ASSOCIATION
PUBLISHED WEEKLY
CHICAGO, ILL., U.S.A.
Subscription price, Five Dollars Per Annum in Advance
Single Copies, Fifteen Cents
Entered as Second-Class Matter, May 2, 1912
Postpaid
Acceptance for mailing at special rate of postage provided for in Act of October 3, 1917
Authorized by Act of October 3, 1917
Copyright, 1918, by American Medical Association
Printed at the American Medical Association, 535 North Dearborn Street, Chicago, Ill.
Second-Class Postage Paid at Chicago, Ill.
Postmaster: This publication is entered as second-class matter under Post Office No. 100, Chicago, Ill., and is paid for at special rate of postage provided for in Act of October 3, 1917. It is published weekly except on Sundays and public holidays. It is published for the American Medical Association, of which it is the official journal. It is published for the American Medical Association, of which it is the official journal. It is published for the American Medical Association, of which it is the official journal.

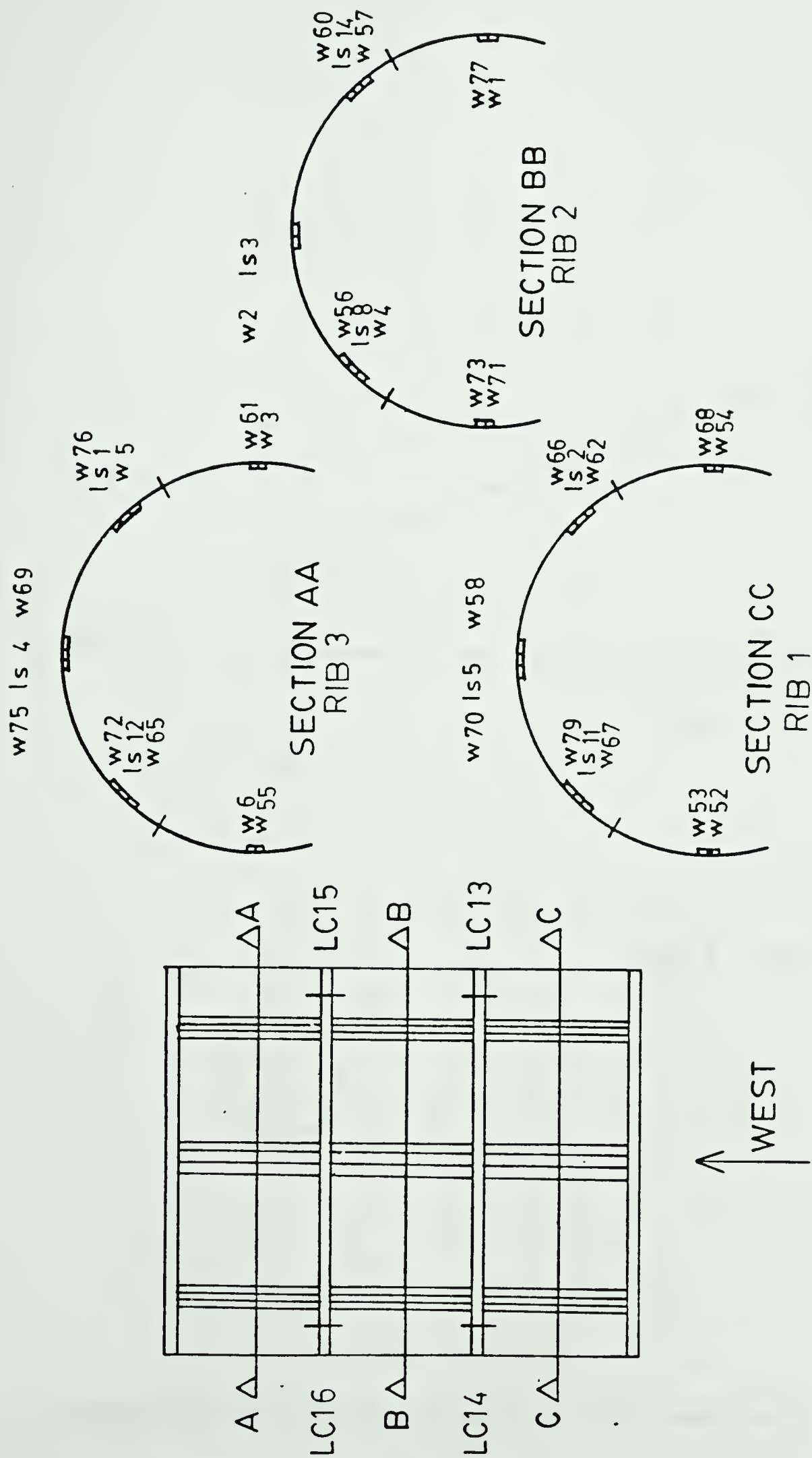


Figure 5.15 Configuration of Test Section 4

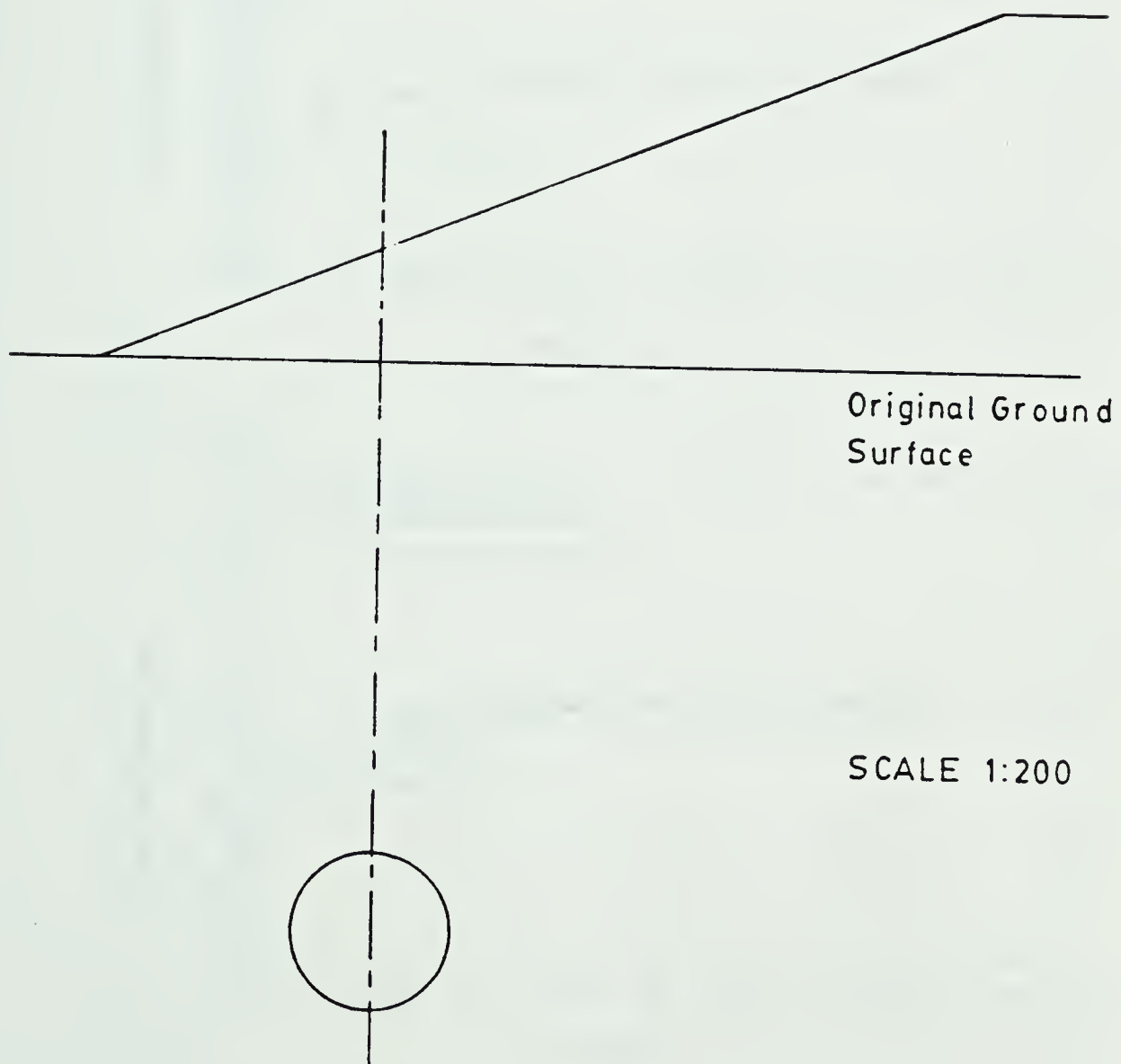


Figure 5.16 Overburden Details at Test Section 4

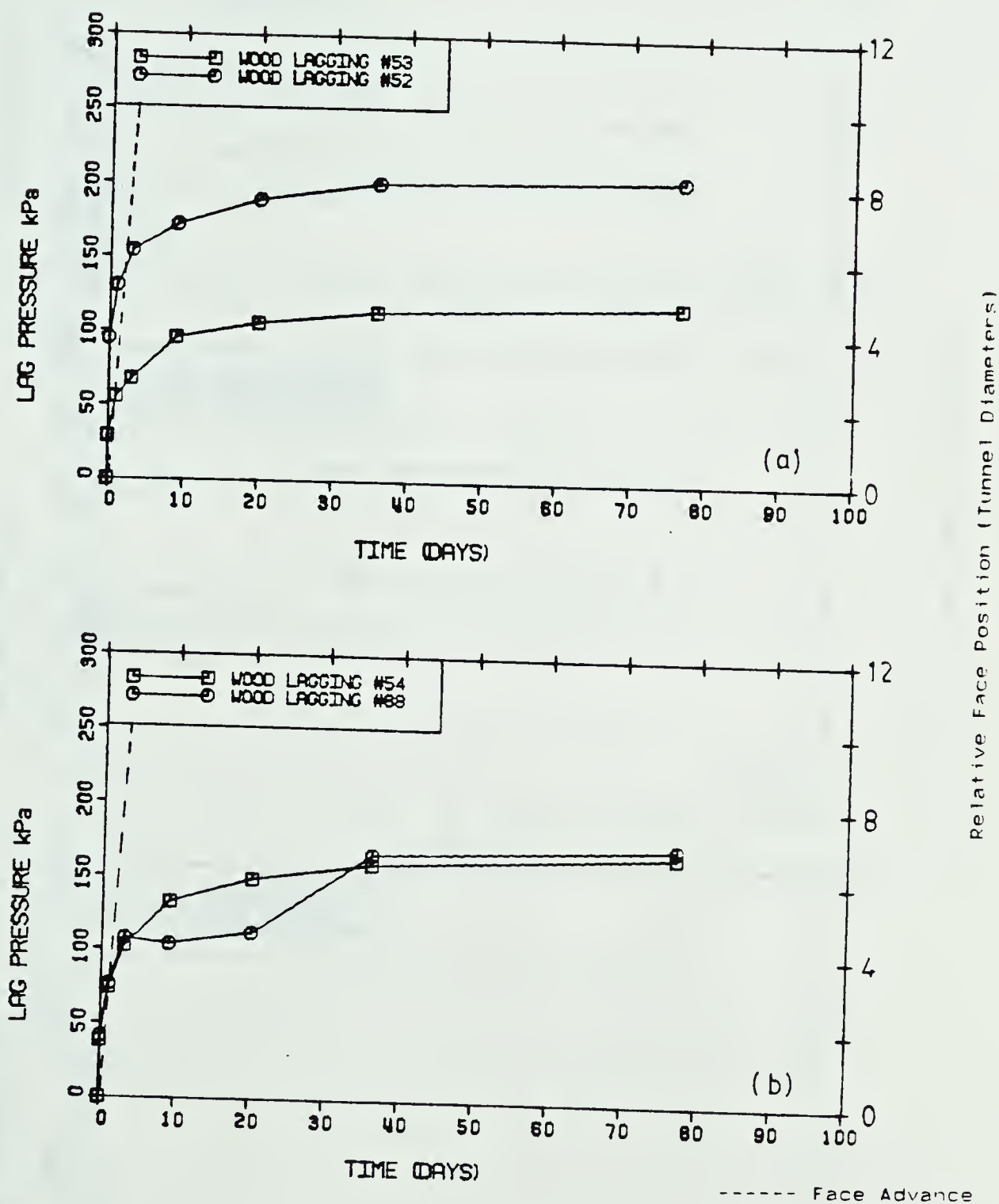


Figure 5.17 Test Section 4 : Rib1 Tunnel Springline Pressures

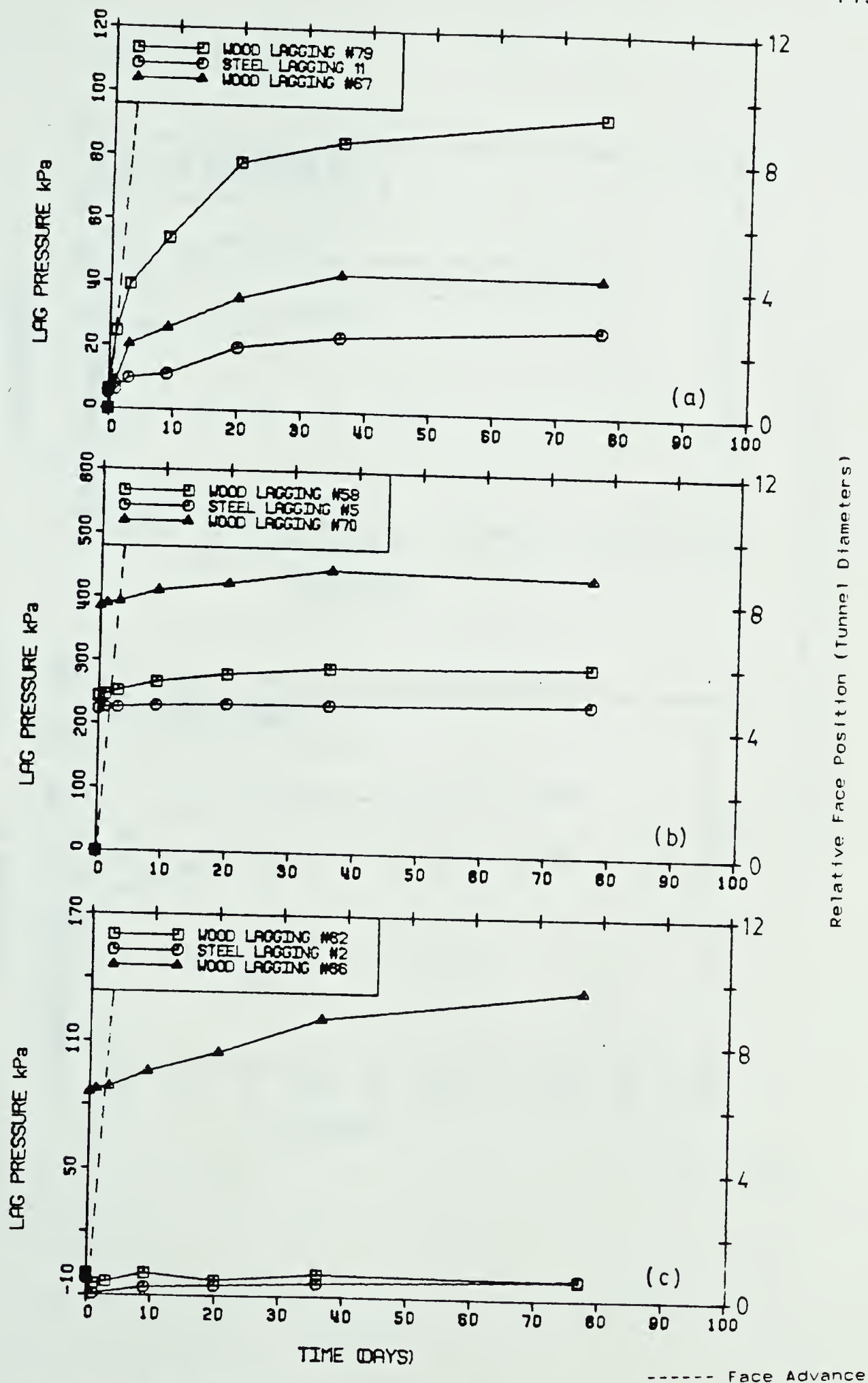


Figure 5.18 Test Section 4 : Rib1 Tunnel Crown Pressures

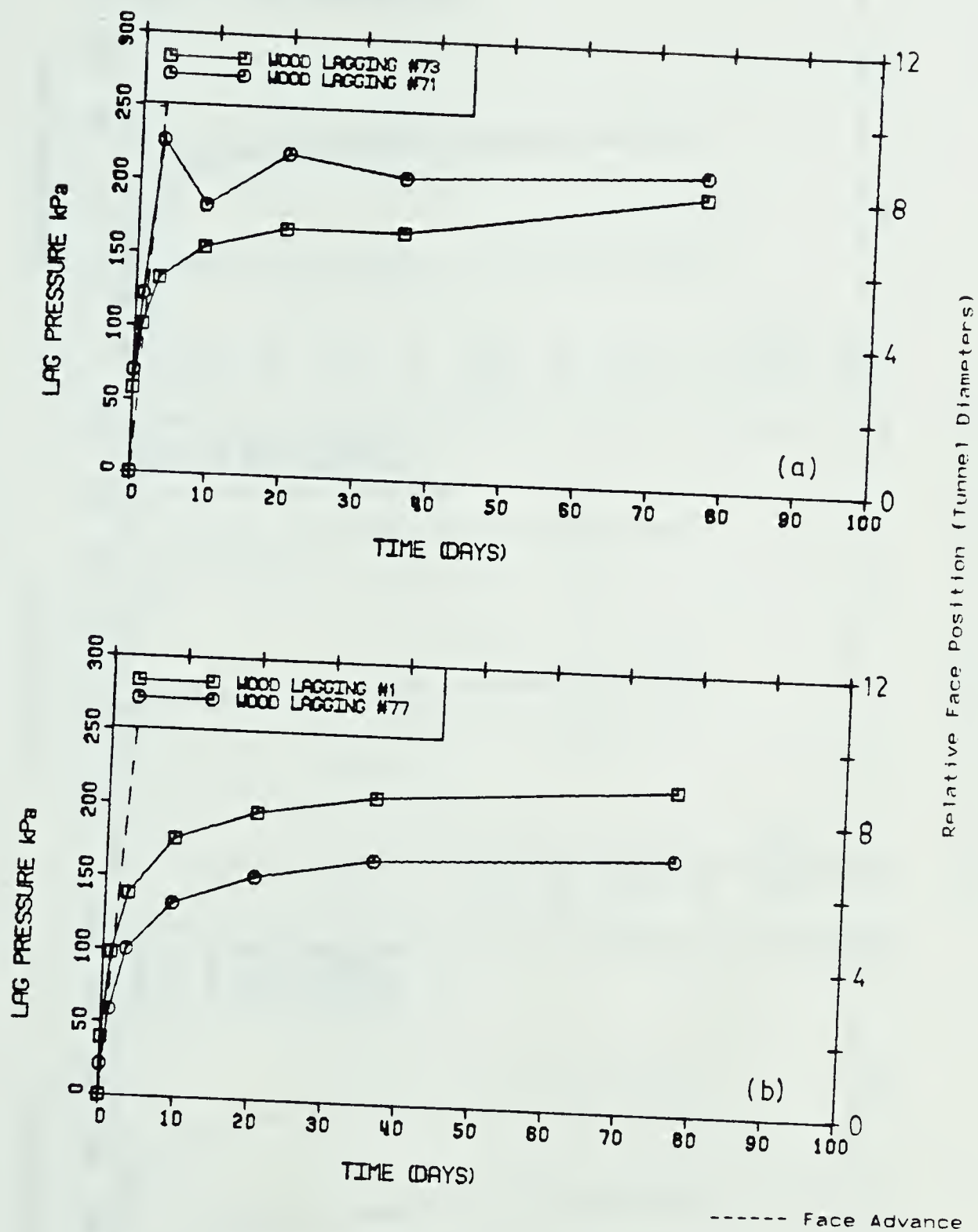


Figure 5.19 Test Section 4 : Rib2 Tunnel Springline Pressures

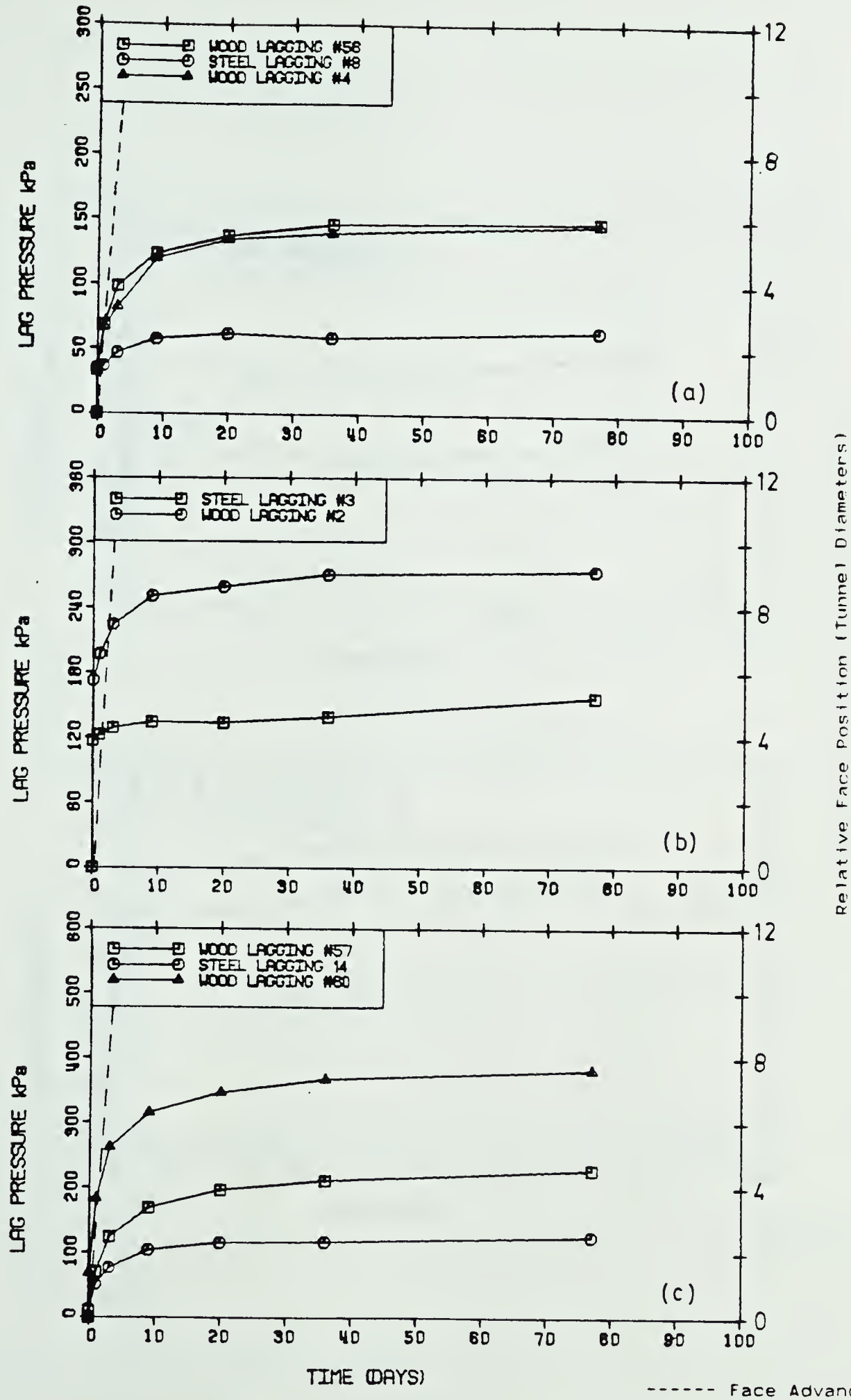


Figure 5.20 Test Section 4 : Rib2 Tunnel Crown Pressures

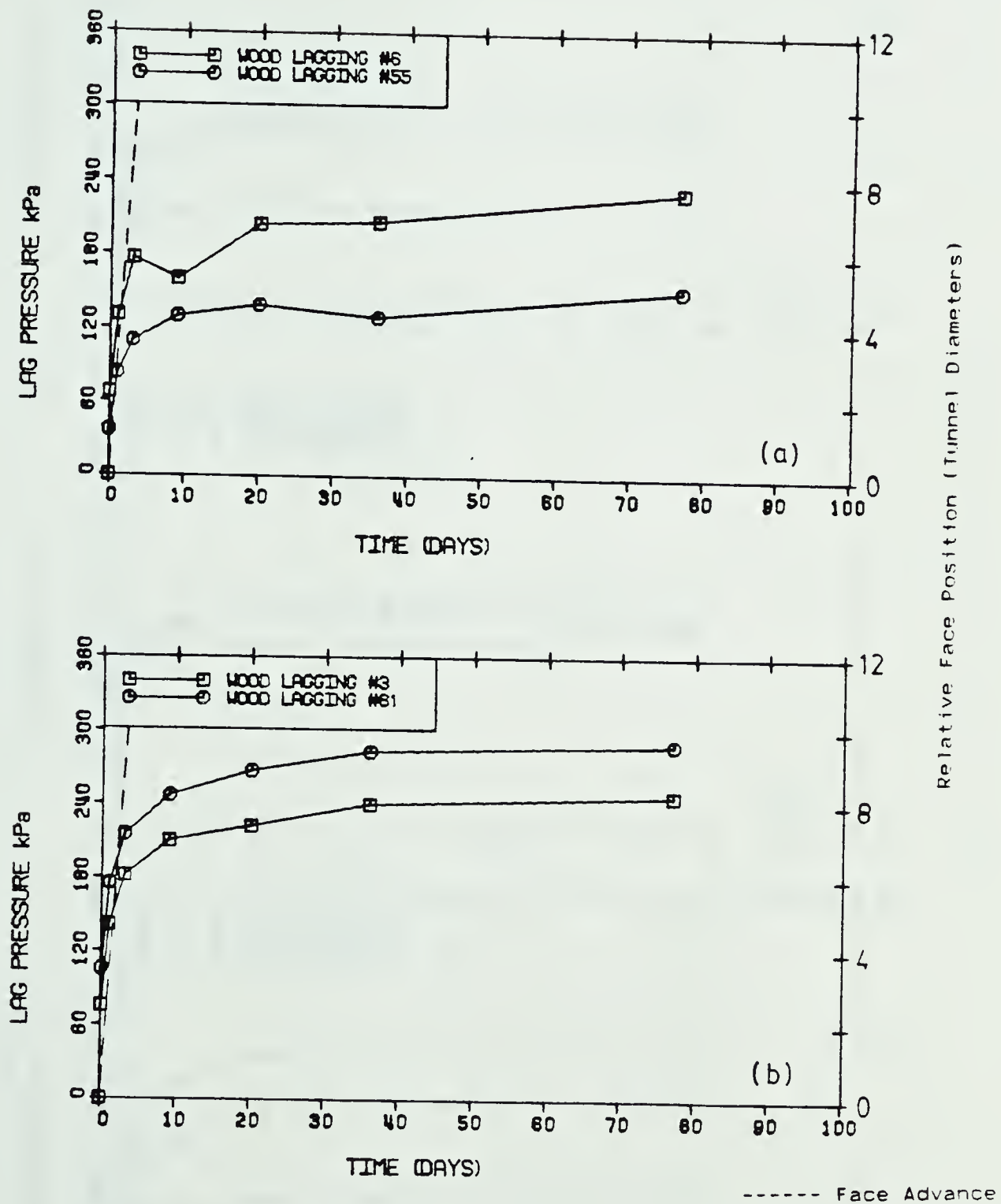


Figure 5.21 Test Section 4 : Rib3 Tunnel Springline Pressures

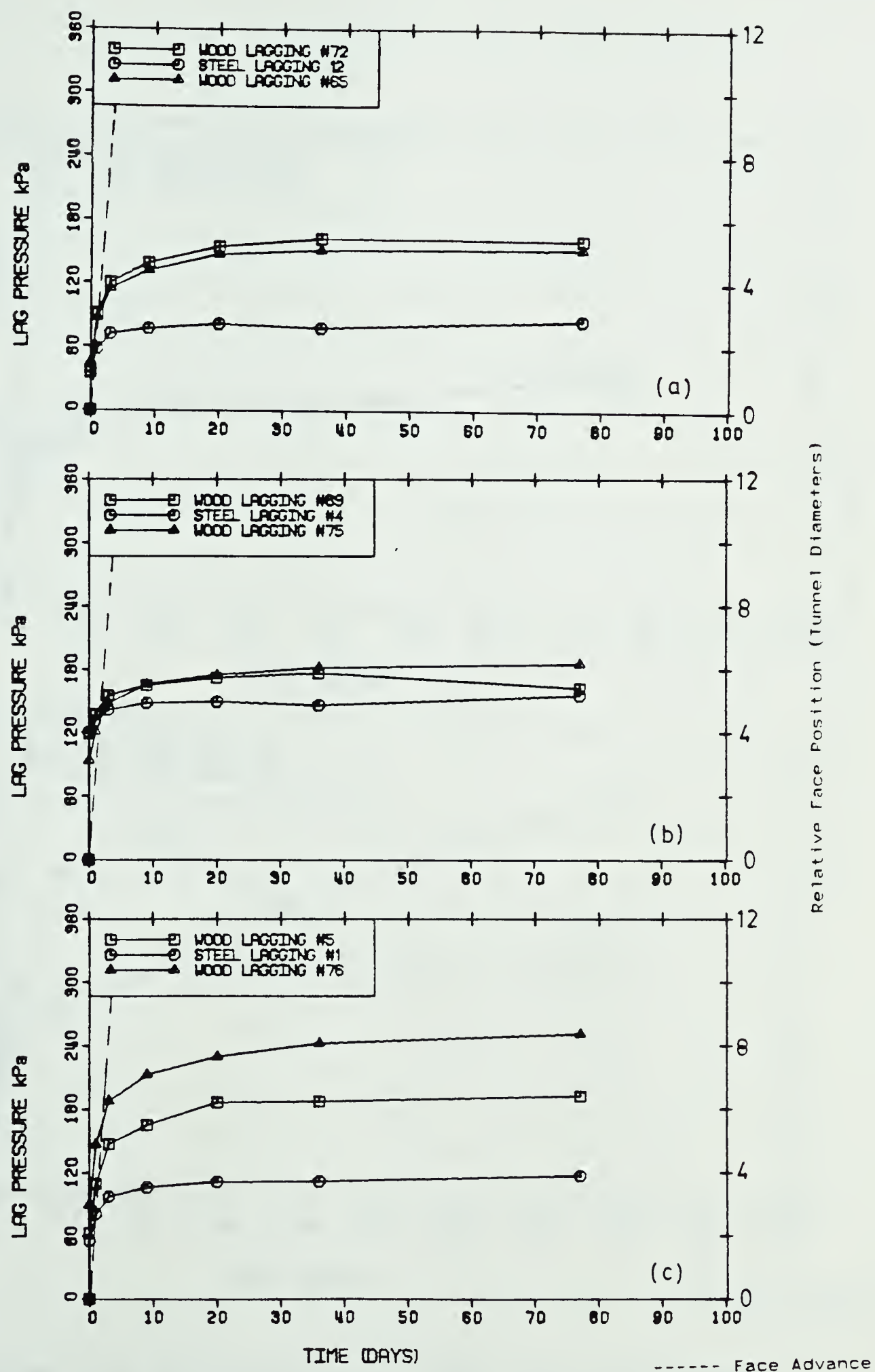


Figure 5.22 Test Section 4 : Rib3 Tunnel Crown Pressures

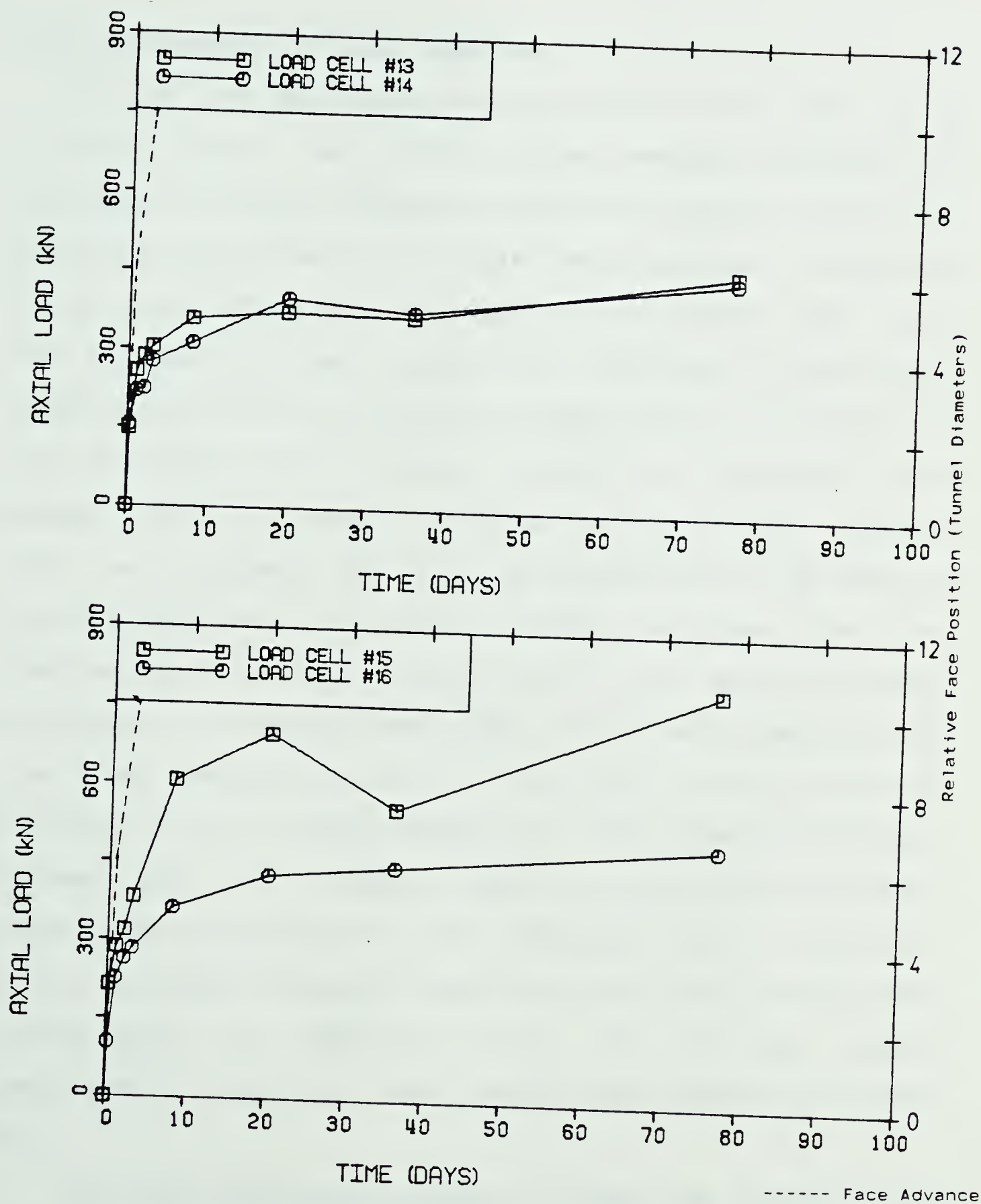


Figure 5.23 Test Section 4 : Load Cell Axial Loads

5.2 Discussion of Tunnel Support Pressure Measurements

5.2.1 Performance of Wood Laggings

As has been mentioned previously one of the main aims of this project was to test whether adequate accuracy for prediction of support pressures could be obtained utilizing deflection measurements of regular wood laggings, as opposed to the relatively expensive lagging simulations. With this aim in mind it was decided to instrument a particular location using sets of simulated steel laggings flanked by two calibrated wood laggings. Using this technique it was assumed that the pressures observed by the steel lagging could be calculated with high enough accuracy to be used in direct comparison with pressure values obtained from the wood laggings. As shown in Figure's 5.2, 5.7 and 5.15, sets, or groups of 3 laggings(wood steel wood), were placed at the crown and shoulder points of a rib. Shear forces around the periphery of the lining, caused by the relative movement between soil and lining, result in load vector rotation which is more pronounced at the shoulder point locations. For this reason pressures observed in the crown region were investigated for compliance with the already stated performance criterion. These results are tabulated in Table 5.1 .

The data presented in Table 5.1 show that observed wood lagging pressure values were consistently lower than those for the steel laggings in the first two sections with the

Table 5.1 Comparison Values Between Steel and Wood Lagging Pressures

Test Section #	Rib #	Derived Pressures (kPa)			
		Wood Left	Steel Centre	Wood Right	Average
1	1	17.80	27.23	0.82	15.30
	2	9.40	24.41	10.60	14.80
	3	12.90	31.60	14.10	19.50
2	1	10.10	4.60	-	7.40
	2	7.10	32.00	9.90	16.30
	3	1.80	16.50	7.80	8.70
4	1	437.00	240.00	298.00	325.00
	2	274.00	157.00	-	215.50
	3	185.00	155.00	162.00	167.30

reverse occurring in the highly loaded Test Section 4. Initially, therefore, it could be concluded that our performance criterion had not been met. Considering the full loading history it is seen, however, (e.g. Figure 5.22) that immediately after rib expansion, the steel and wood laggings show a very similar loading history, i.e., parallelism between all three boards as would be expected. From this it was inferred, that during expansion of the laggings plus associated shoving forces from the mole, something different happened between lagging types resulting in the observed pressure differences. This dissimilarity is believed to be directly attributable to a slight difference in length between the wood and steel laggings, i.e., the steel laggings were constructed a little shorter than the rib spacing so that end effects would not occur. The wood laggings, which were not treated in this manner, may have been loaded by end moments resulting from the two mechanisms outlined in Figure 5.24. While the mechanisms outlined in Figure 5.24 could be readily identified, their exact magnitudes were almost impossible to predict for a variety of reasons.

Mechanism 1

1. The exact geometry was not known and was dependent on the lateral position of the expansion ram.
2. The expansion force was not known accurately

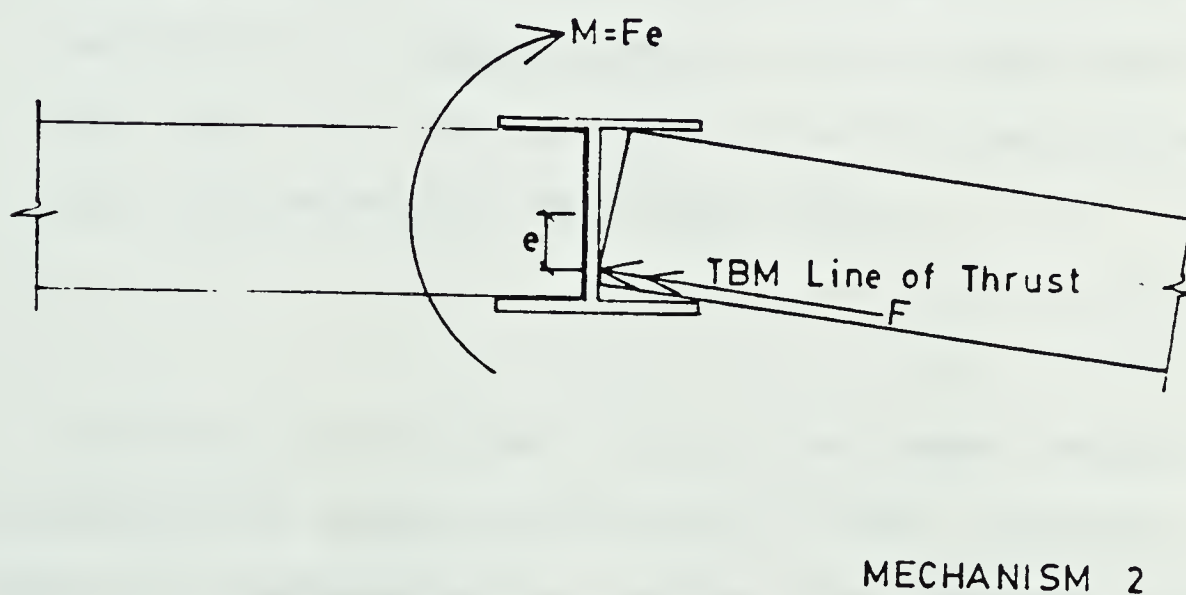
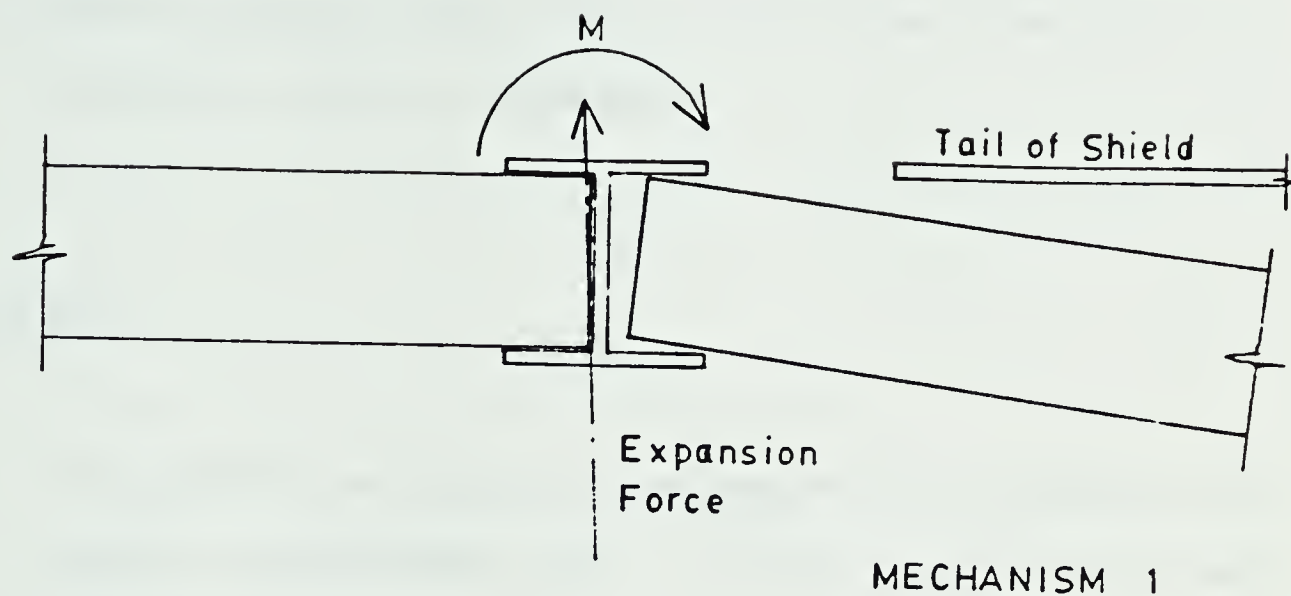


Figure 5.24 Mechanisms for TBM Induced Lagging Moments

although it is suggested for future works that this force be recorded as a regular part of construction activity.

3. Some laggings were affected more than others due to variable lagging thickness.

Mechanism 2

1. Force "F" from the mole was not known although it is again recommended that a record of this be kept during shoving.
2. The eccentricity of the force was unknown and very difficult to obtain.
3. Some boards were affected more than others due to variability in lagging lengths, i.e., total push of the mole only goes through an unknown percentage of all the boards in a particular rib.

Having qualitatively identified some causes for variability in lagging deflections it was necessary to obtain a "representative value" for induced lagging pressures. Because of problem complexity this could not be calculated and therefore must instead be estimated from field measurements. Investigation of the pressure time curves of Test Sections 1 and 2 (Figures 5.3 to 5.5

and 5.8 to 5.13) yielded an apparent mean induced pressure due to expansion related activities in the order of -10kPa . This value was determined mainly from shoulder point boards where soil loads were less dominant. Although larger extreme values did exist, this appeared to be a good average. This conclusion was reinforced by a much improved correspondence between steel and wood lagging pressures, as listed in Table 5.1, when wood values are incremented by 10 kPa .

Considering pressure diagrams (Figures 5.17 to 5.22) from Test Section 4 it can be seen that a reverse in pressure values existed, i.e., wood pressures were larger than those of the steels. As in Test Sections 1 and 2 similar loading histories were observed after emergence from the mole influenced area. In this instance the pressure disparity was believed to be attributable to differences in the stiffness of the steel and wood laggings at this section, i.e., steel laggings were one third the stiffness of the woods. This stiffness difference resulted in a large difference between observed steel and wood deflections, i.e., $\delta u = 5\text{-}10\text{mm}$. These deflection variances may have caused some stress transfer to occur over the softer steel lagging.

Although the original performance criterion of pressure equality was not been met for reasons previously stated, confidence in the predictive

capability of wood laggings was gained from observation of similar load history records for wood and steel, after emergence from the mole effected area. Further confidence in the wood laggings was gained from the development of similar records of two wood laggings installed at the same location(e.g.Figures 5.8, 5.16a, 5.18, 5.19a).

It is from load history records and pressure similarities at the same location that we have concluded wood laggings can be used to predict lining pressures.

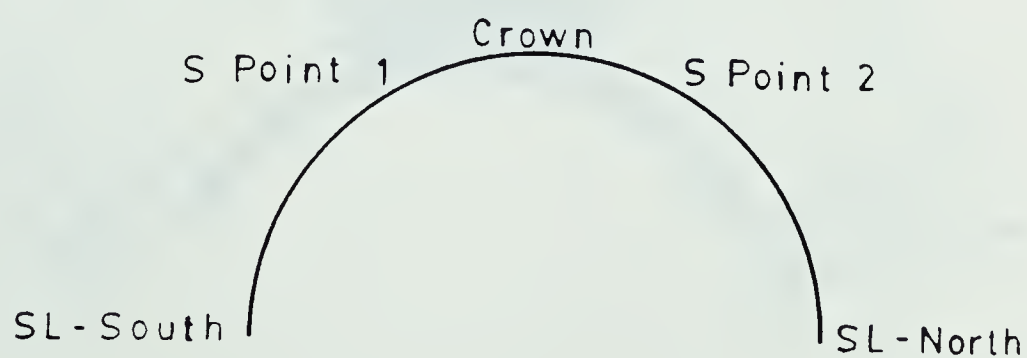
While confident in pressures obtained by the wood laggings, it must be remembered that an approximate underestimation of 10kPa because of mole related activities was concluded. While this error magnitude is small it will have a very dominant effect on predicted pressures under conditions of low soil pressure.

5.2.2 Discussion of Lagging Pressures

Resultant pressure distributions derived from lagging measurements are presented in Figures 5.25, 5.26 and 5.27 for Test Sections 1, 2 and 4 respectively. The pressure plotted in these diagrams was an average of the three(or two) laggings located together. Where negative pressures existed, zero was assumed, unless after obtaining a negative value upon expansion the pressure curves began to show an increase. In this instance the net increase was taken as the pressure. These pressures have been summarized in Table 5.2.

Table 5.2 Average Lagging Pressures for Test Section 1, 2 and 4

Test Section #	R1b #	AVERAGE LAGGING PRESSURE (kPa)				
		SL-South	S Point 1	Crown	S Point 2	SL-North
1	1	-	0.0	15.9	4.7	-
	2	-	3.3	14.8	2.2	-
	3	-	4.2	19.6	3.2	-
2	1	10.0	7.3	11.5	2.7	9.9
	2	0.0	0.7	16.4	3.6	6.1
	3	6.5	0.6	9.3	10.2	10.6
4	1	162.2	54.6	324.4	49.7	170.1
	2	206.8	119.1	215.5	244.7	197.5
	3	192.1	133.1	167.8	186.4	267.5



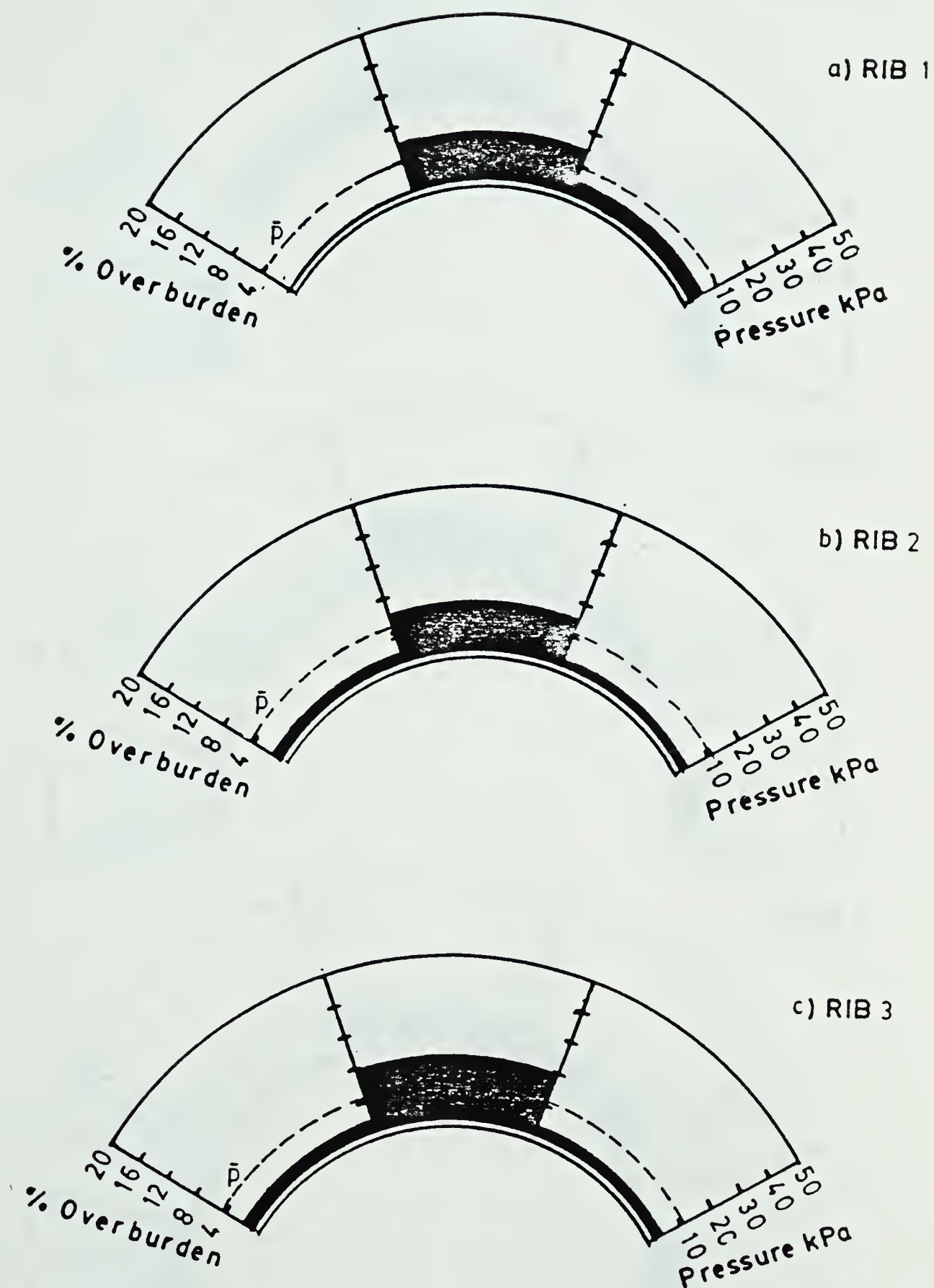


Figure 5.25 Average Pressures for Test Section 1

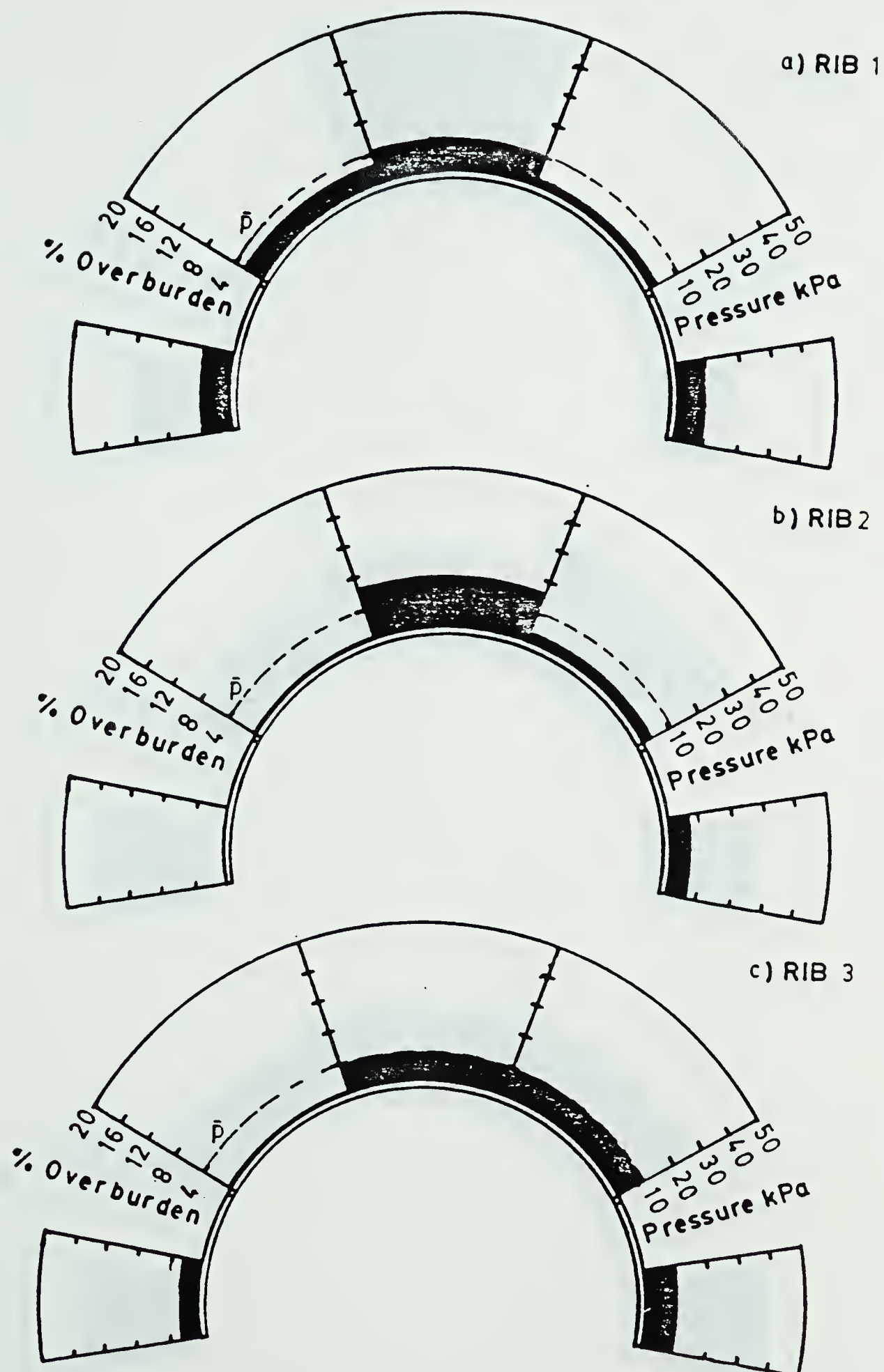


Figure 5.26 Average Pressures for Test Section 2

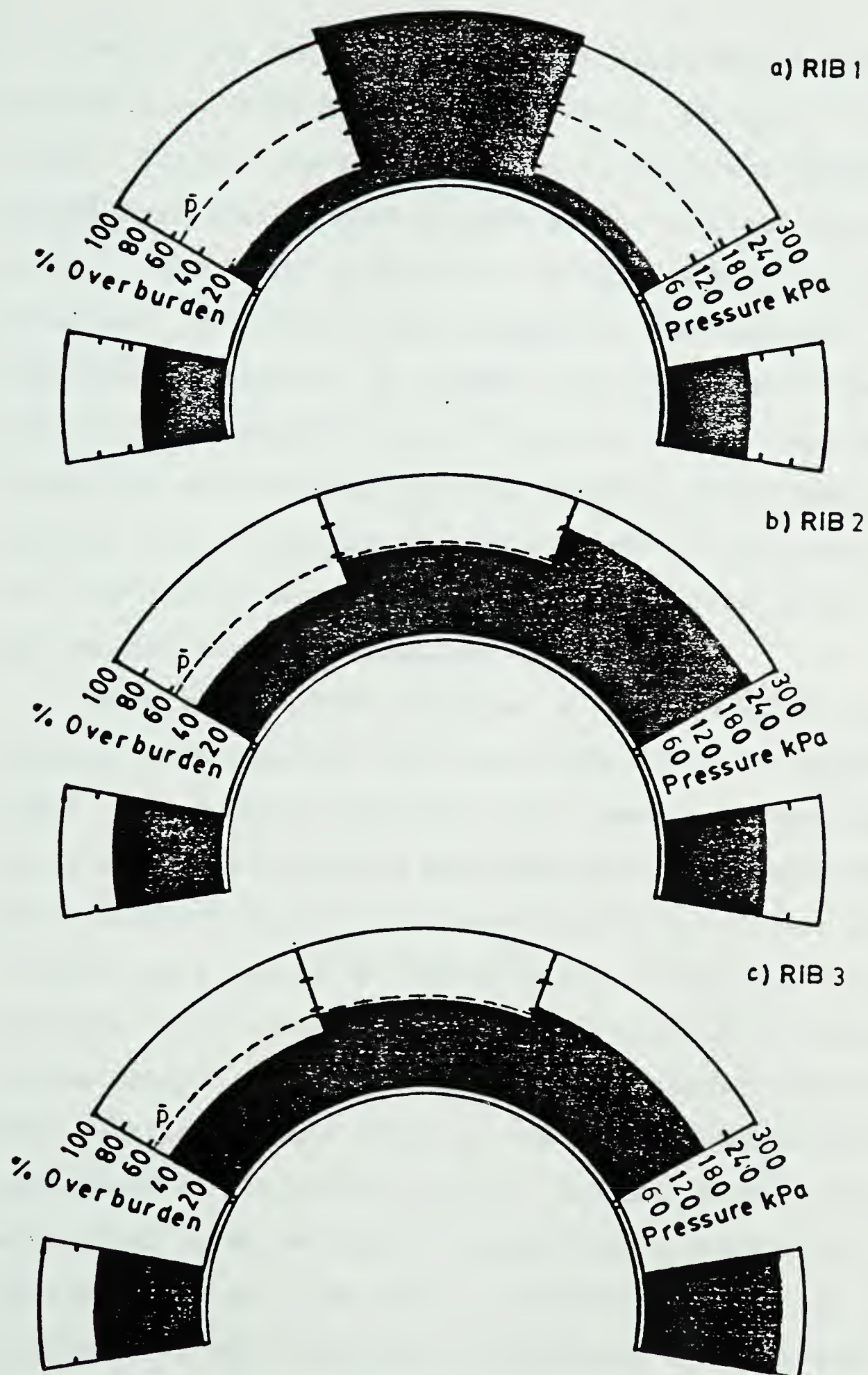


Figure 5.27 Average Pressures for Test Section 4

Near Test Sections 1 and 2 the loads were small with a maximum of only 8% of overburden (Test Section 1 Rib 3, Figure 5.25c). Furthermore, most of the rings demonstrated symmetrical loading with respect to the vertical axis of the tunnel. At Test Section 2 (Figure 5.26) equality of pressures at crown and springline was observed. This observed symmetry of loads and crown-springline load equality were expected for a flexible lining system (Peck, 1969) such as the steel and wood lagging system used in this project. Minor discrepancies were caused by mole activities as previously discussed and also because the lining system was neither perfectly flexible or symmetric.

Focusing on Test Section 4 (Figure 5.27), observed pressure distributions were again approximately symmetrical about the tunnel vertical axis. Near equal pressures at crown and springline were also observed. Pressure magnitudes were however, greatly increased over those of Test Sections 1 and 2 (by a factor of approximately 10). This pressure increase could be directly related to poor ground conditions at the section location coupled with increased overburden at the section brought about by the recent construction of an embankment on the ground surface (Figure 5.16). Using an equivalent area rectangle, as previously explained, a depth of overburden = 16.7m and a vertical stress of 318kPa ($\gamma=19\text{kN/m}^3$) were obtained. Using this field stress value, extremely high lagging pressures, typically 65 to 75% of overburden were calculated. These pressures may have been

slightly high as they were undoubtedly influenced by excessive deflections of the ribs at Test Section 3 (Figure 5.1), just 1.2m from Rib 1 Test Section 4. This bending of the ribs, which occurred due to the formation of a void along the north side of the tunnel was remedied by creating a stiffer section using shoring techniques. After overloading of these ribs stress transfer mechanisms around the void in directions perpendicular and longitudinal to the tunnel axis was thought to have occurred. Occurrence of these mechanisms was demonstrated by the higher pressures in Ribs 1 and 2 of Test Section 4 and the slightly higher pressures on the north side of the tunnel. Ignoring these slight abnormalities, it was still evident that high earth pressures existed in this region. This reflected the influence of excess overburden and poor ground conditions.

Regarding Rib 1 Test Section 4, the very low shoulder point pressures observed were believed to be related to void influence, i.e., due to the proximity of the void little pressure was applied to the north side of this rib. As pressure began to build up on the south side of the rib it moved bodily northwards until activating pressures from the south ceased.

Finally, regarding all sections it was observed that pressure distributions were typical of those expected for a flexible lining system. These pressures, in the main part controlled by wood lagging determinations, are further evidence of the predictive capabilities of wood laggings.

5.2.3 Discussion of Load Cell Results

Recorded axial loads, calculated using the method presented in Chapter 3, are shown in Figure's 5.6, 5.14 and 5.23 for Test Sections 1, 2 and 4 respectively.

Considering Test Sections 1 and 2 (Figures 5.6 and 5.14) placed in what was considered similar ground, gave dissimilar load development in time and magnitude, i.e., magnitude of approximately 60kN in Test Section 1 compared with 30kN in Test Section 2. This contradicted information from the measured pressures in these two sections (Figure 5.25 and 5.26) which showed similar loads. Load development in the load cells was, however, in keeping with that recorded by the laggings, i.e., Test Section 1 showed a steady increase with time while Test Section 2 remained essentially constant. This soil creep behaviour, reported by Peck (1969), was only present in Test Section 1 and the only area in this project where any appreciable time dependancy was detected. This loading difference was thought to be the result of subtle construction differences between sections. The earlier reported 3 day delay before expansion of Rib 3 of Test Section 2 was also believed a contributory factor towards the observed differences. It should be noted with regard to load magnitudes in these sections, that due to over design the Load Cells were operating at less than 10% of their design maximum, therefore actual magnitudes may be in error.

Finally with regard to magnitude trends, it was seen that similar axial thrust on opposite sides of the steel set have developed. Again, this was expected for a flexible liner and corresponded with observations from lagging pressures, i.e., symmetry of loads.

Focusing on Test Section 4 (Figure 5.23), it was observed as with lagging pressures that an enormous increase in load magnitude occurred relative to those of Test Sections 1 and 2. Irrespective, however, of load increase, symmetry of loads was still observed, especially good in Figure 5.23a. In Figure 5.23b the exact magnitude of Load Cell 15 was not known as the elastic limit of the cell, calculated at 500kN, was exceeded. It can be assumed, however that its load was more than that observed by Load Cell 16, present in the same steel set. The higher load at this location (south side) was in response to higher shoulder point pressures observed on the north side of the tunnel (Figure 5.27b and c).

With regard to load history it was observed, unlike in Test Sections 1 and 2, that a contrast between load build up on the laggings compared to the load cells existed. In the laggings, pressure after 10 days increased by an amount approximately 10% of the 10 day load while the load cells showed an increase of 30 to 40% over the same time period. This difference was thought to be directly attributable to consolidation of the material found at the section. That is, during excavation, generation of temporarily high pore

pressures reduced the effective stresses in the cohesionless material and afterwards, as the tunnel acted as a drain material consolidation with an associated increase in strength was facilitated. With this strength gain, stress transfer mechanisms in the longitudinal direction between ribs according to Terzaghi (1943) could develop. This stress transfer thus isolated the laggings from further increase in load by transferring it directly onto the steel sets.

5.2.4 Interrelation of Lagging Pressures and Steel Set Loads

A very important relationship for a steel set and wood lagging liner with regard to tunnel monitoring and design is that of loads carried by the laggings compared with those carried by the steel sets. As a lower bound all lagging loads would be expected to be transferred directly to the steel set. However, it has been found (Branco, 1981) that the loads in the steel set may be as much as 3 times those attributable to lagging pressures. This difference is a result of stress transfer mechanisms in the longitudinal direction between ribs. The development of stress transfer mechanisms between ribs was also aided by the large stiffness disparity between the steel sets and laggings.

Before making comparisons between observed lagging loads and steel set loads the problem of having lagging loads in the form of pressures while steel set loads take the form of a normal force had to be overcome. Treating the top steel set as a simply supported arch and analysing the

vertical equilibrium of the the system, it was decided to use two comparison criterion as explained subsequently :

Pressure Comparison

In this case an average pressure "p bar" was calculated such that the calculated pressure would account for the resultant vertical force in the load cells. A ratio between "p bar" and the average measured pressure around the steel set was then calculated.

Vertical Load Comparison

The resultant pressure diagrams as presented in Figure's 5.25, 5.26 and 5.27 were analysed such that the total vertical force attributable to the pressure distribution was calculated. The ratio of this load and the resultant vertical force in the load cells was thus found.

For calculation of the ratios, lagging loads were assumed equal to the average value obtained from the two flanking ribs surrounding the load cell infiltrated steel set. The results of this exercise are contained in Table

TEST SECTION #	RIB #	Equivalent Pressure (p bar) (kpa)	Average Meas Pressure (kpa)	p bar/ Av Pressure	(a) Vert Force Load Cells (kN)	(b) Vert Component Meas Pressure (kN)	(a)/(b)
1	1-2	26.40	10.25	2.57	98.50	25.50	3.86
	2-3	27.40	11.80	2.32	102.20	29.10	3.51
2	1-2	16.20	10.60	1.53	60.10	24.40	2.46
	2-3	12.20	10.25	1.19	45.40	25.20	1.80
4	1-2	241.20	168.00	1.44	779.40	564.10	1.38
	2-3	278.50	177.80	1.57	1039.20	569.20	1.83

Table 5.3 Steel Set to Lagging Load Calculation Values

5.3. In Table 5.3 the self weight of the lining was not considered as it was small (2kN) relative to the loads. For clarity the calculated equivalent pressures were plotted in Figures 5.25 to 5.27 .

In the author's opinion the integrated vertical load is more correct as this more correctly takes into account the influence of higher crown pressures. It was reassuring to note, however, that the pressure and load ratios were quite similar.

Considering the magnitude of observed ratios a range of 1.19 to a high of 3.86 was found. Ignoring extreme values a range of 1.38 to 2.57 includes nine out of the reported twelve values. This range is similar to that reported by Branco (1981) of 1.85 to 3.13 .

It has already been noted that quite different steel set loads between Test Sections 1 and 2 were observed which have resulted in quite different lagging to steel set load ratios for both sections. It was expected that as ground conditions deteriorated the value of lagging load to steel set load would tend to unity. Results obtained were inconclusive due to insufficient data. It was seen however that Test Section 4 in bad ground had low ratios while Test Section 1 in good ground had high values. Test Section 2 ratios do not fit readily into this scheme.

Accepting an average ratio of 1.5 to 3.0 to exist between rib and lagging load in Edmonton, this leads to an important design compatibility criterion, i.e., the ultimate

capacity of the laggings should range between 33 to 66% of the steel rib ultimate capacity. This conclusion is based on the ultimate capacity of the formulated lagging ring with regard to safety and integrity at failure, i.e., under conditions of high load excessive deformation of the lagging is more desirable and safer for escape of workmen than buckling failure of the steel sets which could totally block the tunnel, possibly trapping workmen. This finding casts doubt on present City of Edmonton tactics of reducing rib spacing in bad ground while keeping the same steel set dimensions. This results from a simple comparative analysis, which shows that as the rib spacing is reduced from 1.53m (5feet) to 1.22m (4feet) to 0.91m (3feet) the lagging capacity is increased by 56 and 178%, respectively. For the same reduction in spacing, the capacity of the steel sets is only increased by 25 and 67%. Hence, under a given ground pressure, the factor of safety of the steel sets is increasing less rapidly than the factor of safety of the laggings which results in an undesirable change in the mode of failure, i.e, the steel sets will collapse before the lagging exhibits large deformations. This incompatibility is reflected by the observed excessive deflections of the steel ribs in the tunnel when rib spacing was reduced from 1.21m to 0.91m in an area of high load. It is therefore recommended, that systems of compatible steel ribs and wood laggings be investigated for varying lagging lengths and thicknesses.

5.2.5 Conclusions

1. Wood laggings can be used to measure lining pressures although they seem more sensitive to construction activities than simulated steel laggings. Alternatively, slightly shorter laggings could be used for monitoring purposes.
2. Lagging pressures varied from less than 10% overburden at Test Sections 1 and 2 to 65-75% overburden at Test Section 4. The drastic increase is believed directly attributable to poor ground conditions at Test Section 4.
3. In keeping with theory regarding flexible liners, it was found that equalisation of pressure at crown and springline occurred and that axial thrusts in the steel sets were symmetrical.
4. The ratio between steel and lagging load vary typically from 1.38 to 2.57 with lower values being found in poorer ground conditions. This leads to an important design compatibility criterion for steel and lagging systems in Edmonton: Ultimate capacity of the wood laggings should lie between 33 and 66% that of the steel ribs.

5.3 Prediction of Lining Loads

The prediction of lining loads for the subsequent design of liners or lining systems has always been the aim of tunnel engineers. Problems exist however because of the

variability of soft ground tunnel conditions. To combat this a host of semi-empirical methods of prediction have evolved e.g. Hewitt and Johansson (1922), Washington Metro Method (Sczechy, 1966), Moscow Method (Sczechy, 1966). Terzaghi, in an attempt to take ground conditions into account introduced various qualitative loadings for different ground conditions. These loads, given for long and short term, have been reproduced in Proctor and White (1977). Terzaghi's loads are based on an expected amount of arching for a particular soil type and in this respect it is one of the first references to soil strength influence on lining loads.

Lining load is, however, a soil interaction problem and in this respect Peck (1972) introduced the terms

- a) Flexibility Coefficient
- b) Compressibility Coefficient.

These terms, which can be found defined in the cited reference, are measures of lining flexibility and compressibility compared to the medium in which the tunnel is placed. Peck (1972) presents charts from which design moments and thrusts based on values of the above parameters can be obtained. In this method the two main problems are determination of a representative Young's Modulus for a composite lining system and, more difficult, a representative Young's Modulus for the ground. This last parameter is in fact the controlling factor for a given

lining system as to what magnitude of loads the lining will be subjected too. While it is good that a predictive method incorporates a ground mechanical property, Peck has chosen one of the most difficult, possibly most innaccurate and expensive to obtain. It would therefore, be advantageous if another interaction method incorporating more reliable and inexpensive parameters could be used.

Such a method is that referred to as the Convergence Confinement Method which has been studied extensively by Daemen (1975). The method and development of Daemen (1975), expanded in the following section, was chosen here as it takes into account well understood shear strength parameters and relates this to expected load on the lining. The dependency of load on ground strength parameters is thus established.

A summary of structural design models in common use for design of tunnel final liners is given by Duddeck and Erdmann (1982). In this paper all models, with the exception of one proposed by Muir Wood (1975), assume pressures equal to the original ground stresses. This condition is based on the assumption that in the long term original conditions will prevail. Evidence stating that this is overconservative has not yet been found but certainly for design pressures on temporary liners this is much too conservative. One model presented in Duddeck and Erdmann (1982) that of Schulze and Duddeck uses a beam model which in simple terms considers the equilibrium of block failure

above the tunnel for various ratios of ground to support stiffness. Discussions presented in Chapter 4 of this thesis cast light on the kinematics of such a model by suggesting that such a failure occurred progressively. It is the ability of the Convergence Confinement Method as presented in Section 5.3.1 to consider the intermediate states of such a block failure which makes this method so potentially useful in soft ground tunnelling.

5.3.1 Convergence Confinement Method

The convergence confinement method (CCM) refers to the ground support interaction which occurs between excavated tunnel and installed liner. The convergence, refers to the inward movement of the tunnel boundary (Ground Convergence Curve) in direct response to the insertion of the stress free boundary (tunnel wall) in the original in-situ stress field. Confinement is the response of the liner installed to arrest these deformations which results in pressure build up within the liner (support reaction curve) until an equilibrium point is reached. These facets of the CCM are demonstrated diagrammatically in Figure 5.28. The ordinate in Figure 5.28 is the amount of internal pressure required at a particular displacement to secure equilibrium.

Required support pressure is seen to decrease as tunnel wall displacement increases. This dependence on tunnel wall movements stems from the fact that for ground around the opening to absorb the stress loss brought about by tunnel

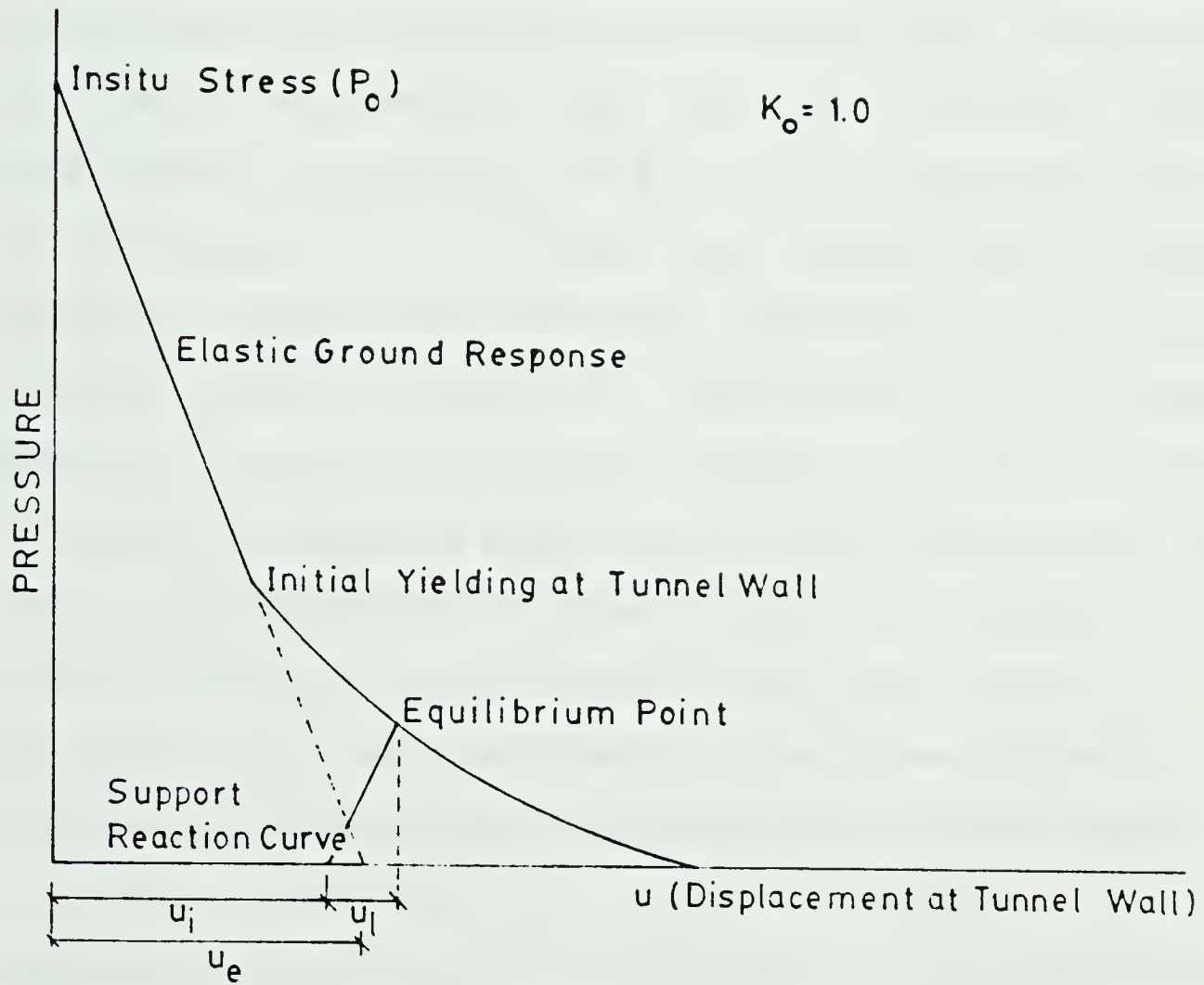


Figure 5.28 Facets of the Convergence Confinement Method

excavation, it must assume a load carrying function by mobilising some of its own inherent strength. This process requires movements which are subsequently manifested by the inward movement of the tunnel walls.

Depending on the size of the tunnel, the strength of the material and the in-situ stress field, the stresses near the tunnel may exceed the ground strength causing overstressing (yielding) of the ground. This may result in the development of a yield zone around the opening. Depending largely on material mechanical properties this yielding usually results in some degree of strength reduction accompanied by development of plastic strains. This point of yielding signifies the start of the non linear portion of the ground convergence curve, i.e., prior to this initial yielding, ground response was linear elastic. It is the shape of the convergence curve after yielding which reflects the behaviour and thus stability of the tunnel.

After yielding, as shown in Figure 5.28, the convergence curve goes off to the right, i.e., displacements increase. In Figure 5.28 the convergence curve does stabilise but this is not always the case. In practise the non linear portion may either stabilise as shown or may, depending on the degree of strength loss in the yielded zone, show an increase in required support pressure with displacements. This phenomenon of an upward turning convergence curve, according to Daemen (1975), is common under conditions of low field stress, such as are found in

shallow tunnels, when gravity terms dominate within the lower strength yield zone. They are also common where large post peak strength losses occur. As will be shown later it is the amount of retained friction angle in the yield zone which has a very dominant effect on the shape of the convergence curve and thus on the lining pressure. This dependence on residual friction angle can be viewed as the self retaining capacity of a block "d" in width and height " $R-d/2$ " from slipping into the tunnel where R is the extent of the yield zone and "d" is the diameter of the tunnel. The lower the angle the less it is retained and the more support pressure must be supplied for stability.

Another type of convergence curve is that which initially starts downward and only after some displacement does it begin to turn upward. This delayed upward trend is a result of moderate strength loss in a low field stress situation (shallow tunnel). Initially the effect of gravity is minimal but after expansion of the yield zone its effect begins to dominate over stress uptake by intact material. These three types of curve are shown diagrammatically in Figure 5.29.

Having identified that certain types of ground convergence curves exist, some of which represent more beneficial modes towards tunnel stability, for any design situation the whole curve is required. Field measurement of the curves involves measurement of the tunnel wall closure before and after face advance plus measurement of lining

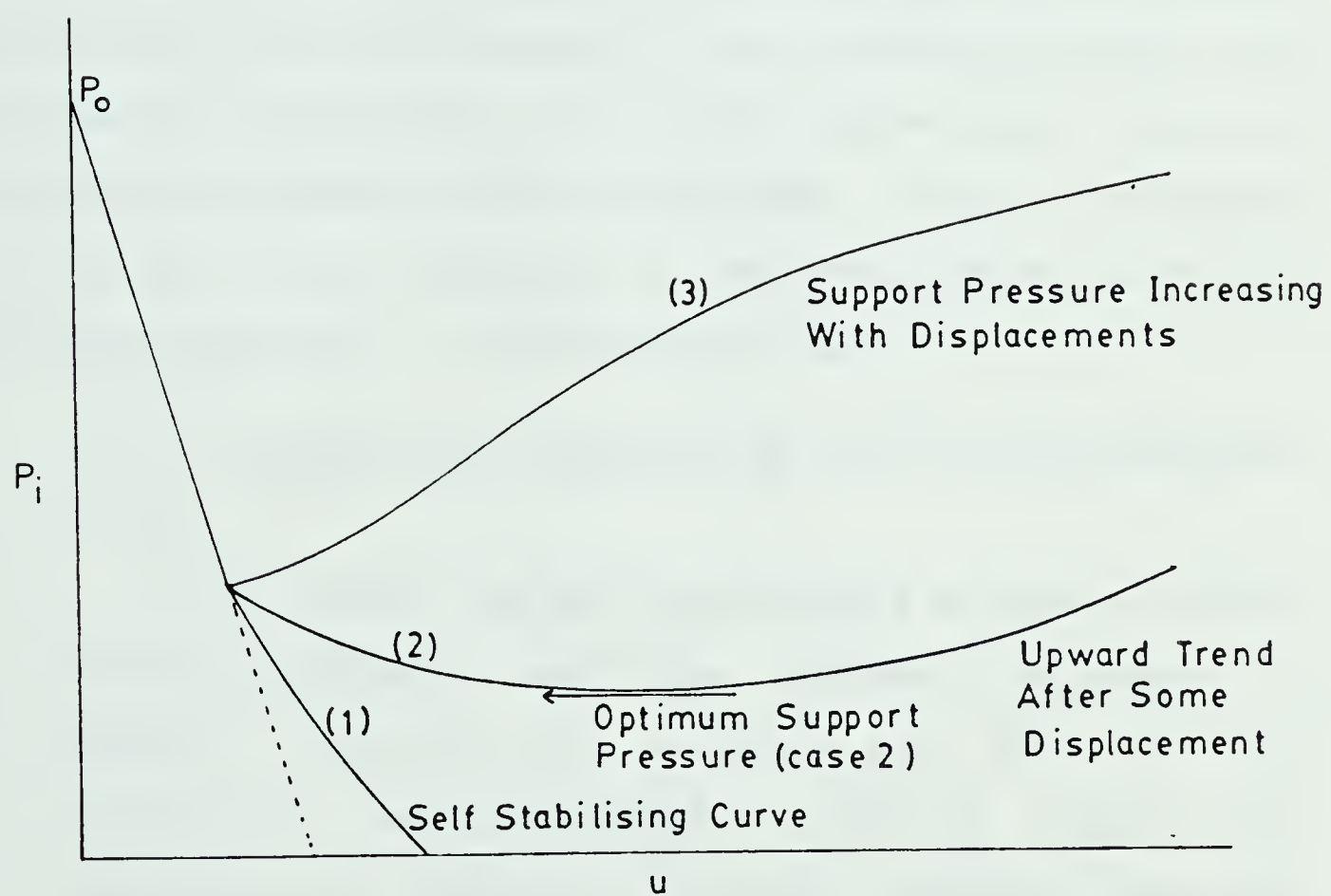


Figure 5.29 Typical Shapes of Ground Convergence Curves

pressure. In reality only the latter can relatively accurately be measured which only yields one point on the ground convergence curve provided some knowledge of ground displacements exist at the section. As field measurements are inadequate we must therefore develop theoretical curves for varying ground conditions in the hope that field measurements will reinforce the developed curves and prove their value for future works. In the following sections, the theoretical development of ground convergence curves as presented by Daemen (1975) is reviewed. Ground convergence curves are then generated for varying strength parameters thought applicable to the present project.

5.3.1.1 Theoretical Prediction of the Ground Convergence Curve

This topic has been extensively studied by Daemen (1975) who adopts a continuum mechanics approach. In Daemen's opinion this is preferable over the too simplistic pseudo-empirical approach and over sophisticated approach of numerical methods. Daemen was however forced, like many other workers in Geotechnique, to make simplistic assumptions regarding material behaviour and problem geometry. Recognizing these shortcomings Daemen (1975) developed equations knowing that they would not provide exact numbers but rather that they would show trends of parameter dependence. It is this parameter dependence that we would like to isolate for the Kennedale tunnel and hence use to

predict pressures along the crown of the tunnel.

Summary of Daemen's Theoretical Model

Daemen (1975) considers a circular opening of radius "a" being driven through a ground under a hydrostatic stress "p" ($K_0=1$). The ground (Daemen originally undertook this analysis for rock) is assumed homogeneous, isotropic and linearly elastic prior to tunnelling. After excavation it is assumed that the induced stresses exceeds the ground strength causing the development of a homogeneous, isotropic, cylindrical yield or broken zone of radius "R". This is shown diagrammatically in Figure 5.30.

All material is assumed to follow the Mohr-Coulomb failure criterion with the initial material having strength parameters of c and ϕ while material in the broken zone has values of c_r and ϕ_r (r denoting residual). The magnitude of c_r and ϕ_r become one of the most dominant variables in this analysis ranging between $0 < c_r < c$ and $0 < \phi_r < \phi$.

For purposes of modelling soft ground behaviour Daemen's c_r and ϕ_r shall be redefined as the apparent shear strength parameters c^* and ϕ^* . This shall therefore avoid any confusion with Skempton's residual shear strength parameters. In the following analysis the values of c^* and ϕ^* represent temporary strength losses

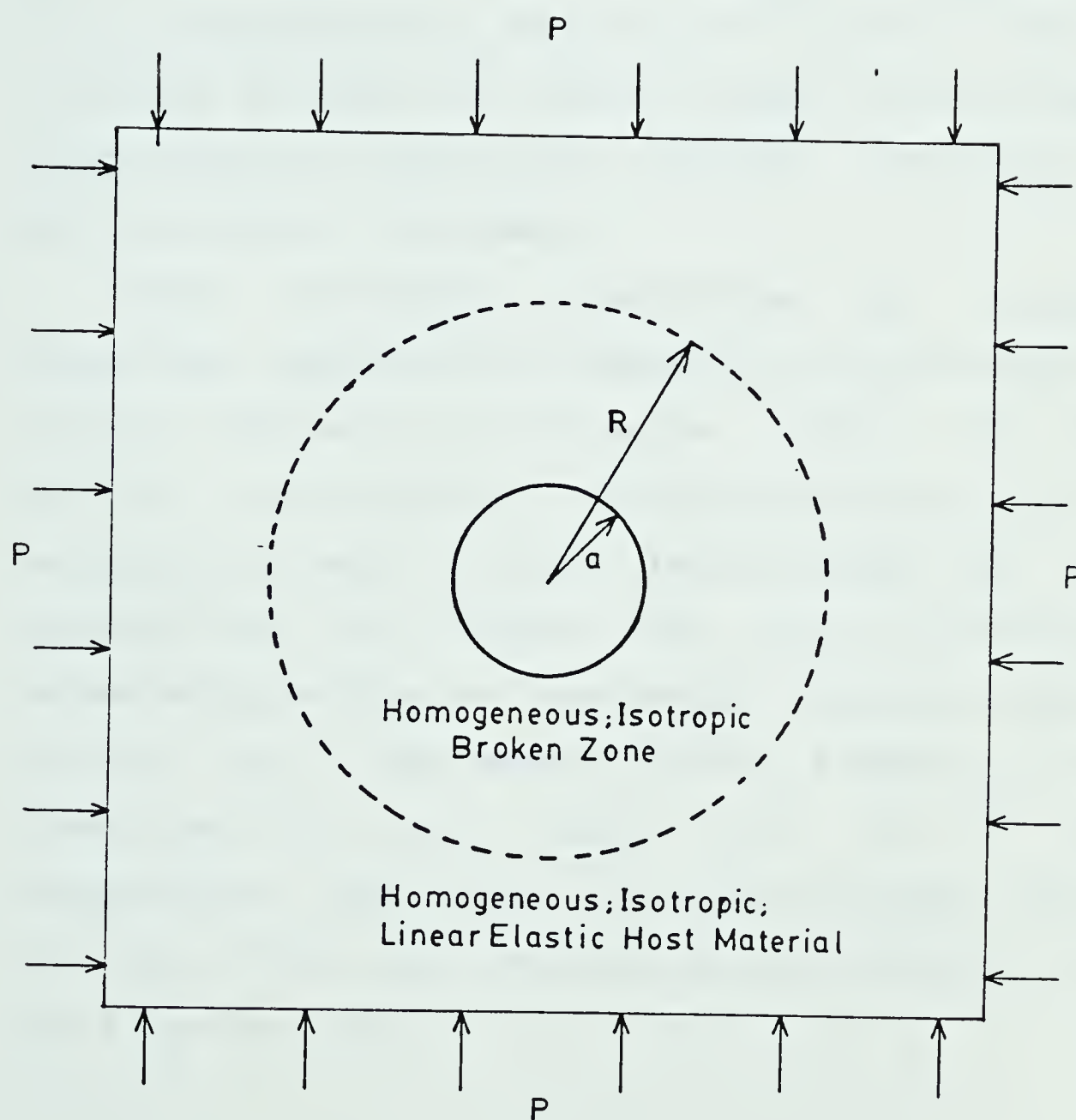


Figure 5.30 Boundary Conditions for Analysis of Daemen(1975)

as a result of tunnel excavation and only in materials which exhibit post peak strength losses do they represent long term conditions. Like Daemen, the magnitude of c^* and ϕ^* vary such that $0 < c^* < c$ and $0 < \phi^* < \phi$. Physically the values of c^* and ϕ^* in the following analysis were chosen to model strength losses brought about by excess pore pressures, loosening and other excavation disturbances.

After introducing equilibrium and boundary conditions together with constitutive relationships the solution follows two fundamental stages. The first requires a calculation of stress distribution under the assumption of small strains. Relationships from this analysis are then coupled with material deformation parameters providing a relationship between internal pressure (p_i), the ratio R/a and u_a ; where u_a is the displacement at the tunnel wall. For a more comprehensive development the reader is again referred to Daemen (1975). The governing equation resulting from the first stage is:

$$\begin{aligned}
p_i = & [p(1-\sin\phi) - c\cos\phi - c^* \cot\phi^*] \\
& [(a/R)^{(2\sin\phi^*)/(1-\sin\phi^*)}] - [c^* \cot\phi^*] \\
& \pm a\gamma\{[(1-\sin\phi^*)/(1-3\sin\phi^*)][(a/R)^{(3\sin\phi^*-1)/(1-\sin\phi^*)} - \\
& 1]\}
\end{aligned}$$

Eq. 5.1

where p_i = internal support pressure
 γ = weight density

Considering the terms present in Equation 5.1 it is seen that the first two terms are primarily concerned with strength mobilisation while the third controls the effects of gravity in the loosened yield zone. In the floor of the tunnel the loosened material acts as a stabilizer, i.e., its weight acts with the internal pressure thereby aiding stability in the floor region and reducing the internal pressure required to achieve equilibrium. Hence, the gravity term has a negative sign in Equation 5.1 for the floor. In the crown area gravity acts against the internal pressure thereby increasing the internal pressure required to achieve equilibrium. Hence, the gravity term assumes a positive sign in Equation 5.1.

When Equation 5.1 is coupled with material deformation parameters and made dimensionless Equation 5.2 is obtained :

$$\begin{aligned}
 u/a = & [(R/a)^2 (p \sin \phi^* + c \cos \phi^*) (1 + \nu)/E] + \\
 & [(p + c \cot \phi^*) (1 - 2\nu) ((R/a)^2 - 1)/E] - \\
 & (1 - 2\nu + \nu \sin^2 \phi^*) / (a^2 E) \{ \pm (2\gamma (R^3 - a^3) / 3(1 - 3\sin \phi^*) + \\
 & ((R/a)^{a+2} - a^{a+2}) / a^a \} [p_i + \\
 & c \cot \phi^* \mp (a\gamma(1 - \sin \phi^*)) / (1 - 3\sin \phi^*)] \}
 \end{aligned}
 \tag{Eq. 5.2}$$

$$\begin{aligned}
 \text{where } a_r &= (2 \sin \phi^*) / (1 - \sin \phi^*) \\
 E &= \text{material deformation modulus}
 \end{aligned}$$

Several other equations can be derived from Equations 5.1 and 5.2 by imposing special values of ϕ^* and c^* (see Daemen 1975).

Using Equations 5.1 and 5.2 it was possible to calculate ground convergence curves for assumed peak strength parameters coupled with variable apparent shear strength parameters. The apparent shear strength parameters

With reference to information presented in Chapter 2 it was decided to use peak values of $c' = 10 \text{ kPa}$ and $\phi' = 35$ degrees with the best approximation of a deformation modulus being 60 MPa and a weight density $\gamma = 19 \text{ kN/m}^3$. It should be noted that in Daemen's analysis he assumes similar deformation modulus values in both the intact and plastic zone. Although this is highly unlikely it should not adversely effect the shape of the curves presented subsequently even though specific displacements at any support pressure may be underestimated.

To obtain a lower bound value to internal pressure or lining pressure required for stability it was assumed that no strength decrease occurred in the yield zone while for an upper bound an assumption of zero strength ($c^* = 0$, $\phi^* = 0$) in the yield zone would suffice. An intermediate strength case with $\phi^* = 19.5$ degrees ($\sin \phi^* = 1/3$) and $c^* = 0 \text{ kPa}$ was also considered. In all cases the field stress was assumed equal to that present at the centre line of the tunnel with a K_0 value of 1 being assumed and more importantly the effect of the proximity of the ground surface was neglected, i.e., the tunnel was modeled as deep.

Generation of the ground convergence curves for the three cases outlined above required for each case that relationships between p_i and R/a using Equation 5.1 be obtained. Having obtained these discrete values for a particular case under consideration they were then used in conjunction with Equation 5.2 to obtain p_i versus u/a

relationships, i.e., the desired ground convergence curve. The three cases considered are shown in Figures 5.31, 5.32 and 5.33 where ground convergence curves for roof, floor and springlines are included. As most of the field pressure information was obtained for the roof area the three ground convergence curves as obtained for the crown area in each case are presented in Figure 5.34 for increased clarity of predicted roof pressures with changing ground conditions.

Considering Figures 5.31 to 5.34 an enormous change in pressures required for equilibrium with decreasing apparent shear strength properties in the yield zone occurred. Inspection of Equation 5.1 illuminates pressure build up dependencies upon yield zone strength parameters. With regard to apparent cohesion it is seen for the zero gravity case (springline) that pressure due to the friction angle decreased monotonically towards zero leading to the conclusion that if the material exhibits some apparent cohesion the springline will self stabilise even if it does mean a very large yield zone radius. With regard to yield zone apparent friction, large increases in the gravity term of Equation 5.1 occur as the friction angle decreases. Possible post peak strength losses with respect to developing a full block failure above a tunnel were cited qualitatively in Section 4.1.2 as a possible cause for increasing loads and deformations in tunnels. Evidence in support of this has emerged from the investigations presented in this section. This increase in the "gravity

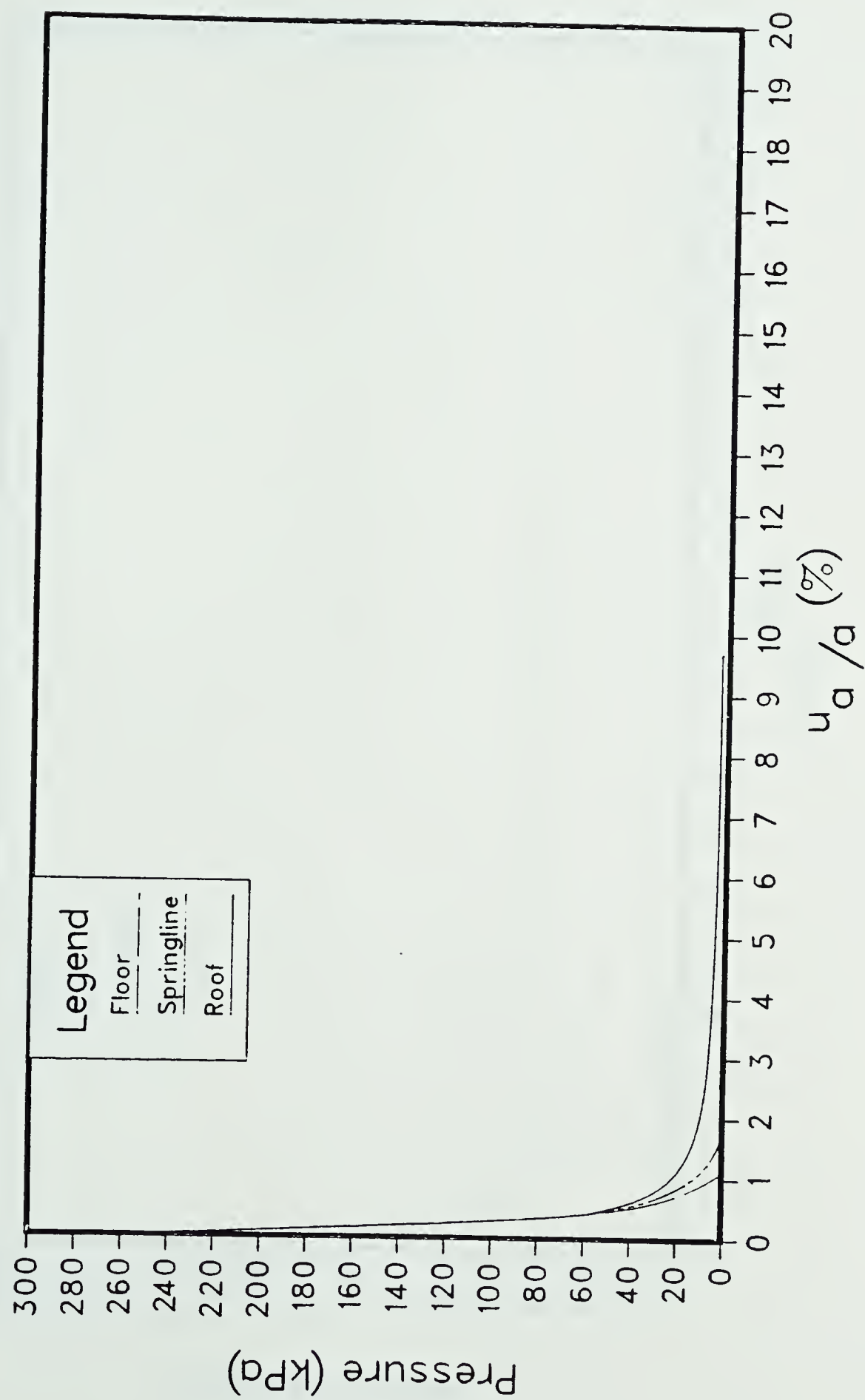


Figure 5.3.1 Ground Convergence Curves Generated under the assumption of $\phi^* = 35^\circ$; $\phi^* = 35^\circ$; $c = 10 \text{ kPa}$; $c^* = 10 \text{ kPa}$

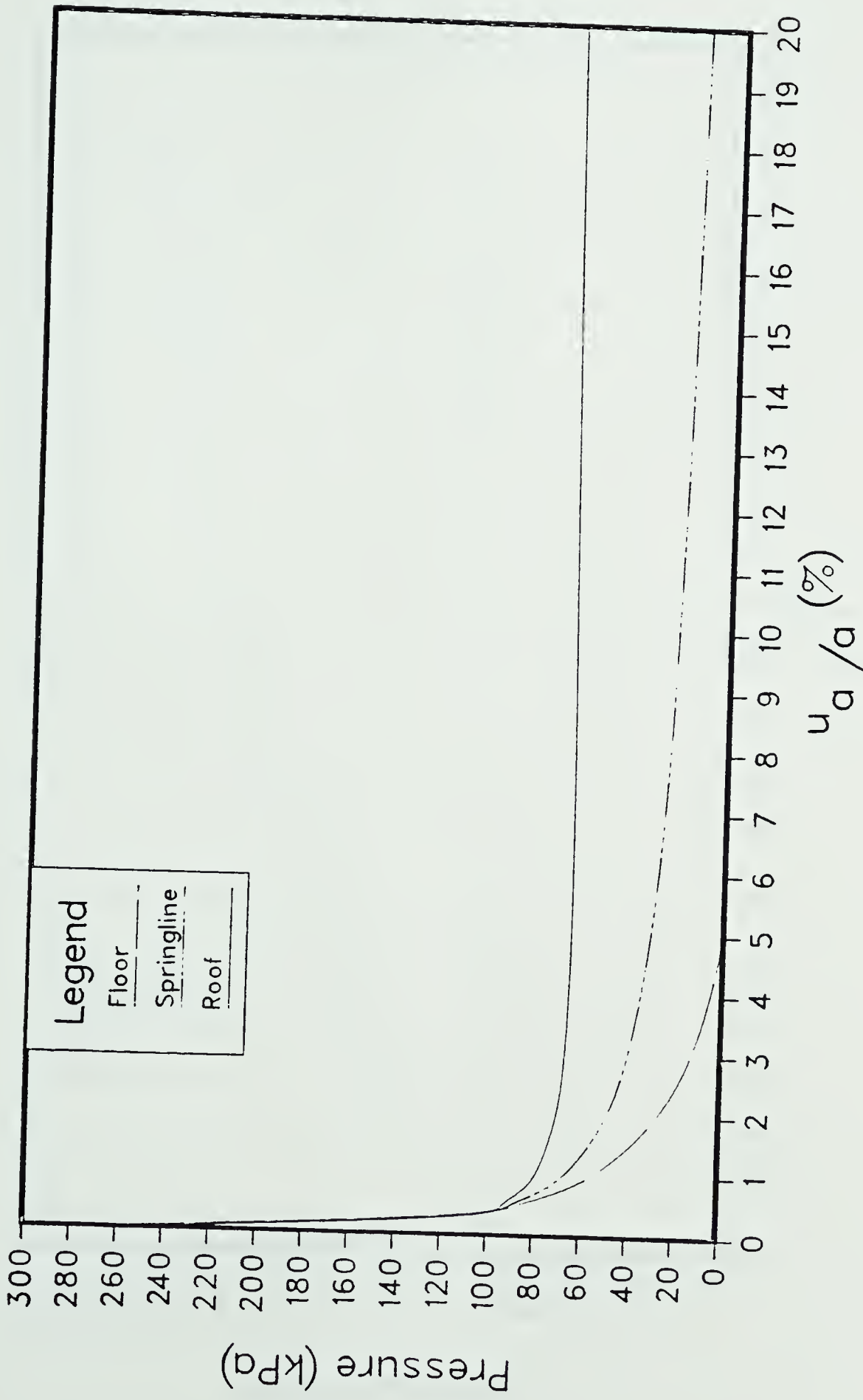


Figure 5.13.2 Ground Convergence Curves Generated under the assumption of $\phi = 35^\circ$; $\phi^* = 19.5^\circ$; $c = 10 \text{ kPa}$; $c^* = 0 \text{ kPa}$

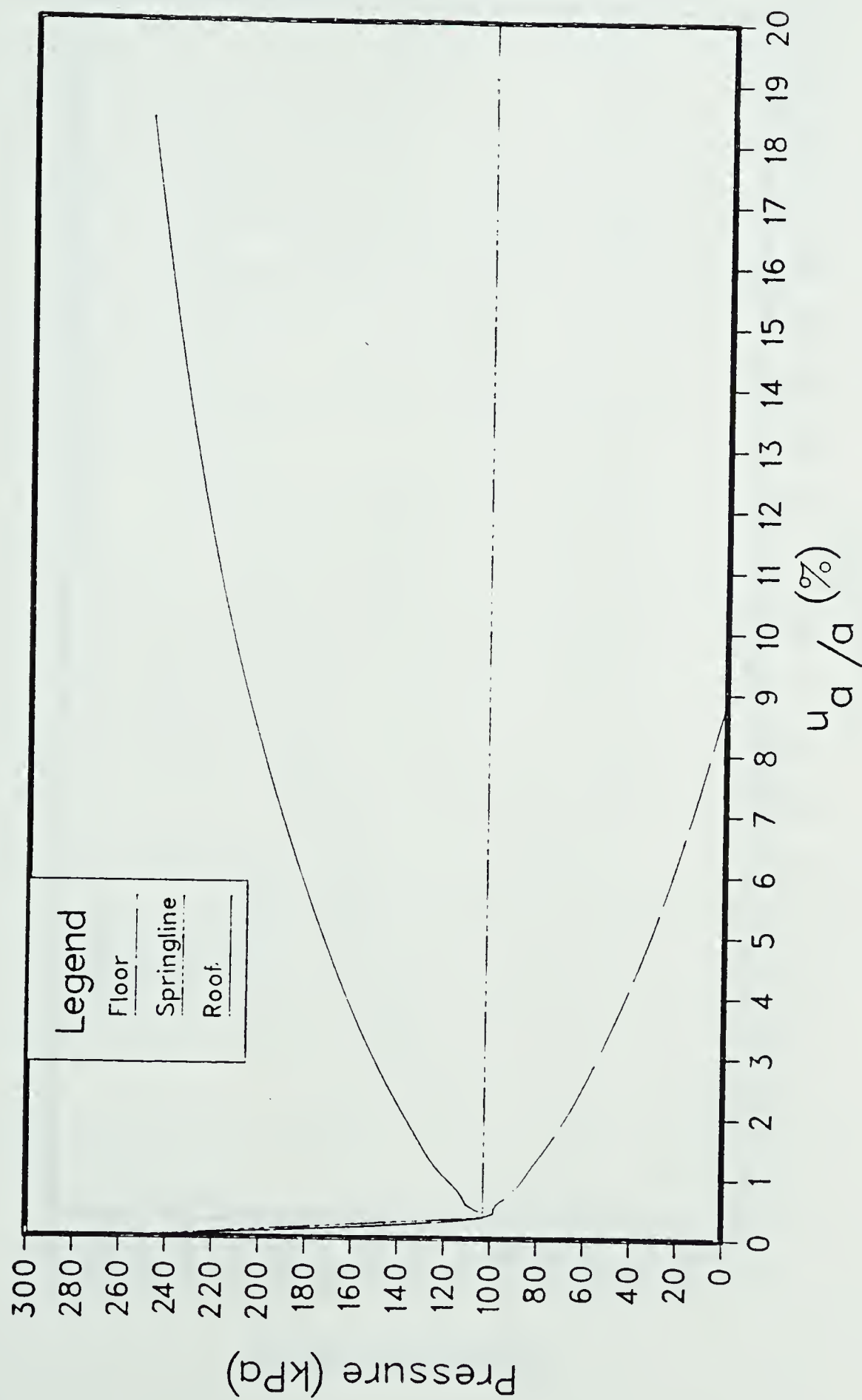


Figure 5.33 Ground Convergence Curves Generated under the assumption of $\phi^* = 0^\circ$; $\phi^* = 35^\circ$; $c = 10 \text{ kPa}$; $c^* = 0 \text{ kPa}$

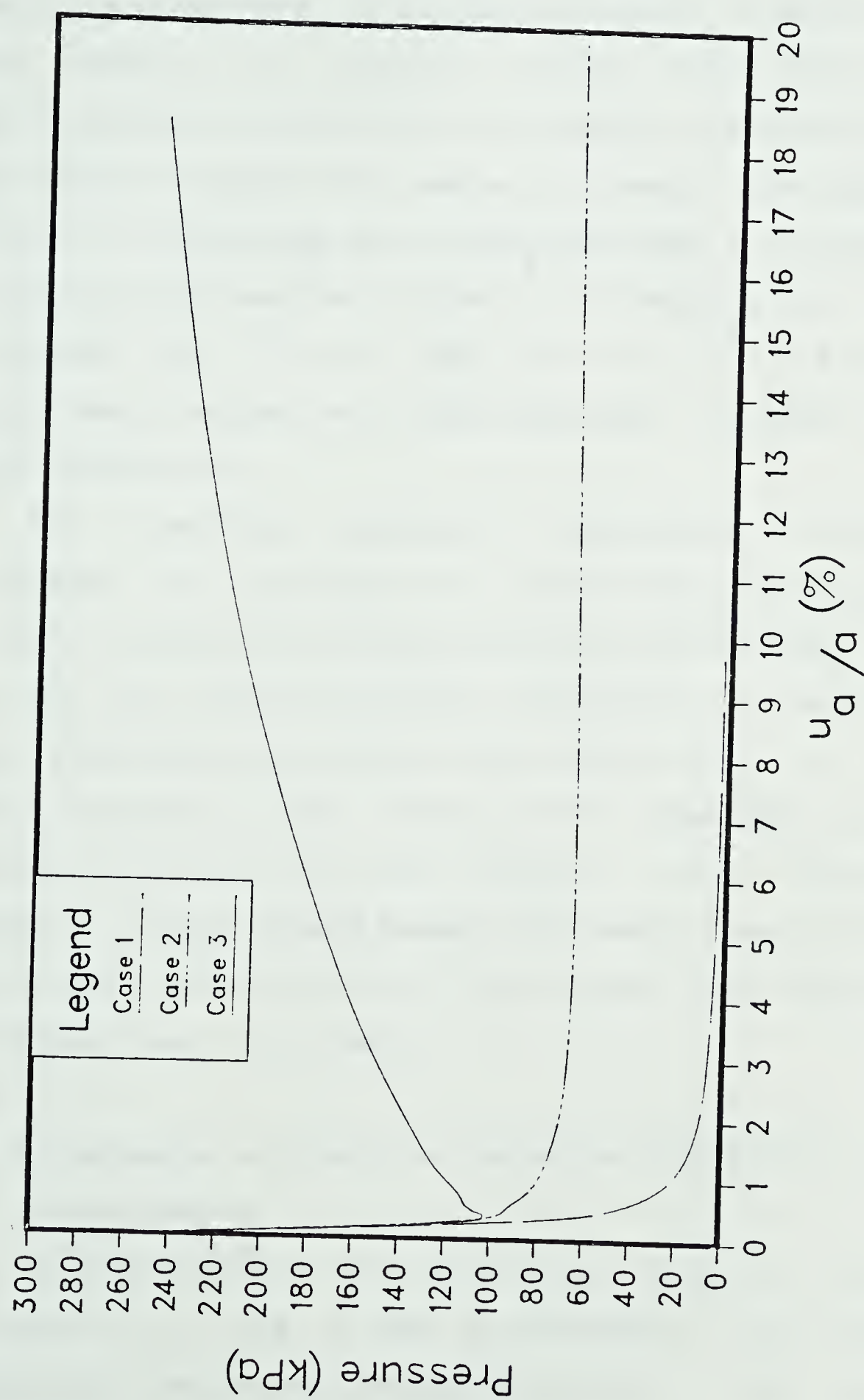


Figure 5.34 Crown Convergence Curves for the three Strength Cases Considered

pressure" with respect to decreasing apparent friction is especially pronounced, as stated previously, in areas of low field stress, i.e., shallow tunnels. This increase in gravity pressure manifested in increasing roof pressures, is emphasized in Figure 5.34 where the major strength loss factor of decreasing the friction was seen to increase the minuscule roof pressures of the $\phi^* = 35$ degrees case to full overburden for $\phi^* = 0$ case. For the $\phi^* = 0$ case the displacements become very large which was recorded in the field (Chapter 4).

The preceding parameter dependence discussion emphasizes the importance of preserving as much apparent friction as possible during construction which may involve the use of ground improvement techniques, eg. drainage of water saturated sand pockets where temporarily, c' and ϕ' could approach zero. This proven dependence of roof pressures upon friction angle supports field evidence as observed on soft ground tunnels for years, i.e., the poorer the ground conditions (low ϕ^*) the larger the deformations and higher the lining loads.

5.3.2 Discussion of Predicted Pressures Compared with Field Measurements

In this section only pressures obtained from Test Sections 1, 2 and 4 will be discussed in the context of convergence confinement predictions while a more detailed general discussion of the method and results will be given

in Section 5.4.

Firstly let us consider what pressures and/or forces would be predicted using conventional methods. Using predictive methods we must first consider what is a "design earth pressure" for a tunnel lining. One line of reasoning suggests that a design pressure should be an envelope of all possible pressures which can occur along the tunnel, i.e., design for full overburden. Design for full overburden is prudent with regard to the long term where it is assumed original conditions will eventually return. Such an outlook, even for a permanent, and definitely for a temporary liner, is conservative and contradictory to general engineering practice which tend to apply a factor of safety to an expected load to account for unforeseen elements as opposed to having a design load which can not physically be surpassed. In tunnelling slightly different conditions do prevail compared to usual geotechnical practice, as workmen safety is always of paramount importance and generally the extent of site investigations is limited. If ground conditions could be fixed more firmly with increased investigation, it would certainly be economical with regard to primary liner design if areas of expected constant pressure could be delimited to which a rational factor of safety could be applied to ensure adequate safety.

Presently only design pressures given by Terzaghi (reproduced in Proctor and White, 1977) give varying predictions depending on ground type while those of Peck

The first part of the paper discusses the importance of the study and the objectives of the research. It also outlines the methodology used in the study and the results obtained. The second part of the paper discusses the implications of the study and the conclusions drawn from the research. It also outlines the limitations of the study and the areas for further research. The third part of the paper discusses the significance of the study and the contributions it makes to the field. It also outlines the practical applications of the study and the policy implications of the research. The fourth part of the paper discusses the future of the study and the potential for further research. It also outlines the challenges facing the study and the opportunities for future research. The fifth part of the paper discusses the role of the study in the broader context of the field and the importance of the research. It also outlines the impact of the study on the field and the potential for future research. The sixth part of the paper discusses the role of the study in the broader context of the field and the importance of the research. It also outlines the impact of the study on the field and the potential for future research. The seventh part of the paper discusses the role of the study in the broader context of the field and the importance of the research. It also outlines the impact of the study on the field and the potential for future research. The eighth part of the paper discusses the role of the study in the broader context of the field and the importance of the research. It also outlines the impact of the study on the field and the potential for future research. The ninth part of the paper discusses the role of the study in the broader context of the field and the importance of the research. It also outlines the impact of the study on the field and the potential for future research. The tenth part of the paper discusses the role of the study in the broader context of the field and the importance of the research. It also outlines the impact of the study on the field and the potential for future research.

(1972) and Schulze and Duddeck (Duddeck and Erdmann, 1982) present designs based on full overburden assuming no displacements at the tunnel wall prior to lining installation. As mentioned previously designs of Peck (1972) and Schulze and Duddeck are meant for long term based on the assumption that initial conditions will eventually return.

An investigation of estimated pressures and loads as would be predicted from the aforementioned methods as well as those obtained from the CCM will now be discussed. Referring to Table 7.2 (Proctor and White 1977) it was found that flowing ground was the best description of the ground conditions for Test Section 4 which yielded a roof pressure of 120 kPa. For Test Section 1 and 2 confusion abounded as to which ground description most accurately described those encountered. Taking "Homogeneous Squeezing Ground" as the most appropriate a pressure of 30 kPa was obtained which is in quite good agreement to that measured. The predicted low pressure for Test Section 4 accounts for the Tables' inability to take account of the surface embankment.

Using Peck's method (Peck 1972) it was found, as previously mentioned, difficult to adequately decide on an appropriate lining stiffness value. Thrust however is not that dependent on compressibility factor for flexible linings and subsequent analysis led to a predicted lining thrust of 400 kN in Test Sections 1 and 2 and 440 kN for Test Section 4. Schulze and Duddeck estimate similar magnitudes. While the estimated thrust was correct for Test

Section 4 it largely overestimated those of Test Sections 1 and 2 by a factor of 10. The correct magnitudes in the poor ground conditions were predictable as assumptions for both of these methods are only met at Test Section 4, i.e., ground failure extending to surface resulting in loads close to full overburden. When failure did not extend to the surface, as in Test Sections 1 and 2, the methods did not take this into account and hence the large overestimations.

Considering the convergence curves of Figure 5.34 it was necessary to gain information regarding crown movement before it was possible to use the curves. From information presented in Chapter 4 the ground surface above Test Sections 1 and 2 went down approximately 8 mm. Information from multipoint extensometers, also presented in Chapter 3 indicated near constant movement with depth in the same area. As an upper bound therefore to expected pressure it was assumed that a crown movement equal to that occurring at the surface, yielding a percentage displacement $u/a = 0.5\%$ would suffice. While extensometer results show near constant displacement with depth it was assumed that close to the crown displacements increased due to loosening and hence as a lower bound to expected pressure it was assumed that displacements equalled 2 times those at surface, yielding a u/a ratio of 1%. From Figure 5.34 using the $\phi^* = 35$ degrees and $c^* = 10$ kPa curve, thought most applicable, an estimated pressure range of 42 kPa to 24 kPa was obtained. This agrees quite closely with typical measured values of 20 kPa

indicating the chosen strength parameters represent the actual ground response quite accurately.

Considering Test Section 4 where no ground displacements were measured but surface settlements obtained under similar ground conditions showed displacements in the order of 300 mm from which it was assumed that the u/a ratio was at least 10%. Ground conditions at the section location are known to be a fine silty cohesionless sand, therefore, $c^* = 0$ was quite reasonable. As for the assumed ϕ^* , the area had a high water table recently preloaded with an embankment therefore pore pressures were initially high. Construction induced pore pressures were also likely, leading to the conclusion that effective friction angle was small and closely approximated by $\phi^* = 0$. From the appropriate curve in Figure 5.34 a pressure of at least 210 kPa, in keeping with those measured was obtained but this curve changes so rapidly at this point that full overburden can be assumed under conditions such as those described above. Actual measurements showed pressures in the order of 250 kPa. It should be noted that the upper curve in Figure 5.34 has not been corrected for the higher stress field existing at Test Section 4 but since close to full overburden had already been predicted it was not necessary.

Information presented here shows that conventional methods were quite insensitive to changing ground conditions while pressures predicted using the Convergence Confinement Method can take account of varying conditions with predicted

values close to those actually measured. While more experience with the CCM is required, it is seen here that a design pressure to which a factor of safety could be applied can be obtained using the CCM.

5.4 Load Variation Along Tunnel

5.4.1 Test Section 3

5.4.1.1 Section Details and Purpose

Located adjacent to Test Section 4 (Figure 5.1) this section consisted of three ribs with load cells positioned as shown in Figure 5.35. Unlike previous sections no calibrated laggings were included in this section but instead regular construction laggings were employed. For two of the ribs (1 and 2) initial deflection measurements, using the technique set out in Chapter 3 employing central reference nails, were taken such that deformations directly attributable to pressure increase could be ascertained. No initial readings were taken on the third rib where for analysis, a zero deflection, as obtained from results presented in Chapter 3 was assumed.

It was initially expected that over a distance of three ribs conditions would be quite similar resulting in similar pressure distributions in all three ribs. Under this assumption, it was hoped that resultant derived pressure distributions for the ribs would be

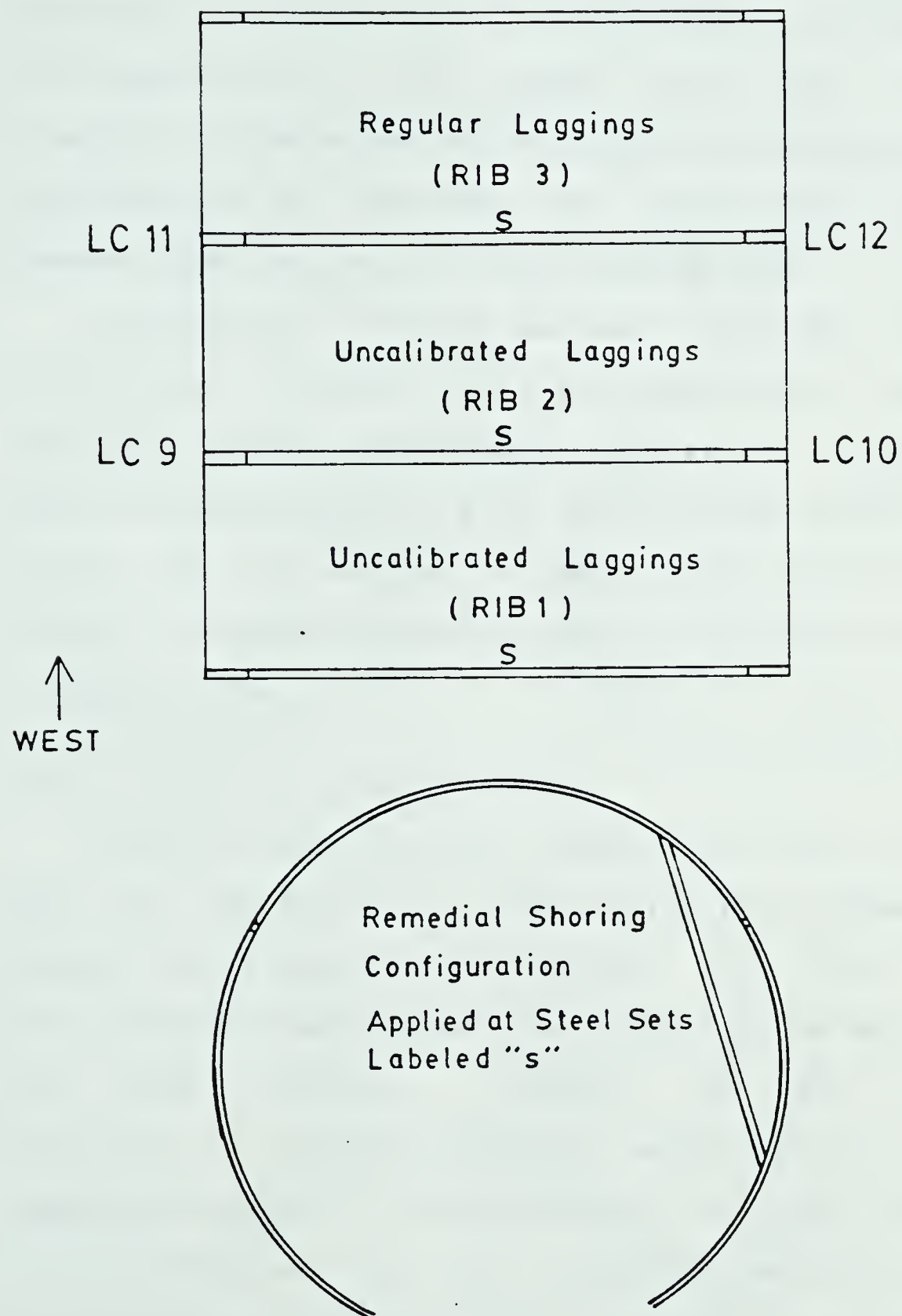


Figure 5.35 Configuration of Test Section 3

similar thereby proving conclusively that zero deflection readings were not critical. From the load cells positioned in the middle steel sets, it was intended to assess the accuracy of the deduced pressure distributions by relating load cell loads to the pressure distributions of the flanking ribs.

Installation of the section followed typical construction procedure, with the exception of load cell insertion. During excavation, however, a large void occurred along the north side of the tunnel which led to failure of the section 8 days after installation. Remedial measures took the form of shoring as outlined in Figure 5.35.

5.4.1.2 Lagging Pressure Details

Pressure distributions, obtained from each lagging board are presented in Figure 5.36 which shows large pressure variations to exist between ribs even though the distance covered by the three ribs is only 3.7m. This large variation, evidence of soft ground tunnelling variability, makes it very difficult to draw comparisons between ribs negating our original objective for this section. This high variability was believed to be directly attributable to the construction void and remedial shoring pattern.

As was expected, considerable pressure build up was detected around the points of shoring (especially pronounced in Rib 2). This indicates sensitivity of the

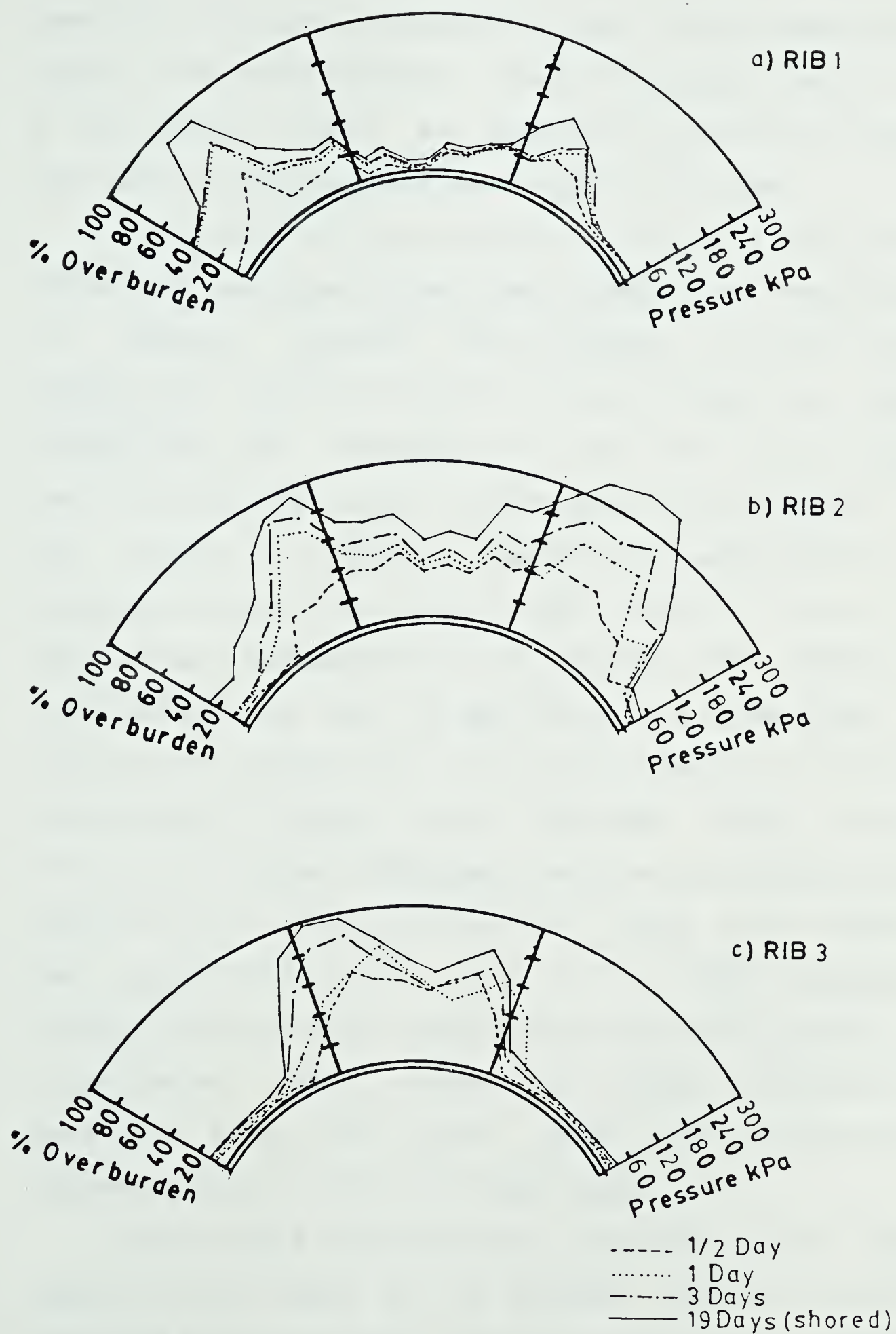


Figure 5.36 Crown Pressure Measurements of Test Section 3

measuring technique, an essential part of any monitoring system. Good repeatability , another important factor in a monitoring system, was observed in Figure 5.36 from the measured lagging load development with time.

Evaluation of the induced error by not taking zero deflection measurements was not possible from comparison of adjacent pressure distributions although the distribution obtained for Rib 3 (Figure 5.36c) was very similar to that obtained in the first rib of Test Section 4 (Figure 5.27a). To circumvent this problem it was decided to reanalyse deflection measurements of laggings between Ribs 1 and 2, Test Section 3 using an assumed zero deflection for all laggings. The results of this analysis for the 19 day case are presented in Figure 5.37 together with the original derived "correct" distribution. Figure 5.37 indicates very little difference between predicted pressures by both methods. Duplication of predicted pressures using both methods was especially close for Rib 2. This apparent insensitivity to exact lagging zero deflection prior to installation, gives credence to results obtained at locations along the tunnel where no information regarding initial deflection was known.

The pressure distributions presented within this section were based on an average flexural rigidity obtained from calibration tests as presented in Chapter 3. No attempt was made to investigate the effects of

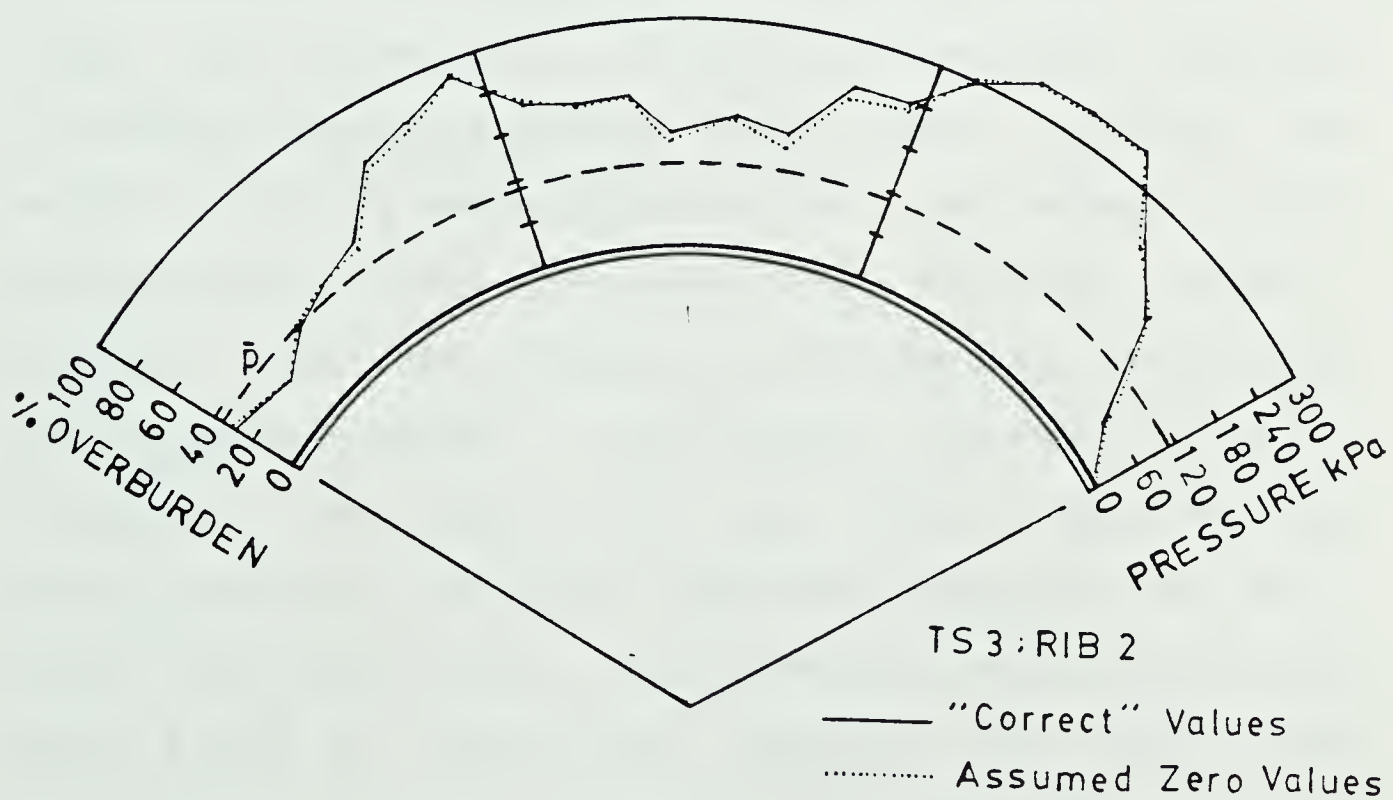
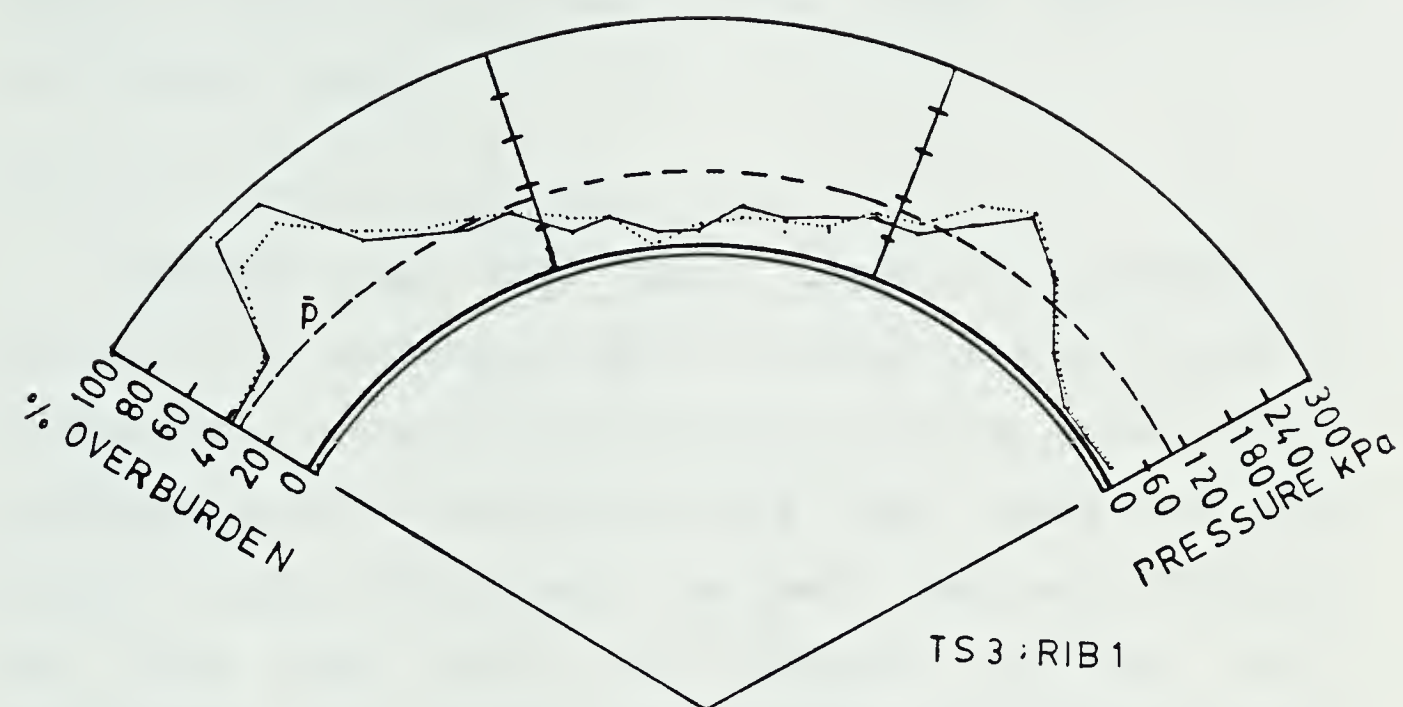


Figure 5.37 Pressure Comparison Obtained between "Correct Pressures" and those Obtained Under the Assumption of Zero Initial Deflection

this assumption on the calculated pressure distribution. Knowledge of individual lagging stiffness would only serve to smooth the pressure curve, rather than effect its average value.

5.4.1.3 Load Cell Results

Derived Load Cell axial loads, are presented in Figure 5.38. Uncharacteristic of other load cell results presented, a consistent discrepancy between axial thrust measured by two Load Cells in the same steel set was observed. Not surprisingly the lower loads were recorded by those Load Cells found adjacent to the void. Indication of movement was evident from the load time relationships where load drop-offs were found after 3 days. As indicated in Figure 5.38 load after shoring increased slightly although some erratic readings do exist. To verify measured pressures it was hoped to back calculate equivalent pressures from measured thrusts. However, with the addition of the shoring, accounting for an unknown amount of load uptake, the exact value of thrust in the steel sets was unknown. Assuming the system remains in balance, equivalent pressures (p bar) were calculated using the thrusts as measured by Load Cells 9 and 11 (positioned opposite the void). The calculated values are presented in Figure 5.37.

Calculated equivalent pressures agree fairly well for Rib 1 while largely underestimating those of Rib 2. The large underestimation for Rib 2 was predictable as a

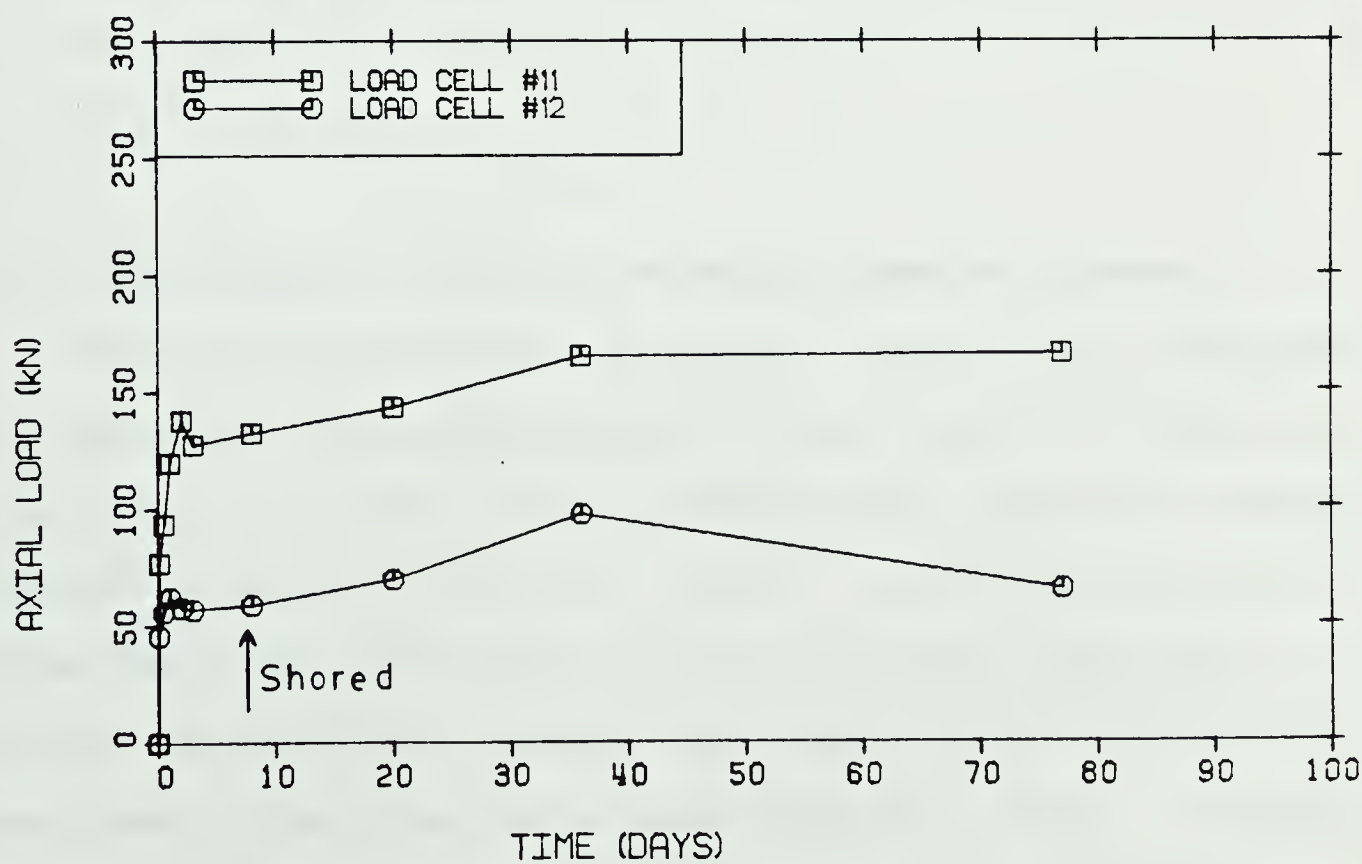
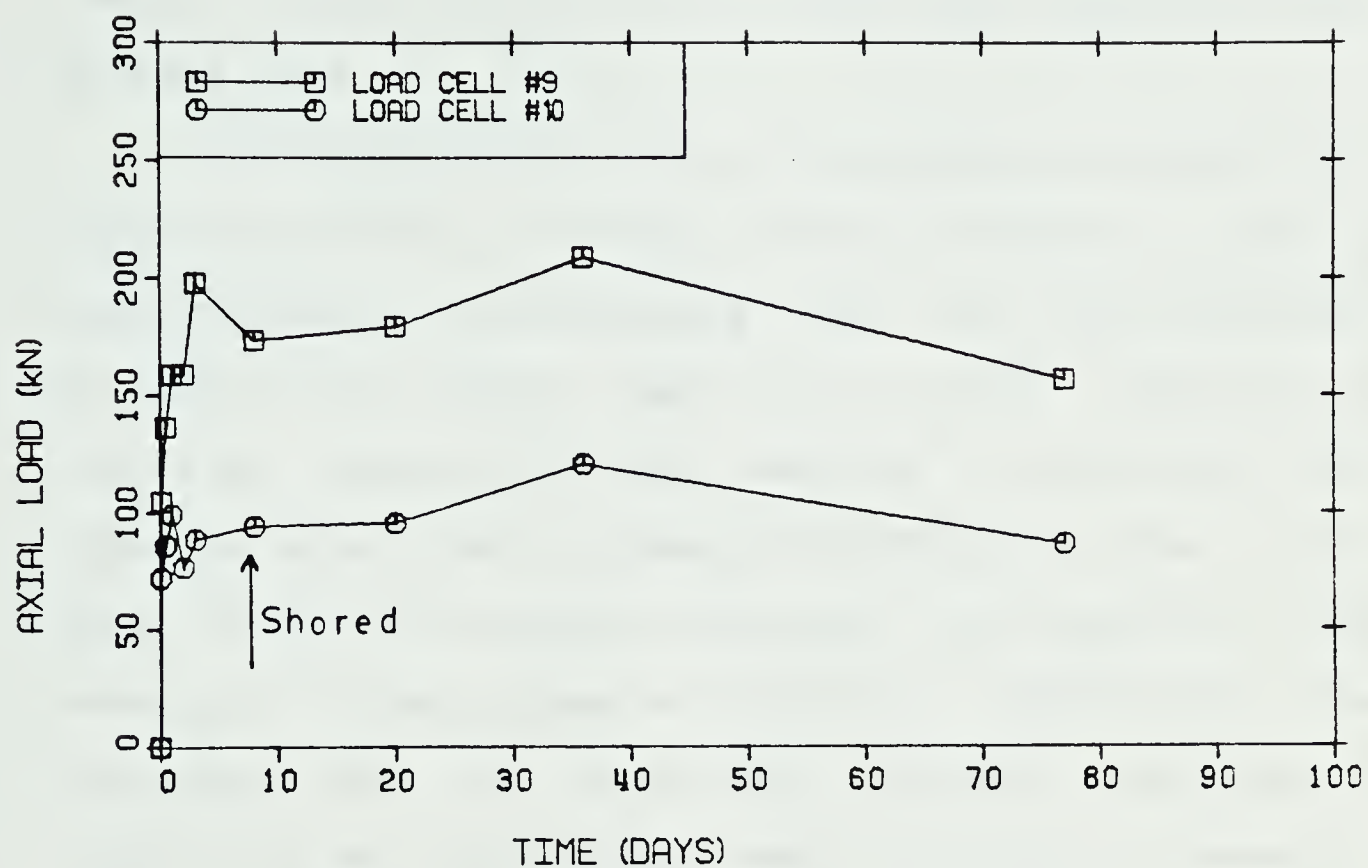


Figure 5.38 Load Cell Axial Loads for Test Section 3

pressure bias over the point of shoring was measured. This bias pressure undoubtedly resulted in the shoring taking a larger amount of the load than that registered by Load Cell 11.

Concerning the validity of pressures obtained from the new measuring technique direct evidence, due to uncontrollable circumstances, was not found. Obtained pressures have however complied with those obtained at the more controlled Test Section 4 and also have appeared sensitive to pressure build up in areas where such build up would be expected. This sensitivity and seemingly correct pressure estimation, coupled with the knowledge that the structural analysis involved is simple and well understood, leads the author to conclude that typical "average" pressures can be obtained using this technique.

5.4.2 Measurement of Lining Pressure Along the Tunnel

This was accomplished using the measurement technique as described and investigated in Test Section 3. Under the assumption of zero initial deflection and an average flexural rigidity of 45.11 kNm^2 , 16 Sections along the tunnel were measured. Each section involved measurement of lagging deflections around the crown third of the rib. Measurements taken on two adjacent lagging rings, totaling typically 48 measurements, constituted one Uncalibrated Section (UC). UC locations, shown in Figure 5.1, were chosen

to lie directly below a surface settlement point such that some knowledge pertaining to ground movements at the section was known. Measurements were taken long after tunnel excavation (months) and subsequent presented pressures can only be considered as long term. Data presented prior to this Section showed little time dependency and therefore these results are not likely to have increased significantly since their 10 day value.

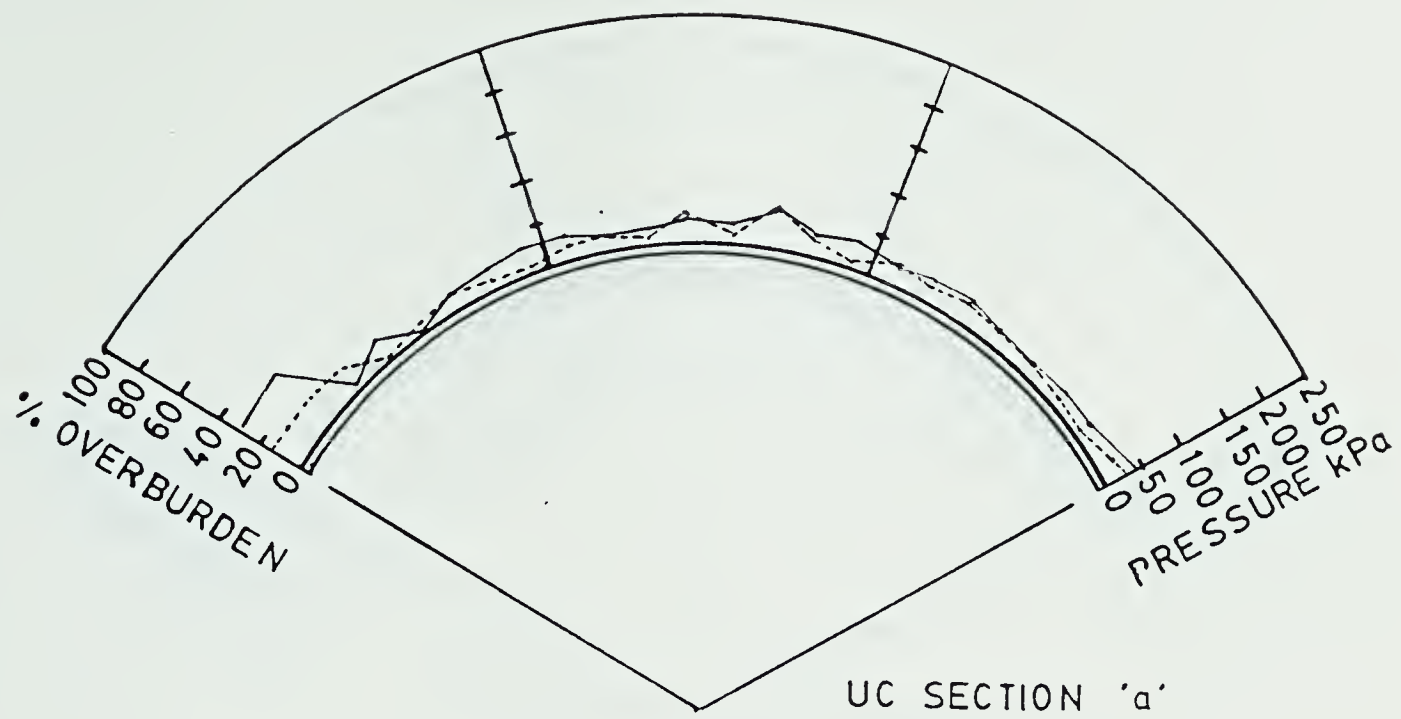
Pressure plots obtained from the 16 Uncalibrated Sections (UC'a' to UC'p') are presented in Figures 5.39 to 5.46. In these plots the two different lines represent the pressures obtained from the two lagging rings which made the total section.

5.4.3 Discussion on Load Variation along the Tunnel

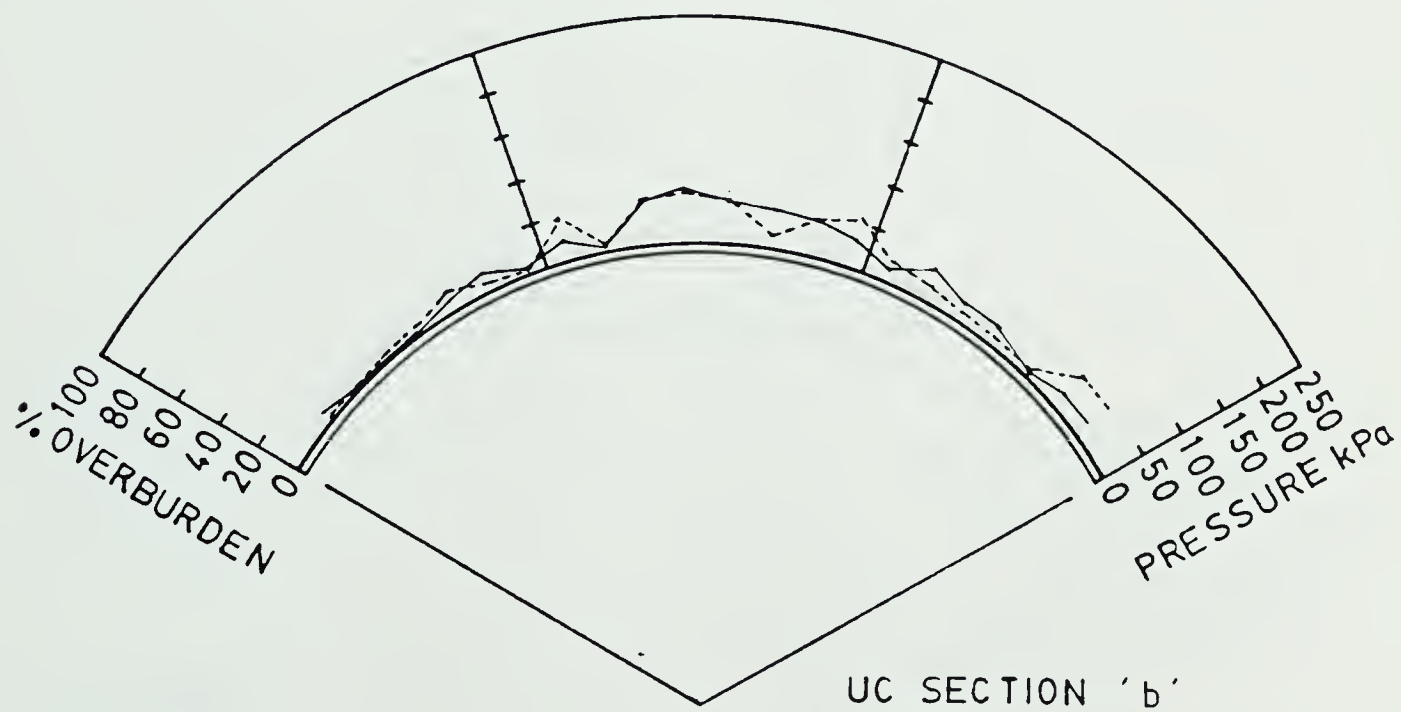
While instrumented Test Sections 1 to 4 have given insight into local behaviour of a tunnel with respect to pressure build up in the steel sets and the laggings, information contained in Figures 5.39 to 5.46 allow investigation of loading variability along the tunnel.

Information contained in Figures 5.39 to 5.46 show two areas of major variability:

1. Magnitude of pressure: this varies from a low of 11.97 kPa at UC'd' (4.8% overburden) to a high value of 123.3 kPa at UC'o' (49.3% of overburden).
2. Pressure distribution around the periphery : symmetrical uniform as in Section UC'c', symmetrical with dominant



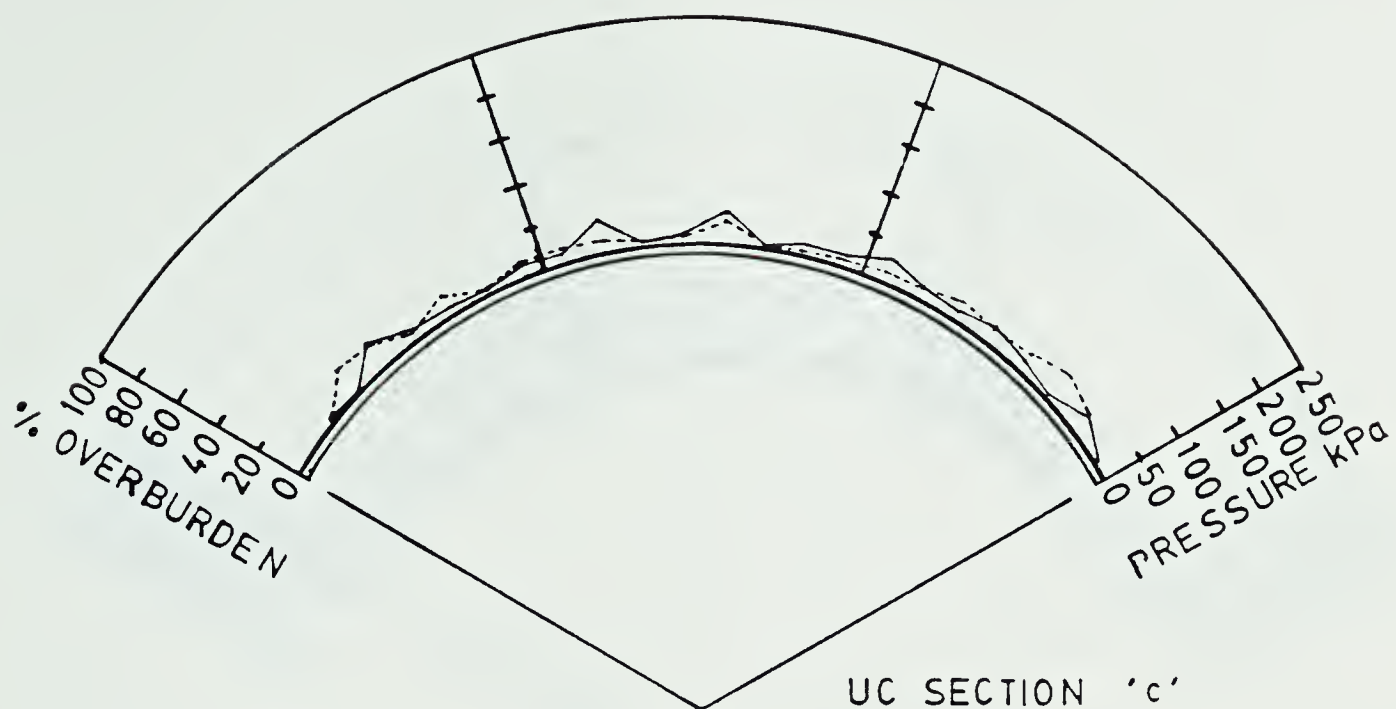
AVERAGE PRESSURE= 23.8 kPa



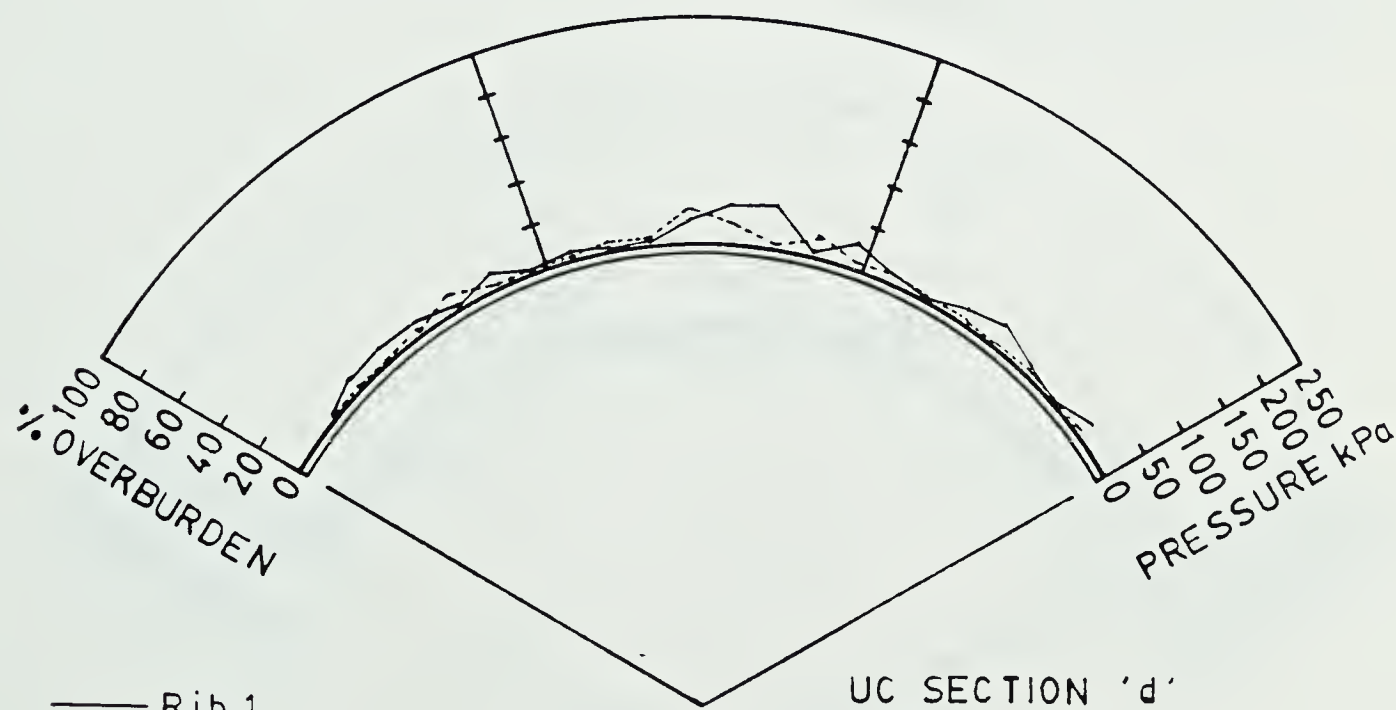
— Rib 1
 ---- Rib 2

AVERAGE PRESSURE= 23.8 kPa

Figure 5.39 Crown Pressure Distributions for Uncalibrated Sections UC a and UC b

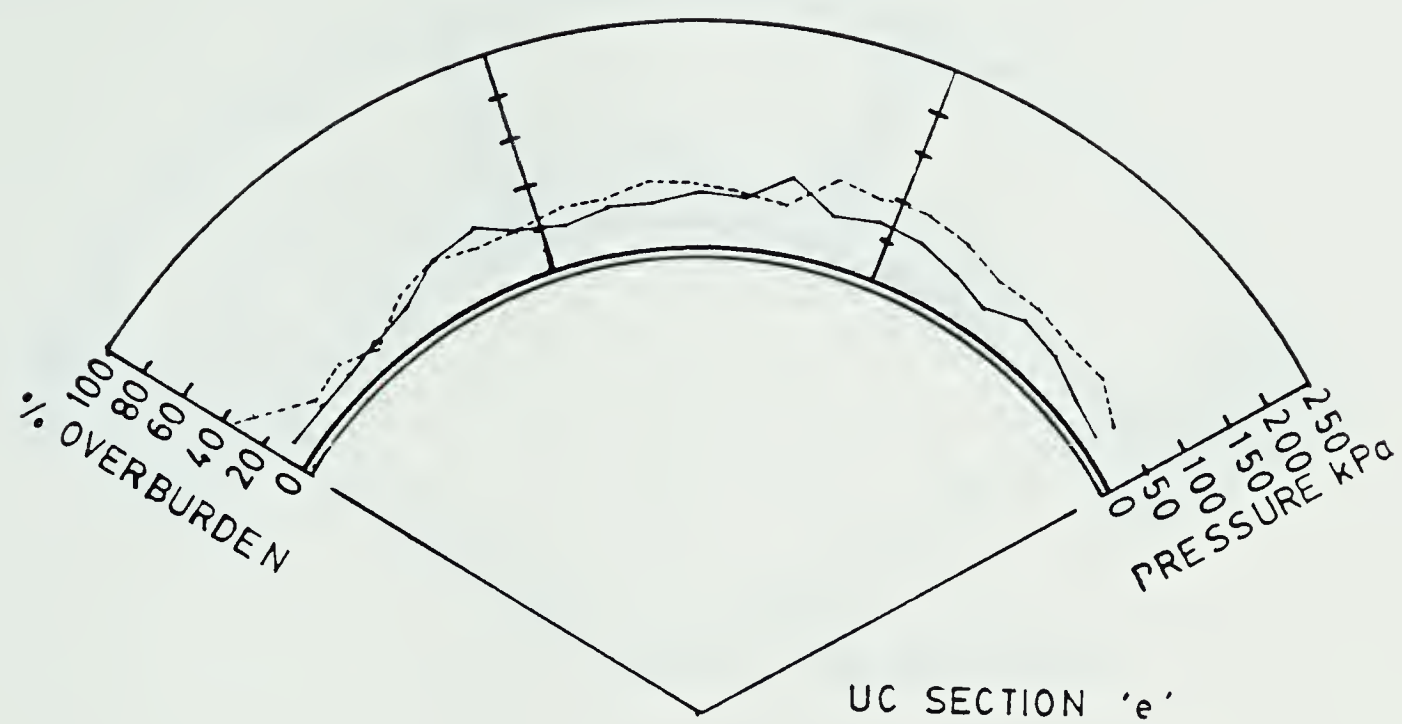


AVERAGE PRESSURE= 16.7 kPa

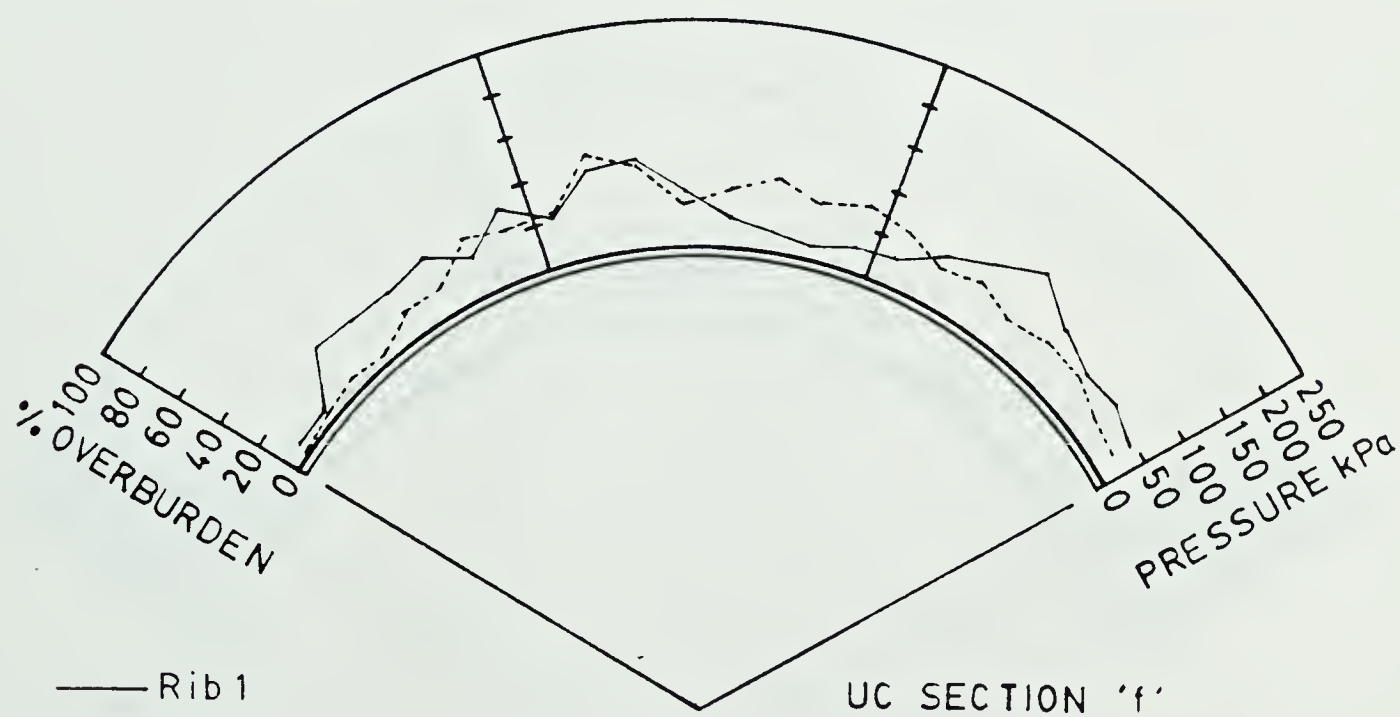


AVERAGE PRESSURE= 11.9 kPa

Figure 5.40 Crown Pressure Distributions for Uncalibrated Sections UC c and UC d

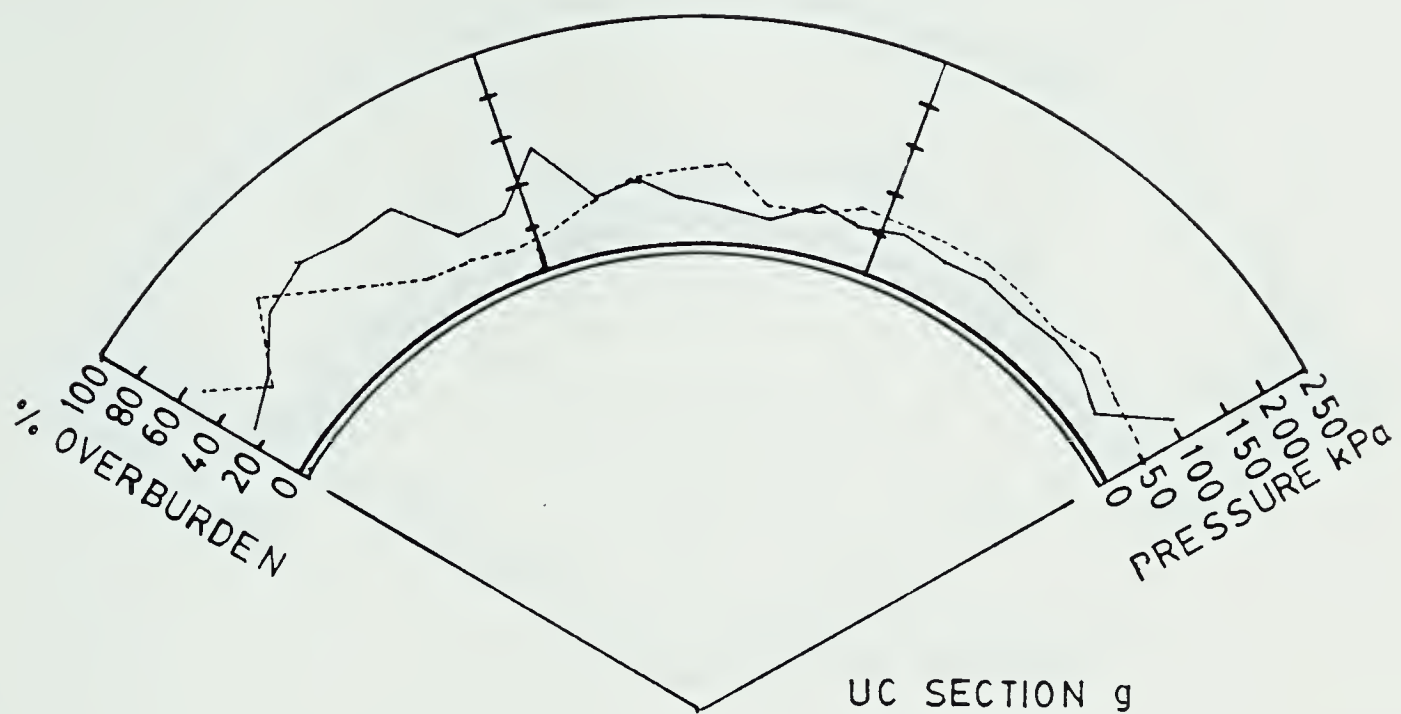


AVERAGE PRESSURE= 56.1 kPa

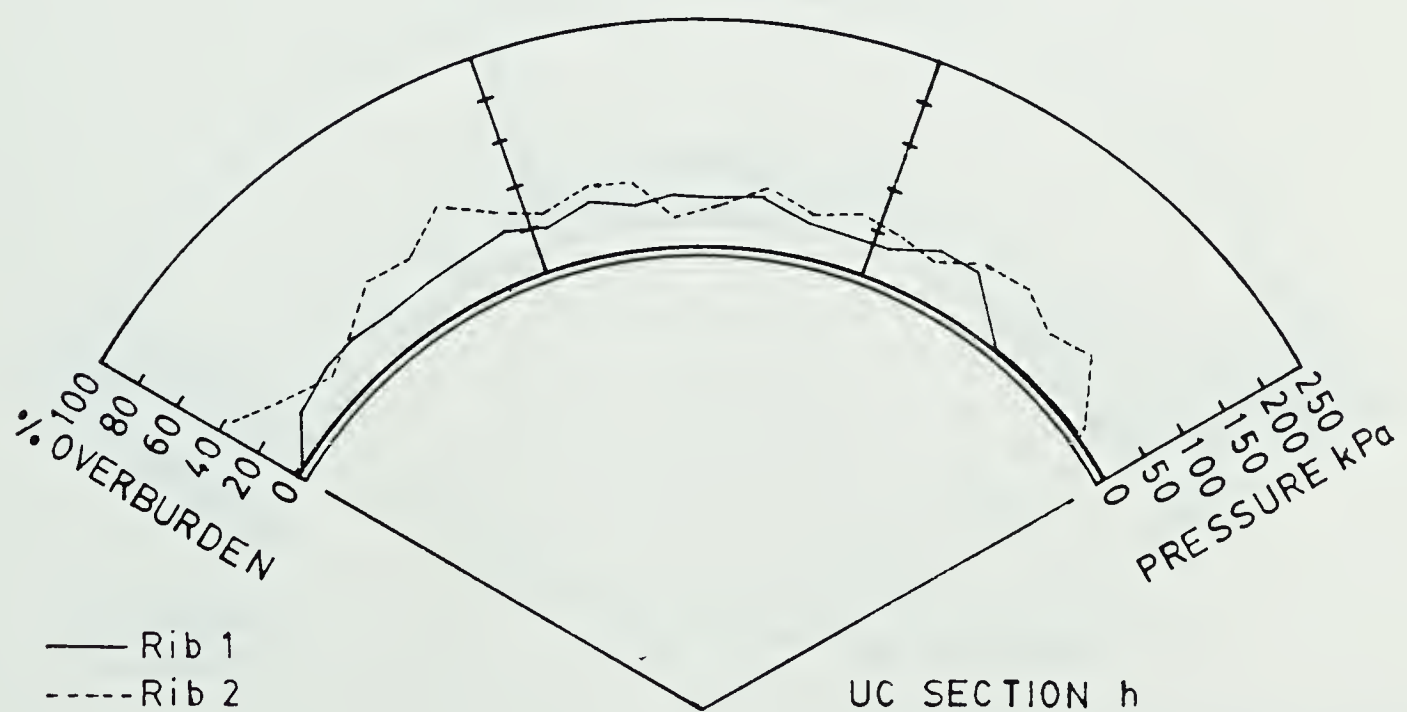


AVERAGE PRESSURE= 53.1 kPa

Figure 5.41 Crown Pressure Distributions for Uncalibrated Sections UC e and UC f

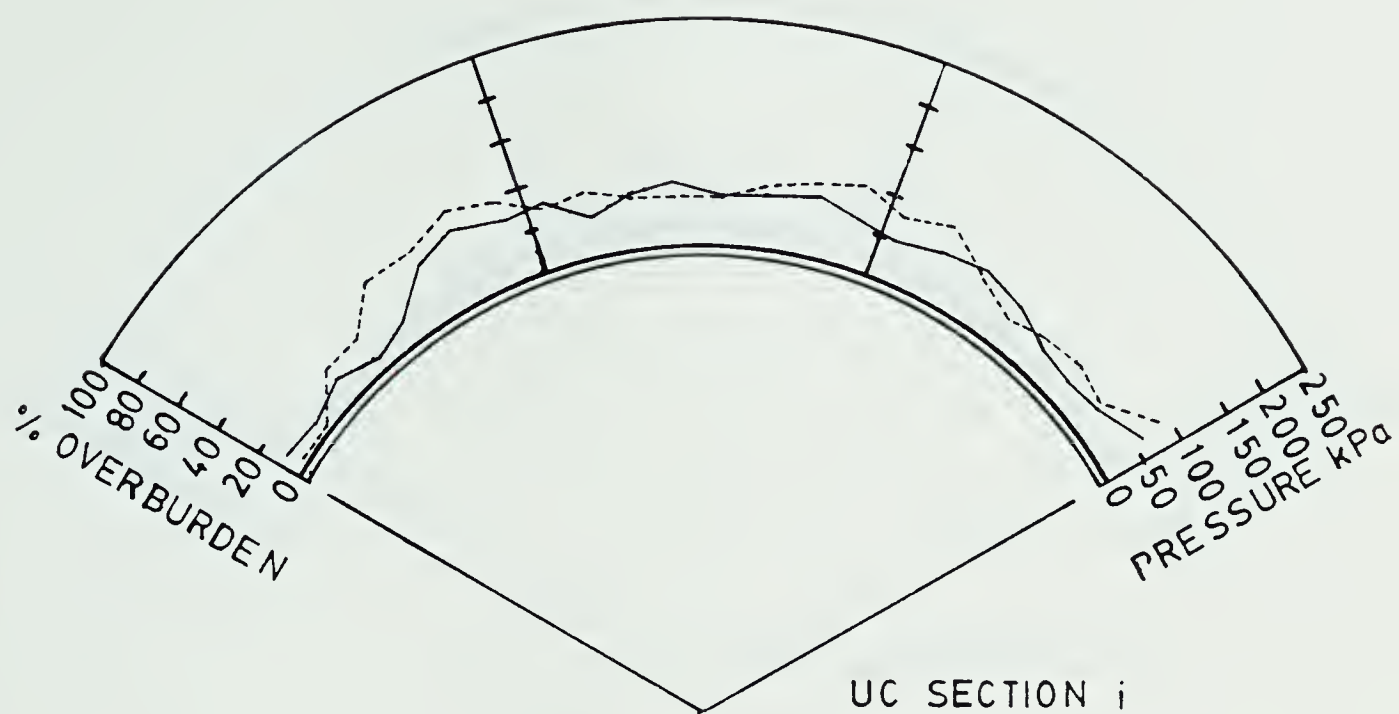


AVERAGE PRESSURE= 72.3 kPa

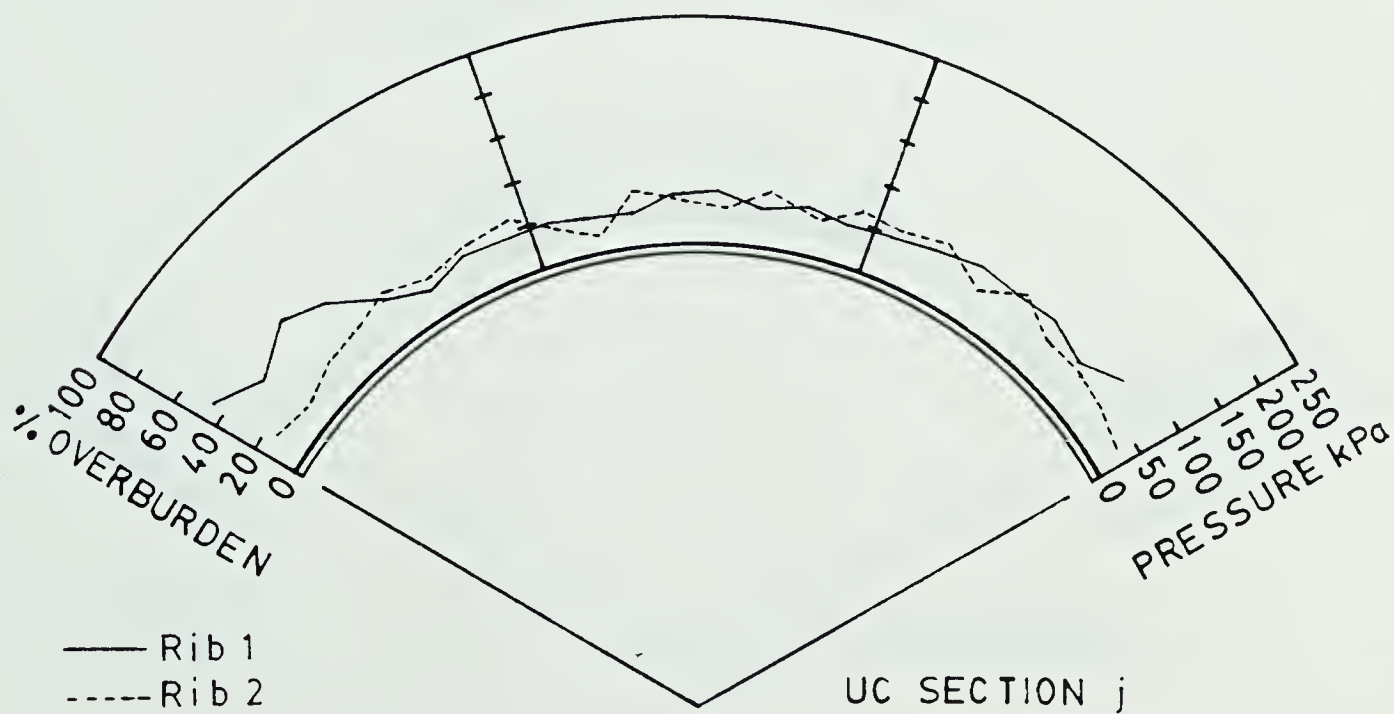


AVERAGE PRESSURE= 50.54 kPa

Figure 5.42 Crown Pressure Distributions for Uncalibrated Sections UC g and UC h

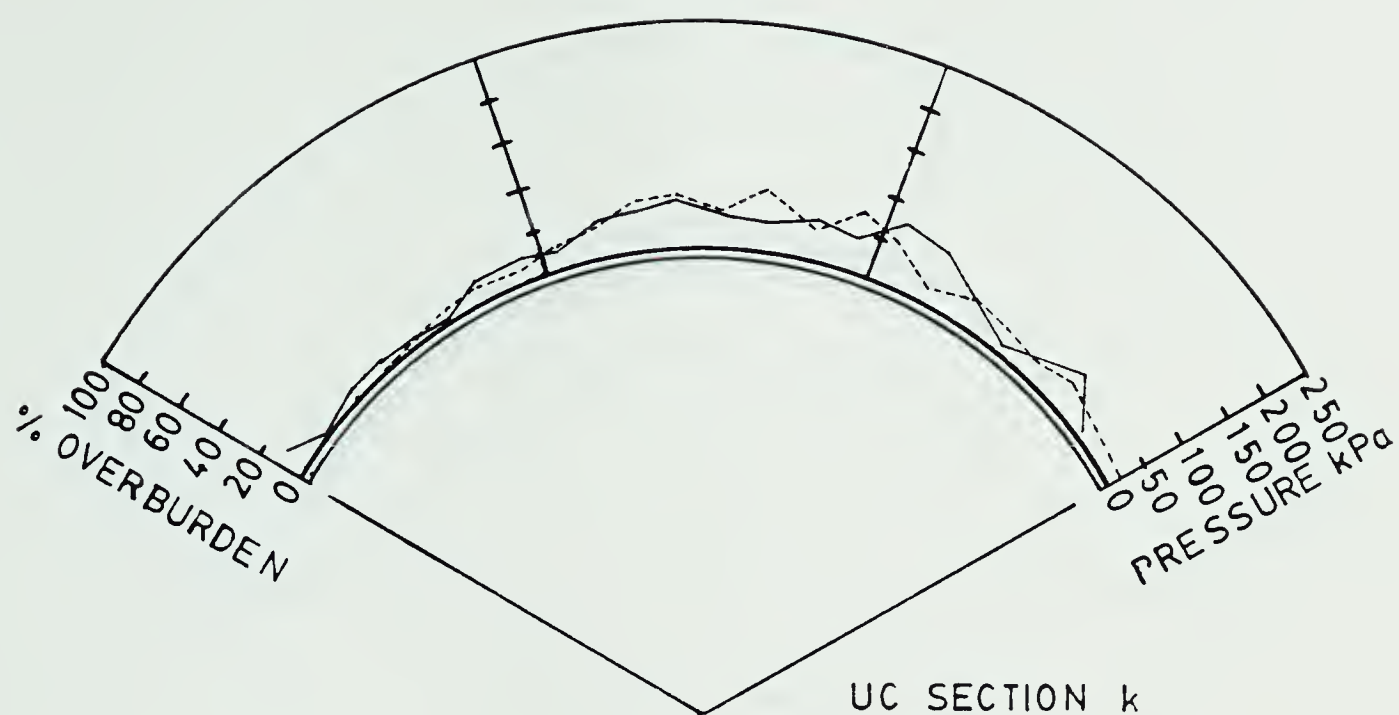


AVERAGE PRESSURE= 54.7 kPa

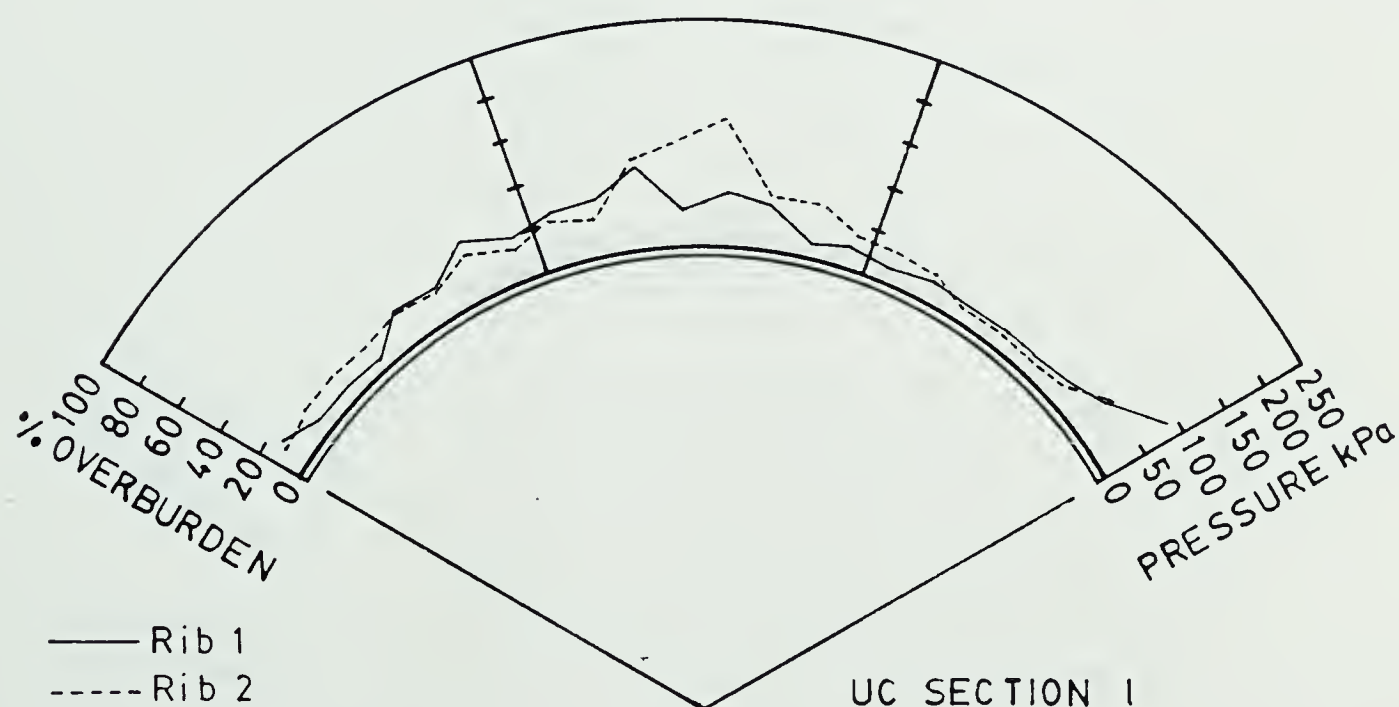


AVERAGE PRESSURE= 53.0 kPa

Figure 5.43 Crown Pressure Distributions for Uncalibrated Sections UC i and UC j



AVERAGE PRESSURE= 26.5 kPa



AVERAGE PRESSURE= 41.8 kPa

Figure 5.44 Crown Pressure Distributions for Uncalibrated Sections UC k and UC l

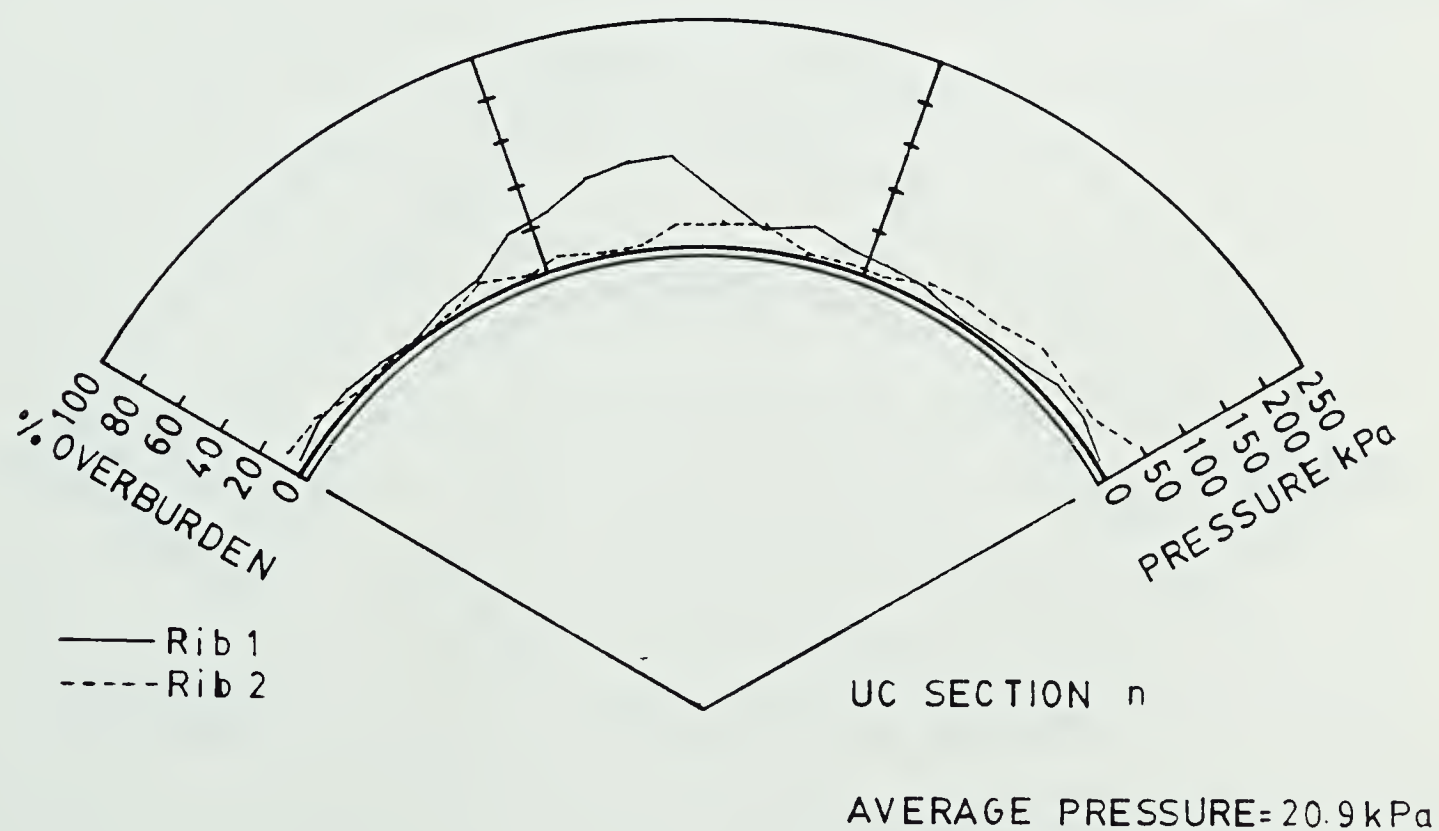
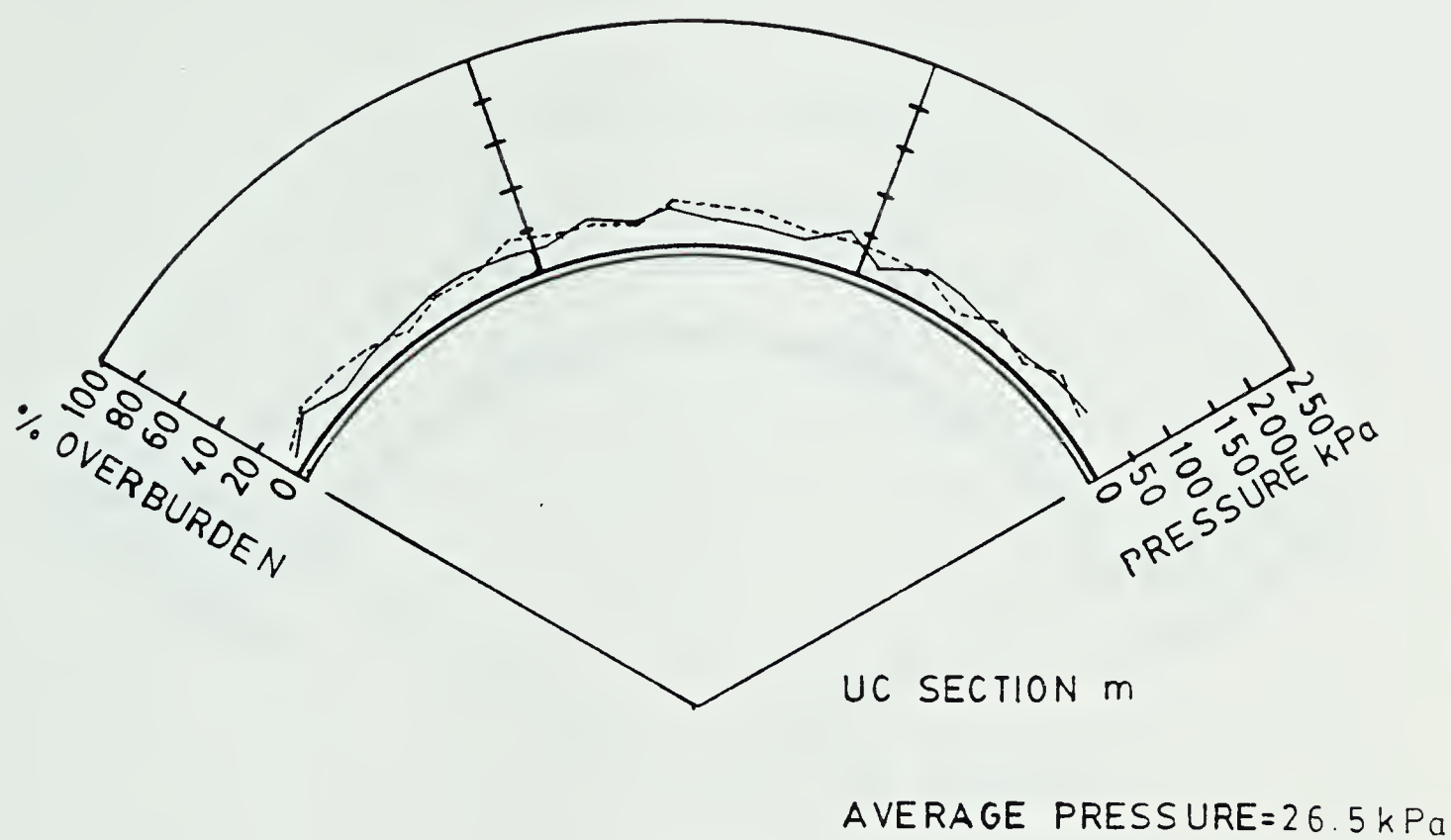
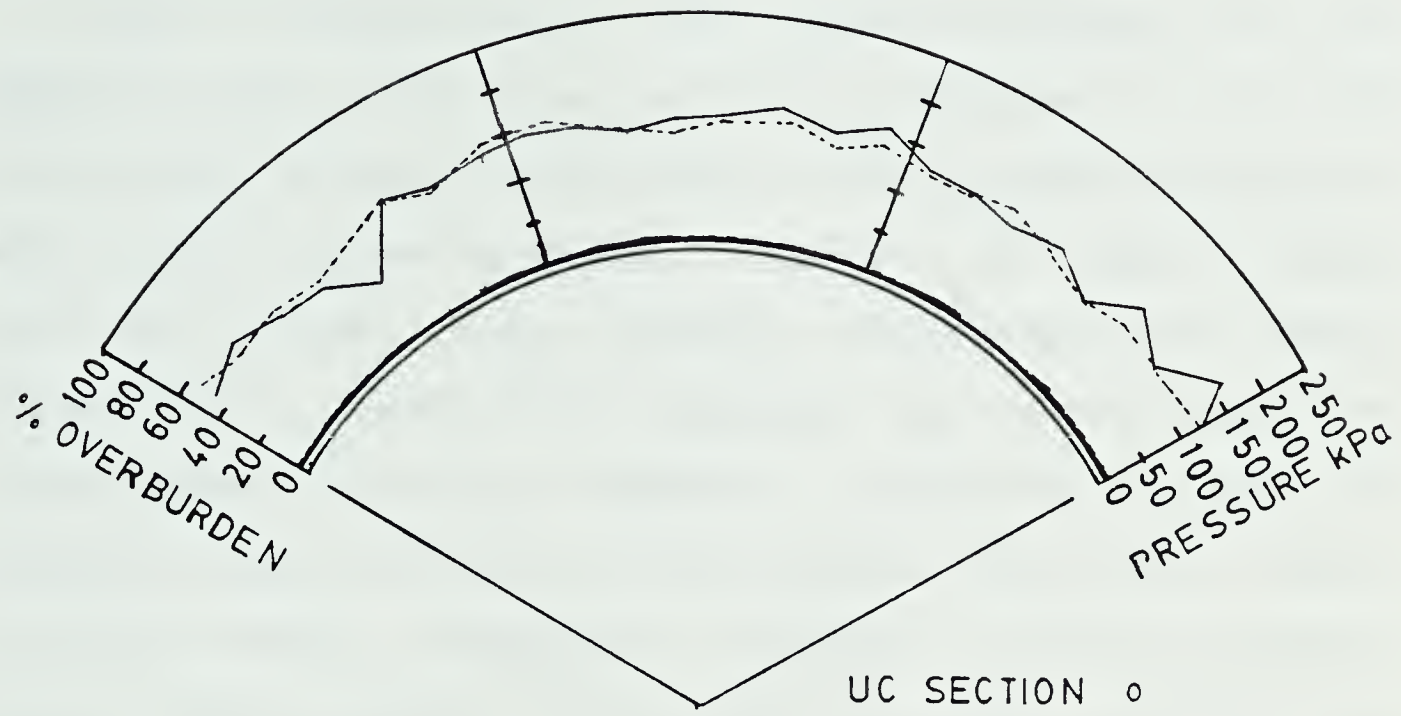
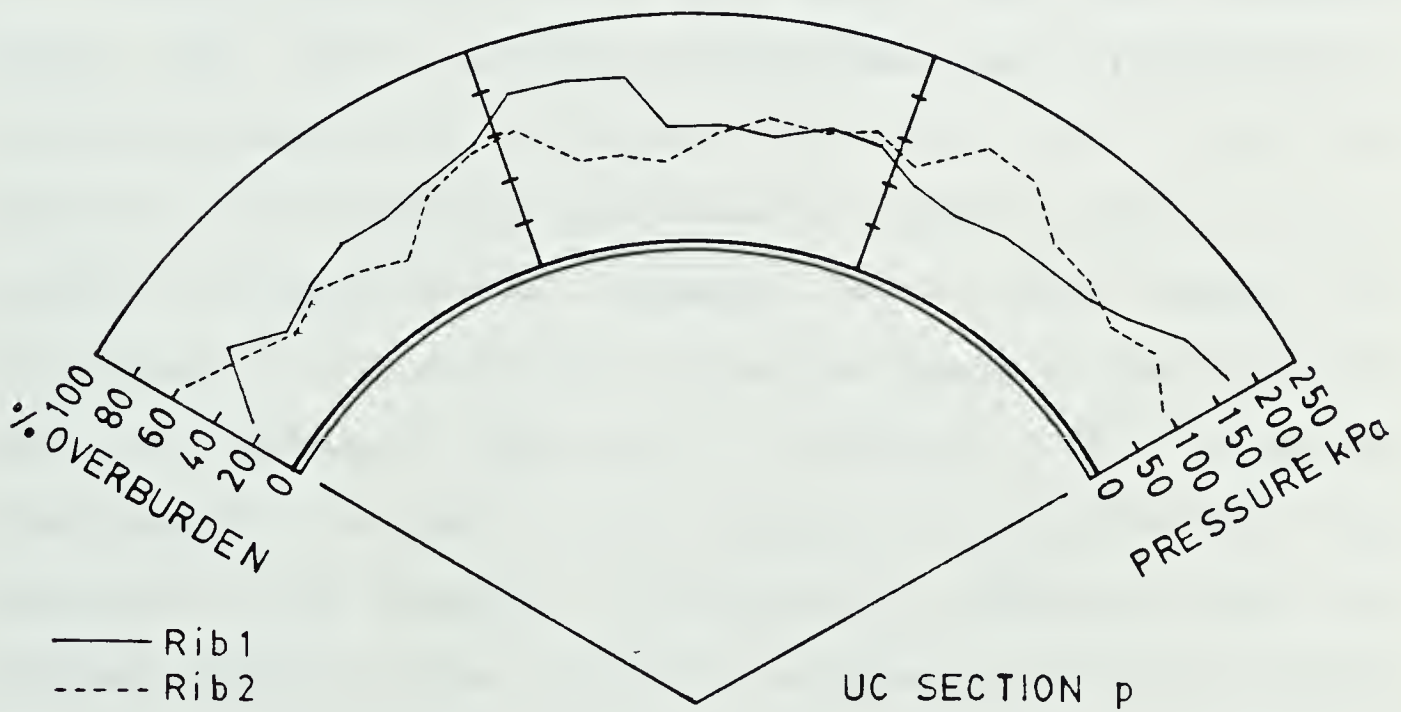


Figure 5.45 Crown Pressure Distributions for Uncalibrated Sections UC m and UC n



AVERAGE PRESSURE=123.3 kPa



AVERAGE PRESSURE=122.2 kPa

Figure 5.46 Crown Pressure Distributions for Uncalibrated Sections UC o and UC p

crown pressure as in UC'b' and heavily bias to one side as in UC'g'.

Minor differences in the derived pressures from two adjacent rings, shown in all of the UC sections is believed attributable to minor tunnelling variations such as slightly more overcut between sections; formation of small random side wall voids; minor geologic differences and small differences in construction procedure, eg. varying times of installation; different expansion pressures (related to overcut); force build up in the installed liner as a result of mole shoving (especially prominent around alignment turns). These observed differences virtually nullify the concept of similar tunnel sections.

Considering point 2 it was seen that the pressure around the liner was not always symmetrical or uniform as would be expected for a flexible liner. The three types of pressure distributions mentioned in regard to point 2 were present, irrespective of pressure level. With regard to structural analysis of the lining the shape of the pressure bulb is extremely important, assuming the pressure distribution obtained in the lagging is duplicated for the steel rib. One pressure distribution observed often in Figures 5.39 to 5.46 is that of unsymmetrical bias loading (UC e, f, g, h, i and k). This loading condition, thought to be a product of the expansion procedure, is critical with regard to moment generation at the joints. Its common occurrence measured in these sections, explains the large

amount of joint failure due to bending observed in the Kennedale tunnel. This undesirable pressure distribution is believed a direct result of continual similar first side expansion of the lining, i.e., whilst expanding the first side less pressure was activated in the lagging, because of the lack of constraint offered by the other side of the lining. Also, the material into which it was expanding was probably quite disturbed due to excavation. Both of these conditions combine to create more circumferential slip than vertical expansion. Upon expansion of the second side, conditions were much more constrained resulting in almost total vertical expansion of the lining, creating increased lagging pressures. This problem is compounded by similar first side expansion of every rib. In the future to offset these undesirable pressure bulbs it is recommended that either stage expansion of the ribs be done or every rib have a different side expanded first.

To investigate loading variability along the tunnel and to eliminate the influence of expansion related pressures, crown pressures based on the eight centrally located boards in each ring were calculated. The results of this exercise together with calculated standard deviations for the average crown pressures are presented in Table 5.4. Given also in Table 5.4 are magnitudes of observed surface settlements above the Uncalibrated Sections.

Pressures in Table 5.4 show a large variation reflecting the influence of differing ground conditions. The

reported large standard deviations are a reflection of local pressure variations coupled with stiffness variations around the assumed mean.

Everything being constant it would be expected that tunnel loads were primarily dependent on ground conditions which should also be true for surface settlements, i.e., increased loads increased settlements. Convergence confinement method predicts that high loads may be obtained with small settlements if the equilibrium point is on the initial arm of the convergence curve. In most soft ground tunnels the ability to install the lining prior to moving substantially down the convergence curve are quite remote, certainly under conditions of shield tunnelling when the face has advanced typically 2 diameters before lining activation. Using ground surface displacement data as presented in Table 5.4, it was possible to construct Figure 5.47. Although a few anomalous values exist a definite trend between crown pressure and surface settlement exists. Accepting a constant ratio between movement at crown and that at surface, Figure 5.47 is proof of lining pressure dependency upon ground displacements.

Ground displacement increases can be expected under conditions of decreasing ground strength and stiffness. This expected increase in displacements and loads has been recognized in clay tunnels where the OFS value, as discussed in Chapter 4, has been used as an indicator of expected tunnel performance. In this study, in an attempt to model

Table 5.4 Uncalibration Section Pressures

Uncal Section i.d.	Mean Average Pressure (kPa)	CROWN PRESSURE DETAILS (kPa)			Surface Settlement (mm)	"n"
		Mean	Stand Dev	% DBurden		
a	23.82	27.89	15.12	11.1	7.1	1.22
b	23.86	35.00	20.85	14.0	7.1	1.53
c	16.71	12.95	10.8	5.2	11.3	0.60
d	11.97	19.65	16.8	7.9	11.1	0.86
e	56.13	66.86	13.9	26.7	9.1	2.93
f	53.10	62.24	29.2	24.9	10.7	2.73
g	72.30	60.23	24.2	24.1	13.7	2.64
h	50.54	54.96	12.0	22.0	15.0	2.41
i	54.70	63.63	10.9	25.5	18.8	2.79
j	52.93	44.60	10.9	17.8	15.6	1.96
k	26.48	37.91	12.5	15.2	8.8	1.66
l	41.80	61.02	32.4	24.4	8.1	2.68
m	26.45	31.51	8.1	12.6	8.0	1.38
n	20.88	34.04	31.6	13.6	7.6	1.49
o	123.30	125.61	22.1	50.2	352.0	5.50
p	122.20	133.10	27.8	53.2	315.0	5.83

"n" = Mean Crown Pressure/ γD

where γ = Weight Density

D = Rib Spacing (1.22m)

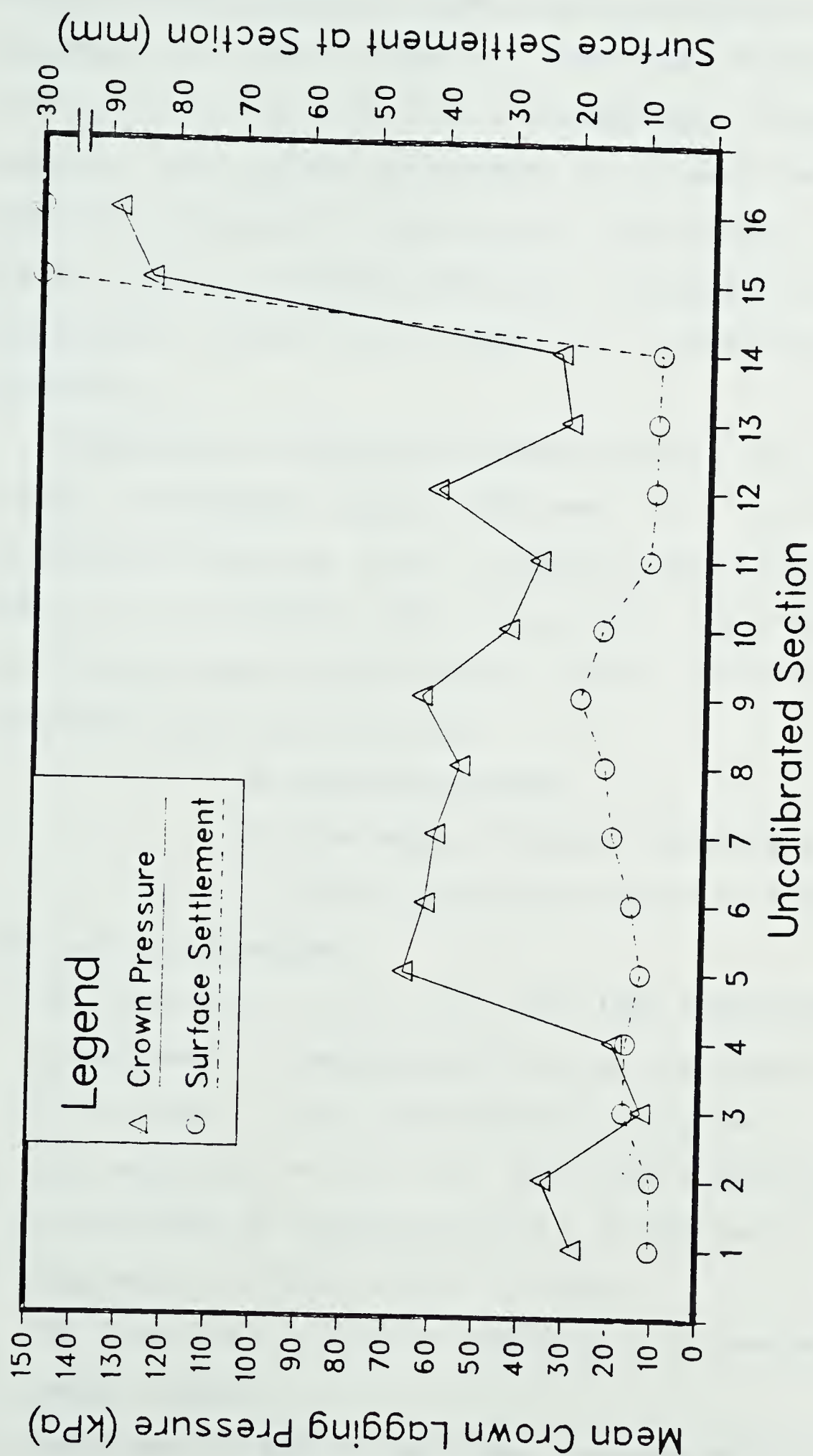


Figure 5.47 Uncalibrated Section Crown Pressures versus Surface Settlement

ground strength changes, three ground convergence curves as presented in Figure 5.34 were generated. Referring to the trend shown in Figure 5.47 of interdependency between lining pressure and surface settlements it is seen that this same dependency is present in the ground convergence curves of Figure 5.34. It should therefore be possible to use the convergence curves as a means of predicting lining pressures.

Referring to Figure 5.34 which contains the generated ground convergence curves obtained for the three cases considered in Section 5.3.1. These curves were produced under the assumption that they were representative of conditions present at the project area. Estimating ground conditions qualitatively from

- a) field knowledge
- b) knowledge of surface settlements
- c) defined geologic regions of Figure 2.4.

the following emerges:

1. UC sections 'a' to 'd' were best represented by the curve based on parameters of $\phi = \phi^* = 35$ degrees and $c = c^* = 10$ kPa, i.e., good ground conditions.
2. UC sections 'e' to 'l' were best represented by the curve based on parameters of $\phi = 35$ degrees; $\phi^* = 19.5$ degrees; $c = 10$ kPa and $c^* = 0$ kPa.
3. UC sections 'm' and 'n' probably lie somewhere between case 1 and 2.
4. Sections 'o' and 'p' were best represented by the curve

based on parameters of $\phi = 35$ degrees; $\phi^* = 0$ degrees; $c = 10$ kPa and $c^* = 0$ kPa .

Using estimates of crown settlements varying from 1 to 2 times that observed at the surface we obtain the following ranges :

1. Using a typical surface settlement of 8 mm the limits of crown movements were 0.5% to 1.0% . This yields a pressure range of 42 kPa to 24 kPa which agrees quite well with the measured range of 35 kPa to 12.9 kPa obtained from UC sections 'a' to 'd'.
2. Using a typical surface settlement of 13 mm the limits of crown movement were 0.85% to 1.7%. This yields a pressure range of 85 kPa to 72 kPa which is slightly above the measured range of 66.9 kPa to 37.9 kPa.
3. no estimation given.
4. In this area the surface settled over 300 mm which corresponds to a crown movement percentage of 20% from which full overburden would be predicted. In reality only 50% overburden was measured by the laggings.

Information from this pressure predictive exercise is quite good and approaching accuracies acceptable for more economical tunnel design in intermediate ground conditions.

Predicted pressures in poorest ground conditions were suspect but in these ground conditions it is already prudent for design on full overburden pressure.

Further illumination of the Convergence Confinement Method is obtained from Figure 5.48 . In this Figure, average crown lagging pressure (Table 5.4) normalised to full overburden pressure, was plotted against the surface settlement measured at the UC section. Superimposed on this Figure are the ground convergence curves as obtained presented in Figure 5.34. Transferral of the ground curves onto Figure 5.48 was achieved under the assumption that the ratio of surface settlement to crown settlement (S_c / S_s) was 0.67. The value of 0.67 is slightly less than the reported values of close to unity in Chapter 4. However, the multipoint extensometers of Chapter 4 were not able to detect an expected increase in displacements due to loosening and/or yielding close to the tunnel crown. For this reason the value of 0.67 was chosen as representative average. Using this ratio the movements at the crown were adjusted to the corresponding movement at surface.

Measured pressures obtained from uncalibrated sections of tunnel sections along the tunnel, presented in Figure 5.48, are seen to fall into two distinct clusters one of which is intersected by the ground convergence curve generated under the assumption of $\phi = \phi^* = 35^\circ$ and $c = c^* = 10\text{kPa}$. The second cluster, although lying slightly to the left of the intermediate strength curve ($\phi = 35^\circ$; $\phi^* = 19.5^\circ$; c

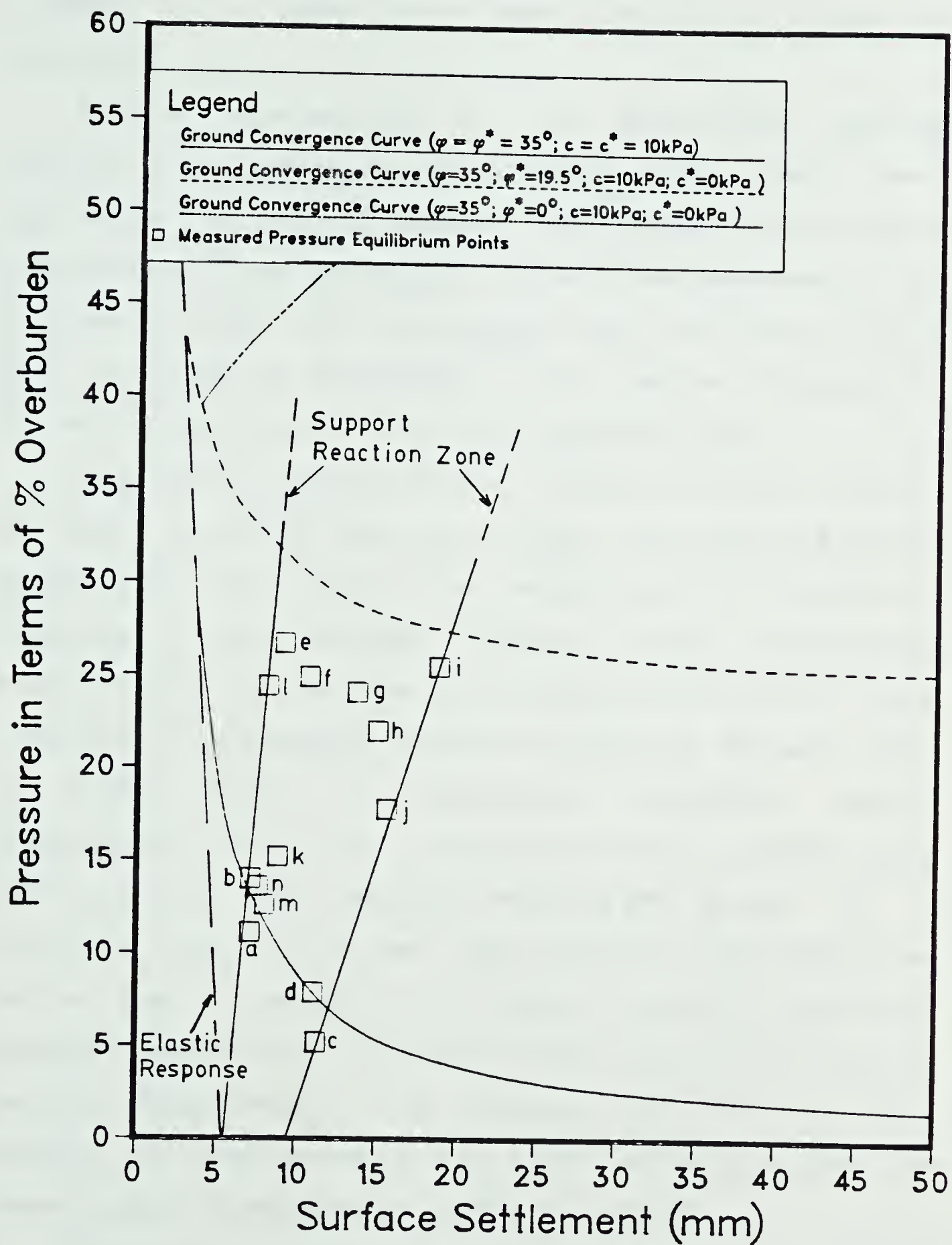


Figure 5.48 Uncalibrated Section Pressures in terms of Percentage Overburden versus Surface Settlement

= 10kpa; $c^* = 0$ kPa), has a trend line similar to that of the curve.

Earlier discussions on the Uncalibrated Lagging Sections, cited groups of sections that were thought best represented by typical ground convergence curves. Figure 5.48 supports these groupings with only one measurement (UC k) lying far away from its assigned curve. Sections UC m and UC n, not given any designation in the earlier discussion, lie very close to the $\phi = \phi^* = 35^\circ$ strength case.

From the measured pressures a "Support Reaction Zone", as shown on Figure 5.48 can be drawn. The shape and extent of this zone casts light on the support-ground interaction responses of the selected support system for differing ground conditions along the tunnel. Interpretation of this Convergence Confinement diagram is aided by the fact that, for Figure 5.48, no assumptions regarding initial displacements prior to lining installation, has been made before plotting the measured equilibrium points. It is therefore possible to see the effects of local variances such as overcut; variability in support expansion pressure; delayed installation time which have resulted in increased surface displacements. The pressures are seen to drop rapidly in good ground ($\phi = \phi_r = 35^\circ$) and only slightly in poorer ground conditions ($\phi = 35^\circ$; $\phi^* = 19.5^\circ$).

Theoretical predictions in Section 5.3.1 indicate that significant pressure decreases for inward movement of the tunnel wall are only to be expected under conditions of

relatively high strength. This has been confirmed by the measured field pressures resulting in the Support Reaction Zone of Figure 5.48. This zone shows that the range of surface settlements widens as increased pressures, which have been brought about by ground strength decreases, occur. It also demonstrates clearly that the support pressure largely depends on the ground quality while surface settlements, although dependent on the ground conditions, can be controlled to a larger extent if good construction techniques are employed.

A ground reaction zone, instead of a unique line, is observed for two principal reasons:

1. With decreasing ground quality it becomes increasingly difficult to control the ground at the tunnel face and larger movements occur;
and more importantly
2. Under strong ground conditions, a little inward movement results in quite a large uptake of the stress loss by the ground, thereby decreasing the support pressure required for equilibrium. Under poorer conditions, the ability of the ground to take up the stress loss is reduced and therefore larger displacements, extending into the soil mass and eventually to the surface, are required to achieve a significant reduction in required equilibrium support pressure.

Evidence in support of point 2 is seen from Figure 5.48 by examination of the behaviour of the two individual

measured clusters. The lower cluster is seen to tend rapidly to lower pressures with increasing movements while there is little change in pressure for the second cluster. In the first case only modest movements and hence a narrow Support Reaction Zone is observed. Cluster 2 exhibits very little variation in pressure but has a larger range of surface settlements, hence, the Support Reaction Zone widens. Further evidence of this widening of the Support Reaction Zone is obtained from measured values for UC'o' and UC'p' (not plotted on Figure 5.48) which have values of 50% overburden pressure and over 300mm of surface settlement. This indicates that, as the Support Reaction Zone approaches the $\phi^* = 0^\circ$ and $c^* = 0\text{kPa}$ ground convergence curve, ground control at the tunnel face deteriorates rapidly and stress uptake by the ground is very low resulting in largely uncontrollable displacements and significantly higher pressures. It is however of interest to note that even under conditions of extreme yielding, only 50% of overburden pressure was measured on the lagging. Minor differences in the Support Reaction Curve can be attributed to variations in lining stiffness but this variability is much less than that of the varying ground conditions.

In summary, the ground conditions constitutes the most important factor with regard to the expected support pressures while the support characteristics (stiffness, overcut, expansion pressure, installation time etc.) dominate the ground displacements for any constant strength

situation.

6. SUMMARY AND CONCLUSIONS

This investigation of tunnel performance by extensive monitoring along the length of a soft ground tunnel, provided valuable information on the variability of loads and displacements. Contrary to other studies, the influence of changing ground conditions and strength could be evaluated, as encountered ground conditions ranged from very stable through to flowing. For this project, regions of different geologic conditions could be closely correlated with magnitudes of surface displacements and lining loads. Larger values of both were observed as ground conditions deteriorated.

The investigation for the project focused on the variability along the tunnel in two main areas:

1. Ground Displacements; and
2. Load Measurements on lagging and in the Steel Sets.

Conclusions arising from this project can be grouped accordingly.

Ground Displacements

Observed settlements, found to range between 6 and 300mm, could be related to increased difficulty in tunnelling conditions as different defined geologic regions were encountered. It was found that ground settlements were affected by the quality of ground control at the tunnel face and the reduced ability to limit ground movements prior to

lining activation (Figure 5.48). Only in very poor ground was the performance entirely dominated by the ground control at the face.

Information from ground displacements at depth and subsequent analysis cast light on the kinematics of a fully developed block failure above a tunnel. Arising from the field measurements it was observed, that under conditions of no yield ($OFS = 0.86$; undrained factor of safety against block failure = 10; drained factor of safety = 3.3) equal vertical displacements with depth, indicating "block like" movements, occurred above the centre line of the tunnel. This movement profile, considered analogous to elastic movements at the centre of a deep elastic beam, is similar to the profiles observed in highly overstressed ground. However, the magnitude of displacement (approximately 10mm) is much smaller. Hence, analysis of the shape of the vertical displacement profile to determine the extent of yielding is not sufficient but must be used in conjunction with knowledge of the whole displacement field. Discussion presented in Chapter 4, however, suggest that yielding can be estimated from the point of non linearity in the vertical displacement profile.

Measurement of horizontal displacements indicated under conditions of good ground very little movement toward the face ($<1\text{mm}$) occurred. In poor ground, however, observed vertical surface settlements exceeding 300mm caused slumping of the ground to occur at least 3 diameters ahead of the

face. This slumping was reflected in large horizontal movements ($>10\text{mm}$) at the surface. Large movements, such as these, are potentially very dangerous to surface structures.

Tunnel Load Measurements

Before fulfilling one of the project objectives, that of obtaining load variability along the tunnel, it was necessary to solve another initial objective of the project, i.e., develop a simple, accurate and inexpensive measurement technique. Both these objectives were achieved by:

1. postulation of a measurement technique;
2. validation of technique accuracy; and
3. utilization of the technique for load measurement along the tunnel.

The measurement technique postulated involved measuring deflections on typical construction wood laggings. After attaining knowledge of the flexural rigidity of the lagging, measured deflections could be used to calculate equivalent uniform pressures on the lagging. For measurement of deflection a "University of Alberta Deflectometer" was designed and constructed.

The accuracy of wood lagging pressures was investigated using 4 controlled test sections, each of which took the format of three instrumented lagging rings with load cells being inserted in the two middle steel set rings. Using

simulated steel laggings, assumed to give pressure values accurate enough to be used in direct comparison with those derived from the wood lagging, it was found that wood lagging was more prone to TBM influence. After emergence from the TBM affected area, however, similar load records were obtained for steel and wood laggings, indicating the reliability and predictive capabilities of the wood laggings. Accepting TBM influences and uninvestigated moisture effects to give a larger natural variation in predicted pressures, the ability to cheaply and easily take measurements over longer tunnel sections than is usually considered economic was felt to compensate for this reduced accuracy. For these reasons it is concluded that the monitoring of wood lagging deflections along a tunnel can be used as an effective and adequate means of establishing load magnitudes for the appraisal of factor of safety of the temporary support. Further similar studies on the variability of pressures within tunnels, would aid greatly in tunnel design.

In this project measured loads agreed with typical structural design loads only under conditions of full failure to the surface. This was expected as models of Peck (1972) and those presented in Duddeck and Erdmann (1983) assume full overburden. Only loads by Terzaghi (Proctor and White, 1977) gave intermediate loads for comparison with those measured and in general they agreed quite well.

Information on the local behaviour of this tunnel, obtained from the formal test sections, indicated symmetry with regard to lining pressures and steel set axial thrusts. Equalisation of pressure at crown and springline was also observed. Such distributions are typical of a flexible lining system (Peck, 1969).

Investigation of steel set to lagging load ratios indicated values ranging typically from 1.5 to 3.0, with the lower values being obtained in poorer ground conditions. It can thus be concluded that as ground conditions deteriorate the ratio of steel set loads to lagging loads will tend toward unity.

From these measured ratios of 1.5 to 3.0 an important design compatibility criterion emerges for steel set and wood lagging primary liners in Edmonton, i.e., the ultimate capacity of the laggings should lie between 33 - 66% of the steel set capacity. Further investigation on compatibility of steel set and wood lagging systems showed that as rib spacing is reduced, while maintaining steel sets of similar dimensions, the factor of safety of the steel set reduces faster than that of the wood lagging. This may lead to undesirable modes of deformation or instability. From this it was concluded that design of compatible steel sets for varying lengths and thicknesses of lagging should be investigated.

Satisfied with the accuracy of the new measuring technique, it was subsequently used to measure lining crown

pressures at 16 sections along the tunnel. These sections, which covered a plan distance of approximately 700m, showed a pressure range of 5.2 - 53.2% of full overburden on the laggings. As with increasing surface displacements, pressure increases could be correlated with deteriorating ground conditions. Study of the interaction between loads and displacements was possible because all 16 sections were chosen to lie under surface settlement points. A plot of surface displacement and mean crown pressure (Figure 5.47) showed a definite relationship between the two.

The interaction of lining pressures and displacements was further investigated using the convergence confinement method :- a method generally thought only applicable to deep tunnels. Using assumed ground peak strength parameters coupled with varying strength parameters in the yield zone, three ground convergence curves were generated assuming different apparent shear strength parameters (ϕ^* and c^*) in the yield zone. These apparent shear strength parameters were chosen to model temporary ground losses resulting from excavation activities. While they are temporary parameters they dominate the support equilibrium pressure found to have occurred within approximately 10 days or 10-15 diameters after installation for this project. These curves, transferred to represent surface displacements, compared well with measured conditions. In this fashion a support reaction zone could be derived to describe the support performance. This zone (Figure 5.48) was seen to widen as

the support pressure, required for equilibrium, increased as a result of decreasing ground strength. Measured equilibrium points, presented in Figure 5.48, showed two clusters with each cluster representing points obtained in regions where ground conditions were approximately similar. Generated ground convergence curves, obtained with varying ground strength parameters thought applicable, proved to lie very close to each of these clusters.

From investigation of the interaction of displacements and pressures it was concluded that:

1. the magnitude of lining pressure is primarily a function of ground strength;
2. the amount of ground displacements, observed for any ground condition, is largely controlled by construction sequence (mainly time of installation and activation) and the support characteristics;
3. ground convergence curves generated by assuming apparent shear strength parameters, thought active in the yield zone around the tunnel, gave expected ranges of lining pressures along lengths of the tunnel which agreed quite well with those actually measured. The magnitudes of the apparent shear strength parameters(c^* and ϕ^*) were chosen arbitrarily to model expected strength losses resulting from excavation procedures and differing material types. Further investigations, with an aim to prove and justify more appropriate strength loss parameters, are however necessary. Research into

The first part of the paper discusses the importance of the study and the objectives of the research. It also outlines the methodology used in the study and the results obtained. The second part of the paper discusses the implications of the study and the conclusions drawn from the research. It also outlines the limitations of the study and the areas for further research.

The third part of the paper discusses the implications of the study and the conclusions drawn from the research. It also outlines the limitations of the study and the areas for further research. The fourth part of the paper discusses the implications of the study and the conclusions drawn from the research. It also outlines the limitations of the study and the areas for further research.

The fifth part of the paper discusses the implications of the study and the conclusions drawn from the research. It also outlines the limitations of the study and the areas for further research. The sixth part of the paper discusses the implications of the study and the conclusions drawn from the research. It also outlines the limitations of the study and the areas for further research.

The seventh part of the paper discusses the implications of the study and the conclusions drawn from the research. It also outlines the limitations of the study and the areas for further research. The eighth part of the paper discusses the implications of the study and the conclusions drawn from the research. It also outlines the limitations of the study and the areas for further research.

the development of more analytically correct models for the deformation mechanisms are also required.

REFERENCES

- Atkinson, J.H., Cairncross, A.M. and James, R.G. 1974. Model tests on shallow tunnels in sand and clay. *Tunnels and Tunnelling*, Volume 6, No.??, pp. 28-32.
- Atkinson, J.H., Brown, E.J. and Potts, D.M. 1975. Collapse of shallow unlined tunnels in dense sands. *Tunnels and Tunnelling* Volume 7, No. 3, pp. 81-87.
- Atkinson, J.H. and Potts, D.M. 1977. Subsidence above shallow tunnels in soft ground. *Journal of Geotechnical Engineering Division*, American Society of Civil Engineers, Volume 103, pp. 307-325.
- Burland, J.B., Moore, J.F.A. and Smith, P.D.K. 1972. A simple and precise borehole extensometer. *Geotechnique*, Volume 22, pp. 174-177.
- Attewell, P. 1977. Ground movements caused by tunnelling in soil. *Proceedings Institute of Structural Engineers. Conference on large ground movements and structures.* University of Wales Institute of Science and Technology, 4-7 July 1977, pp. 812-948.
- Benham, P.P. 1965. *Elementary mechanics of solids.* Oxford,

Pergamon, 264p.

Bjerrum, L. 1967. Progressive failure in slopes of overconsolidated plastic clay and clay shales. Journal of Soil Mechanics Division, Proceedings American Society of Civil Engineers, Volume 93, SM5, pp. 3-39.

Burland, J.Q., and Moore, J.F.A. 1973. The measurement of ground displacements around deep excavations. Field Instrumentation in Geotechnical Engineering, Butterworth and Co., London, pp. 70-84.

Branco, P., 1981. Behaviour of a Shallow Tunnel in Till. M.Sc. Thesis, Department of Civil Engineering, University of Alberta, Edmonton, Alberta, 351p.

Broms, B.B. and Bennermark, H. 1967. Stability of clay at vertical openings. Transactions American Society Civil Engineers, Volume 93, SM1, pp. 71-94.

Carlson, V.A. 1967. Bedrock topography and surficial aquifers of the Edmonton district, Alberta. Alberta Research Council, Report 66-3, 21p.

City of Edmonton 1983a. Moisture tests on tunnel timbers. Report prepared for the City of Edmonton, Department of Water and sanitation by the City of Edmonton, Department

of Materials and Testing. Report No. 71158(402.10.1).

City of Edmonton 1983b. Wood timber test results. Report prepared for the City of Edmonton, Department of Water and sanitation by the City of Edmonton, Department of Materials and Testing. Report No. 754487(402.10.1).

Cording, E.J. and Hansmire, W.H. 1973. Displacement around soft ground tunnels. General report. Proceedings 5th Panamerican Conference on Soil Mechanics and Foundation Engineering, Buenos Aires, Argentina, Volume 4, pp. 571-633.

Cording, E.J., Hendron, A.J., PacPherson, H.H., Hansmire, W.H., Jones, R.A., Mahar, J.W. and O'Rourke, T.D. 1975. Methods for geotechnical observations and instrumentation in tunnelling. Report prepared for U.S. National Science Foundation, Washington, D.C. NTIS No. PB252585-PB252586.

Daemen, J.J.K. 1975. Tunnel support loading caused by rock failure. Ph.d. Thesis, Department of Civil Engineering, University of Minnesota, Minnesota, U.S.A.

Dejong, J. and Morgenstern, N.R. 1973. Heave and settlement of two tall building foundations in Edmonton, Alberta. Canadian Geotechnical Journal, Volume 10, pp. 261-281.

- Duddeck, H. and Erdmann, J. 1982. Structural design models for tunnels. Tunnelling 82'. Institute of mining and metallurgy, pp. 83-91.
- Dunnicliff, C.J. 1971. Equipment for field deformation measurements. Proceedings 4th Panamerican Conference on Soil Mechanics and Foundation Engineering, San Juan, Volume 2, pp. 319-332.
- Eisenstein, F. and Morrison, N.A. 1973. Predictions of foundation deformations in Edmonton using an in-situ pressure probe. Canadian Geotechnical Journal, Volume 10, pp. 193-210
- El-Nahhas, F. 1977. Field measurements in two tunnels in the City of Edmonton. M.Sc. Thesis, Department of Civil Engineering, University of Alberta, Edmonton, Alberta, 85p.
- El-Nahhas, F. 1980. The behaviour of tunnels in stiff soils. Ph.D. Thesis, Department of Civil Engineering, University of Alberta, Edmonton, Alberta, 305p.
- Hanna, T.H. 1973. Foundation instrumentation. Trans. Tech. Publications, Cleveland.

- Heuer, R.E., 1976. Catastrophic ground loss in soft ground tunnels. Proceedings of the 3rd North American Rapid Excavation and Tunnelling Conference, pp. 278-295.
- Hewett, B.H.M. and Johannesson, S. 1922. Shield and compressed air tunnelling. McGraw Hill Book Company, New York.
- Irish, E.J.W. 1970. The Edmonton group of south central Alberta. Bulletin of Canadian Petroleum Geology, Volume 18, pp. 125-155.
- Kathol, C.P. and MacPherson, R.A. 1975. Urban geology of Edmonton. Alberta Research Council, Bulletin 32, 61p plus maps.
- Kovari, K., Amstad, C.H., Fritz, P. 1977. Integrated measuring technique for rock pressure. International Symposium on Field Measurements in Rock Mechanics, Zurich, pp.289-316.
- May, R.W. and Thomson, S. 1978. The geology and geotechnical properties of till and related deposits in the Edmonton, Alberta area. Canadian Geotechnical Journal, Volume 15, pp. 362-370.
- Mello, V.F.B. 1981. Proposed basis for collating experiences

for urban tunnelling design. Proceedings of the Symposium on Tunnelling and Deep Excavations in Soils, Sao Paulo, Brazil, pp. 197-235.

Mendes, R.H., Brown, E.L., Moreau, R. and Boyer, B. 1970. Supervision of the behaviour of Daniel Johnson Dam (Manicouagan 5). Transactions of 10th International Congress on Large Dams, Montreal, Volume III, pp. 1183-1205.

Muir Wood, A.M. 1975. The circular tunnel in elastic ground. Geotechnique, Volume 25, pp 115-127.

Negro, A. and Eisenstein, Z. 1981. Ground control techniques compared in three Brazilian water tunnels. Part 3. Tunnels and Tunnelling, Volume 13, No. 11 pp. 48-51.

Palmer, J.H.L. and Belshaw, D.J. 1980. Deformations and pore pressures in the vicinity of a precast, segmented concrete-lined tunnel in clay. Canadian Geotechnical Journal, Volume 17, pp. 174-184.

Peck, R.B. 1969. Deep excavations and tunnelling in soft ground. State of the Art Report. Proceedings 7th International Conference on Soil Mechanics and Foundation Engineering, Volume 3, Mexico City, Mexico, pp. 225-290.

- Peck, R.B., Deere, D.U., Monsees, J.E. and Parker, H.W. 1969. Some design considerations in the selection of underground support system. Report for the U.S. Department of Transportation NTIS No. PB 190 443.
- Peck, R.B., Hendron, A.J. and Mohraz, B. 1972. State of the art of soft ground tunnelling. Proceedings of the 1st North American Rapid Excavation and Tunnelling Conference, Volume 1, pp. 259-286.
- Proctor, R.V. and White, T.L. 1977. Earth tunnelling with steel supports. Commercial Shearing, Inc., Youngstown, Ohio, U.S.A., 274p.
- Savigny, K.W. 1980. In-situ analysis of naturally occurring creep in ice-rich permafrost soil. Ph.D. Thesis, Department of Civil Engineering, University of Alberta, Edmonton, Alberta, 439p.
- St. Onge, D.A. 1972. Sequence of glacial lakes in north-central Alberta. Geologic survey of Canada. Bulletin 213, 16p.
- Szechy, K. 1966. Art of Tunnelling. Translated from Hungarian, Published by Akademiai Kiado Budapest.

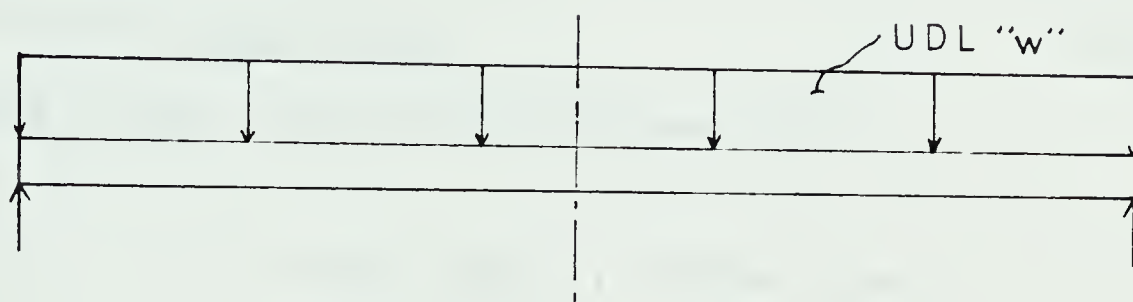
- Terzaghi, K. 1943. Theoretical Soil Mechanics. John Wiley and Sons, New York.
- Tiedemann, C.E. 1984. The characterization of tills in the Edmonton area using standard penetration test results. M.Eng. Report, Department of Civil Engineering, University of Alberta, Edmonton, Alberta, 30p.
- Thomson, S. and El-Nahhas, F. 1980. Field measurements in two tunnels in Edmonton, Alberta. Canadian Geotechnical Journal, Volume 17, pp 20-33.
- Thomson, S. and Yacyszyn, R. 1977. Slope instability in the City of Edmonton. Canadian Geotechnical Journal, Volume 14, No. 1 pp. 1-16.
- Westgate, J.A. 1969. The Quaternary geology of the Edmonton area, Alberta. In Pedology and Quaternary research. Edited by S. Pawluk. University of Alberta printing Department, Edmonton, Alberta, pp. 129-151.
- Wilson, S.D. 1967. Investigations of embankment performance. Journal Soil Mechanics and Foundation Division, American Society of Civil Engineers, Volume 93, No. SM4, pp.135-166.
- Wittebolle, R.J. 1983. The influence of microfabric on the

engineering properties of glacial tills. M. Sc. Thesis.
Department of Civil Engineering, University of Alberta,
Edmonton, Alberta.

APPENDIX A

Calculation of Equivalent Uniformly Distributed Pressure on Laggings

Diagram of System



For a uniformly distributed load the deflection at the centre of a beam, which is also the maximum deflection, is obtained by the expression

$$v_{\max} = v_{cl} = 5wl^4/384EI$$

where v_{cl} = deflection at the beam centre line
 w = load per unit length on beam
 l = length of beam
 EI = flexural rigidity of beam

Therefore for a measured central deflection, the pressure magnitude "w" is

$$w = v_{cl} \frac{384EI}{5l^4} \text{ [F/L]}$$

Eq. A1.1

The calculated "w" from Eq. A1.1 is in the form of a load per unit length of the beam, whereas we wish to have a pressure (p). As "w" is calculated from the expression

$$w = p * \text{beam width}$$

"p" is obtained from

$$p = w / \text{beam width} \quad \text{Eq. A1.2}$$

In this project the parameter values were

$$l = 1114\text{mm (wood)} ; 1187\text{mm (steel)}$$

$$b = 130\text{mm (wood)} ; 100\text{mm (steel)}$$

$$v_{cl} = \text{variable}$$

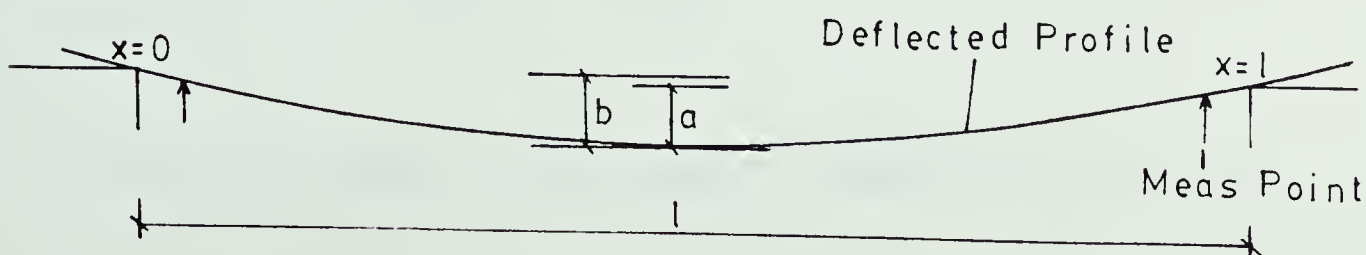
Using these values the following expressions are obtained

$$w (\text{steel}) = w (\text{wood}) = 4.812 * 10^{-11} v_{cl} EI \text{ [N/mm]} \quad \text{Eq. A1.3}$$

$$p (\text{wood}) = 4.812 * 10^{-11} v_{cl} EI / 130 \text{ [N/mm}^2\text{]} \quad \text{Eq. A1.4}$$

$$p (\text{steel}) = 4.812 * 10^{-11} v_{cl} EI / 100 \text{ [N/mm}^2\text{]} \quad \text{Eq. A1.5}$$

The above calculated values must be altered by a correction because the fitted end measuring points were not at end of the lagging. The effect of this is shown diagrammatically below



a = deflection measured

b = actual total deflection

Because the measured deflection is smaller than that actually occurring, pressures predicted by Equations A1.4 and A1.5 will be smaller than actual. To calculate the appropriate correction factor it is first necessary to calculate the deflected shape of the beam, i.e., variation of deflection (v) along the length of the beam. Having obtained the deflected shape of the beam it will be possible to calculate the relative magnitudes of deflections occurring at the measuring points to the maximum value. Using Macaulys' method (Benham, 1965) the moment variation for a uniformly distributed load along the beam is given by

$$EI(d^2v/dx^2) = -wlx/2 + wx^2/2 \quad \text{Eq. A1.6}$$

Integration of Eq. A1.6 twice yields:

$$EI(dv/dx) = -wlx^2/4 + wx^3/6 + A \quad \text{Eq. A1.7}$$

$$EIv = -wlx^3/12 + wx^4/24 + Ax + B \quad \text{Eq. A1.8}$$

Introducing boundary conditions

$$x = 0 ; v = 0$$

$$x = l ; v = 0$$

yields $B = 0$ and $A = wl^3/24$

Deflected shape of the beam is therefore given by:

$$v = [-wlx^3/12 + wx^4/24 + wl^3x/24]/EI \quad \text{Eq. A1.9}$$

which gives:

$$v_{cl} = v_{557} = 2.0 * 10^{-6} w/EI$$

For the wood laggings measuring points were fitted 50mm from the lagging end, therefore:

$$v_{50} = 1.714 * 10^{-6} w/EI$$

Therefore % underestimation = $(2.0 - 1.714)/2.0 * 100\% = 14.3\%$

In otherwords the calculated value is 85.7% of the actual pressure and therefore the correction factor $1/0.857 = 1.167$ must be applied to the woods.

$$p(\text{wood}) = [4.812 * 10^{-11} v_{cl} EI / 130] * 1.167 [F/L^2] \quad \text{Eq. A1.10}$$

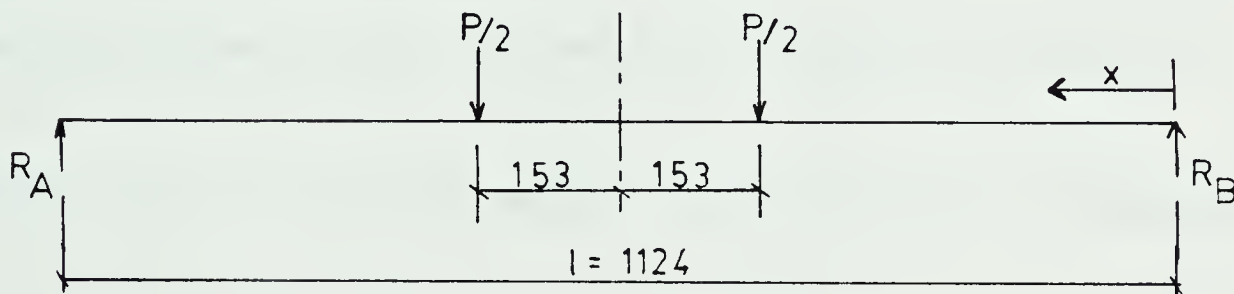
For the steel laggings where $l = 1187\text{mm}$ and the measuring points were fitted at a distance of 87.5mm from the end, a correction factor of 1.305 is found. Therefore:

$$p(\text{steel}) = [4.812 * 10^{-11} v_{cl} EI] * 1.305 [F/L^2] \quad \text{Eq. A1.11}$$

APPENDIX B

Calculation of Flexural Rigidities

To utilise laboratory deflection measurements the deflected shape of the beam must be calculated for the loading configuration used for calibration. This loading configuration is shown diagrammatically below



Using Macaulys' method (Benham, 1965) the required moment variation along the beam can be calculated. With reference to the diagram above moments are taken around R_B and using step functions Equation A2.1 as shown below was obtained. The important thing about step functions is that if the value inside the $[]$ is < 0 the expression is assumed equal to zero.

$$M = EI(d^2v/dx^2) = -Px/2 + P/2[x-409] + P/2[x-715] \quad \text{Eq. A2.1}$$

Integration of Eq. A2.1 twice yields the deflected shape

$$EI (dv/dx) = -Px^2/4 + P/4[x-409]^2 + P/4[x-715]^2 + A \quad \text{Eq A2.2}$$

$$EIv = -Px^3/12 + P/12[x-409]^3 + P/12[x-715]^3 + Ax + B \quad \text{Eq A2.3}$$

Boundary conditions $x = 0$; $v = 0$ yields $B = 0$

$$x = l \text{ ; } v = 0$$

Using the second boundary condition Eq. A2.3 becomes:

$$0 = -P1124^3/12 + P/12[715]^3 + P/12[409]^3 + 1124A$$

which yields $A = 73108P \text{ mm}^2$

General Equation for the deflected shape is therefore:

$$EIv = -Px^3/12 + P/12[x-409]^3 + P/12[x-715]^3 + 73108xP \text{ [Nmm}^3\text{]} \quad \text{Eq. A2.4}$$

The calibration technique involved measurement of the central deflection therefore substituting $x = 562\text{mm}$ gives:

$$v_{\text{max}} = [26593100P]/EI \text{ mm}$$

therefore

$$EI = 26593100P/v_{\text{meas}} \text{ [Nmm}^2\text{]} \quad \text{Eq. A2.6}$$

Because the measuring points were not at the end of a correction factor as explained in Appendix A must be applied. For the woods the measuring points were located 55mm from the end, therefore substituting this value for "x" into Eq A2.4 yields:

$$v_{55} = 4005200P \text{ [EI ignored]}$$

In the calibration tests only the relative displacement

between v_{ss} and v_{cl} was measured. Therefore we measure

$$v_{meas} = 26593100P - 4005200P = 22587900P$$

whereas the correct deflection is:

$$v_{correct} = v_{cl} = 26593100P$$

If EI is calculated from v_{meas} , an overestimation of the flexural rigidity by an amount $= v_{cl} / v_{meas}$ would occur. This value is 1.17 therefore a correction factor equal to $1/1.17 = 0.847$ must be applied to calculated wood values.

Therefore:

$$EI \text{ (wood)} = [26593100P / v_{meas}] * 0.847 \text{ Nmm}^2 \text{ Eq. A2.6}$$

Using a similar development for the steel laggings where $l = 1187\text{mm}$ with measuring points fitted 87.5mm from the end yields:

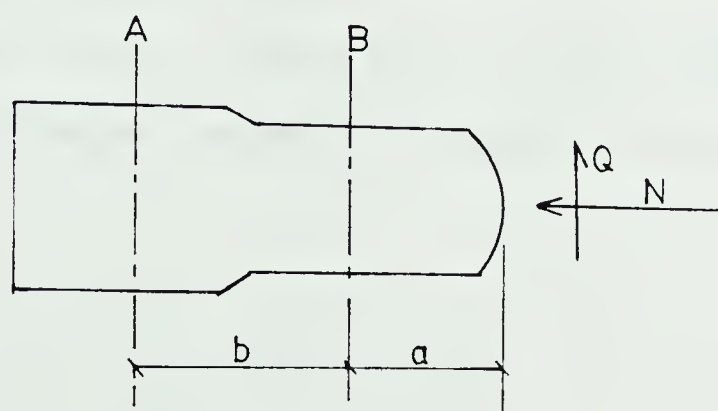
$$EI \text{ (steel)} = [31667598P / v_{meas}] * 0.775 \text{ Nmm}^2 \text{ Eq. A2.7}$$

APPENDIX C

Load Cell Design Details

Design of the cells was such that shear force, bending moment and axial load could be calculated from the cell. Design of this cell followed principles published by Kovari et al. (1977).

Kovari Principles



Moment equilibrium at section B

$$M_B = Qa$$

Moment equilibrium as section A

$$M_A = Q(a+b) = Qa + Qb$$

Substitution yields $M_A = M_B + Qb$

therefore
$$Q = (M_A - M_B) / b$$

To incorporate the above principles it is necessary to instrument the load cell at two sections such that it is possible to calculate the bending moments at those sections. To achieve this it was decided to place four strain gauges equally spaced around the periphery of the circular cells.

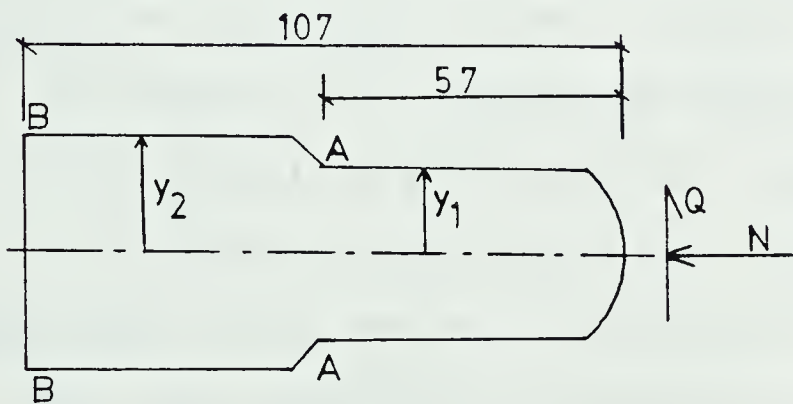
Structural design

Material steel with $\sigma_{\text{yield}} = 250\text{Mpa}$

Design normal load = 500kN

Design shear force = 100kN (20% of the normal force)

The design problem is shown diagrammatically below



The longitudinal section lengths were chosen in regard to allowable length permitted during expansion of the steel sets. Critical design sections are at "A" and "B".

Critical stress at section A is given by

$$\sigma_{\max} = N/A + M * y_{\max} / I = 250\text{Mpa/FS}$$

Manipulation of the above equation for section "A" and "B" results in

$$y_1 = 35\text{mm}$$

$$y_2 = 40\text{mm}$$

Overall cross-section details are given in Figure 3.12.

Calibration

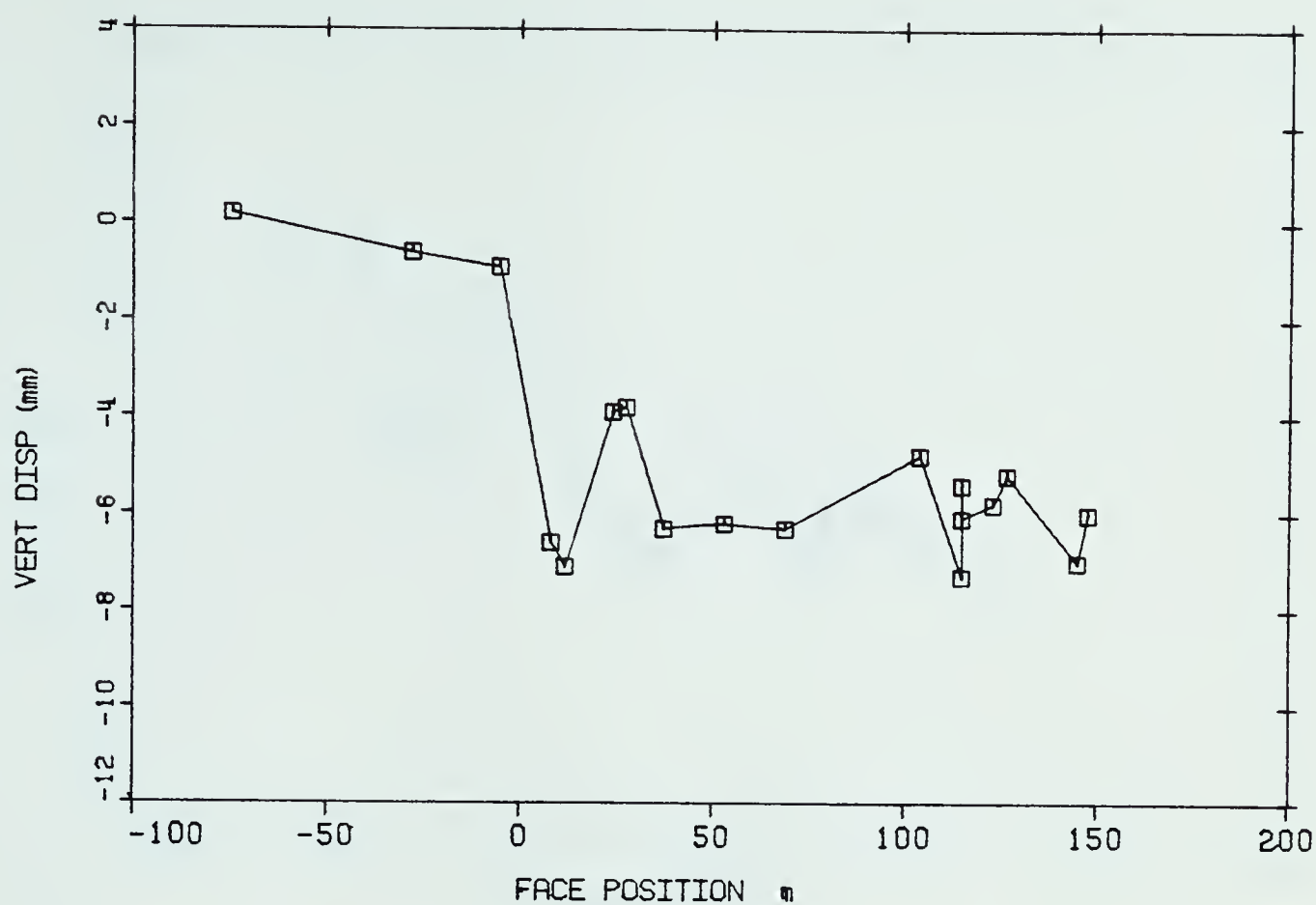
To obtain the moment present at a section it is necessary to have each of the 8 fitted strain gauges (4 top cell; 4 bottom cell) calibrated under conditions of normal load. In an effort to achieve this the cells were loaded from 0 to 800kN in increments of 100kN under conditions of assumed axial load. Prior to recording strain gauge readings the cell was loaded and unloaded for at least 4 cycles. To check the cell ability to predict moment and shear force inclined load tests were also performed.

Due to problems such as non axial calibration force, stress concentrations, variability in symmetry of the cell etc. it was not found possible to get accurate calibration factors for each gauge and as a result the original purpose of the cell was not fulfilled. By totaling all the compressive strains, however, obtained by the four strain

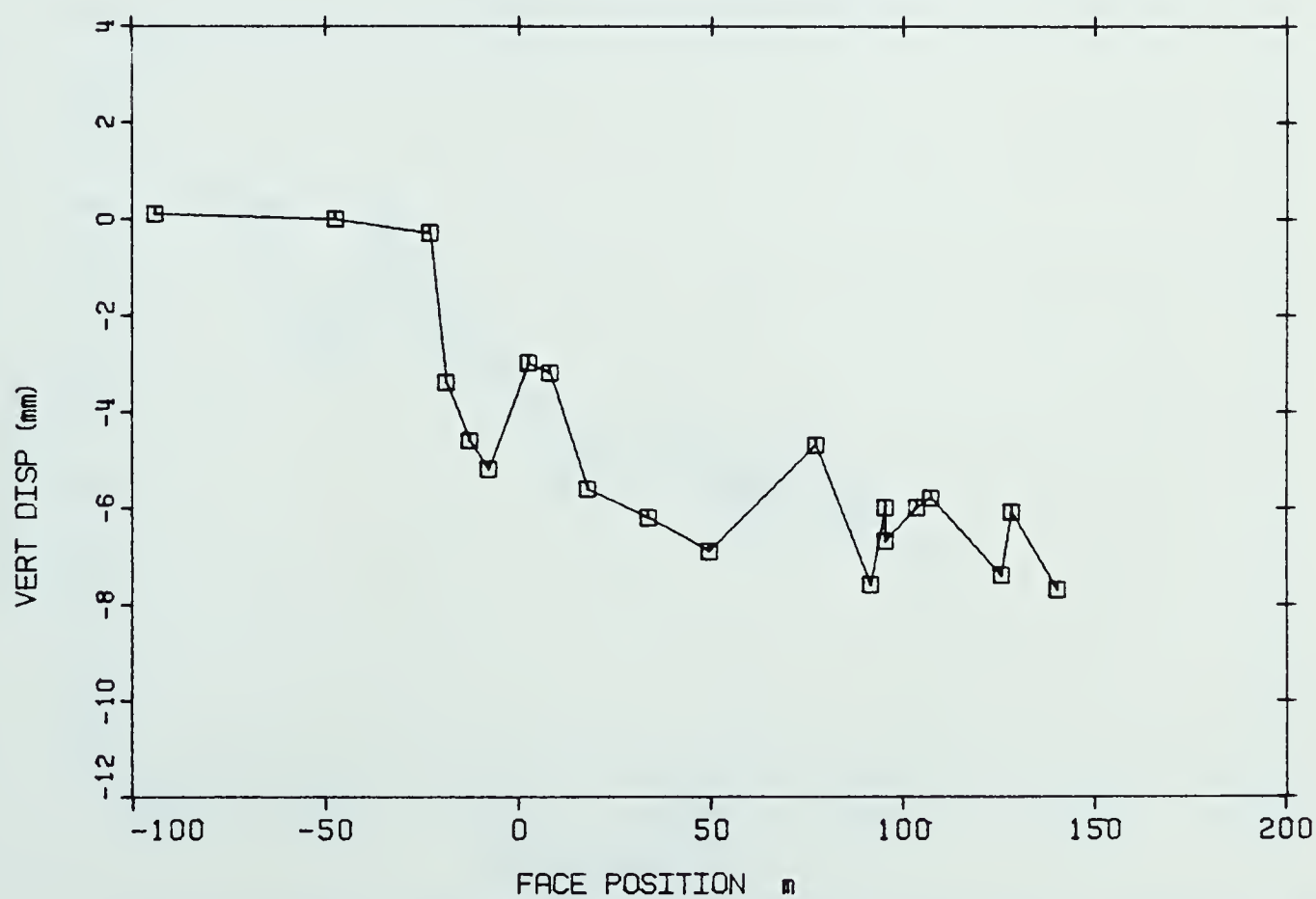
gauges located at a particular section and putting a best fit line through calibration values the axial force could quite accurately be predicted (Table 3.2).

Future design of a cell based on the principles presented by Kovari et al. 1977, require that the cell be made longer and have a more comprehensive analysis on generated moments throughout the cell, if its use is to be successful.

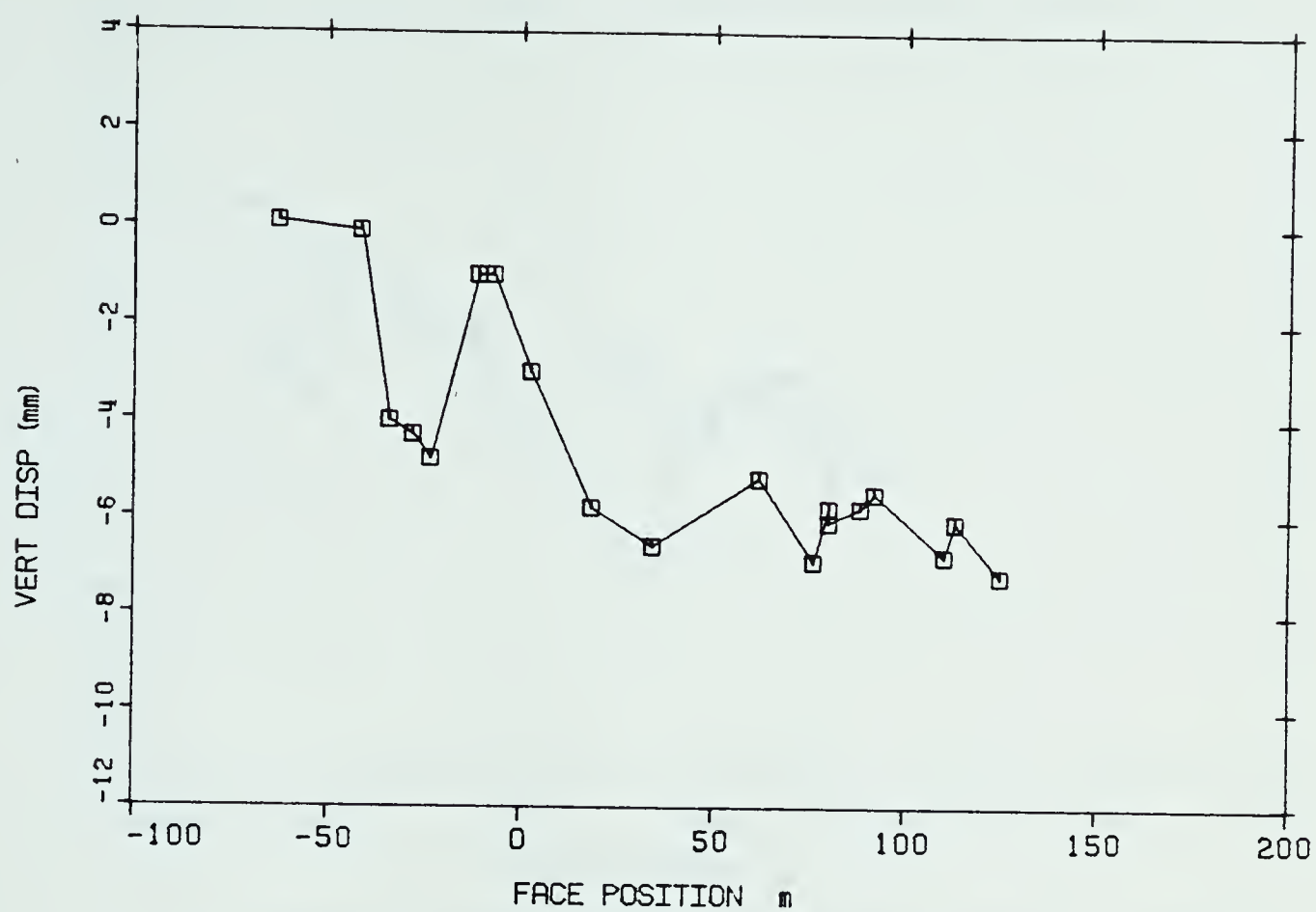
APPENDIX D



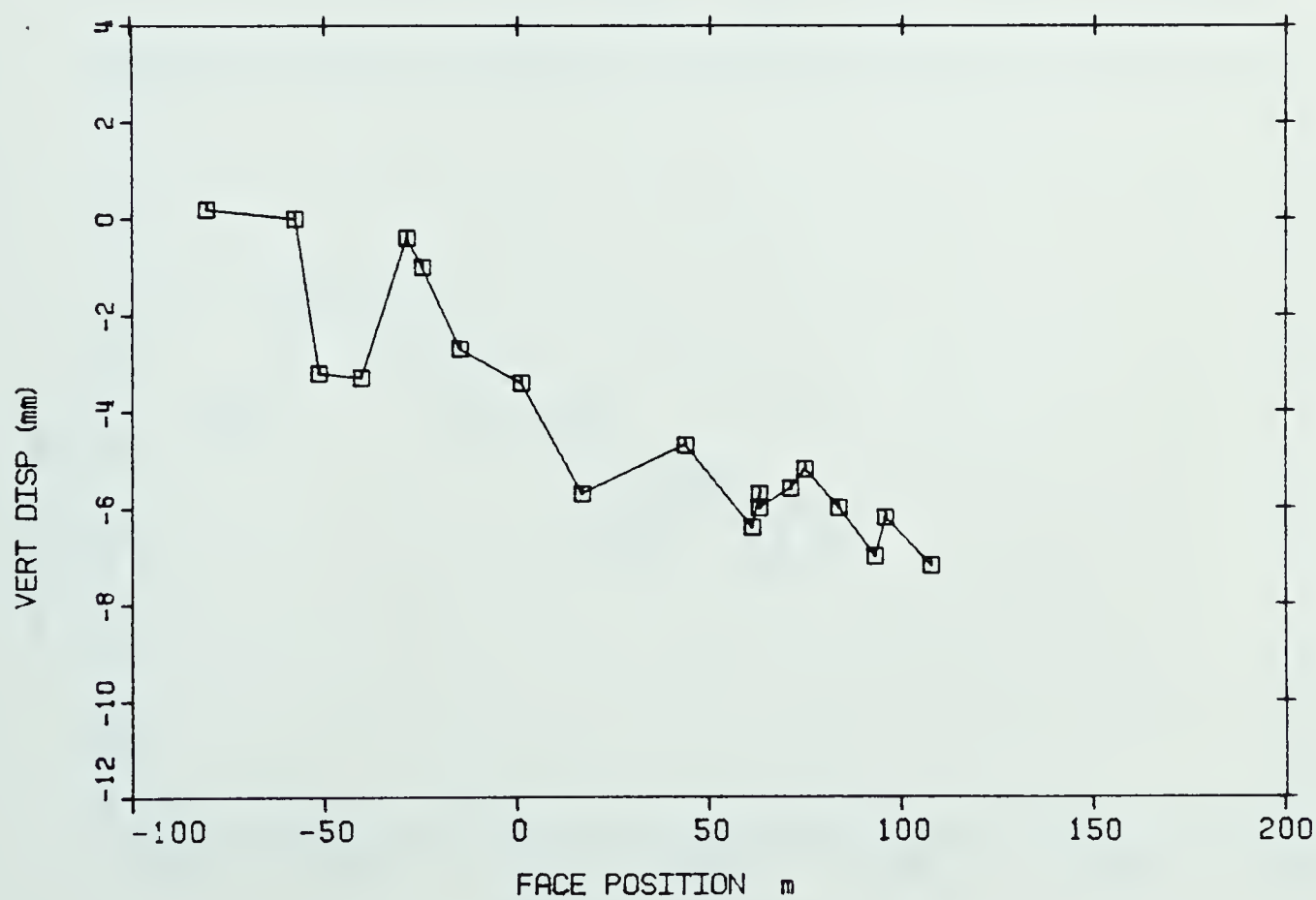
SETTLEMENT VERSUS FACE POSITION FOR S. POINT #1



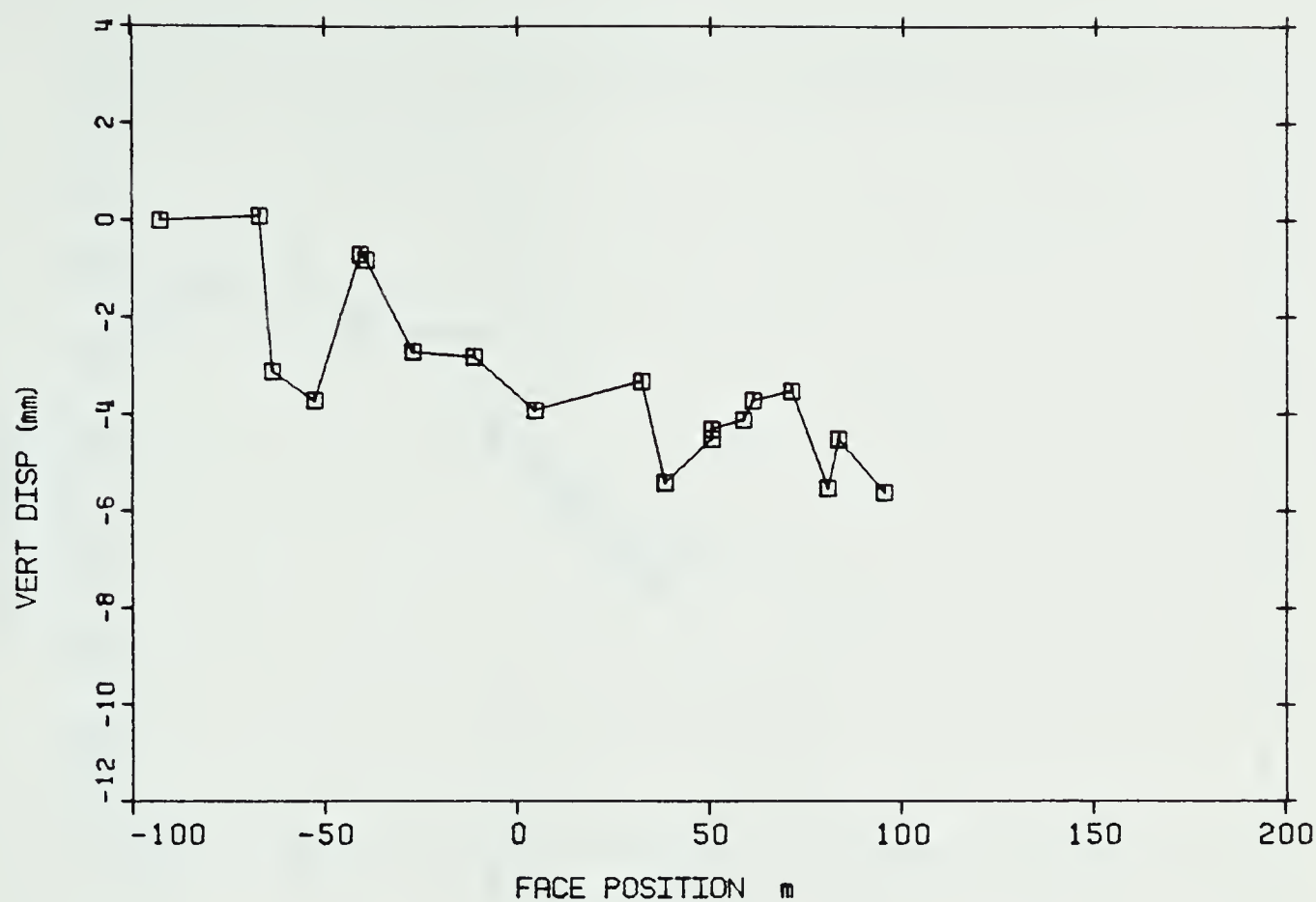
SETTLEMENT VERSUS FACE POSITION FOR S. POINT #2



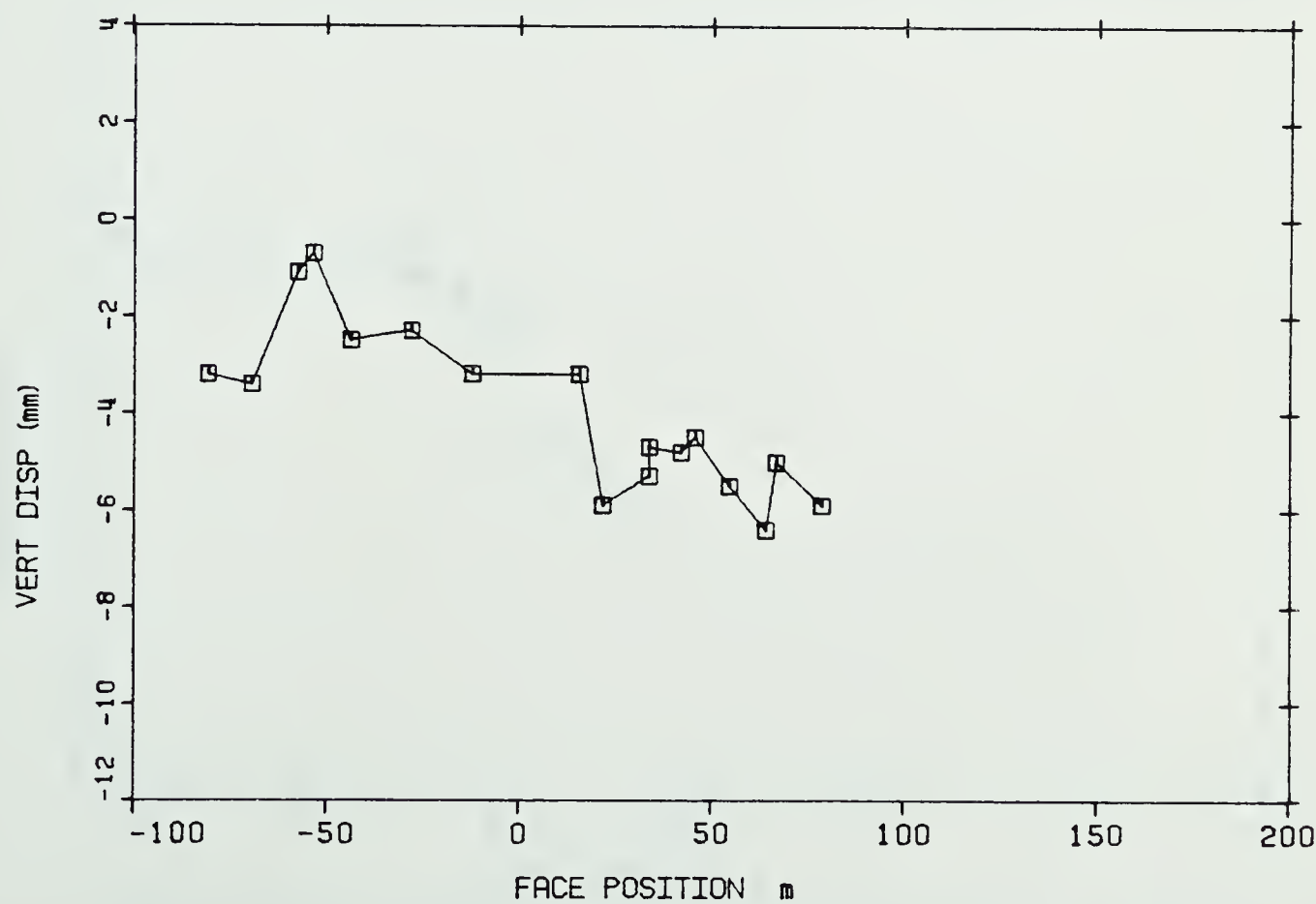
SETTLEMENT VERSUS FACE POSITION FOR S. POINT #3



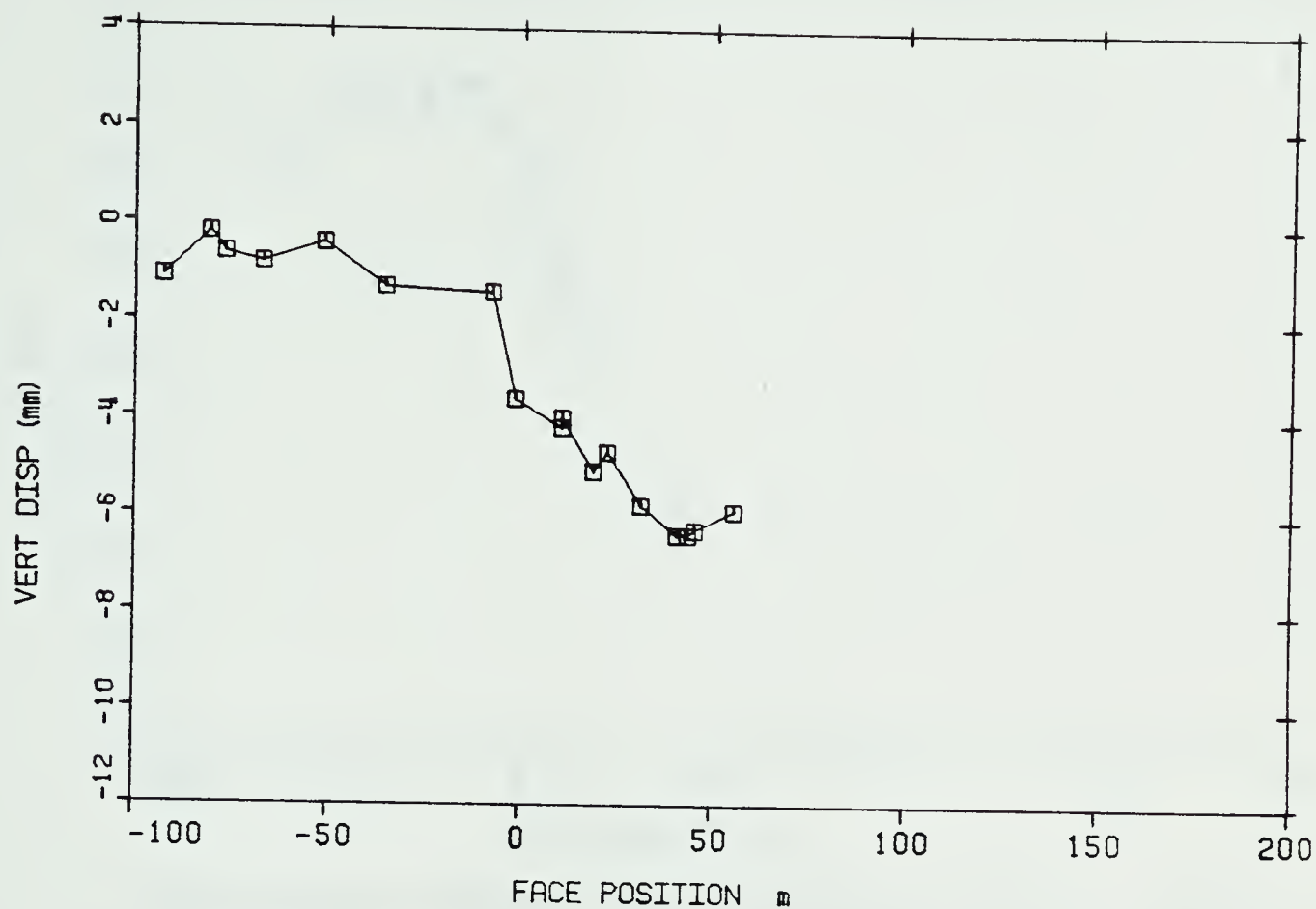
SETTLEMENT VERSUS FACE POSITION FOR S. POINT #4



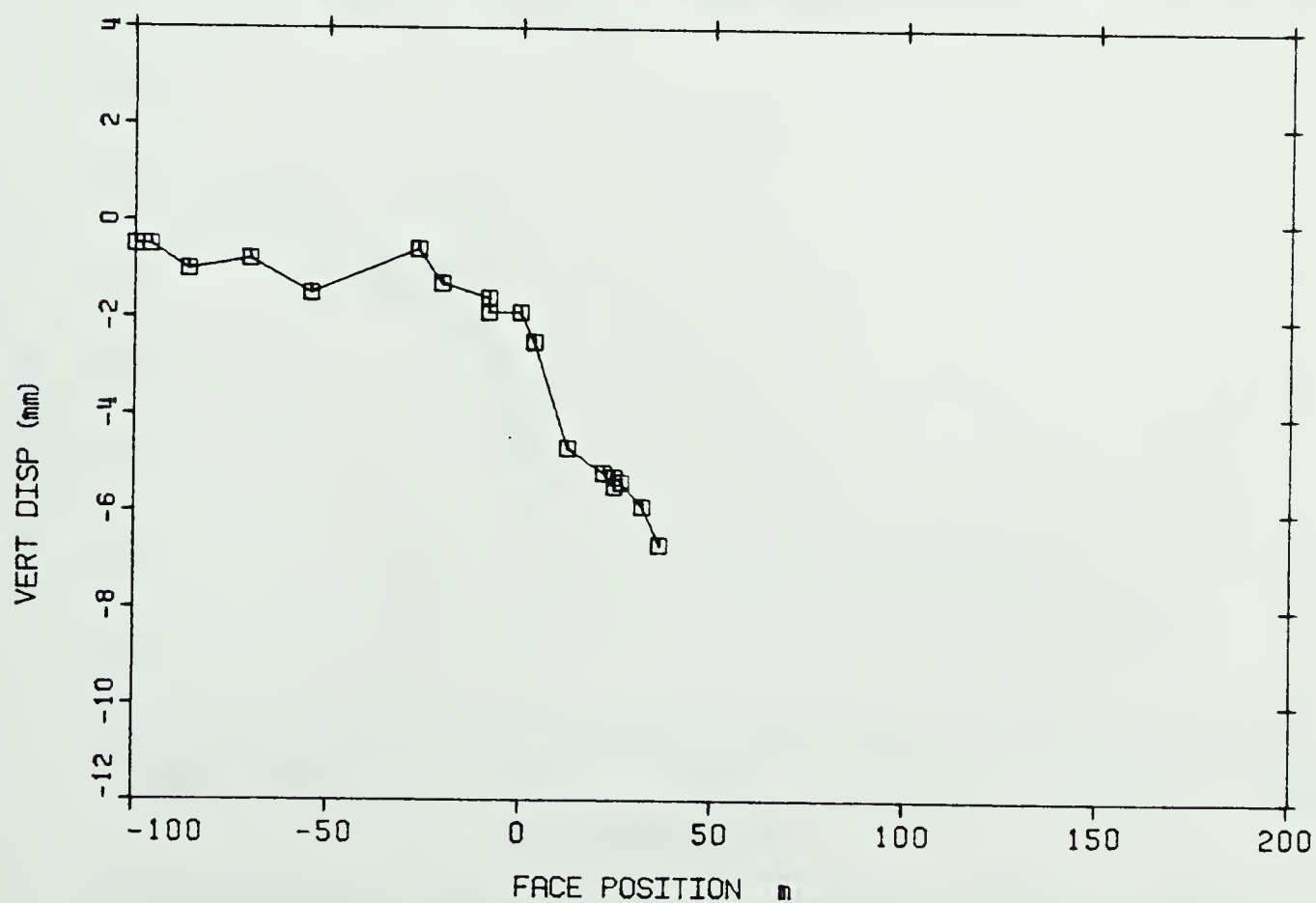
SETTLEMENT VERSUS FACE POSITION FOR S. POINT #5



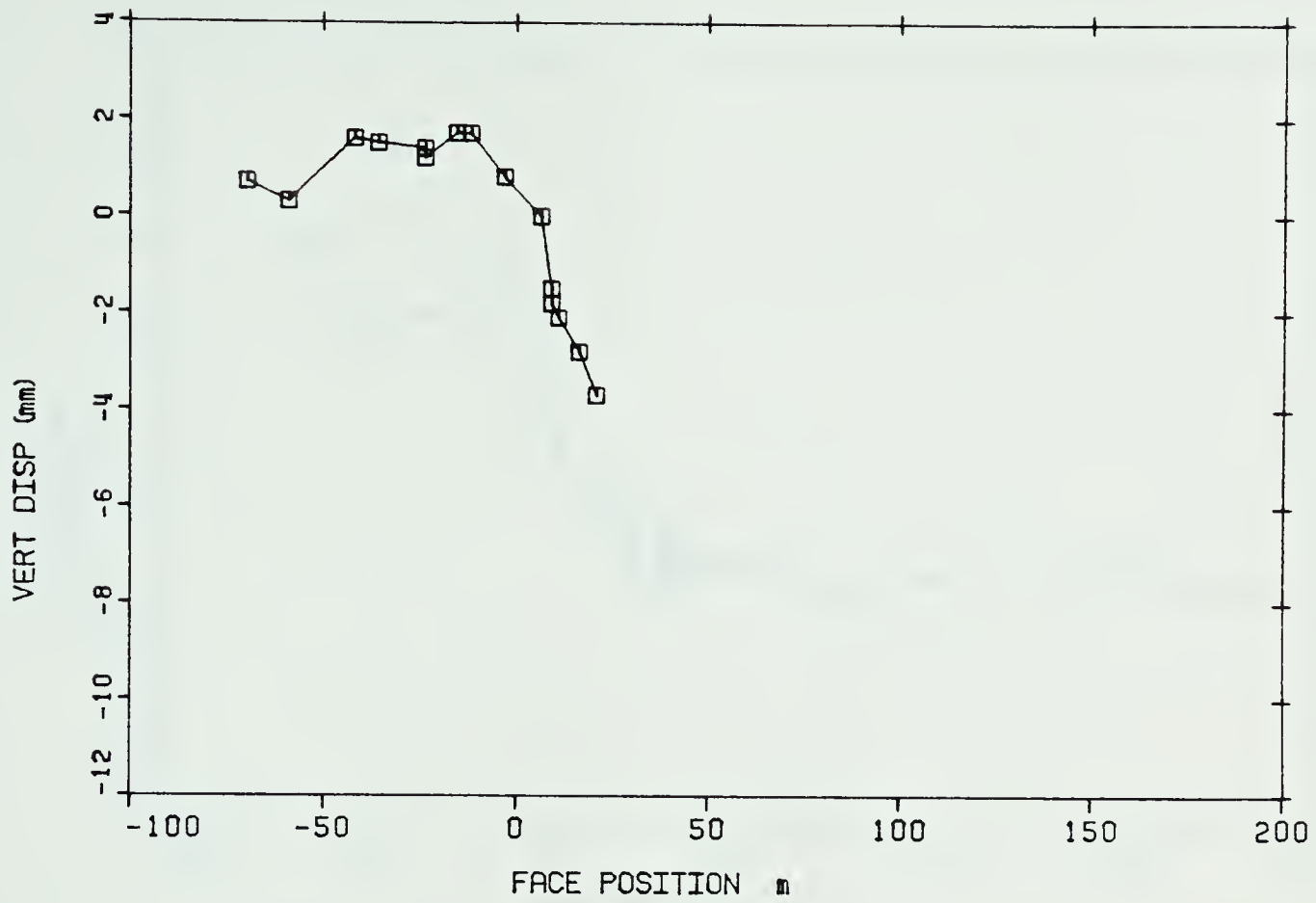
SETTLEMENT VERSUS FACE POSITION FOR S. POINT #6



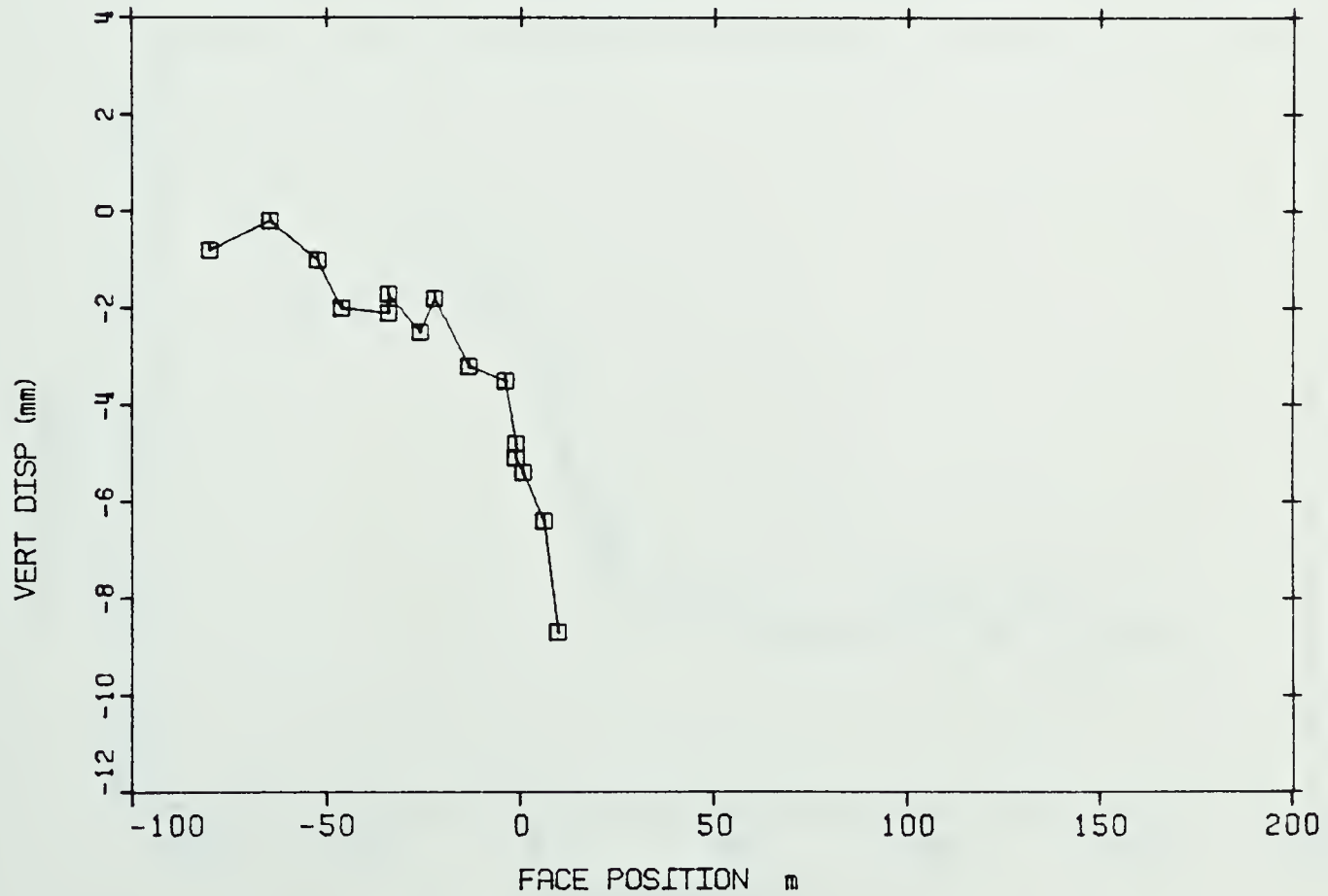
SETTLEMENT VERSUS FACE POSITION FOR S. POINT #7



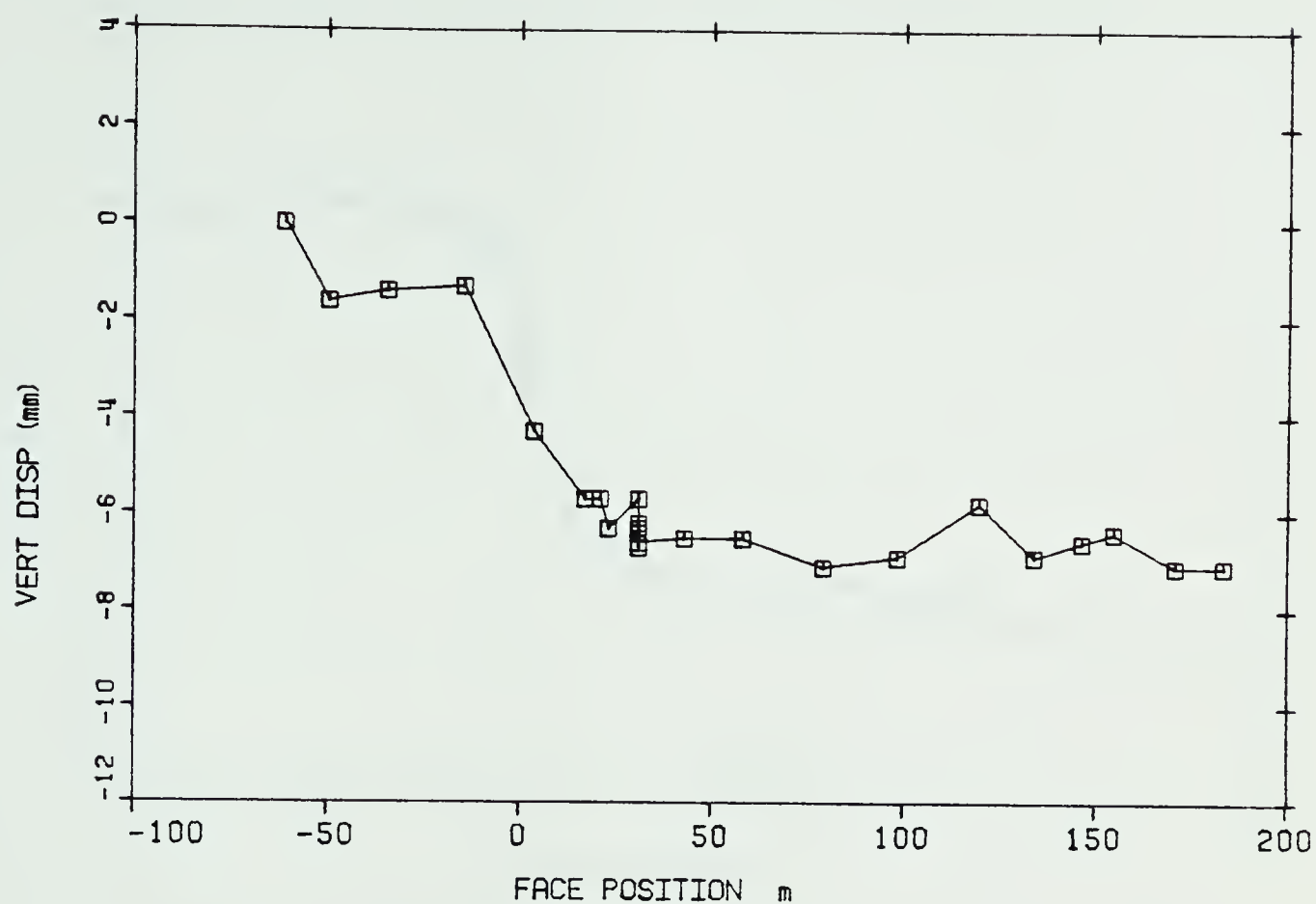
SETTLEMENT VERSUS FACE POSITION FOR S. POINT #8



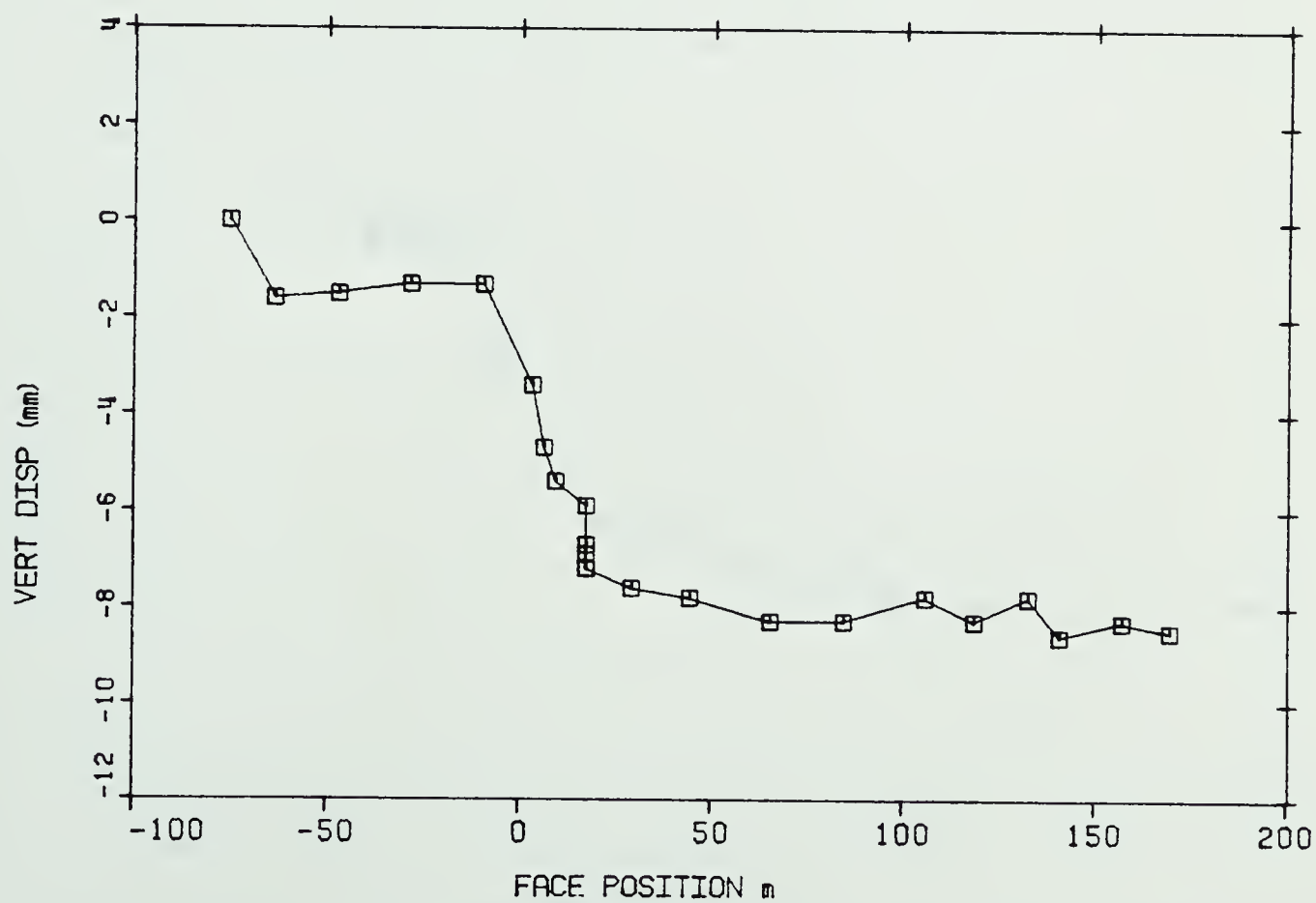
SETTLEMENT VERSUS FACE POSITION FOR S. POINT #9



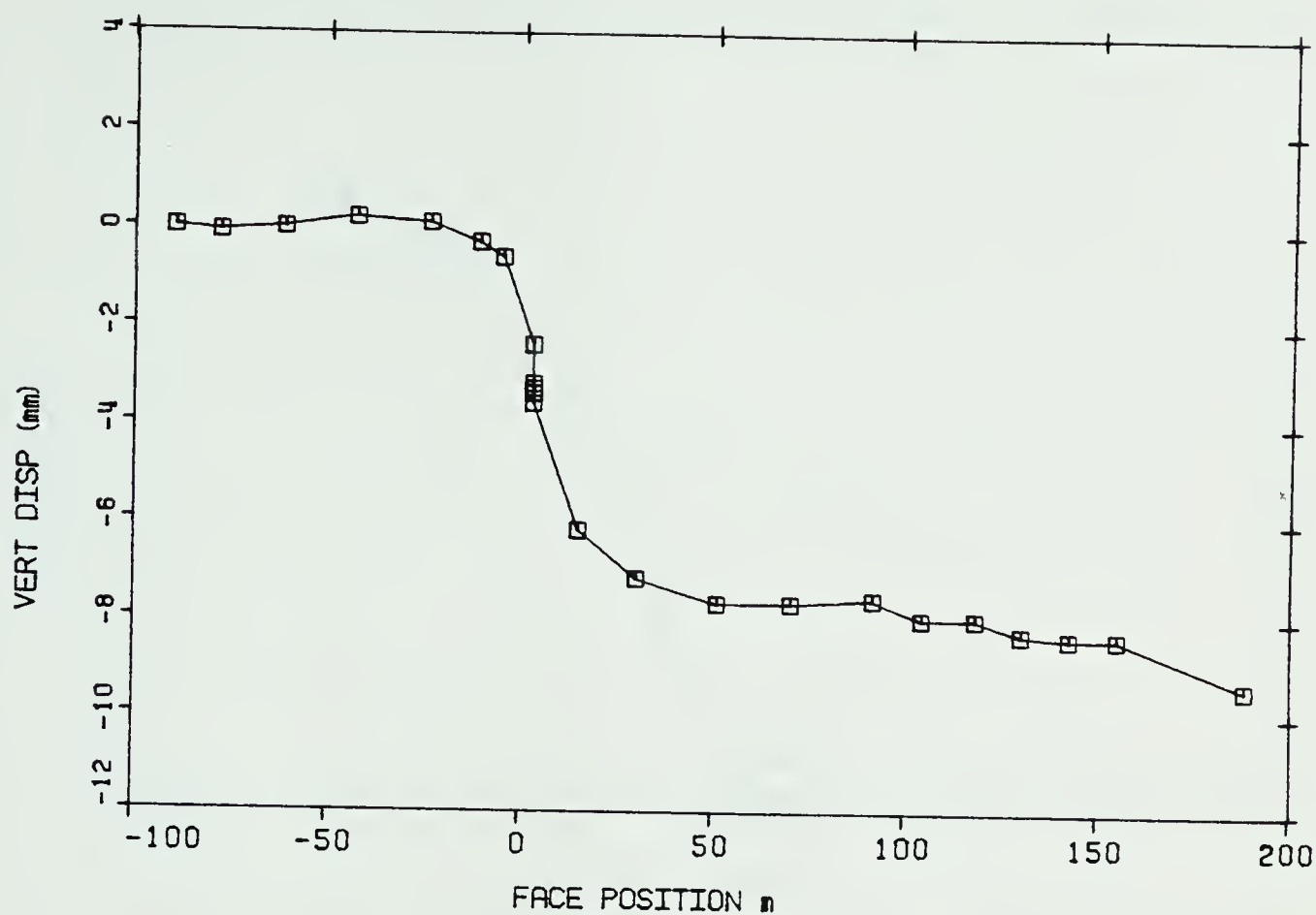
SETTLEMENT VERSUS FACE POSITION FOR S. POINT #10



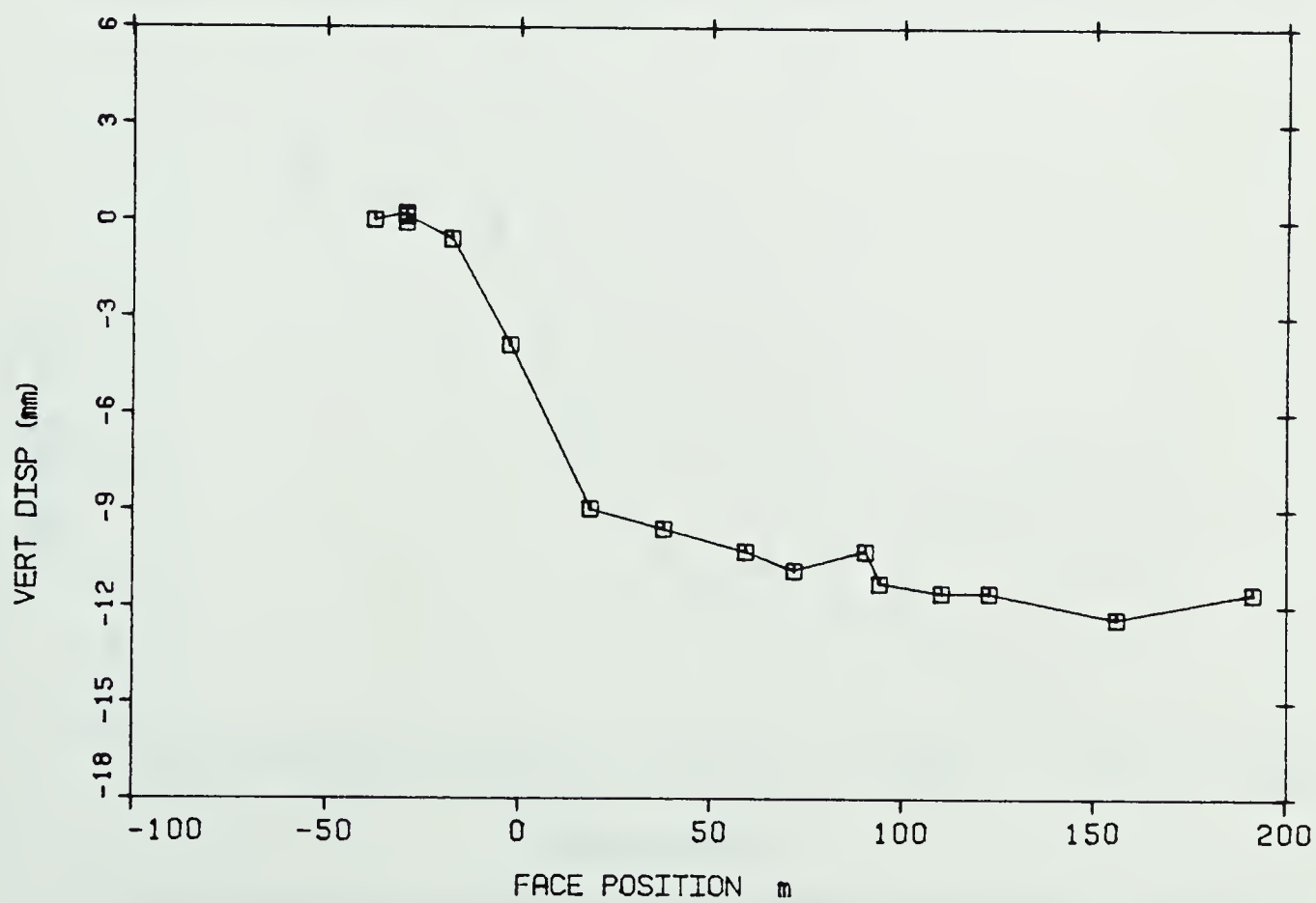
SETTLEMENT VERSUS FACE POSITION FOR S. POINT #11



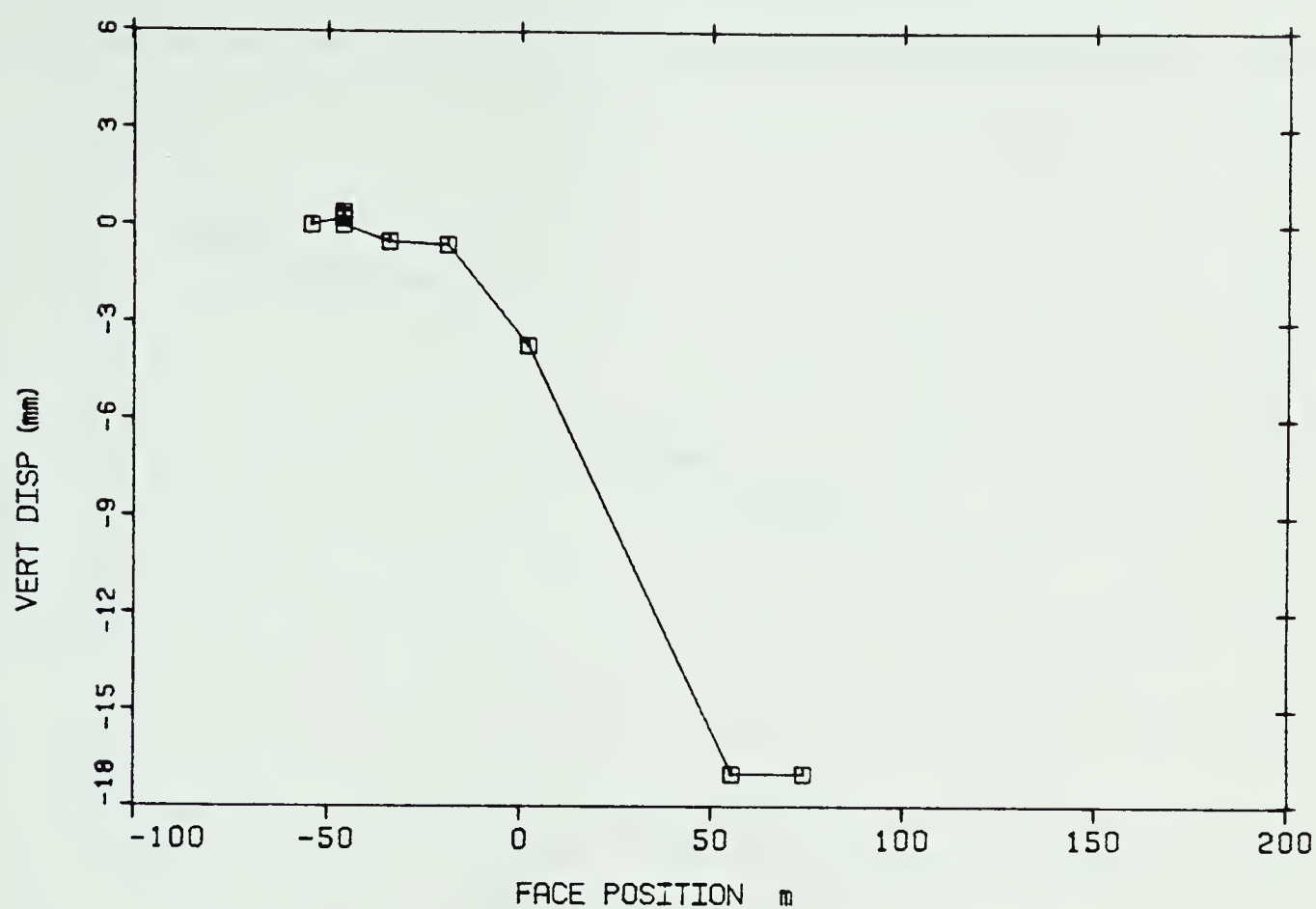
SETTLEMENT VERSUS FACE POSITION FOR S. POINT #12



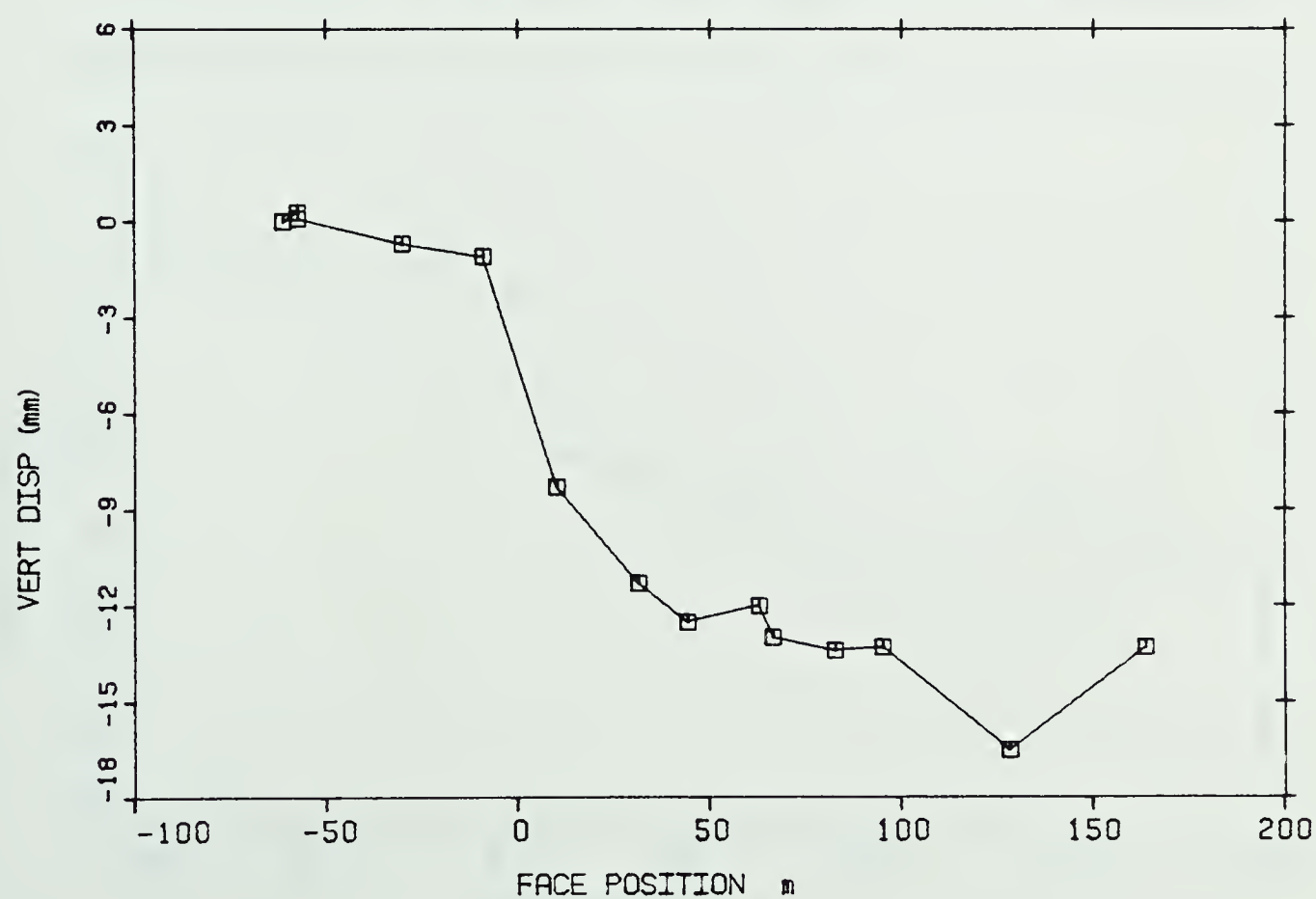
SETTLEMENT VERSUS FACE POSITION FOR S. POINT #13



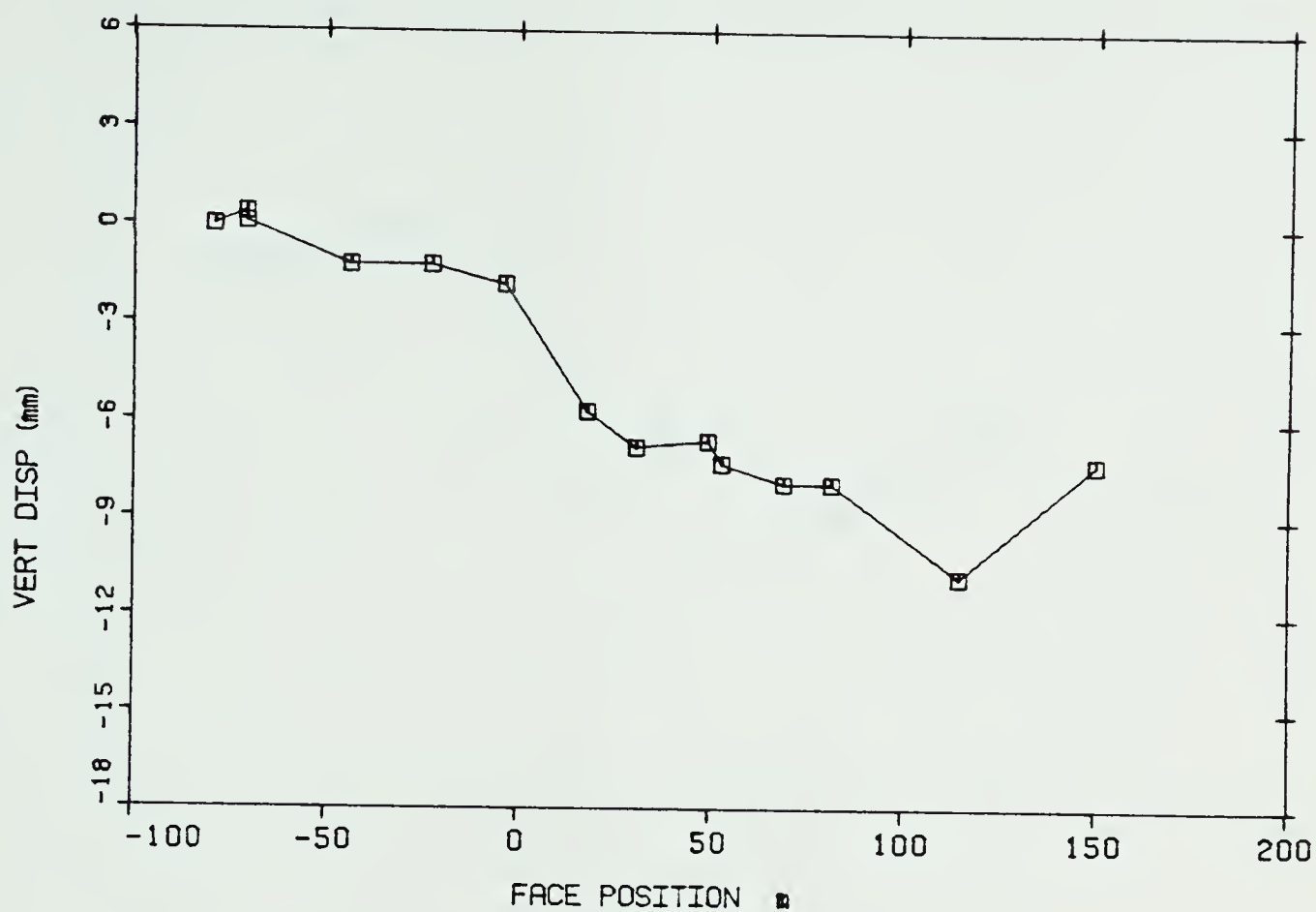
SETTLEMENT VERSUS FACE POSITION FOR S. POINT #14



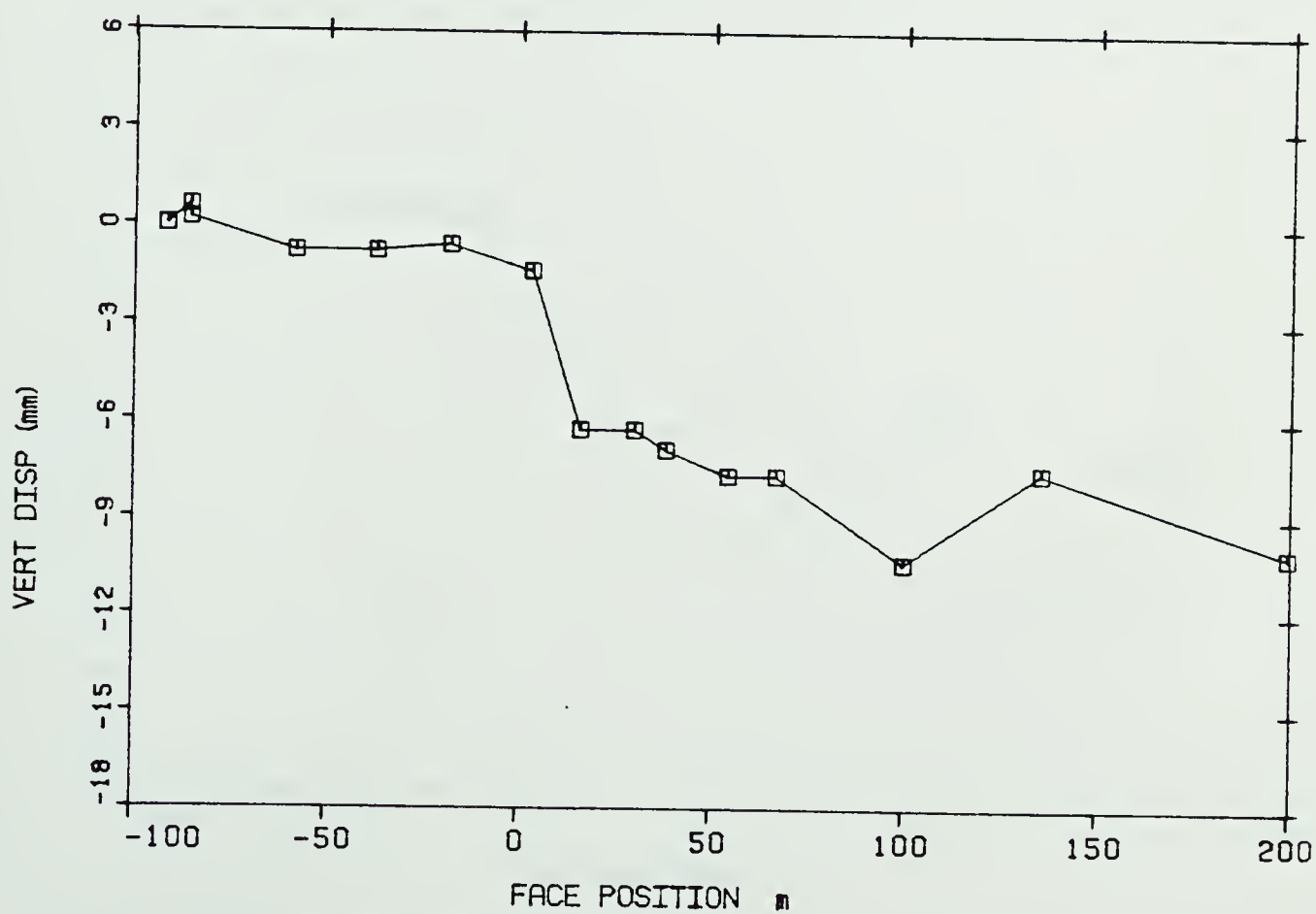
SETTLEMENT VERSUS FACE POSITION FOR S. POINT #15



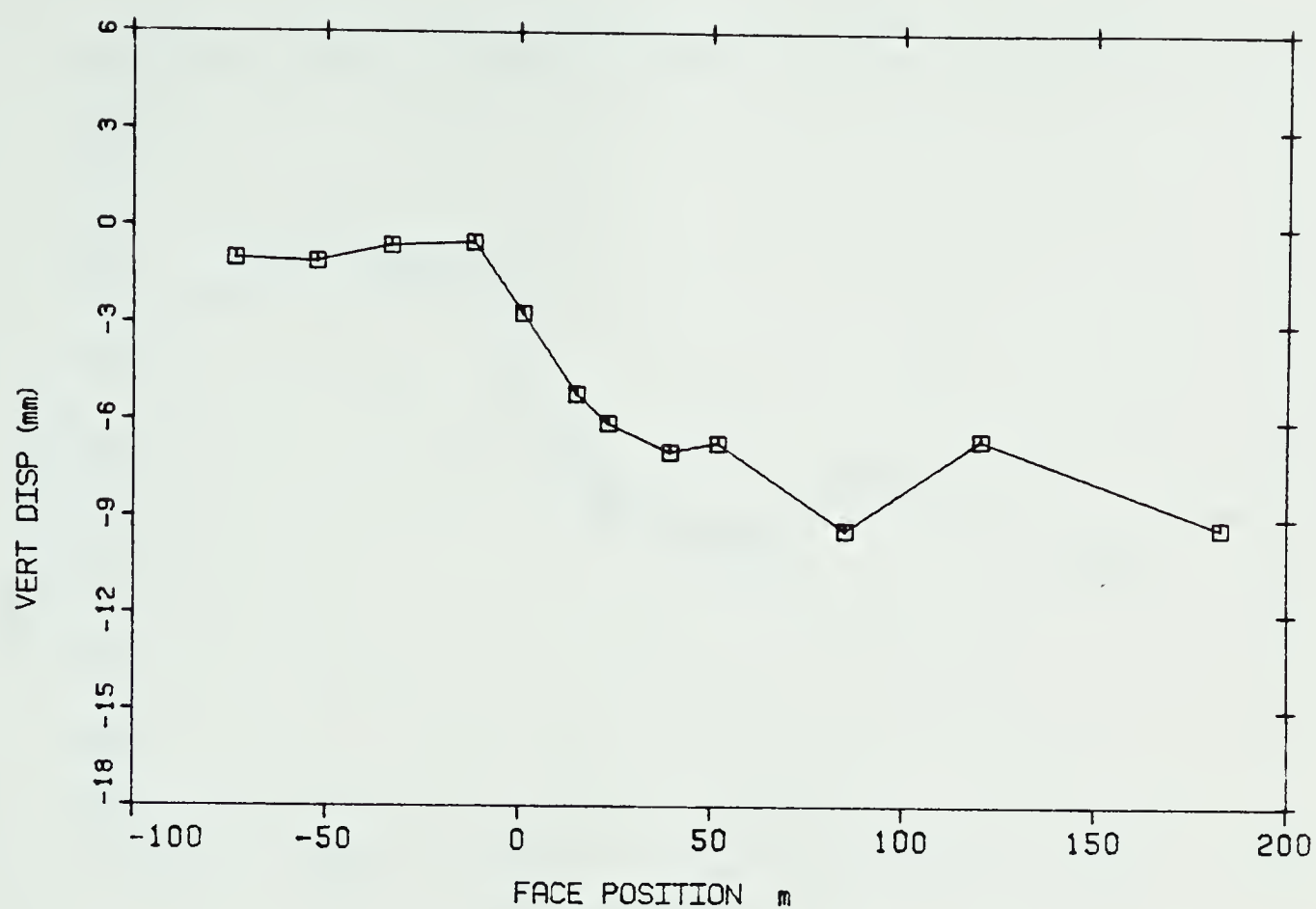
SETTLEMENT VERSUS FACE POSITION FOR S. POINT #16



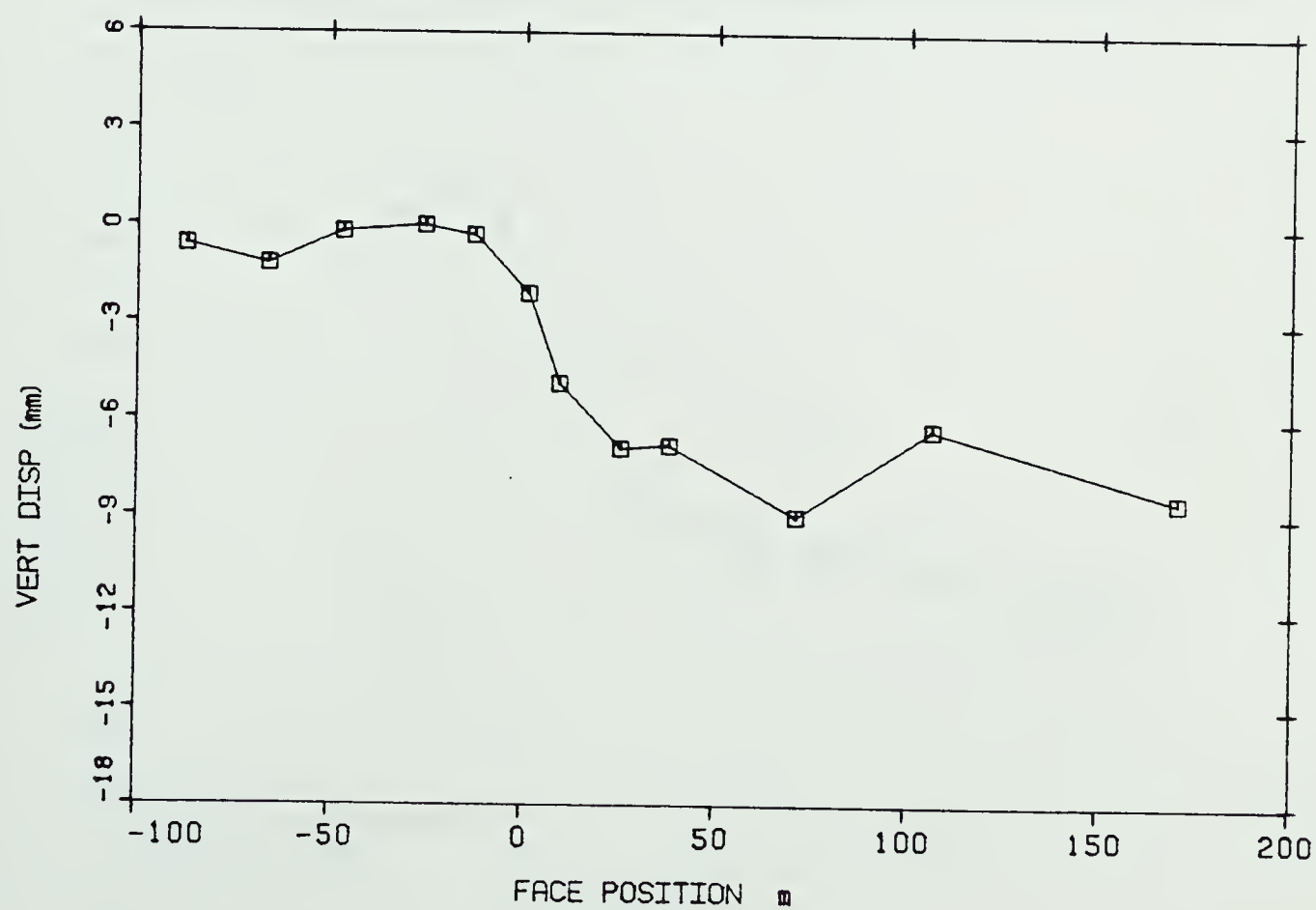
SETTLEMENT VERSUS FACE POSITION FOR S. POINT #17



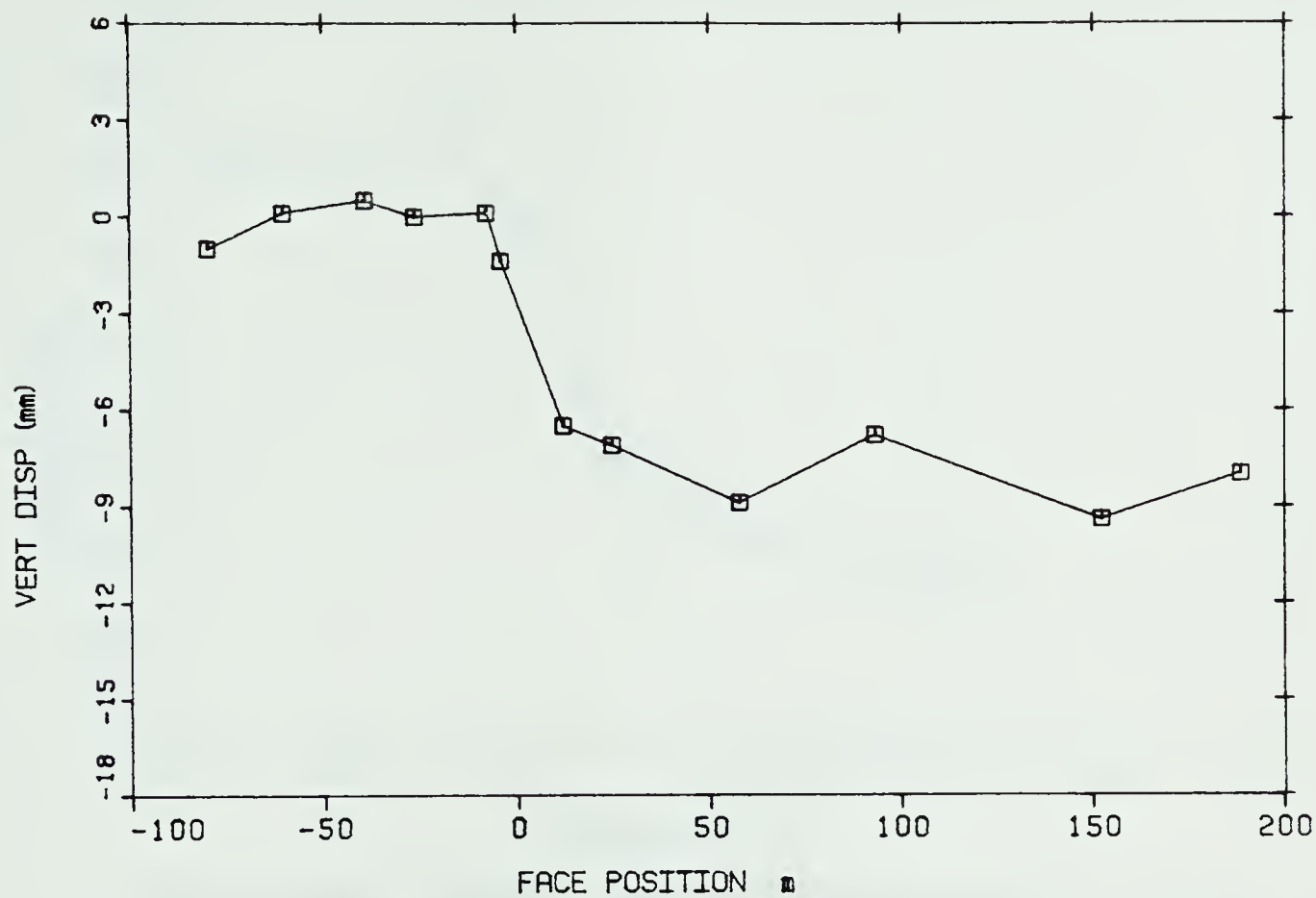
SETTLEMENT VERSUS FACE POSITION FOR S. POINT #18



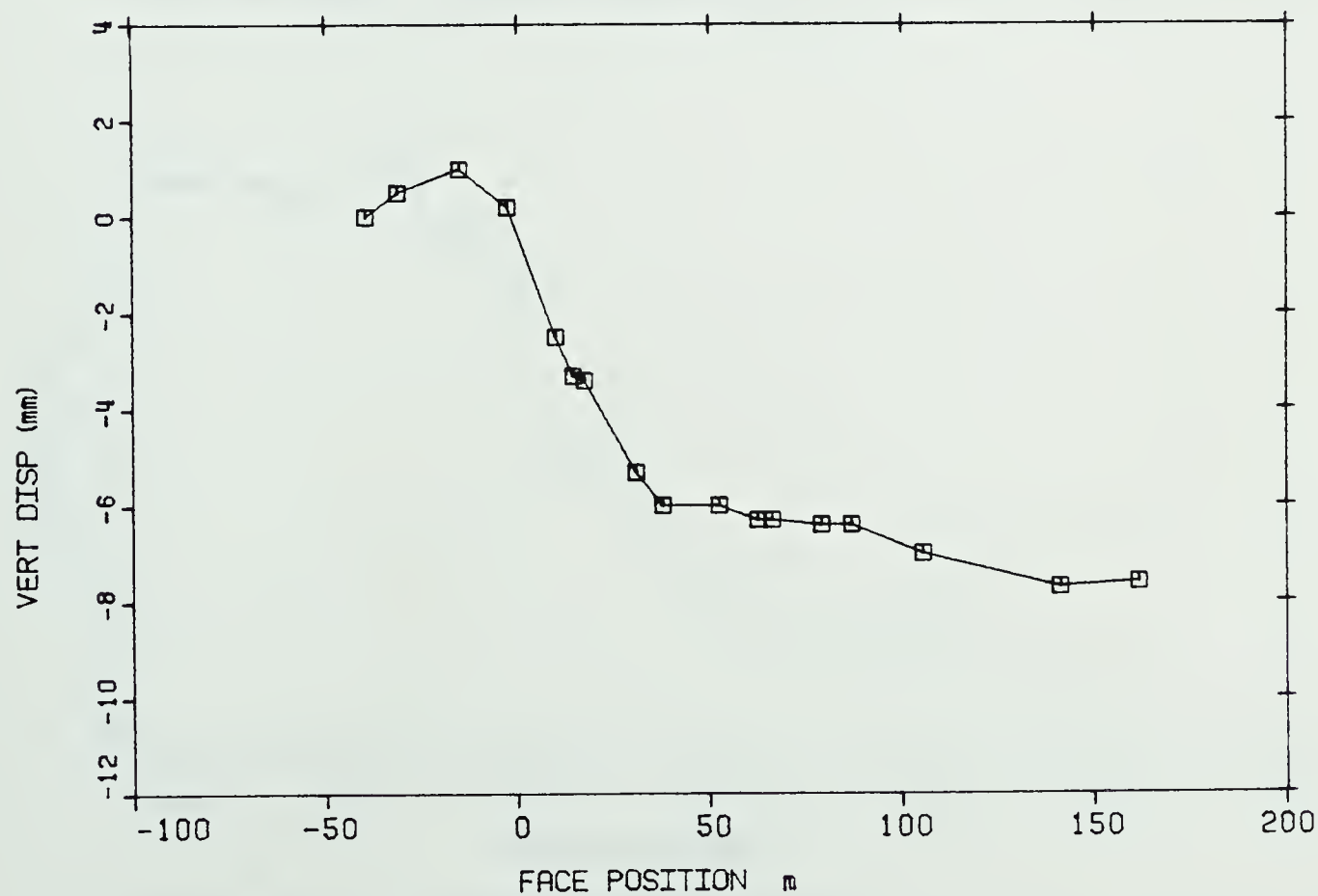
SETTLEMENT VERSUS FACE POSITION FOR S. POINT #19



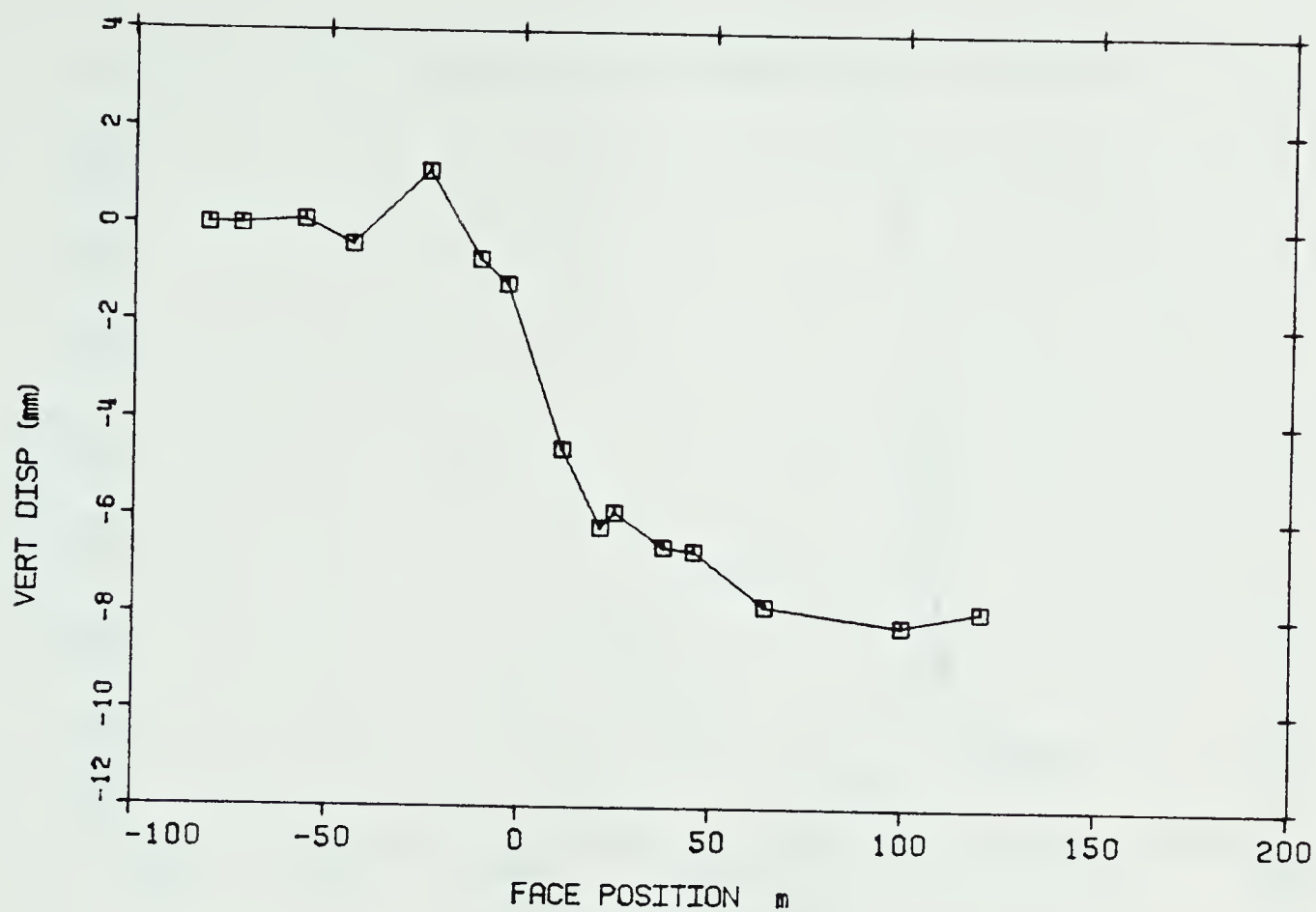
SETTLEMENT VERSUS FACE POSITION FOR S. POINT #20



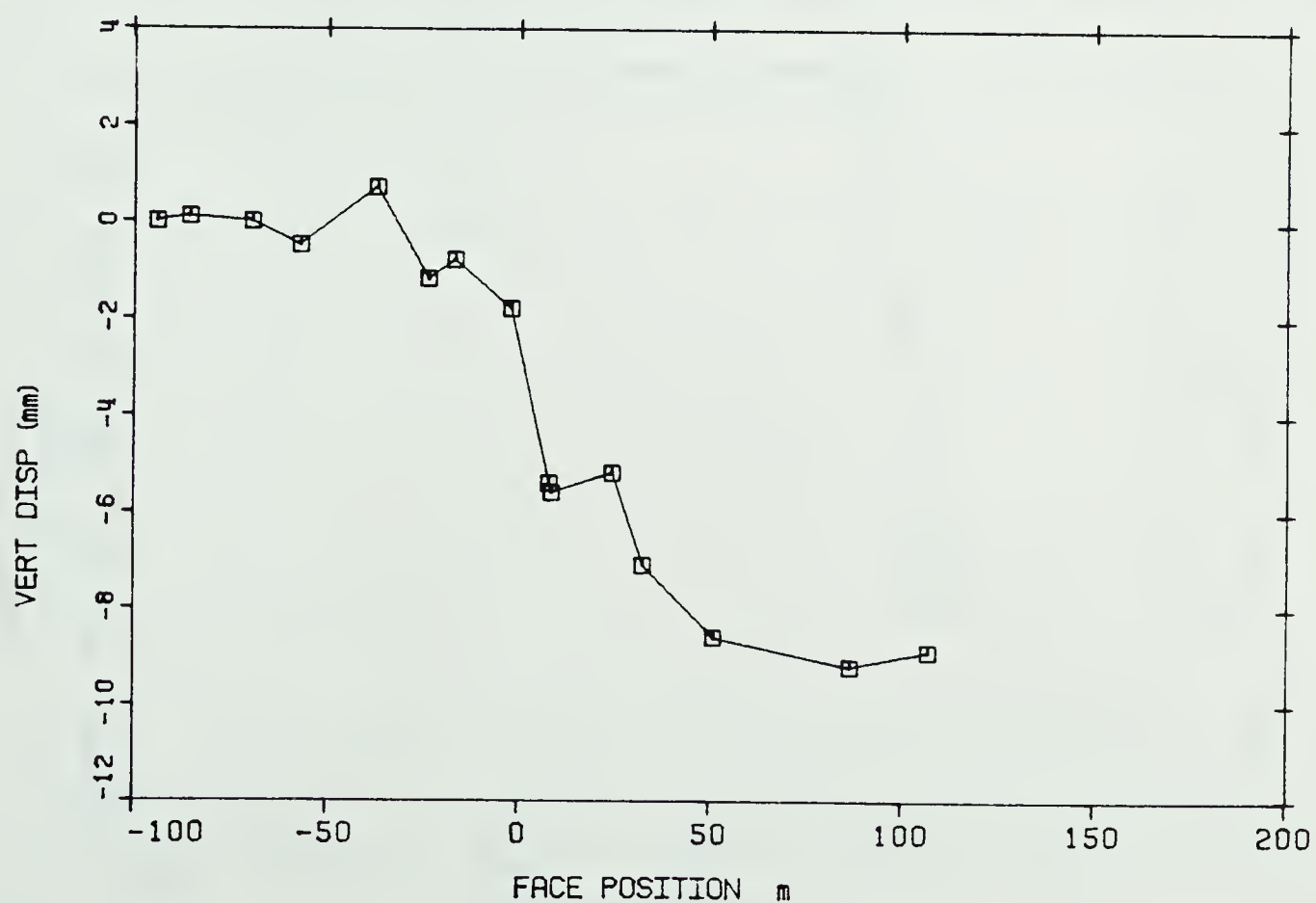
SETTLEMENT VERSUS FACE POSITION FOR S. POINT #21



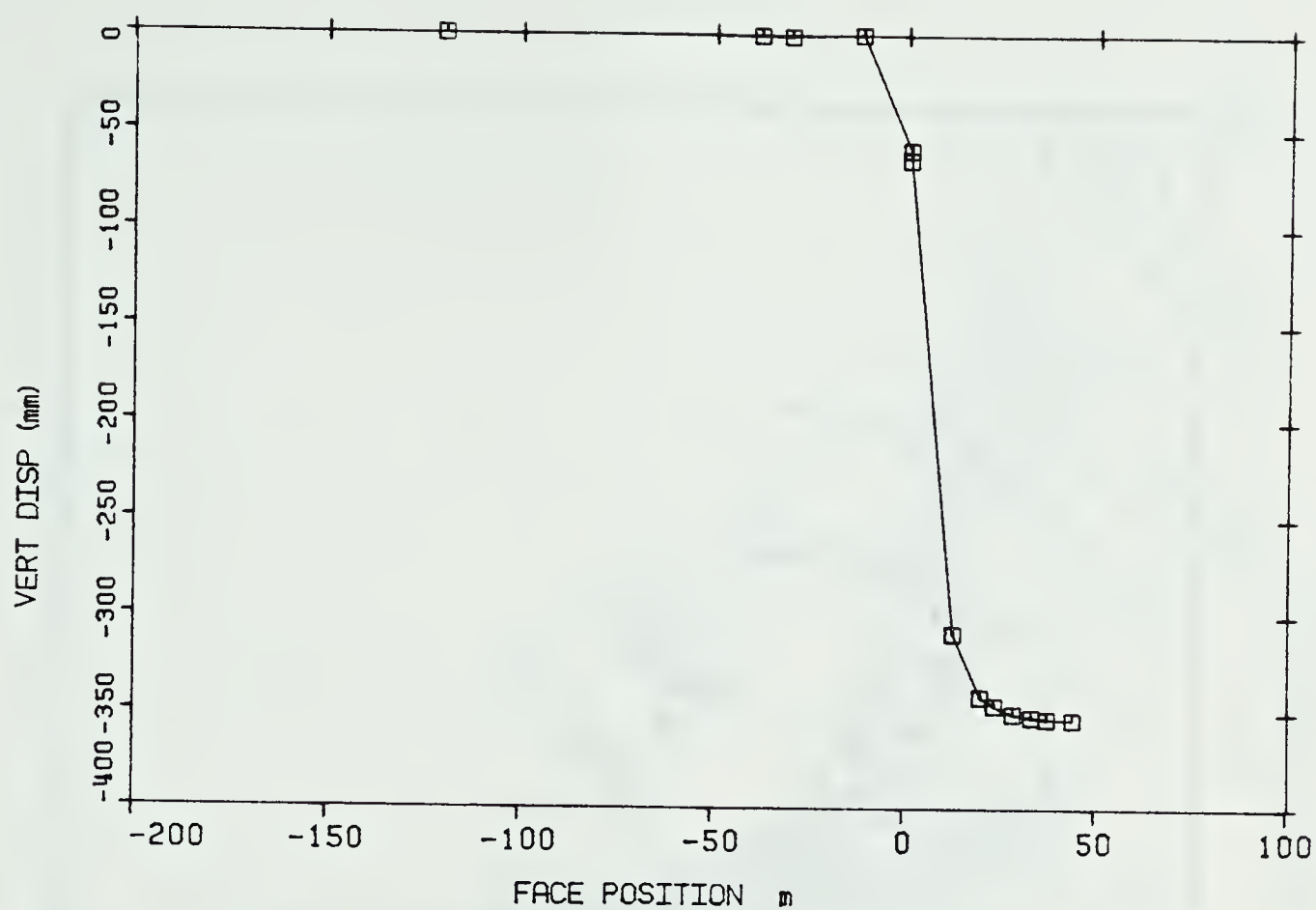
SETTLEMENT VERSUS FACE POSITION FOR S. POINT #22



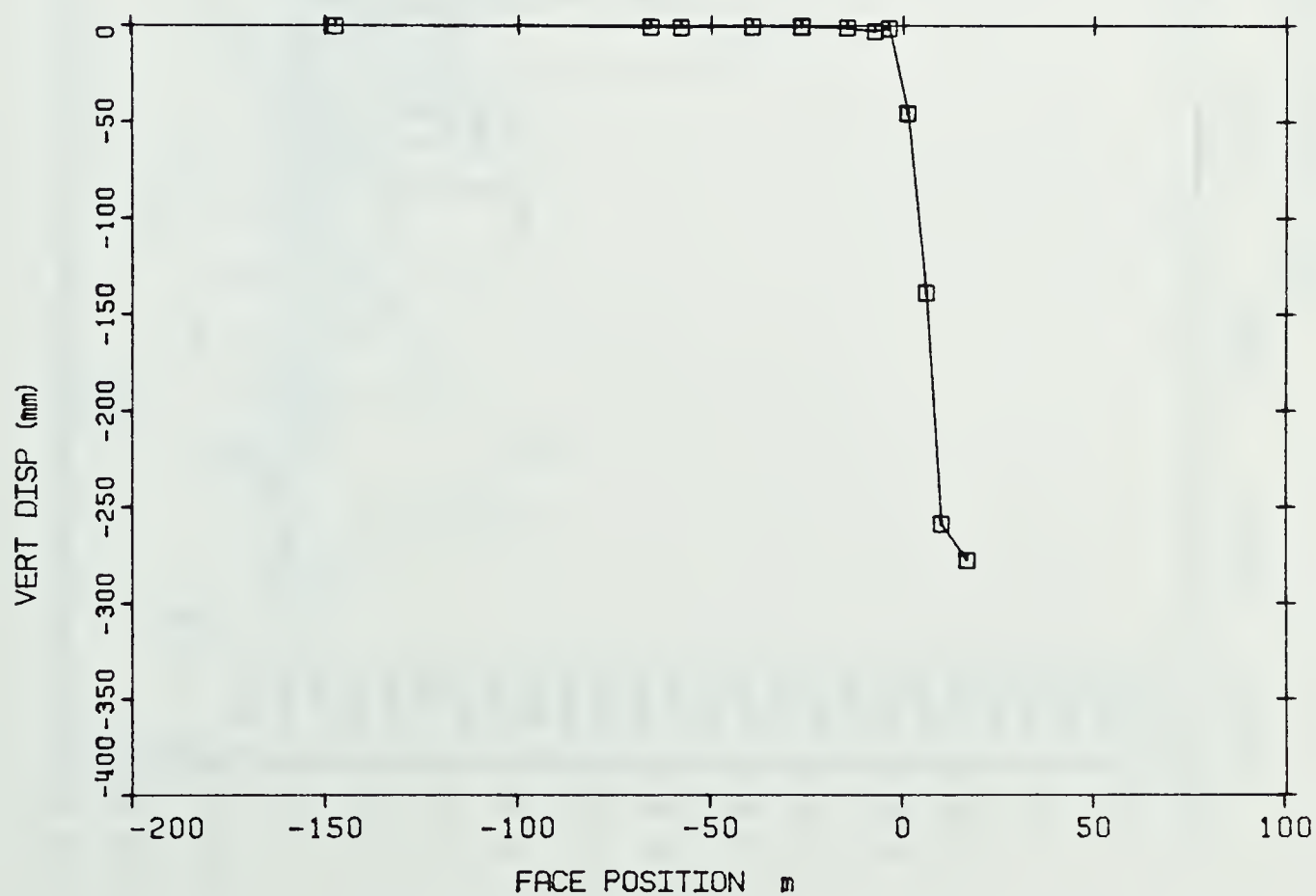
SETTLEMENT VERSUS FACE POSITION FOR S. POINT #23



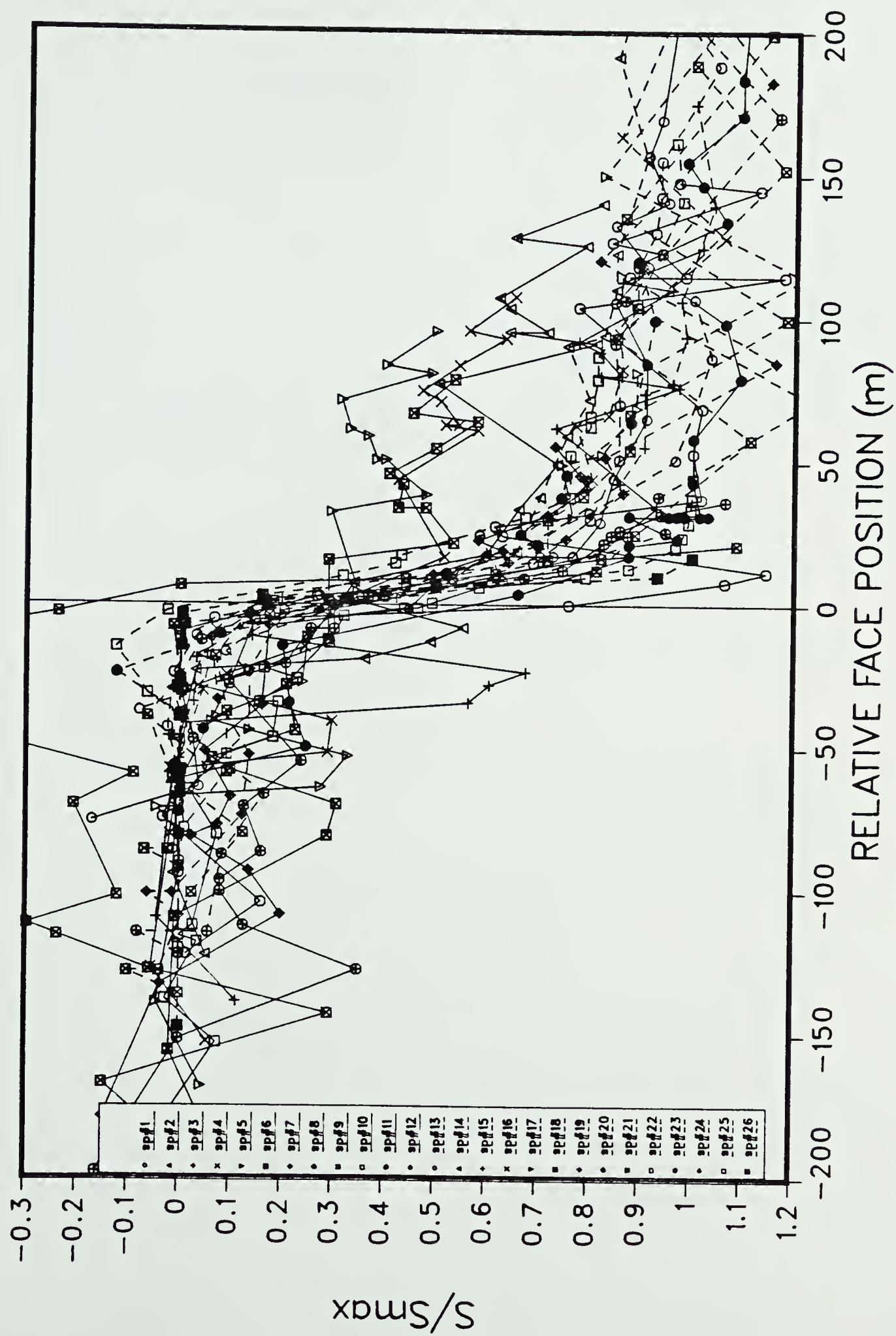
SETTLEMENT VERSUS FACE POSITION FOR S. POINT #24



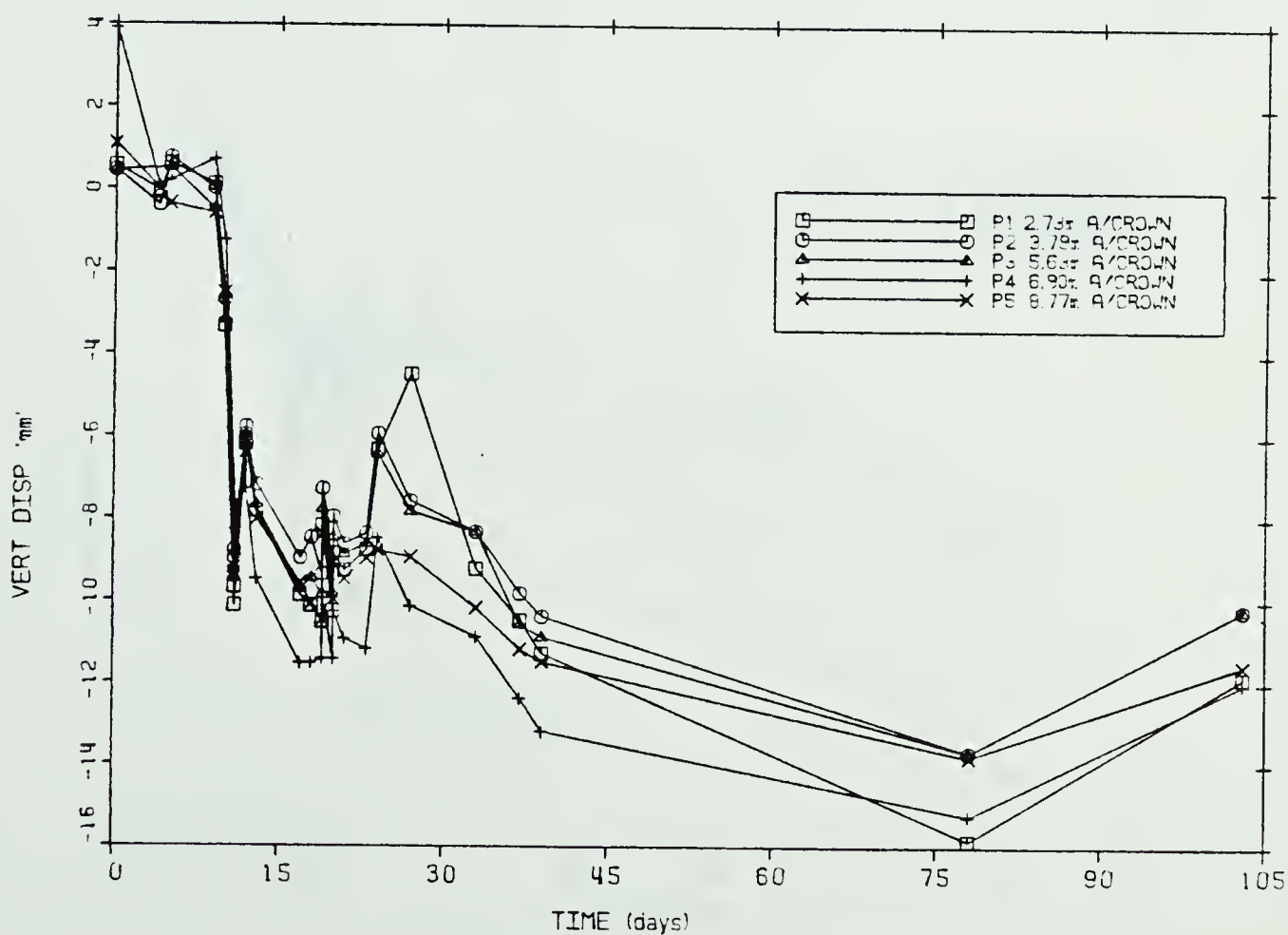
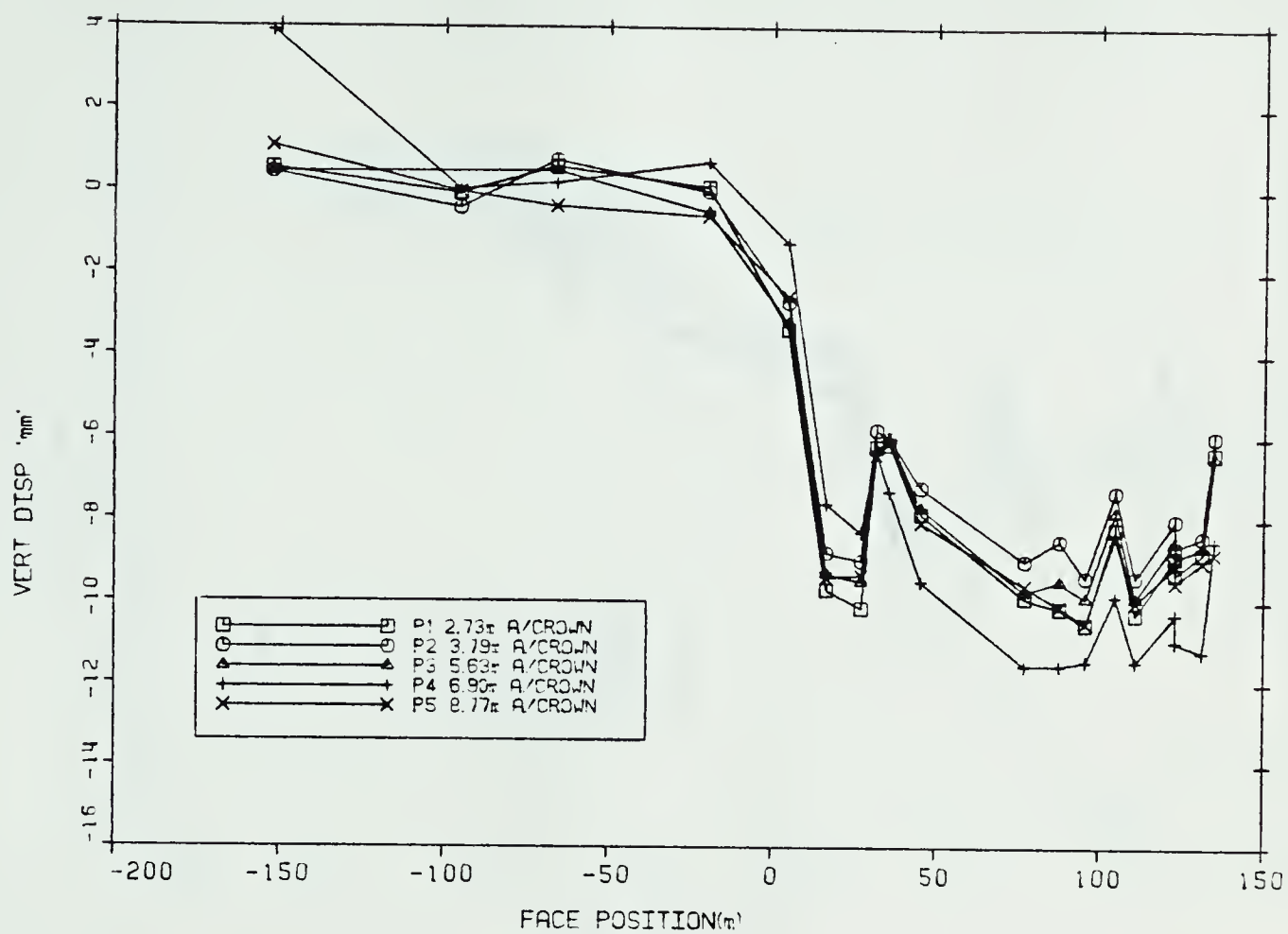
SETTLEMENT VERSUS FACE POSITION FOR S. POINT #25



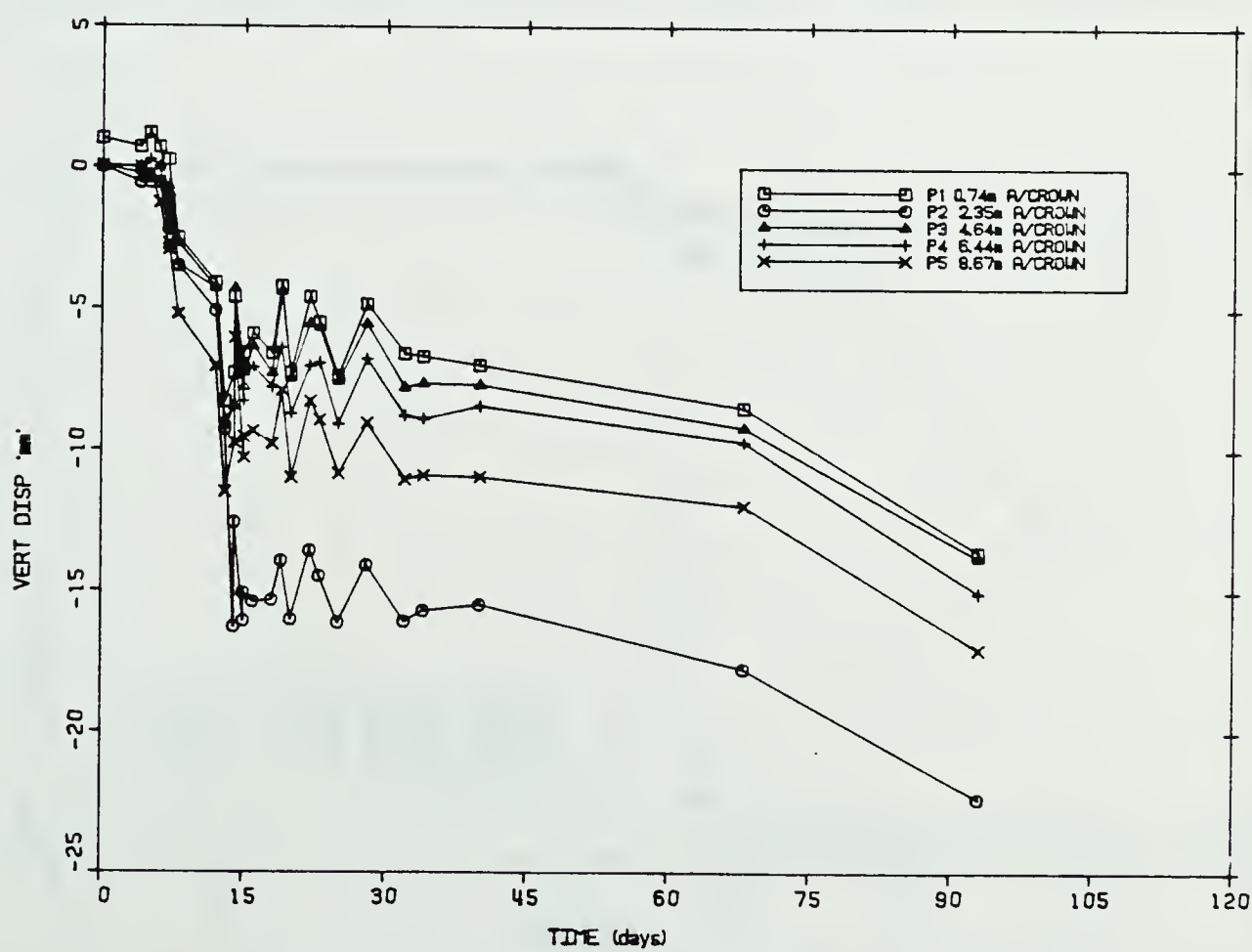
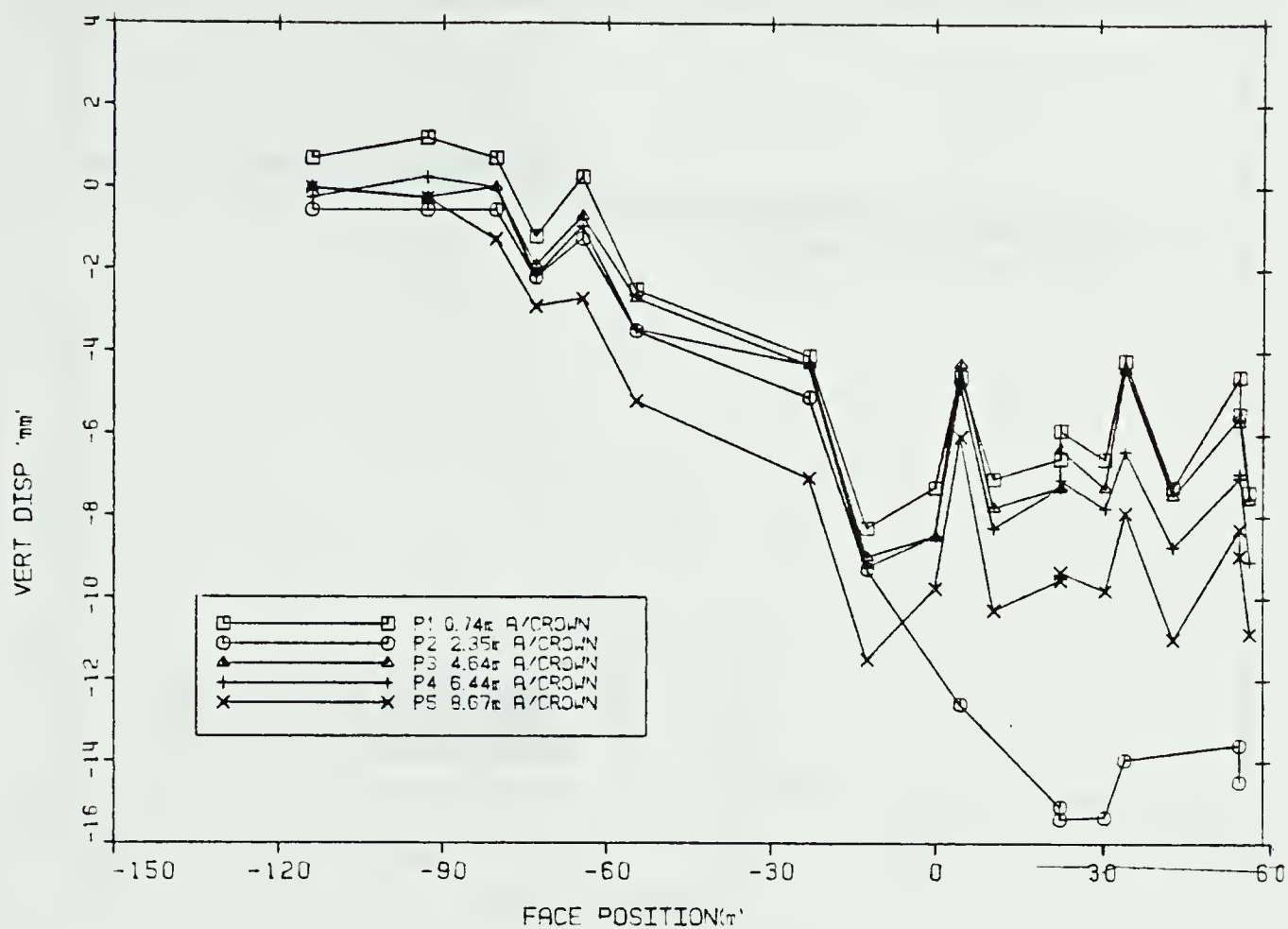
SETTLEMENT VERSUS FACE POSITION FOR S. POINT #26



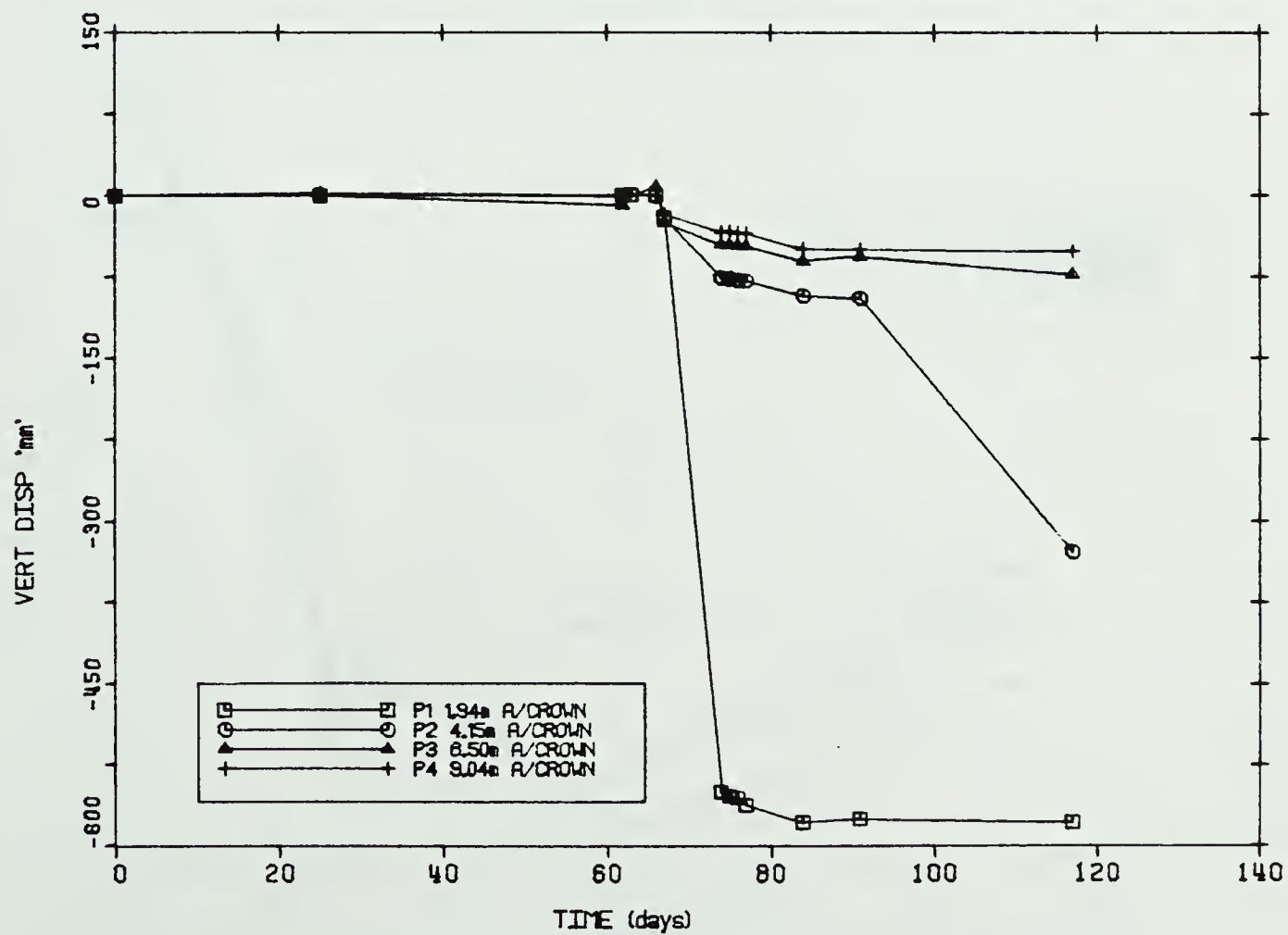
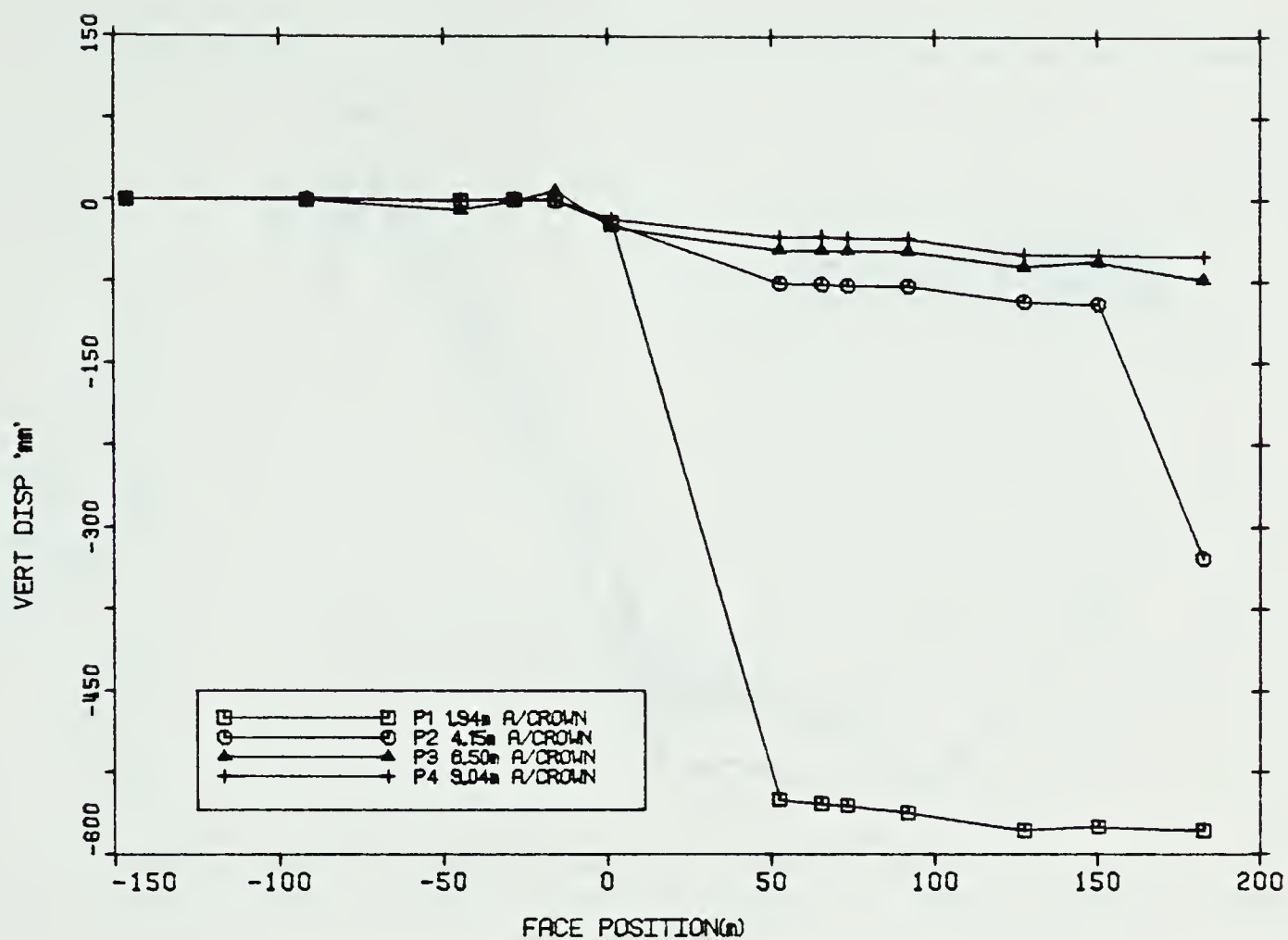
APPENDIX E



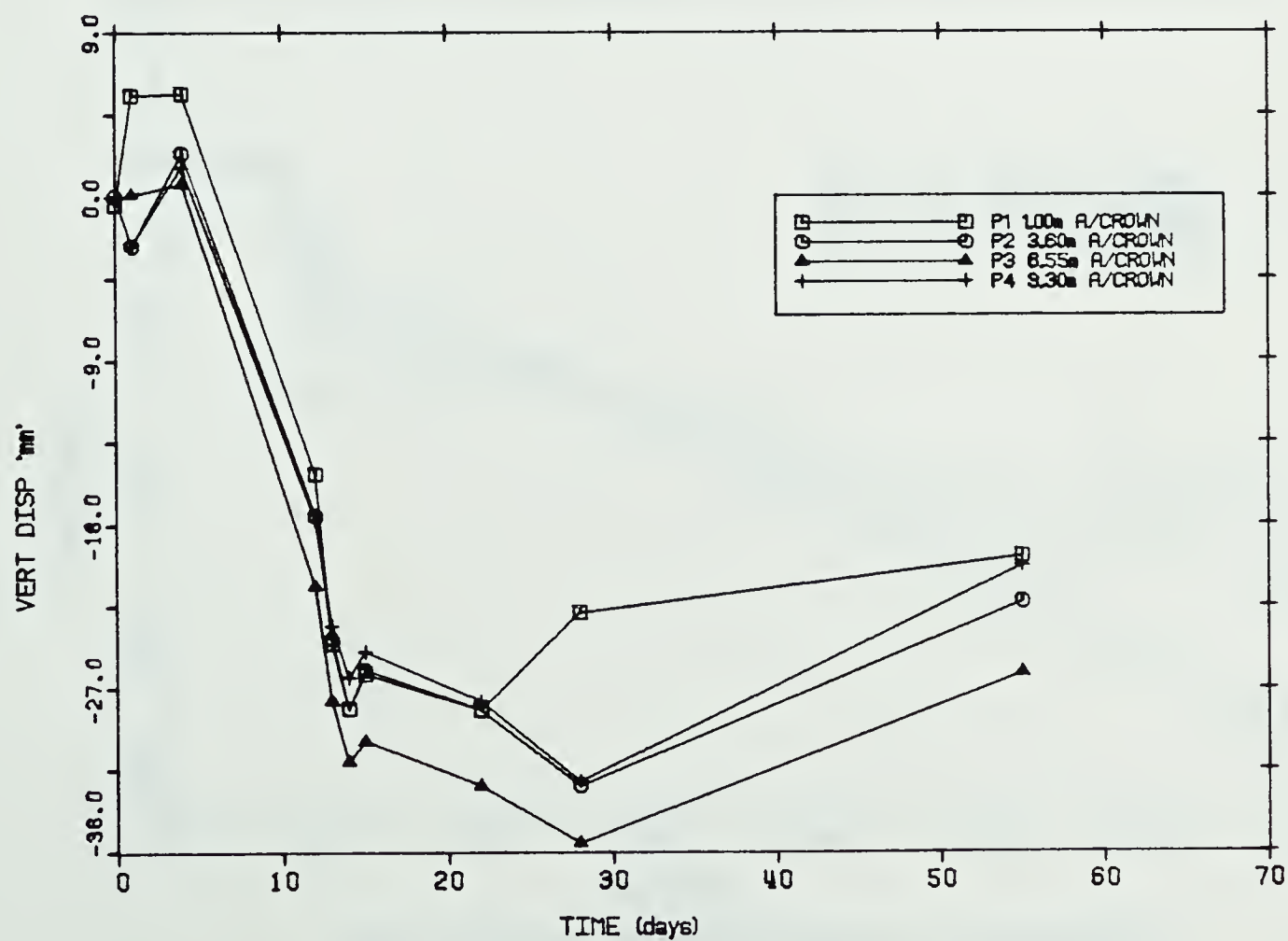
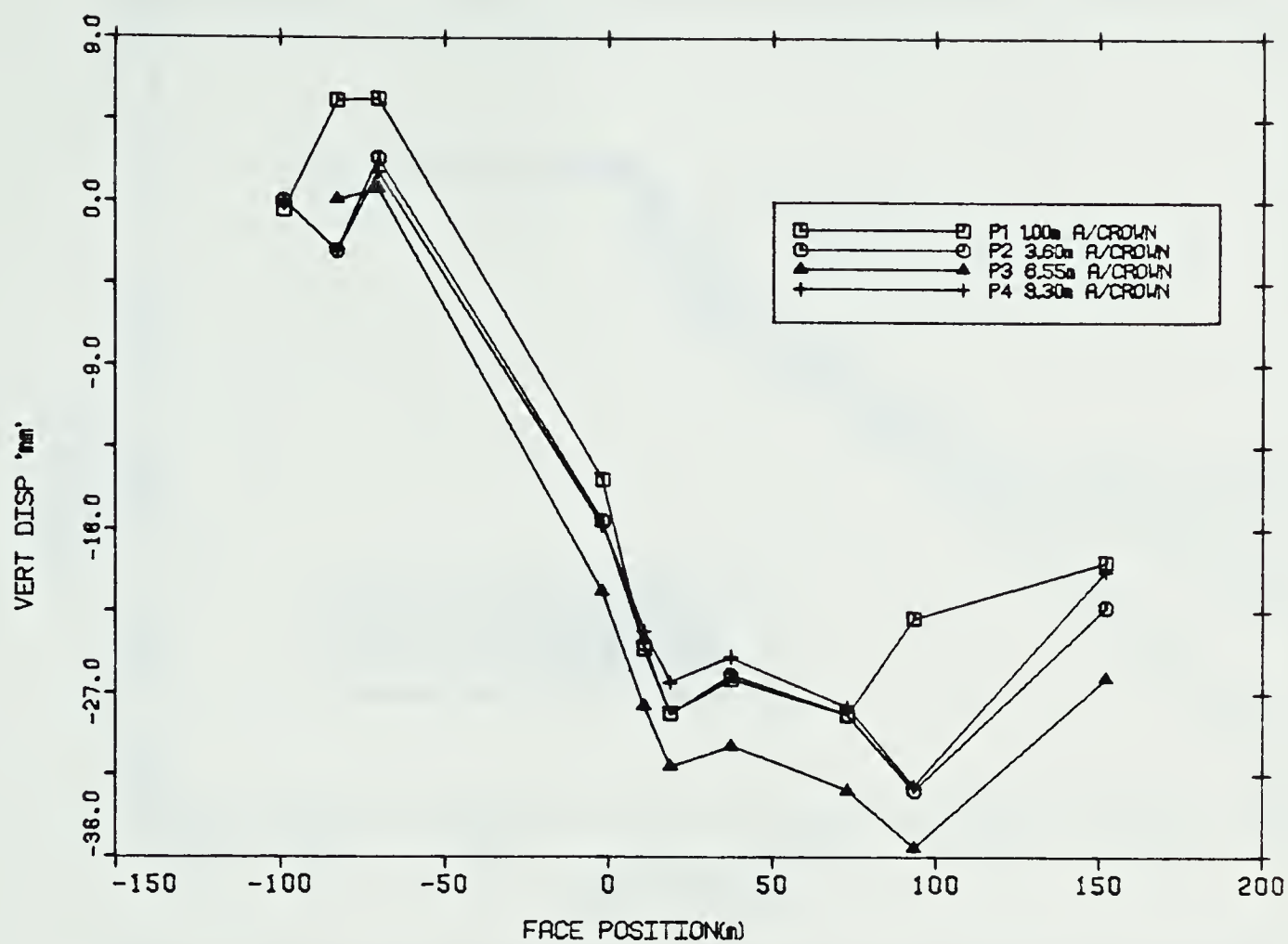
MULTIPOINT EXTENSOMETER #1 MOVEMENTS



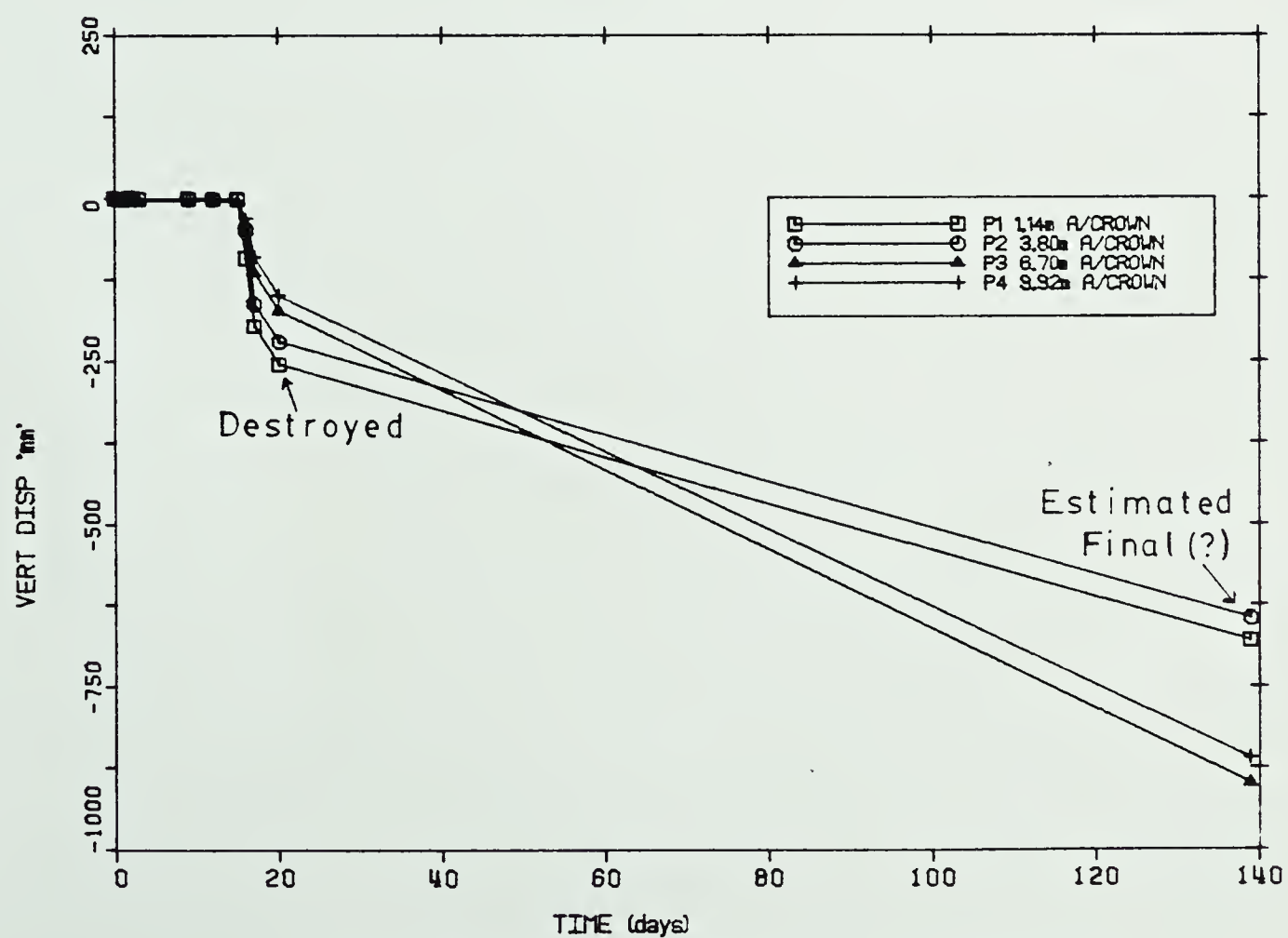
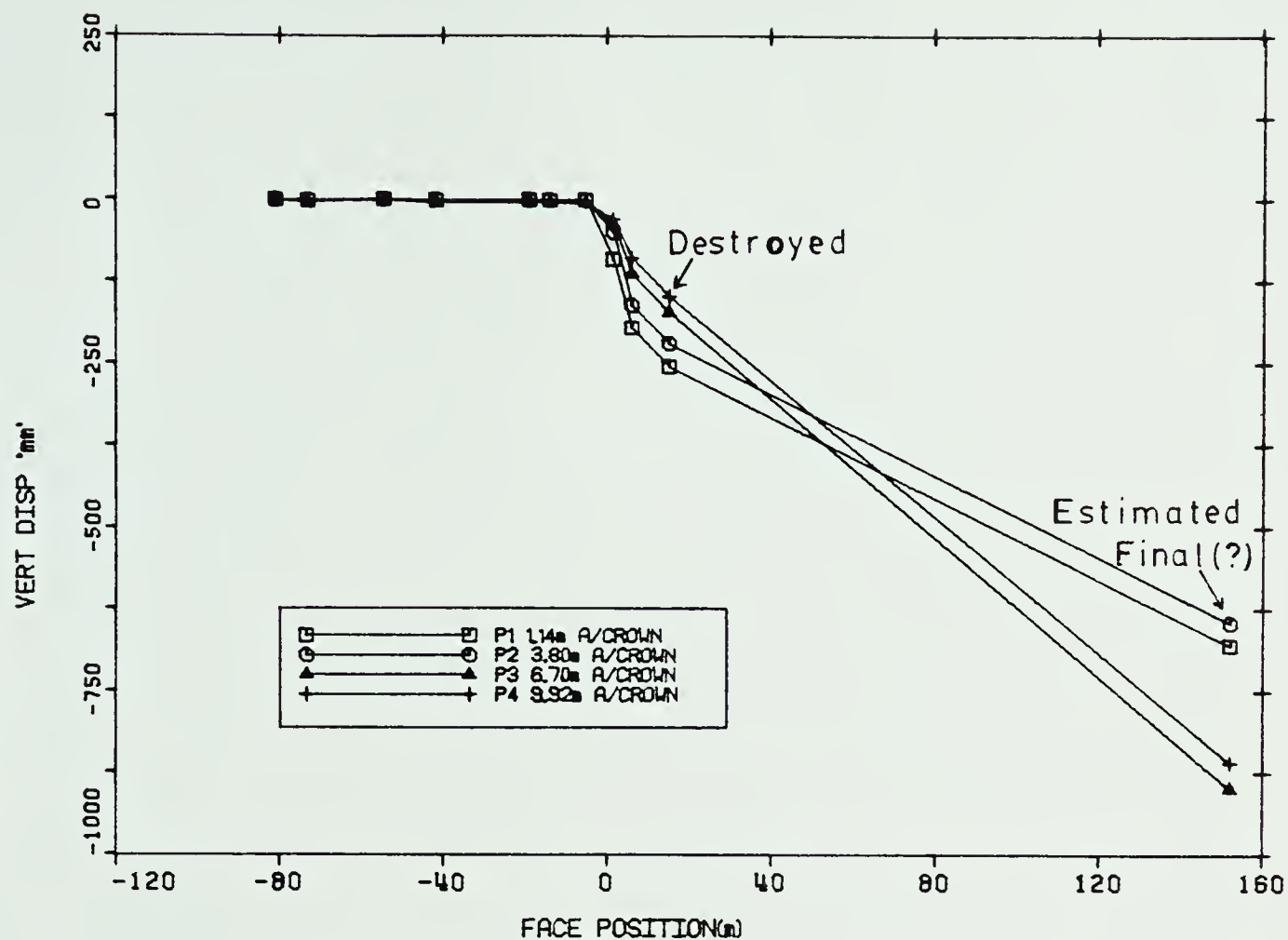
MULTIPOINT EXTENSOMETER #2 MOVEMENTS



MULTIPOINT EXTENSOMETER #3 MOVEMENTS



MULTIPOINT EXTENSOMETER #4 MOVEMENTS



MULTIPOINT EXTENSOMETER #5 MOVEMENTS

B30412